A REVISED AND EXPANDED STRUCTURE HIERARCHY OF NATURAL AND SYNTHETIC HEXAVALENT URANIUM COMPOUNDS

Aaron J. LUSSIER[§] and Rachel A.K. LOPEZ

Department of Civil & Environmental Engineering & Earth Sciences, University of Notre Dame, Notre Dame, Indiana, USA, 46556

Peter C. BURNS

Department of Civil & Environmental Engineering & Earth Sciences, University of Notre Dame, Notre Dame, Indiana, USA, 46556
Department of Chemistry and Biochemistry, University of Notre Dame, Notre Dame, Indiana, USA, 46556

ABSTRACT

Over the past four decades, the number of inorganic oxide and oxy-salt phases containing stoichiometric quantities of hexavalent uranium has increased exponentially from a few dozen to well over 700, and these structures have become well-known for their remarkable compositional diversity and topological variability. Considering the entirety of these compounds (*i.e.*, crystal structures, conditions of synthesis, and geological occurrences) offers significant insight into the behavior of uranium in the solid state and in the nascent (typically aqueous) fluids. The structure hierarchy approach adopted here aims specifically to facilitate the recognition of useful patterns in the crystal-chemical behavior of hexavalent uranium (U^{6+}). This work represents the third attempt at a structure hierarchy of U^{6+} compounds, with the first two being those of Burns *et al.* (1996) and Burns (2005), which considered 180 and 368 structures, respectively. The current work is expanded to include the structures of 727 known, well-refined synthetic compounds (610) and minerals (117) that contain stoichiometric quantities of U^{6+}. As in the previous works, structures are systematically ordered on the basis of topological similarity, as defined predominantly by the polymerization of high-valence cations. The updated breakdown is as follows: (1) isolated polyhedra (24 compounds/0 minerals); (2) finite clusters (70 compounds/10 minerals); (3) infinite chains (94 compounds/15 minerals); (4) infinite sheets (353 compounds/79 minerals); and (5) frameworks (186 compounds/13 minerals). Within each of these major categories, structures are sub-divided on the basis of increasing connectivity of uranium (nearly always uranyl) polyhedra. In addition to elucidating common trends in U^{6+} crystal chemistry, this structure hierarchy will serve as a comprehensive introduction for those not yet fluent in the domain of uranium mineralogy and inorganic, synthetic uranium chemistry.

Keywords: Structure hierarchy, actinides, crystal chemistry, uranium mineralogy, crystal structures, uranyl ion, nuclear waste.

INTRODUCTION

The modern societal importance of uranium originates with the discovery of fission in 1938 and the subsequent development of electricity generation from fission reactors, as well as the production of nuclear weapons on a massive scale. The exploration for, and exploitation of, uranium is important to many economies around the globe. The use of uranium as an energy source is almost certain to be a critical part of meeting future global demand, while also serving to reduce CO_2 emissions. Subsurface and aeolian uranium transport are serious ecological threats, and risks associated with uranium as a radiotoxin and heavy metal have many potential negative consequences to human health. The development of safe, long-term disposal strategies for spent nuclear fuel ($\sim$96% UO_2) and other forms of nuclear waste remain largely unrealized. Recent work has shown myriad examples of how the remarkably versatile chemistry of uranium

§ *Corresponding author e-mail address*: aaron.j.lussier@gmail.com

can be used to develop novel materials, with potentially useful functional properties. Central to the safe and effective use of uranium as a resource is our ability to understand its chemical, mineralogical, and geochemical behavior.

In the solid state, uranium is most commonly present in 6+ or 4+ valence states, with 5+ rather rare and difficult to stabilize in the presence of water. U^{4+}, the most common uranium oxidation state in the solid crust of Earth by volume, forms a relatively small number of compositionally and structurally simple mineral species (*e.g.*, uraninite, coffinite, euxenite). U^{6+}, although less common overall in the crust, is essential in nearly 200 mineral species that show an extensive range of compositions and structures. Owing to the efforts of mineralogists and synthetic chemists, the quantity of characterized inorganic compounds of U^{6+} has increased nearly exponentially.

Here we present an updated and expanded structure hierarchy of U^{6+} compounds, in which inorganic structures containing U^{6+} are systematically organized on the basis of the increasing dimensionality of their structural units. We limit ourselves to extended structures, choosing to exclude the structurally diverse category of uranyl-peroxo nanoclusters that have been reviewed elsewhere recently (Burns 2011, Qiu & Burns 2013). This is the third presentation of a structure hierarchy for inorganic uranyl compounds, after Burns *et al.* (1996; 180 structures) and Burns (2005; 367 structures). The near doubling of known structures over the past decade alone prompts this reexamination. This current hierarchy examines the structures of 727 well-characterized inorganic crystal structures containing U^{6+}, 117 of which are minerals. Consistent with the basic classification scheme proposed in the previous structure hierarchies, these are placed into five structural classes that are based on the dimensionality of polymerization within their structural units: isolated polyhedra (24 compounds, no minerals), finite polyhedral clusters (70 compounds, 10 minerals), infinite chains (94 compounds, 15 minerals), infinite sheets (353 compounds, 79 minerals), and frameworks (186 compounds, 13 minerals). The number of species with sheets and frameworks has grown considerably since 2005. Where possible, subdivisions are introduced to further highlight structural comparisons and facilitate the extraction of useful information.

The structure hierarchy approach

The concept of the structure hierarchy has existed for nearly a century, and was codified by Hawthorne (1983) who stated, "crystal structures may be ordered or classified according to the polymerization of those coordination polyhedra (not necessarily of the same type) with the higher bond valences." This concept has been applied to the development of hierarchies for several mineral groups, such as silicates, uranyl oxide-hydroxides (Burns *et al.* 1996, Burns 2005), copper oxysalts (Eby & Hawthorne 1993), borates (Hawthorne *et al.* 1996), berylates (Hawthorne & Huminicki 2002), sulfates (Hawthorne *et al.* 2000), and phosphates (Huminicki & Hawthorne 2002). More recently, Hawthorne (2014) states that a structure hierarchy has two functions: (1) to coherently organize knowledge of crystal structures; and (2) to facilitate the recognition of linkages between the mechanistic details of crystal stability and behavior and the interaction of those features with the environment. This structure hierarchy is compiled with this explicitly in mind. The categories initially proposed by Burns *et al.* (1996) and Burns (2005) are retained; however, we attempt to create useful sub-divisions within these categories to facilitate recognition of common topological features within a wide array of structures. It is also noteworthy that the striking increase in the number of known structures in certain categories (particularly frameworks) necessitates the implementation of some degree of sub-division, as grouping such a large number of structures together seems in violation of Hawthorne's proposed functions. It is noted that the function of this structure hierarchy of uranyl phases differs profoundly from those developed for the other oxyanion mineral phases in that the number of known uranyl phases continues to increase rapidly. Hence, it serves not only as an epistemological tool, but also (hopefully) as a source of inspiration to synthetic chemists.

URANYL COORDINATION POLYHEDRA

In nearly all crystal structures, U^{6+} occurs as the collinear uranyl ion, UO_2^{2+}. This ion consists of a central U^{6+} cation that is triple-bonded to two apical oxygen atoms with short bond distances of $\sim$1.8 Å (Fig. 1). The $U–O_{yl}$ bonds provide between 1.6 and 1.7 *vu* to the oxygen atom, nearly satisfying its bond valence requirements. Thus, the yl oxygen atoms are most often terminal, interacting with low-valence/highly-coordinated cations or (H_2O) present in the interstitial complex. The formal charge of the uranyl ion is +2, which impacts its incorporation into coordination polyhedra. In these, ligands (usually anions) are located in an equatorial plane that is perpendicular to the axis of the uranyl ion, such that bipyramidal polyhedra result with the uranyl ion oxygen atoms defining the bipyramid apices. In the majority of structures, oxygen (as O, OH, or H_2O) is the coordinating ligand; however, compounds with
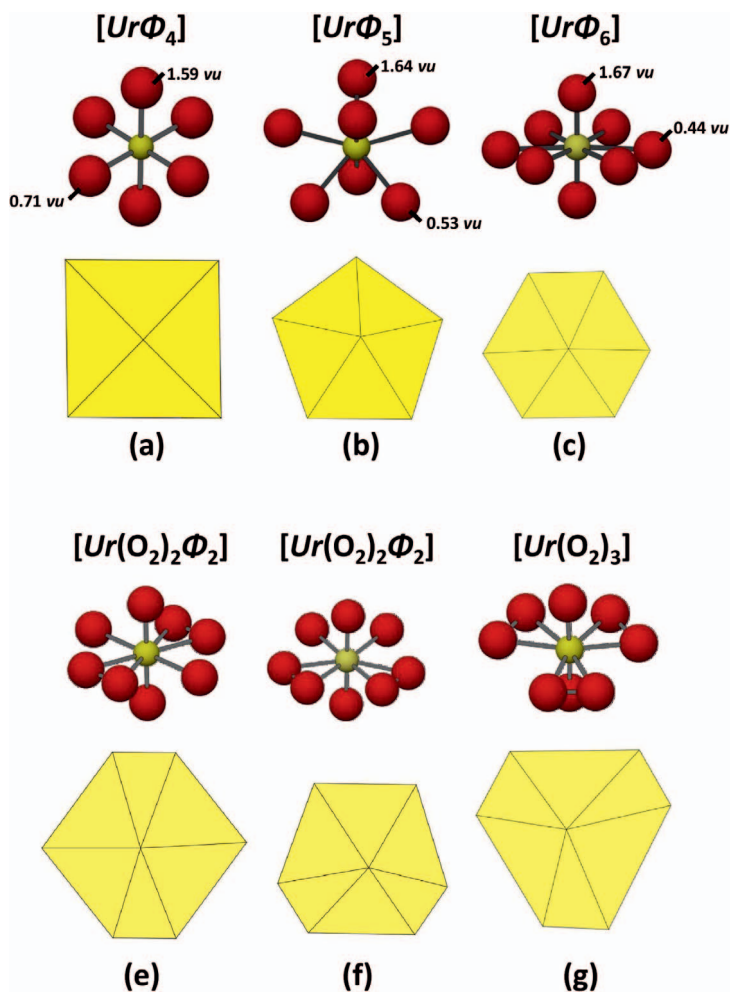
FIG. 1. Uranyl (*Ur*) coordination polyhedra observed in the compounds discussed in this work. Top row: uranyl bipyramids [(a) square, (b) pentagonal, and (c) hexagonal] containing only single anions at each equatorial position [$\Phi = O^{2-}$, $(OH)^-$, (H_2O), Cl, Br, F]. Bottom row: three configurations of uranyl hexagonal bipyramids with peroxide (O_2) at the equatorial positions [(d) $Ur(O_2)_2\Phi_2$, (f–g) graphical isomers of $Ur(O_2)_3$].

variable numbers of equatorial halogens are also known (*e.g.*, Nazarchuk *et al*. 2011).

Three types of coordination polyhedra are commonly observed: (1) square bipyramids (four equatorial ligands), (2) pentagonal bipyramids (five equatorial ligands), and (3) hexagonal bipyramids (six equatorial ligands); these are illustrated in Figure 1. Burns *et al*. (1997a) examined ~100 well-refined U^{6+} structures and discussed the distribution of observed bond lengths in each coordination polyhedron in detail, and derived refined bond-valence parameters, focusing only on polyhedra in which all of the equatorial ligands are O, (OH), or (H_2O). Burns (2005) updated the inventory of bond lengths and

angles to 222. The findings from these works are briefly summarized here, as aspects are germane to the discussions below.

A bimodal distribution of bond lengths is observed for uranyl pentagonal and hexagonal bipyramids. For both, the $U–O_{yl}$ bond lengths in the uranyl ion are significantly shorter than the $U–O_{eq}$ bonds. The average $[7]U^{6+}–O_{yl}$ is 1.793 Å ($\sigma = 0.035$ Å); $[7]U^{6+}–O_{eq}$ is 2.368 Å ($\sigma = 0.100$ Å). The average $[8]U^{6+}–O_{yl}$ is 1.783 ($\sigma = 0.030$ Å); $U^{6+}–O_{eq}$ is 2.460 Å ($\sigma = 0.107$ Å).

The situation regarding $[6]U^{6+}$ is more complicated. Most commonly, the UO_2^{2+} cation is coordinated by four equatorial ligands with an average $U–O_{yl}$ of 1.816

Å ($\sigma = 0.050$ Å) and U–O$_{eq}$ of 2.264 ($\sigma = 0.064$ Å). However, well-refined structures also contain U^{6+} in regular (or distorted) octahedral coordination, where the average bond lengths are ~2.1 Å. Further, in at least two reported structures (Wu *et al*. 2009, Unruh *et al*. 2010), [6]-coordinated U^{6+} adopts an unusual tetraoxido core, wherein the four equatorial bonds of the octahedra are short, at ~1.8 Å, and the polar bonds are long, at ~2.3 Å.

Furthermore, $^{[6]}$U^{6+} coordination geometries range between the specific cases of uranyl square bipyramids, tetraoxido, and octahedral, defining coordination geometry structural pathways (Weng *et al*. 2012). The corresponding U–O bond valences for the three most common uranyl coordination polyhedra, given in Burns (2005) using the parameters of Burns *et al*. (1997a), are shown in Figure 1a–c and listed here: $^{[6]}$U^{6+}–O$_{yl}$ = 1.59 valence units (*vu*), $^{[6]}$U^{6+}– O$_{eq}$ = 0.71 *vu*, $^{[7]}$U^{6+}–O$_{yl}$= 1.64 *vu*, $^{[7]}$U^{6+}–O$_{eq}$ = 0.53 *vu*, $^{[8]}$U^{6+}–O$_{yl}$ = 1.67 *vu*, $^{[8]}$U^{6+}–O$_{eq}$ = 0.44 *vu*. Hence, the significant residual bond valence to the equatorial anions results in the tendency for uranyl polyhedra to polymerize, forming structures with higher dimensionality (*i.e.*, chains, sheets, and frameworks).

The uranyl ion readily bonds with the peroxide molecule (O$_2$), forming hexagonal bipyramids with O$_2$ at the equatorial anion positions. The resulting polyhedra have the general formula [Ur_4(O$_2$)$_x$Φ$_{6-2x}$], and those observed in the structures presented in this work are illustrated in Figure 1e–g. Research over the past decade (Kubatko & Burns 2006a, Kubatko *et al*. 2007, Unruh *et al*. 2009) has shown that these peroxide coordination polyhedra may occur in synthetic, extended inorganic structures of varying dimensionality (*i.e.*, isolated polyhedra, finite clusters, and sheets). Infinite chains of edge-sharing di-peroxide polyhedra occur in two known mineral phases: studtite and metastudtite (Burns & Hughes 2003). Further, the uranyl peroxide polyhedra are essential to the formation of an ever-growing class of discrete, soluble nanostructured materials referred to as uranyl peroxide nanoclusters (see Qiu & Burns 2013 and references therein).

Although rare in compounds containing U^{6+}, one or both of the yl oxygen atoms occasionally bridge to other uranyl ions, with the interaction referred to as a cation-cation interaction (CCI) for historic reasons (Sullivan *et al*. 1961). The current work lists 21 structures with cation-cation interactions in Table 18 and illustrates these in Figure 19. Cation-cation interactions are much more common in Np^{5+} compounds, owing to the decreased electrostatic repulsion as well as the weaker bonds in the Np(V) neptunyl cation (Forbes *et al*. 2008).

THE POLYMERIZATION OF URANYL POLYHEDRA

Crystal structures can be divided into two components: (1) the *structural unit*, which consists of the strongly bonded, usually anionic, portion of the structure, and (2) the *interstitial complex*, which consists of the weakly bonded, usually cationic, portion of the structure. Following the approach proposed by Hawthorne (1983) and previous uranyl oxo-structure hierarchies (Burns *et al*. 1996, Burns 1999a, Burns 2005), structures of inorganic compounds are arranged here on the basis of increasing topological dimensionality and complexity of the structural unit. The structural units readily separate into five classes that are defined by the dimensionality of polyhedral connectedness in the structural unit. *Isolated clusters* (0-dimension) consist of isolated uranyl polyhedra that share no polyhedral elements with any other uranyl polyhedra or polyoxo-anions. Finite clusters (also 0-dimensional) contain one or more uranyl polyhedra linked to various oxyanions, or in some cases, groups of linked uranyl polyhedra. *Infinite chains* (1-dimensional) contain chains of uranyl polyhedra either linked directly to one another or *via* a ligand polyhedron, or both, such that they extend to infinity. *Infinite sheets* involve the polymerization of uranyl and other high-valence cation polyhedra in 2-dimensions. *Frameworks* show polymerization of uranyl polyhedra and other higher valence cation polyhedra in 3-dimensions.

CHEMICAL AND STRUCTURAL TRENDS IN URANYL CRYSTAL CHEMISTRY

Figure 2a shows the systemic changes in the number of known inorganic phases that contain U^{6+} over the past 75 years and demonstrates the nearly exponential increase in the number of synthetic phases starting in the early-to-mid 1990's. The number of minerals whose structures and compositions have been characterized has also increased substantially since this time (nearly 300%), but now represents only about 15% of the total uranyl phases known. Figure 2c illustrates the relative frequency of compounds in which uranyl is paired with various ligands; larger circles represent a larger number of known compounds. Research into the synthetic inorganic chemistry of uranyl has been heavily influenced by the potential interaction of nuclear waste with groundwater in a geological repository. As such, it is likely that the compositional distribution of phases in Figure 2b exhibits a bias for chemical species that are common constituents of natural groundwater (*e.g.*, SiO$_4$$^{4-}$, CO$_3$$^{2-}$, SO$_4$$^{2-}$, PO$_4$$^{3-}$, Li$^+$, Na$^+$, K$^+$, Mg^{2+}, and Ca^{2+}) and nuclear waste packages (*e.g.*, IO$_3$$^-$, Mo, Cs$^+$, Ba^{2+},
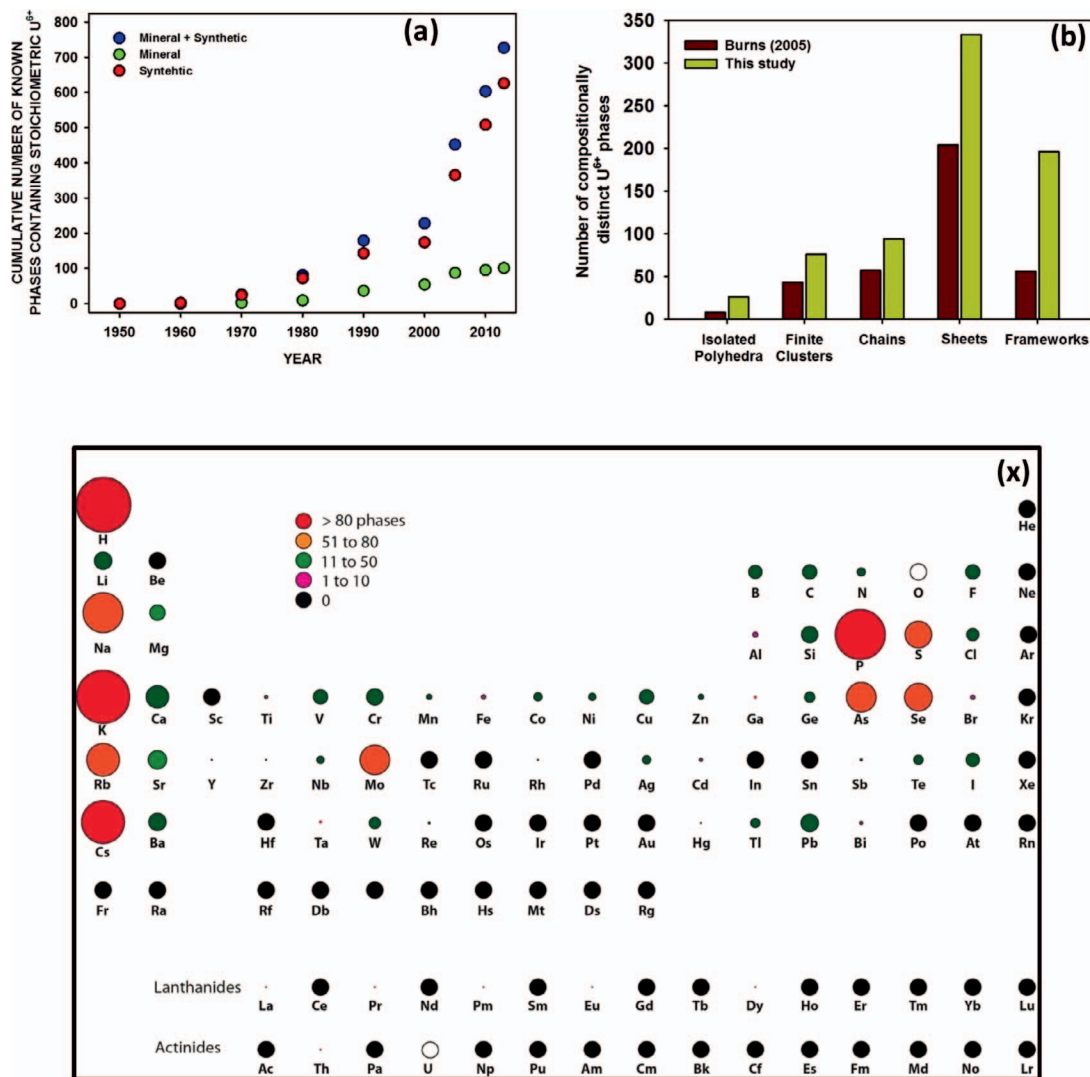
FIG. 2. General information regarding the known U^{6+} compounds. (a) Changes in the number of characterized U^{6+} compounds (synthetics and minerals) since the year 1950. (b) Changes in the number of U^{6+} placed in the structural classes since the publication of hierarchy of Burns (2005). (x) Relationship between the frequency (circle size) and composition of the 727 U^{6+} discussed in this work.

and Sr^{2+}). Certain elements, common in spent nuclear fuel from light water reactors, such as the lanthanides, are currently under-represented, although research in this area appears to be increasing steadily (Pobedina & Ilyukhin 1997, Chapelet-Arab *et al.* 2005, 2006, Mer *et al.* 2012).

Figure 2b shows the evolution of structure types since the hierarchy of Burns (2005). The structures in which the uranyl ion occurs in sheets continue to dominate the inventory; the next most extensive class,

frameworks, has nearly 130 fewer members. The number of sheet- and framework-bearing species has increased far more than the other, less-polymerized classes (although more than 60 uranyl peroxide clusters are excluded from consideration here). The number of sheets has less than doubled, whereas the number of frameworks has more than tripled. Previously, the development of sub-classes for framework structures of uranyl compounds received no attention, as they were both few in number and topologically difficult to group

TABLE 1. U(VI) COMPOUNDS WITH STRUCTURES CONTAINING ISOLATED POLYHEDRA

FORMULA	SG	a (Å)	b (Å)	c (Å)	α (°)	β (°)	γ (°)	SYN[a]	FIG	REF
[$U\Phi_4$]										
$Ca_3[UO_6]$	$P2_1/n$	5.729	5.962	8.299	—	90.56	—	SS[1200]	2a	1
$Sr_3[UO_6]$	$P2_1/n$	6.013	6.214	8.614	—	90.239	—	SS[977]	2a	2
$K_2Li_4[UO_6]$	$P\bar{3}m$	6.193	6.193	5.338	—	—	120	SS[750]	2a	3
$\alpha\text{-}Li_6[UO_6]$	$R\bar{3}$	8.381	8.381	7.383	—	—	120		2a	4
$K_8[(UO_2)_2O_6]$	$P\bar{1}$	6.474	9.698	6.344	101.17	102.3	109.02	SS[750]	2a	5
$(NH_4)_2[(UO_2)Br_4](H_2O)_2$	$P\bar{1}$	6.777	6.822	7.679	98.075	95.036	116.49	A	2a	6
$K_2[(UO_2)Br_4](H_2O)_2$	$P\bar{1}$	6.753	6.825	7.573	93.976	99.495	117.48	A	2a	6
$Rb_2[(UO_2)Br_4](H_2O)_2$	$P\bar{1}$	6.862	6.925	7.736	93.754	99.142	117.36	A	2a	6
$Cs_2[(UO_2)Br_4]$	$P2_1/c$	6.350	9.742	9.927	—	104.51	—	A	2a	6
$Cs_2[(UO_2)Cl_4]$	Cm	12.005	7.697	5.85	—	100.00	—		2a	7
$(NH_4)_2[(UO_2)Br_4](H_2O)_2$	$P\bar{1}$	6.885	6.887	7.737	94.44	98.78	116.79		2a	8
$Rb_2[(UO_2)Cl_4](H_2O)_2$	$P\bar{1}$	6.795	6.929	7.457	91.96	102.13	118.82	Ac	2a	9
$Pb_2Ca[UO_6]$	$P2_1/n$	6.059	5.974	8.526	—	89.92	—	SS[1050]	1a	10
$Ba_2Na_{0.83}U_{1.17}O_6$	$Fm\bar{3}m$	8.617	8.617	8.617	—	—	—	Flx[1050]	1a	11
[$U\Phi_5$]										
$[(UO_2)(H_2O)_5](ClO_4)(H_2O)_2$	$Pbcn$	14.495	9.216	10.675	—	—	—	A	2b	12
$[(UO_2)(H_2O)_5](ClO_4)_2$	$P2_1/n$	5.294	16.454	14.802	—	99.847	—	A	2b	12
$[(UO_2)Cl_2(H_2O)_3]$	$Pnma$	12.738	10.495	5.547	—	—	—		2b	13
$[(UO_2)Br_2(H_2O)_3]$	$P2_1/c$	9.738	6.547	12.818	—	94.104	—	Ae	2b	14
$K_3(UO_2)F_5$	$P2_1/n$	9.160	9.160	18.167	—	—	—	A	2b	15
[$U(O_2)_2\Phi_2$]										
$Na_6[(UO_2)(O_2)_2(OH)_2](OH)_2(H_2O)_{14}$	$P2_1/n$	13.357	5.852	15.948	—	112.29	—		2e	16
[$U(O_2)_3$]										
$Na_4[(UO_2)(O_2)_3](H_2O)_9$	$Cmc2_1$	6.413	17.292	14.186	—	98.52	—		2g	17
$Ca_2[(UO_2)(O_2)_3](H_2O)_9$	$Pbcn$	9.576	12.172	12.314	—	—	—		2g	18
$Na_4[(UO_2)(O_2)_3](H_2O)_{12}$	$P2_1/c$	6.788	16.001	16.562	—	91.92	—		2g	18
$Li_4[(UO_2)(O_2)_3](H_2O)_{10}$	$Pbcn$	13.118	9.236	12.896	—	—	—		2g	19

Note: Double lines (═) indicate major differences in the stoichiometry of the structural unit, as indicated by the corresponding header in the table; single lines (–) indicates different topologic configurations; and dotted lines (- -) separate graphical isomers.

[a] Synthesis column data. HT[T] and SS[T] correspond to hydrothermal and solid state synthesis, respectively, at maximum reported temperature T (°C); V-Cl: vapor phase chlorination; A, aqueous (Ae denotes evaporation to dryness); Ac, concentrated acid; Flx, molten flux; SDg, slow diffusion in gel.

References: (1) Van Duivenboden & Ijdo (1986); (2) Ijdo (1993b); (3) Wolf & Hoppe (1987); (4) Wolf & Hoppe (1985); (5) Wolf & Hoppe (1986); (6) Wilson *et al.* (2011); (7) Tutov *et al.* (1991); (8) van den Bossche *et al.* (1987); (9) Anson *et al.* (1996); (10) Knyazev *et al.* (2011); (11) Roof *et al.* (2010b); (12) Fischer (2003); (13) Debets (1968); (14) Crawford *et al.* (2004); (15) Lychev *et al.* (1986); (16) Zehnder (2008); (17) Alcock (1968); (18) Kubatko *et al.* (2007); (19) Nyman *et al.* (2010).

in a coherent manner. However, as will be elaborated upon in subsequent text, the proliferation of framework structures has prompted development of a more sophisticated framework classification scheme.

In the recent past, compounds incorporating halogens (F⁻, Cl⁻, Br⁻) at equatorial positions of uranyl polyhedra have been synthesized. To date, there are 56 oxyhalogen uranyl compounds with reported structures. In general, these elements tend to occur in lower-dimensionality structures, but the oxyhalogen uranyl compounds are well represented in all five of the structural classes; of the 56, 21% have isolated polyhedra, 27% have finite clusters, 14% have infinite chains, 32% have sheets, and 5% are framework structures.

STRUCTURES CONTAINING ISOLATED POLYHEDRA

There are 24 compounds (Table 1) for which the structural unit consists solely of isolated uranyl polyhedra (as illustrated in Fig. 1), corresponding to only 3.3% of the total U^{6+} structures; none are minerals. Only uranyl square (14 compounds) and pentagonal bipyramids (five compounds) occur isolated in these structures.

$Ur\Phi_4$ polyhedra (Fig. 1a) in these structures have either the composition UrO_4 or UrX_4 ($X = Br^-$, Cl^-). Seven compounds contain equatorial halogen atoms (Cl⁻, Br⁻, F⁻), yet no polyhedra have mixed oxygen and halogen ligands. The isolated $Ur\Phi_4$ polyhedra occur in either anhydrous or hydrous structures. Wilson *et al.* (2011) investigated this issue for the aqueous (UO_2^{2+})–Br system. These authors compared structural information derived from single crystal X-ray diffraction and high-energy X-ray scattering (HEXS) data for an aqueous precursor and found no compelling evidence for the occurrence of $(UO_2)Br_4$ aqueous complexes.

Three compositions of isolated $Ur\Phi_5$ polyhedra (Fig. 1b) are listed in Table 1: $Ur(H_2O)_5$, $Ur(H_2O)_3X_2$ (X = Br, Cl), and UrX_5 (X = F). All but one of these contain (H_2O) as one or more equatorial ligands. $K_2(UO_2)F_5$ is the only compound with an isolated pentagonal bipyramid as well as a cation in the interstitial complex. In the structures of $[(UO_2)X_2(H_2O)_3]$ (X = Cl, Br), the individual polyhedra are stabilized solely by a network of hydrogen bonds between equatorial (H_2O) and Cl (or Br) atoms of adjacent polyhedra. These structures are the only known inorganic uranyl dihalides, of which there are many other examples with organic molecules in the interstitial complexes (see Crawford et al. 2004 and references therein).

The structures of $[(UO_2)(H_2O)_5](ClO_4)_2(H_2O)_2$ and $[(UO_2)(H_2O)_5](ClO_4)_2$ both contain the perchlorate ion (ClO_4^-) as isolated interstitial polyhedra and are synthesized in low temperature environments. This is consistent with the observation that interactions between uranyl and perchlorate ions are unlikely in aqueous environments, although other solid-state structures suggest otherwise (see below).

The uranyl hexagonal bipyramid does not occur as isolated polyhedra in any known extended structure. However, structures are known to contain isolated di-peroxide ($[Ur(O_2)\Phi_2]$; one compound; Fig. 1e) and tri-peroxide ($[Ur(O_2)_3]$; four compounds; Fig. 1g) hexagonal bipyramids; these are also listed in Table 1. The isolated di-peroxide hexagonal bipyramid occurs in the compound $Na_6[(UO_2)(O_2)_2(OH)_2](OH)_2(H_2O)_{14}$, and here the peroxo linkages occur in the equatorial plane in a *trans* configuration. The two non-peroxide equatorial anion positions are occupied by (OH). In a tri-peroxide hexagonal bipyramid, all six equatorial anion positions are occupied by the peroxide molecules (Fig. 1g) in the four compounds listed in Table 1.

STRUCTURES CONTAINING FINITE CLUSTERS OF POLYHEDRA

Finite clusters of polyhedra consist of a grouping of either vertex-sharing or edge-sharing polyhedra (or both) that do not polymerize in any direction. Currently, there are 70 known U^{6+} compounds that contain finite clusters of polyhedra, an increase from the 43 structures discussed in Burns (2005). Despite this increase, only five new clusters have been added (although the large family of uranyl peroxide cage clusters is excluded from discussion here).

The general formula for finite clusters in U^{6+} compounds and minerals is designated Ur_xL_y, where Ur is the uranyl cation in any coordination and L is an oxo-anion such as PO_4, SO_4, or SiO_4. We distinguish between two types of L polyhedra: bridging and non-bridging. Bridging ligand polyhedra are element-sharing with more than one U^{6+} polyhedron, whereas non-bridging ligand polyhedra are terminal. The subscripts x and y denote the number of U^{6+} and ligand polyhedra in the cluster. We use this notation to facilitate hierarchical classification. Structures are grouped on the basis of the value of x and are sub-ordered on the basis of y. This approach naturally groups graphical isomers and facilitates the comparison of structures that may be related by addition (or deletion) of ligand polyhedra.

The majority of synthetic compounds containing either isolated polyhedra (Table 1) or finite clusters (Table 2) were prepared in aqueous media, at either room temperature or under mild hydrothermal conditions (<100 °C). Hence, there may be a relationship between the conformation of the polyhedral unit of finite polyhedral clusters in the aqueous and crystal matrices. In aqueous solution, the uranyl ion is well known to interact strongly with many species of counterions, such as halogens (Wilson et al. 2011), hydroxides (Soderholm et al. 2007), carbonate (Nguyen-Trung et al. 1992, Allen et al. 1995, Clark et al. 1995), nitrate (Nguyen-Trung et al. 1992, de Jong et al. 2005), sulfate (Moll et al. 2000, Neuefeind et al. 2004, Hennig et al. 2007), selenate (Sladkov 2010), arsenate (Rutsch et al. 1999), and phosphate (Sandino & Bruno 1992).

Graphical representations of finite clusters

The topological complexity of crystal structures can often be reduced to its essential elements using a graphical representation. Following the methodology initially proposed by Hawthorne (1983) and Hawthorne et al. (1996), implemented by Burns (2005) for uranyl compounds, the graph of each finite cluster is drawn (Fig. 3). Each is constructed by representing Ur and L polyhedra as solid black and solid white circles, respectively. A solid line depicts every anion common to more than one polyhedron; as such, vertex-sharing and edge-sharing between polyhedra are represented by single and double lines connecting the corresponding circles, respectively.

U_1L_y-type finite clusters of polyhedra

Ten topologically unique clusters of polyhedra containing one uranyl polyhedron form the structures of 70 compounds listed in Table 2 and illustrated in Figure 3. These clusters may be decorated by either vertex- or edge-sharing polyhedra. The anhydrous structure of $Cs_2[(UO_2)Cl_3(NO_3)]$ contains a finite cluster of the type U_1L_1 (Fig. 3a). Here three of the five equatorial ligands are Cl^- that are non-bridging, whereas two O^{2-} serve to bridge the triangular NO_3 to

TABLE 2. U(VI) COMPOUNDS WITH STRUCTURES CONTAINING FINITE CLUSTERS OF POLYHEDRA

MINERAL	FORMULA	SG	a (Å)	b (Å)	c (Å)	α (°)	β (°)	γ (°)	SYN[a]	FIG	REF
$^0[U_1L_x]$ clusters											
U_1L_1											
	Cs$_2$[(UO$_2$)(NO$_3$)Cl$_3$]	P2$_1$/n	10.375	9.468	12.554	—	110.28	—	HT[205]	3a	1
	(H$_3$O)$_2$(UO$_2$)(SeO$_4$)$_2$(H$_2$O)$_3$	Pnma	14.033	11.641	8.215	—	—	—	Ae	3b	2
	[(UO$_2$)(ClO$_4$)$_2$](H$_2$O)$_3$	P2$_1$/c	5.454	18.111	10.325	—	90.02	—	A	3c	3
U_1L_2											
	(UO$_2$)(NO$_3$)$_2$(H$_2$O)$_6$	Cmc2$_1$	13.197	8.035	11.467	—	—	—	A	3d	4
	(UO$_2$)(NO$_3$)$_2$(H$_2$O)$_2$	P2$_1$/c	14.124	8.432	7.028	—	108.0	—	A	3d	5
	(UO$_2$)(NO$_3$)$_2$(H$_2$O)$_3$	P$\bar{1}$	7.036	7.173	10.084	81.69	82.04	63.64	Ae	3d	6
	[(UO$_2$)(NO$_3$)$_2$(H$_2$O)$_2$](H$_2$O)	P2$_1$/c	7.179	8.954	14.301	—	99.40	—	Ac	3e	7
	K$_4$[U(CO$_3$)$_2$O$_2$(O$_2$)](H$_2$O)$_{2.5}$	P2$_1$/n	6.908	9.233	21.809	—	91.31	—		3f	8
	K$_4$[UO$_2$(O$_2$)(CO$_3$)$_2$](H$_2$O)	P2$_1$/n	6.967	9.216	18.052	—	91.51	—		3f	9
U_1L_3											
Liebigite	Ca$_2$[(UO$_2$)(CO$_3$)$_3$](H$_2$O)$_{11}$	Bba2	16.699	17.557	13.697	—	—	—		3g	10
Schröckingerite	NaCa$_3$[(UO$_2$)(CO$_3$)$_3$](SO$_4$)F(H$_2$O)$_{10}$	P$\bar{1}$	9.634	9.635	14.391	91.41	92.33	120.26		3g	11
Bayleyite	Mg$_2$[(UO$_2$)(CO$_3$)$_3$](H$_2$O)$_{18}$	P2$_1$/a	26.56	15.256	6.505	—	92.90	—		3g	12
Swartzite	CaMg[(UO$_2$)(CO$_3$)$_3$](H$_2$O)$_{12}$	P2$_1$/m	11.080	14.634	6.439	—	99.43	—	A	3g	13
Andersonite	Na$_2$Ca[(UO$_2$)(CO$_3$)$_3$](H$_2$O)$_5$	R$\bar{3}$mH	17.904	17.904	23.753	—	—	120		3g	14
Čejkaite	Na$_4$[(UO$_2$)(CO$_3$)$_3$]	Cc	9.292	16.099	6.444	—	91.40	—		3g	15
Grimselite	K$_3$Na[(UO$_2$)(CO$_3$)$_3$](H$_2$O)	P$\bar{6}$2c	9.302	9.302	8.260	—	—	120	A	3g	16
Albrechts-chraufite	MgCa$_4$F$_2$[(UO$_2$)(CO$_3$)$_3$]$_2$(H$_2$O)$_{17.29}$	P$\bar{1}$	13.569	13.419	11.622	115.82	107.61	92.84		3g	17
	(U(CO$_3$)$_3$(H$_2$O)$_2$)(H$_2$O)$_2$	P$\bar{6}$2c	9.220	9.220	8.196	—	—	120	HT[170]	3g	18
	Rb$_6$Na$_2$[(UO$_2$)(CO$_3$)$_3$]$_2$(H$_2$O)	P$\bar{6}$2c	9.432	9.432	8.359	—	—	120	Ae	3g	19
	(NH$_4$)$_4$[(UO$_2$)(CO$_3$)$_3$]	C2/c	10.679	9.373	12.850	—	96.43	—	HT	3g	20
	K$_4$[(UO$_2$)(CO$_3$)$_3$]	C2/c	10.247	9.202	12.226	—	95.11	—	A	3g	21
	Tl$_4$[(UO$_2$)(CO$_3$)$_3$]	C2/c	10.684	9.309	12.726	—	94.95	—	HT[70]	3g	22
	Cs$_4$[(UO$_2$)(CO$_3$)$_3$]	C2/c	11.513	9.604	12.918	—	93.77	—	A	3g	23
	Cs$_4$[(UO$_2$)(CO$_3$)$_3$](H$_2$O)$_6$	P2$_1$/n	18.723	9.647	11.297	—	96.84	—	Ae	3g	24
	Sr$_2$[(UO$_2$)(CO$_3$)$_3$](H$_2$O)$_8$	P2$_1$/c	11.379	11.446	25.653	—	93.40	—	Ae	3g	25
	Na$_4$[(UO$_2$)(CO$_3$)$_3$]	P$\bar{3}$c1	9.342	9.342	12.824	—	—	120	HT[220]	3g	26
	Ca$_5$[(UO$_2$)(CO$_3$)$_3$]$_2$(NO$_3$)$_2$(H$_2$O)$_{10}$	P2$_1$/n	6.573	16.517	15.195	—	90.49	—	Ae	3g	27
	Ca$_6$[(UO$_2$)(CO$_3$)$_3$]$_2$Cl$_4$(H$_2$O)$_{19}$	P4/mbm	16.744	16.744	8.136	—	—	—	Ae	3g	27
	Ca$_{12}$[(UO$_2$)(CO$_3$)$_3$]$_4$Cl$_8$(H$_2$O)$_{47}$	Fd$\bar{3}$z	27.489	27.489	27.489	—	—	—	Ae	3g	27
	K[(UO$_2$)(NO$_3$)$_3$]	C2/c	13.488	9.584	7.956	—	116.12	—	Ae	3g	28
	K$_2$Ca$_3$[(UO$_2$)(CO$_3$)$_3$]$_2$(H$_2$O)$_6$	Pnnm	17.015	18.048	18.394	—	—	—	A	3g	29
	Na$_{0.79}$Sr$_{1.40}$Mg$_{0.17}$[(UO$_2$)(CO$_3$)$_3$](H$_2$O)$_{4.66}$	Pa$\bar{3}$	20.290	20.290	20.290	—	—	—	Ae	3g	30
	Ca$_{1.5}$Na$_{0.63}$[UO$_2$(CO$_3$)$_3$](H$_2$O)$_{6.38}$	Pnnm	18.150	16.866	18.436	—	—	—	A	3g	31
	Rb[(UO$_2$)(NO$_3$)$_3$]	R$\bar{3}$cH	9.384	9.384	18.899	—	—	120	Ae	3g	32
	Na[(UO$_2$)(NO$_3$)$_3$]	P2$_1$3	10.632	10.632	10.632	—	—	—	Ae	3g	33
	(NH$_4$)[(UO$_2$)(NO$_3$)$_3$]	R$\bar{3}$cH	9.361	9.361	18.883	—	—	120	A	3g	34
	γ-K[UO$_2$(NO$_3$)$_3$]	Pbca	9.256	12.175	15.808	—	—	—	HT[220]	3g	35
U_1L_4											
	Rb$_2$[(UO$_2$)(NO$_3$)$_4$]	P2$_1$/c	6.42	7.82	12.79	—	108.68	—		3h	36
	(NH$_4$)$_2$[(UO$_2$)(NO$_3$)$_4$]	P2$_1$/n	6.408	7.785	12.446	—	101.24	—	HT[60]/Ae	3h	37
	K$_8$[(UO$_2$)(CrO$_4$)$_4$](NO$_3$)$_2$	P$\bar{1}$	7.039	9.734	9.757	105.85	97.99	93.27	Ae	3i	38
	Cs$_8$[(UO$_2$)(MoO$_4$)$_4$]	P$\bar{1}$	11.613	12.545	14.466	102.71	95.28	106.18	SS[850]	3i	39
	Rb$_6$[(UO$_2$)(MoO$_4$)$_4$]	C2/c	17.312	11.529	13.916	—	127.63	—	SS[700]	3i	40
	Na$_2$[(UO$_2$)(IO$_3$)$_4$(H$_2$O)]	C2	11.381	8.055	7.652	—	90.102	—	HT[180]	3j	41
	Na$_6$[(UO$_2$)(SO$_4$)$_4$](H$_2$O)$_2$	P$\bar{1}$	5.550	11.246	14.256	91.48	92.58	97.59	HT[70]/Ae	3k	42
	Na$_{10}$[(UO$_2$)(SO$_4$)$_4$](SO$_4$)$_2$(H$_2$O)$_3$	Cc	9.307	28.706	9.6152	—	93.40	—	HT[70]/Ae	3k	43
	KNa$_3$[(UO$_2$)(SO$_4$)$_4$](H$_2$O)	C2/c	16.917	5.599	35.340	—	90.44	—	HT[70]/Ae	3k	44
Belakovskiite	Na$_7$[(UO$_2$)(SO$_4$)$_4$(SO$_3$OH)](H$_2$O)$_3$	P$\bar{1}$	5.458	11.329	18.416	104.79	90.09	96.77		3l	45
U_1L_5											
	Na$_6$[(UO$_2$)(MoO$_4$)$_4$]	P$\bar{1}$	7.096	9.566	13.415	73.69	86.62	82.94	SS[850]	3m	46
U_1L_{18}											
	K$_6$[(UO$_2$)B$_{16}$O$_{24}$(OH)$_8$](H$_2$O)$_{12}$	P2$_1$/n	12.024	26.45	12.543	—	94.74	—	A	3n	47

TABLE 2 (CONTINUED). U(VI) COMPOUNDS WITH STRUCTURES CONTAINING FINITE CLUSTERS OF POLYHEDRA

MINERAL	FORMULA	SG	a (Å)	b (Å)	c (Å)	α (°)	β (°)	γ (°)	SYN	FIG	REF
$^0[U_2L_x]$ cluster											
U_2L_0											
	[(UO₂)Br₂(OH)₂]₂	$P2_1/c$	6.057	10.512	10.362	—	99.62	—	HT[100]/Ae	3o	48
	[(UO₂)(OH)Cl₂(H₂O)₂]	$P2_1/n$	17.743	6.136	10.725	—	95.52	—	A	3o	49
	[(UO₂)(OH)₂Br₂(H₂O)₄]	$P2_1/c$	9.840	6.320	10.850	—	115.65	—	A	3o	50
	[(UO₂)₂(OH)₂Cl₂(H₂O)₄]	$P2_1/n$	10.712	6.121	17.662	—	95.47	—	HT[60]/Ae	3o	51
	Ni[(UO₂)F₄(H₂O)₇]	$P112_1/b$	10.141	11.901	9.510	—	—	96.80		3o	52
	K₆[(UO₂)(O₂)₂]₂(H₂O)₇	$Pcca$	15.078	6.669	23.526	—	—	—		3np	53
	Na₂Rb₄[(UO₂)₂(O₂)₃](H₂O)₁₄	$Pbcm$	6.808	16.888	23.286	—	—	—		3q	54
U_2L_2											
	[(UO₂)₄(ReO₄)₂O(OH)₄(H₂O)₇](H₂O)₅ [b]	$P\bar{1}$	7.884	11.443	16.976	83.19	89.39	85.29	HT[170]/Ae	3r	55
	[(UO₂)₂(OH)₂(NO₃)₂(H₂O)₃](H₂O)	$P\bar{1}$	8.622	8.628	10.393	109.57	105.56	99.65		3s	56
	Ba₂[(UO₂)₂(HPO₃)₄](H₂O)₅	$P2_1/c$	10.573	16.683	13.343	—	113.27	—	HT[200]	3t	57
U_2L_4											
	K₄[(UO₂)₂(SO₄)₃]	$Pnma$	13.053	23.200	9.379	—	—	—	SS[550]	3u	58
U_2L_6											
	Na[(UO₂)(ReO₄)₃(H₂O)₂]	$C2/m$	12.311	22.651	5.490	—	109.37	—	HT[170]/Ae	3v	55
	Na₃Tl₃[(UO₂)(MoO₄)₄]	$Pbcn$	20.582	7.439	26.251	—	—	—	HT[120]/Ae	3w	59
U_2L_8											
	Na₆[(UO₂)₂(MoO₄)₄]	$P\bar{1}$	7.637	8.164	8.746	72.33	79.36	65.79	SS[850]	3x	46
Bluelizardite	Na₇[(UO₂)(SO₄)₄Cl](H₂O)₂	$C2/c$	21.151	5.347	34.671	—	104.91	—		3x	60
$^0[U_{>2}L_x]$ clusters											
U_3L_0											
	K₂(Mg(H₂O)₆)₄[(UO₂)₃(O₂)₈](H₂O)₂	$P\bar{1}$	6.555	8.287	18.146	95.06	93.36	94.77		3y	62
	[(UO₂)₃O(OH)₃(H₂O)₆](NO₃)(H₂O)₄	$P\bar{1}$	8.026	11.276	12.346	109.65	99.39	88.62	Ae	3z	63
U_3L_1											
	[(UO₂)₄(ReO₄)₂O(OH)₄(H₂O)₇](H₂O)₅ [b]	$P\bar{1}$	7.884	11.443	16.976	83.19	89.39	85.29	HT[170]/Ae	3aa	55
U_4L_0											
	[(UO₂)₄Cl₂O₂(OH)₂(H₂O)₆](H₂O)₄	$P2_1/n$	11.645	10.101	10.206	—	105.77	—	A	3ab	64
	Rb₄[(UO₂)₄O₂Cl₈(H₂O)₂](H₂O)₂	$P2_1/c$	8.540	8.096	21.735	—	111.74	—	A	3ab	65
	K₂[(UO₂)₄Cl₄O₂(OH)₂(H₂O)₄](H₂O)₂	$P\bar{1}$	12.15	12.33	8.026	110.50	96.30	138.71	A	3ab	66

Note: Double lines (=) indicate major differences in the stoichiometry of the structural unit, as indicated by the corresponding header in the table; single lines (–) indicates different topologic configurations; and dotted lines (- -) separate graphical isomers.

[a] Synthesis column data. HT[T] and SS[T] correspond to hydrothermal and solid state synthesis, respectively, at maximum reported temperature T (°C); V-Cl: vapor phase chlorination; A, aqueous (Ae denotes evaporation to dryness); Ac, concentrated acid; Flx, molten flux; SDg, slow diffusion in gel.

[b] Structure contains multiple cluster types.

References: (1) Nazarchuk *et al.* (2011); (2) Krivovichev (2008a); (3) Fischer (2003); (4) Taylor & Mueller (1965); (5) Dalley *et al.* (1971); (6) Hughes & Burns (2003b); (7) Shuvalov & Burns (2003); (8) Zehnder *et al.* (2005); (9) Goff *et al.* (2008); (10) Mereiter (1982b); (11) Mereiter (1986a); (12) Mayer & Mereiter (1986); (13) Mereiter (1986e); (14) Mereiter (1986f); (15) Plášil et al. (2013); (16) Li & Burns (2001a); (17) Mereiter (2013); (18) Juan *et al.* (2010); (19) Kubatko & Burns (2004b); (20) Serezhkin *et al.* (1983); (21) Anderson *et al.* (1980); (22) Mereiter (1986d); (23) Krivovichev & Burns (2004b); (24) Mereiter (1988); (25) Mereiter (1986c); (26) Li *et al.* (2001b); (27) Li & Burns (2002); (28) Krivovichev & Burns (2004a); (29) Kubatko & Burns (2004a); (30) Effenberger & Mereiter (1988); (31) Vochten *et al.* (1994); (32) Zalkin *et al.* (1989); (33) Backer & Mudring (2010); (34) Belomestnykh *et al.* (2011); (35) Jouffret *et al.* (2011); (36) Kapshukov *et al.* (1971); (37) Belomestnykh *et al.* (2011); (38) Krivovichev & Burns (2003g); (39) Krivovichev & Burns (2002b); (40) Krivovichev & Burns (2002a); (41) Bray *et al.* (2006); (42) Hayden & Burns (2002a); (43) Burns & Hayden (2002); (44) Hayden & Burns (2002b); (45) Kampf *et al.* (2014); (46) Krivovichev & Burns (2001a); (47) Behm (1985); (48) Crawford *et al.* (2004); (49) Aberg (1969); (50) Wilson *et al.* (2011); (51) Huys *et al.* (2010); (52) Ivanov *et al.* (1982); (53) Kubatko *et al.* (2007); (54) Kubatko *et al.* (2007); (55) Karimova & Burns (2007); (56) Perrin (1976); (57) Villa *et al.* (2013a); (58) Mikhailov *et al.* (1977); (59) Krivovichev & Burns (2003c); (60) Plášil *et al.* (2014b); (62) Unruh *et al.* (2009). (63) Aberg (1978); (64) Aberg (1976); (65) Perrin (1977); (66) Perrin & Le Marouille (1977).

the uranyl ion. The structure of the compound (H₂O)₂[(UO₂)(SeO₄)(H₂O)₃] contains a graphically isomeric cluster (Fig. 3b); here the ligand polyhedron is of irregular geometry.

The *UL₂*-type cluster shown in Figure 3c in [(UO₂)(ClO₄)₂(H₂O)₃] contains two perchlorate anions that vertex-share with a uranyl pentagonal bipyramid. This compound is the only example of a direct linkage between U⁶⁺ and (ClO₄)⁻, and its synthesis in concentrated perchloric acid suggests that high activities of (ClO₄)⁻ are required to promote the formation of this linkage. Whereas it is generally assumed that
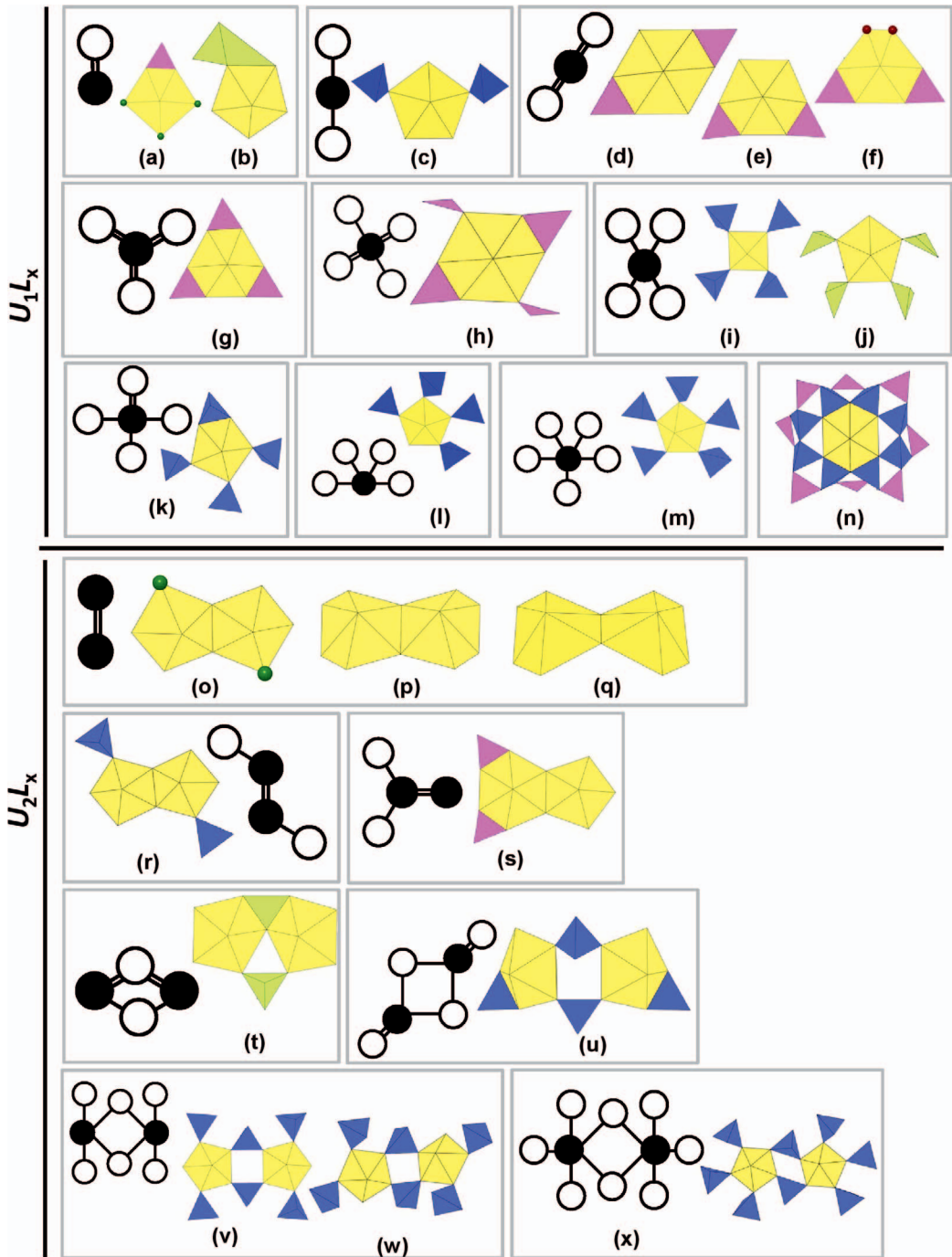
FIG. 3. Finite clusters (graphical and polyhedral representations) of polyhedra observed to occur in the 79 U^{6+} compounds listed in Table 2. As with all following figures, U^{6+} are shown in yellow, and ligand polyhedra are colored according to geometry with $T\Phi_4$ tetrahedra (blue-purple), $D\Phi_3$ triangles (pink), irregular $D\Phi_3E$ tetrahedra (light green), where E corresponds to lone-pair electrons, and regular $M\Phi_6$ octahedra (orange). Green spheres indicate Cl^- anions.

$U_{>2}L_x$

(y)

(z)

(aa)

(ab)
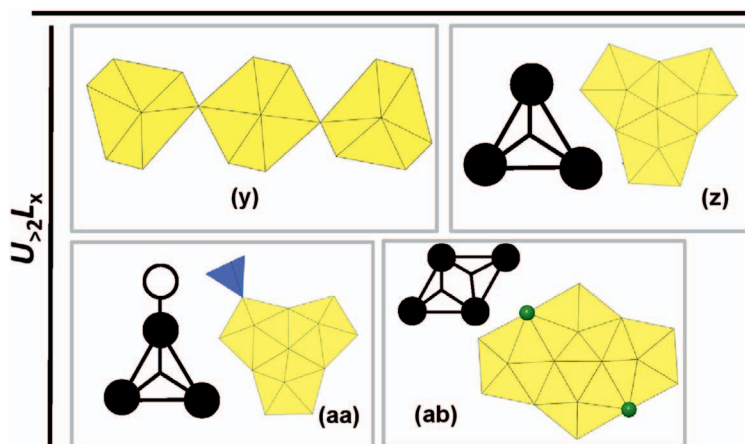
Fɪɢ. 3. Continued.

perchlorate does not coordinate uranyl in aqueous solution, the existence of $[UO_2(ClO_4)_2(H_2O)_3]$ suggests caution with this interpretation, especially at high perchlorate concentrations.

In the structures of four different types of hydrous uranyl nitrates, there are two graphical isomers of UL_2-type clusters with the formula $(UO_2)(NO_3)_2O_2$ (Fig. 3d–e). In both, a central uranyl hexagonal bipyramid shares two equatorial edges with two triangular nitrate polyhedra. In the structure of $[(UO_2)(NO_3)_2(H_2O)_2]$ (H_2O), the decorating NO_3 triangles are located *cis* to each other (Fig. 3e), whereas in $(UO_2)(NO_3)_2(H_2O)_x$ (x = 2, 3, 6), they are in a *trans* configuration (Fig. 3d). Each of the non-bridging equatorial ligands in these clusters is (H_2O). The finite cluster found in the compounds $[K_4[U(CO_3)_2O_2(O_2)](H_2O)_{2.5}$ and $K_4[UO_2(O_2)(CO_3)_2](H_2O)]$ is graphically isomeric with the *cis* UL_2-type. There are two significant differences: (1) (CO_3) triangles substitute for the (NO_3) triangles, and (2) a peroxide molecule (shown as red spheres in Fig. 3f) occurs at the position of the remaining two equatorial anions.

The UL_3-type cluster, with formula $(UO_2)(DO_3)_3$ (Fig. 3g) (where $D = C^{4+}$ or N^{5+}), is, by a significant margin, the most common finite cluster topology observed, occurring in 28 compounds (eight minerals and 20 synthetics). The cluster is always anhydrous, yet the interstitial complex of the structure is often hydrous: 13 of these structures are anhydrous, whereas 15 are hydrous. This is the most common mode for (CO_3) incorporated into the structures of uranyl compounds, occurring in 23 of the 31 total uranyl carbonate phases. Further, of the 11 known uranyl mineral phases containing carbonate, eight are based on these clusters. The analogous tri-nitrate cluster,

$(UO_2)(NO_3)_3$, occurs in only five synthetic compounds.

All synthetic compounds that contain the uranyl triscarbonato cluster formed from aqueous solutions, and minerals containing it dissolve readily in water (*e.g.*, Finch & Murakami 1999). As such, crystals grow due to the prevalence of the $[(UO_2)(CO_3)_3]^{4-}$ complex in the nascent solution. Carbonates are among the most well-characterized of the uranyl complexes, occurring as $(UO_2)(CO_3)_n$ where n = 1, 2, 3. These have been studied by EXAFS, O-17/C-13 NMR, Raman, and IR spectroscopy (Nguyen-Trung *et al*. 1992, Allen *et al*. 1995, Clark *et al*. 1995) and are stable at near-neutral to alkaline pH. The tricarbonates result from evaporative conditions where the pCO_2 is well above atmospheric levels. In contrast, the monocarbonates (rutherfordine, joliotite, blatonite, urancalcarite, and wyartite) appear to precipitate from fresh water with elevated pCO_2 values. In phases where the isolated complex occurs, the solubility is relatively high. Where the carbonate is present in chain or sheet structural units (see below), the compounds are less soluble. Analogous nitrates are also known in synthetic compounds but have received less attention (Nguyen-Trung *et al*. 1992, de Jong *et al*. 2005). These have no mineral analogues, likely owing to their very high solubility (*e.g.*, the uranyl nitrate hexahydrate solubility is 2.5 M).

Ten structures contain U_1L_4-type clusters. The cluster found in the isostructural compounds $X_2[(UO_2)(NO_3)_4]$ (X = Rb, $(NH_4)_2$) (Fig. 3h) bears a topological similarity to that shown in Figure 3d, but it also shares vertices with two additional triangular polyhedra, also in *trans* configuration. The UL_4-type cluster shown in Figure 3i consists of a central uranyl

square bipyramid in which each of the four equatorial vertices are shared with tetrahedral polyhedra. The structures of $K_8[(UO_2)(CrO_4)_4](NO_3)_2$, $Cs_6[(UO_2)(MoO_4)_4]$, and $Rb_6[(UO_2)(MoO_4)_4]$ contain graphically isomeric clusters; however, the structures in which they occur are not isotypic. The structure of $Na_2[(UO_2)(IO_3)_4(H_2O)]$ contains the cluster $(UO_2)(IO_3)_4(H_2O)$ (Fig. 3j), which is the only example of a finite cluster containing polyhedra with a lone-pair stereoactive cation, curiously enough crystallizing in a chiral space-group.

The cluster shown in Figure 3k occurs in the three uranyl sulfates listed in Table 2. Each was grown under relatively low temperature (~70 °C) hydrothermal conditions, indicating that the cluster is sufficiently stable to overcome the electrostatic repulsion expected between the U^{6+} and S^{6+} cations owing to their shared polyhedral edge. This is consistent with work showing the existence of mono- (Neuefeind *et al.* 2004) and bi- (Hennig *et al.* 2007) dentate uranyl sulfate complexes in low-temperature aqueous solutions. Of further interest, Hennig *et al.* (2007) also presented DFT calculations that suggested that mono- and bidentate uranyl sulfate complexes in aqueous solution differ energetically by only ~16 kJ, approaching the limit of the uncertainty of the DFT calculation.

The cluster occurring in belakovskiite, $Na_7[(UO_2)(SO_4)_4(SO_3OH)](H_2O)_3$, is shown in Figure 3l. Here, a central uranyl cation is in pentagonal bipyramidal coordination; four equatorial anions are vertex-sharing with four $(S\Phi_4)$ tetrahedra, with the remaining equatorial anion position occupied by (H_2O).

Only one isolated UL_5 cluster topology is observed, which occurs in $Na_6[(UO_2)(MoO_4)_4]$ (Fig. 3m). It consists of a central uranyl pentagonal bipyramid wherein each equatorial anion is shared with a MoO_4 tetrahedron. The UL_{16} cluster is also unique, occurring only in the complex borate structure of $K_6[(UO_2)(B_{16}O_{24})(OH)_8](H_2O)_{12}$ (Fig. 3n); it is the most highly decorated finite cluster known. The uranyl hexagonal bipyramid is centered in an [8]-membered ring of vertex-sharing borate tetrahedra, four of which are connected to uranyl polyhedra *via* edge sharing. An additional [8]-membered ring of borate triangles links to the borate tetrahedra *via* vertex-sharing; the terminal anions on the BO_3 groups are (OH) groups. Despite its topologic complexity and high degree of connectivity, this structure crystallizes under aqueous conditions at room temperature.

$U_{x>1}L_y$-type finite polyhedral clusters

Isolated finite clusters also occur in which multiple uranyl polyhedra are either bridged by an additional polyhedron or are linked directly *via* the sharing of vertices or edges. Most are dinuclear clusters, with $x = 2$ (15 structures); there are six structures with clusters wherein $x > 2$. The simple clusters are of U_2L_0-type, with two uranyl pentagonal bipyramids linking *via* edge-sharing (Fig. 3o–q, 7 structures). The first four clusters of this type listed in Table 2 contain two halogen ions at non-bridging uranyl polyhedra equatorial positions (one per polyhedron), with the non-halogen equatorial position being occupied by either (H_2O) or (OH). None of these compounds contain interstitial cations, hence the structures are stabilized only by hydrogen bonds emanating from the clusters. The structure of $Ni[(UO_2)F_4(H_2O)_7]$ contains a cluster with the same topology shown in Figure 3o; however, in this structure, two uranyl ions are bridged by two F anions, with the remaining three vertices of each of the uranyl pentagonal bipyramids also occupied by F^-. The peroxide-bearing structures $K_6[(UO_2)(O_2)_2(OH)]_2(H_2O)_7$ and $Na_2Rb_4[(UO_2)_2(O_2)_5](H_2O)_{14}$ both contain topologically similar U_2L_0 clusters of edge-sharing dimers of uranyl peroxide hexagonal bipyramids. In the cluster observed in $K_6[(UO_2)(O_2)_2(OH)]_2(H_2O)_7$ (Fig. 3p), the two uranyl polyhedra are di-peroxide types and are bridged by two (OH) groups. In the cluster observed in $Na_2Rb_4[(UO_2)_2(O_2)_5](H_2O)_{14}$ (Fig. 3q), the two clusters are tri-peroxide types and are bridged by the peroxide ligand.

Of the three uranyl perrhenates currently known, the structures of two are based on finite clusters (the third being an infinite chain structure). The compound $[(UO_2)(ReO_4)_2O(OH_4)(H_2O)_7](H_2O)_5$ (Table 2) contains clusters with two different topologies. One consists of two edge-sharing uranyl pentagonal bipyramids that are decorated by two vertex-sharing tetrahedra (one per cluster; Fig. 3r). The other consists of a trimer of edge-sharing uranyl pentagonal bipyramids with one equatorial anion bridging to a single (ReO_4) tetrahedron (Fig. 3aa).

The unusual cluster in Figure 3s is found only in $[(UO_2)_2(OH)_2(NO_3)_2(H_2O)_3](H_2O)$. This is the only finite cluster that contains uranyl ions in both pentagonal and hexagonal bipyramidal coordinations, linked by a shared edge. Two of the remaining equatorial edges on the hexagonal bipyramid share edges with (NO_3) groups. The two bridging oxygen atoms are (OH) and the remaining three ligands are (H_2O). The structure contains no interstitial cations, and is thus held together solely by hydrogen bonding. The structure of $Ba_2[(UO_2)_2(HPO_3)_4](H_2O)_5$ contains the unique finite cluster shown in Figure 3t. Here, the two uranyl pentagonal bipyramids are linked directly by vertex-sharing. Two irregular polyhedra of hydro-

phosphite (HPO_3) groups further link the polyhedra, (1) *via* vertex-sharing, and (2) *via* edge-sharing.

The finite clusters illustrated in Figure 3u through 3w contain two uranyl pentagonal bipyramids that are linked by two vertex-sharing polyhedra. In Figure 3u, the tetrahedra are (SO_4) groups, and two additional tetrahedra are located at the opposite ends of the uranyl cluster. The (SO_4) tetrahedra are edge sharing with the uranyl polyhedra, and this cluster is found in the anhydrous structure of $K_4[(UO_2)(SO_4)_3]$. In the U_2L_6-type cluster illustrated in Figure 3v, four additional tetrahedra are linked to the uranyl core *via* the sharing of vertices; two equatorial anions (one per bipyramid) are non-bridging. This cluster is found only in the structures of $Na[(UO_2)(ReO_4)_3](H_2O)_2$. A graphical isomer of this cluster, with the non-bridging tetrahedra located at different equatorial anion positions (Fig. 3w) is found in the structure of Na_3Tl_3 $[(UO_2)(MoO_4)_4]$. Attaching two additional vertex-sharing tetrahedra to the non-bridging equatorial anions results in the cluster topology observed in the synthetic compounds $Na_3Tl_3[(UO_2)(MoO_4)_4]$ and $Na_6[(UO_2)(MoO_4)_4]$ as well as bluelizardite, Na_7 $[(UO_2)(SO_4)_4]Cl(H_2O)_2$(Fig. 3x).

Clusters in which x > 2

There are only four cluster topologies in which more than two uranyl polyhedra are directly linked; three have $x = 3$, whereas the fourth has $x = 4$. The U_3L_0-type cluster that occurs in the peroxide-bearing structure of $K_2(Mg(H_2O)_6)_4[(UO_2)_3(O_2)](H_2O)_2$ is illustrated in Figure 3y and consists of a linear, vertex-sharing trimer of uranyl hexagonal peroxide polyhedra. This cluster consists of two uranyl tri-peroxide hexagonal dipyramids (*cf.* 2f) bridged by a central *cis* di-peroxide hexagonal dipyramid (*cf.* 2e). The non-peroxide anions of the central di-peroxo polyhedron link directly to the peroxo-anions of the tri-peroxo polyhedrons at either side. It is noteworthy that this is the only peroxide-bearing compound (extended or caged cluster) to polymerize by vertex-sharing of a peroxide molecule.

The finite clusters shown in (Fig. 3z and 3aa) both consist of trimers of edge-sharing uranyl pentagonal bipyramids; the U_3L_0 cluster in the structure of $[(UO_2)_3O(OH)_3(H_2O)_6](NO_3)(H_2O)_4$ and the U_3L_1 cluster in the structure of $[(UO_2)_4(ReO_4)_2O(OH)_4$ $(H_2O)_7](H_2O)_5$ differ only in the presence of a single vertex-sharing tetrahedral decoration. In both structures the non-bridging equatorial ligands are (H_2O) groups. In the former structure, the (NO_3) triangles are located within the interstitial complex where they are only attached to the cluster *via* hydrogen bonds emanating from it. The only cluster topology in which

$a = 4$ has the stoichiometry $(UO_2)_4\Phi_{10}$ and is shown in Figure 3ab. This cluster is always observed to contain halogen ions. It occurs in the structures of three compounds, $[(UO_2)_4Cl_2O_2(OH_2)(H_2O)_6](H_2O)_4$, $Rb_4[(UO_2)_4O_2Cl_8(H_2O)_2](H_2O)_2$, and $K_2[(UO_2)_4$ $Cl_4O_2(OH)_2(H_2O)_4](H_2O)_2$; curiously, none of these are isostructural. The first is held together by H bonding from the interstitial complexes, whereas the latter two are stabilized by both H bonds and linkages to interstitial cations.

<div align="center">STRUCTURES CONTAINING INFINITE CHAINS
OF URANYL POLYHEDRA</div>

Burns (2005) listed 57 compounds (14 unique chain topologies) containing infinite chains consisting of uranyl polyhedra, whereas there are currently 94 compounds (23 chain topologies) known (Table 3). Burns (2005) noted that the increased number of chain structures since the publication of Burns *et al.* (1996) was largely attributable to research focused on the crystal chemical behavior of ligands based on tetrahedrally coordinated Mo^{6+}, S^{6+}, and Cr^{6+} and lone-pair stereoactive Se^{4+} and I^{5+} cations, all of which seem to promote the formation of infinite chains. With respect to lone-pair stereoactive cations, 43% of uranyl compounds containing these have chain structural units, however 45% have sheets; hence, the structural role of lone-electron-pair stereoactivity remains ambiguous. Below, we separate structures based on the connectivity of uranyl polyhedra. With respect to infinite chains, there are three categories: (1) chains based on the polymerization of only uranyl polyhedra; (2) chains based on the inclusion of bridging ligand polyhedra between uranyl polyhedra; and (3) chains based on the linking of discrete clusters of uranyl polyhedra.

Graphical representation of infinite chains

Similar to the approach taken with respect to finite clusters, the topological complexity of infinite chains can be effectively reduced to its essential elements by a graphical approach. For infinite chains, only a single repeatable unit of the chain is represented, and color distinguishes between bridging (black) and non-bridging ligand polyhedra (red) (Fig. 4).

Chains based on vertex sharing uranium polyhedra

Structures in this category contain chains based on U polyhedra that directly share either a vertex or an edge; these are shown in Figures 4a to 4m. In chains where polyhedral decorations are present (Figs. 4b–c, f, l, m), they are designated as non-bridging, as their removal does not disrupt the connectedness of the

TABLE 3. U(VI) COMPOUNDS WITH STRUCTURES CONTAINING INFINITE CHAINS BASED OF URANIUM POLYHEDRA

MINERAL	FORMULA	SG	a (Å)	b (Å)	c (Å)	α (°)	β (°)	γ (°)	SYN[a]	FIG	REF
Chains based on element-sharing uranyl polyhedral											
	$Na_4[(UO_2)O_3]$	$I4/m$	7.557	7.557	4.641	—	—	—	HT[700]	4a	1
	$Ca_2[(UO_2)O_3]$	$P2_1/c$	7.914	5.441	11.448	—	108.80	—	SS[1000]	4a	2
	$Sr_2[(UO_2)O_3]$	$P2_1/c$	8.104	5.661	11.919	—	108.99	—	SS[1000]	4a	2
	$Li_4[(UO_2)O_3]$	$I4/m$	6.720	6.720	4.450	—	—	—		4a	3
	$Pb_3[(UO_2)O_4]$	$Pnam$	13.719	12.351	8.213	—	—	—	HT[800]	4a	4
	$Na_4[UO_5]$	$I4/m$	7.517	7.517	4.633	—	—	—	SS[750]	4a	5
	$K_2[UO_4]$	$I4/mmm$	4.332	4.332	13.138	—	—	—	SS[750]	4a	6
	$Cs_2[(UO_2)O(MoO_4)]$	$Pca2_1$	12.018	12.438	17.917	—	—	—	SS[870]	4b	7
	$K[(UO_2)(SO_4)(OH)(H_2O)]$	$P2_1/c$	8.052	7.935	11.318	—	107.68	—	HT[150]	4c	8
	$Rb[(UO_2)(SeO_4)(OH)(H_2O)]$	$P2_1/c$	8.273	8.085	11.791	—	107.22	—	HT[100]	4c	9
	$K[(UO_2)(SeO_4)(OH)](H_2O)$	$P2_1/ca$	8.0413	8.0362	11.603	—	106.93	—		4c	76
Adolfpateraite	$K[(UO_2)(SO_4)(OH)(H_2O)]$	$P2_1/c$	8.046	7.926	11.321	—	107.73	—		4c	10
	$[(UO_2)Cl_2(H_2O)]$	$P2_1/m$	5.828	8.534	5.557	—	97.79	—	Flx	4d	11
Moctezumite	$Pb[(UO_2)(Te_2O_3)]$	$P2_1/c$	7.813	7.061	13.775	—	93.71	—		4e	12
	$[(UO_2)(IO_3)_2]$	$P2_1/n$	4.245	16.636	5.284	—	107.57	—	HT[425]	4f	13
Studtite	$[(UO_2)(O_2)(H_2O)_2](H_2O)_4$	$C2/c$	14.068	6.721	8.428	—	123.36	—		4g	14
Metastudtite	$[(UO_2)(O_2)(H_2O)_2](H_2O)_2$	$Immm$	6.51	8.78	4.21	—	—	—		4g	15
	$Ni_3[(UO_2)_2F_{12}(H_2O)_{18}$	$P112_1/b$	9.131	16.925	12.500	—	—	114.62		4h	16
	$Na_3[(UO_2)_2F_7](H_2O)_6$	$P\overline{1}$	6.997	7.176	8.630	77.84	113.30	104.95	SS[1000]/Ae	4h	17
	$Cs_2[(UO_2)_3Cl_2(IO_3)(OH)O_2](H_2O)_2$	$Pnma$	8.272	12.473	17.117	—	—	—	HT[180]	4i	18
	$(Li(H_2O)_2][(UO_2)_2Cl_3O(H_2O)]$	$P\overline{1}$	8.110	8.621	8.739	112.23	96.38	93.67	A	4k	18
	$Cs_{0.9}[(UO_2)OCl_{0.9}]$	$P2_1/m$	8.734	4.118	7.718	—	105.26	—	SS[600]	4k	19
	$Ba[(UO_2)_2(IO_3)_2O_2](H_2O)$	$P2_1/c$	8.062	6.940	21.665	—	98.05	—	HT[180]	4l	20
	$Sr[(UO_2)_2(IO_3)_2O_2](H_2O)$	$P2_1/c$	7.814	6.943	21.434	—	99.32	—	HT[200]	4l	21
	$Pb[(UO_2)_2(IO_3)_2O_2](H_2O)$	$P2_1/c$	7.844	6.933	21.340	—	99.06	—	HT[200]	4l	21
	$Rb_2[(UO_2)_3(IO_3)_4O_2]$	$P\overline{1}$	7.083	7.894	9.092	91.74	105.11	92.21	HT[200]	4m	21
	$Tl_2[(UO_2)_3(IO_3)_4O_2]$	$P\overline{1}$	7.060	7.948	9.018	91.87	105.59	91.578	HT[200]	4m	21
	$K_2[(UO_2)_3(IO_3)_4O_2]$	$P\overline{1}$	7.037	7.773	8.985	93.39	105.67	91.34	HT[425]	4m	20
Chains containing essential bridging ligands											
U_1L_{2+z}– *type chains*											
Walpurgite	$Bi_4O_4[(UO_2)(AsO_4)_2](H_2O)_2$	$P\overline{1}$	7.135	10.426	5.494	101.47	110.82	88.20		4n	22
Orthowalpurgite	$Bi_4O_4[(UO_2)(AsO_4)_2](H_2O)_2$	$Pbcm$	5.492	13.324	20.685	—	—	—		4n	23
Deloryite	$Cu_4[(UO_2)(MoO_4)_2](OH)_6$	$C2/m$	19.940	6.116	5.520	—	104.18	—		4n	24
	$Cu_4[(UO_2)(MoO_4)_2](OH)_6$	$B2/m$	19.839	5.511	6.101	—	—	104.48		4n	25
	$Cu_2[UO_2(PO_4)_2]$	$C2/m$	14.040	5.759	5.028	—	107.24	—	SS[1150]	4n	26
	$Li_2[(UO_2)(MoO_4)_2]$	$P\overline{1}$	5.346	5.829	8.265	108.27	100.57	104.12	SS[650]	4n	27
Derriksite	$Cu_4[(UO_2)(SeO_3)_2](OH)_6$	$Pn2_1m$	5.570	19.088	5.965	—	—	—	—	4o	28
	$Sr_3[(UO_2)(TeO_3)_2](TeO_3)_2$	$C2/c$	20.540	5.655	13.101	—	94.42	—	HT[180]	4o	29
	$\beta-Tl_2[(UO_2)(TeO_3)_2]$	$P2_1/n$	5.477	8.235	20.849	—	92.33	—	HT[210]	4o	29
	$[UF_2O_2(SbF_5)_3]$	$P2_1/n$	11.040	12.438	12.147	—	111.16	—	Ac	4p	30
	$Mn[(UO_2)(SO_4)_2(H_2O)](H_2O)_4$	$P2_1$	6.506	11.368	8.338	—	90.79	—		4q	31
Svornostite	$K_2Mg[(UO_2)(SO_4)_2]_2(H_2O)_8$	$Pmn2_1$	12.785	8.268	11.216	—	—	—		4q	32
	$K_2[(UO_2)(SO_4)_2(H_2O)](H_2O)$	$Cmca$	12.171	16.689	10.997	—	—	—	A	4q	33
	$(UO_2)(H_2PO_2)_2(H_2O)$	$P2_1/n$	7.686	9.275	11.027	—	92.32	—	A/Ac	4q	34
	$[(UO_2)(H_2PO_4)_2(H_2O)](H_2O)_2$	$P2_1/c$	10.816	13.896	7.481	—	105.65	—	HT[80]	4q	35
	$(UO_2)(H_2AsO_4)_2(H_2O)$	$C2/c$	13.164	8.862	9.050	—	124.41	—	Ac	4q	36
	$Mg[(UO_2)(SeO_4)_2(H_2O)](H_2O)_4$	$P2_1/c$	8.467	11.631	13.167	—	90.96	—	Ae	4q	37
	$Zn[(UO_2)(SeO_4)_2(H_2O)](H_2O)_4$	$P2_1/c$	8.449	11.586	13.240	—	92.38	—	Ae	4q	37
	$(H_3O)_6 [(UO_2)_5(SeO_4)_8(H_2O)_5](H_2O)_5$	$P2_1/n$	13.835	13.437	14.310	—	108.00	—	Ae	4q	38
	$Co[(UO_2)(SO_4)_2(H_2O)]_5$	$Pmc2_1$	6.452	8.295	11.288	—	—	—	Ae	4q	39
Demesmaekerite	$Pb_2Cu_5[(UO_2)(SeO_3)_3]_2(OH)_6(H_2O)_2$	$P\overline{1}$	11.955	10.039	5.639	89.78	100.36	91.34		4r	40
	$[UO_2(HSeO_3)_2(H_2O)]$	$C2/c$	9.924	12.546	6.324	—	98.09	—	HT[77]	4r	41
	$[(UO_2)(HSeO_3)_2(H_2O)]$	$A2/a$	6.354	12.578	9.972	—	82.35	—		4r	42
	$Na_4[(UO_2)(CrO_4)_3]$	$P\overline{1}$	7.155	8.442	11.510	80.20	79.31	70.42	SS[300]	4s	43
	$K_6[(UO_2)(CrO_4)_3](NO_3)(H_2O)_3$	$P2_12_12_1$	6.111	12.136	27.464	—	—	—	Ae	4s	44
	$Na_3Tl_5[(UO_2)(MoO_4)_3]_2(H_2O)_3$	$P2_12_12_1$	10.766	11.962	12.899	—	—	—	HT[180]	4s	45
	$Na_{12.9}Tl_{3.1}[(UO_2)(MoO_4)_3]_4(H_2O)_{6.6}$	$P2/c$	19.794	7.191	22.884	—	97.83	—	HT[120]	4s	45
Meisserite	$Na_5[(UO_2)(SO_4)_3(SO_3OH)](H_2O)$	$P\overline{1}$	5.323	11.511	13.556	102.86	97.41	91.46		4s	46

TABLE 3 (CONTINUED). U(VI) COMPOUNDS WITH STRUCTURES CONTAINING INFINITE CHAINS BASED OF URANIUM POLYHEDRA

MINERAL	FORMULA	SG	a (Å)	b (Å)	c (Å)	α (°)	β (°)	γ (°)	SYN[a]	FIG	REF
U_2L_{2+z}-type clusters											
	$[(UO_2)(SO_4)](H_2O)_{2.5}$	$P2_1/c$	6.726	12.421	16.827	—	90.78	—	A	4t	47
	$[(UO_2)(SO_4)(H_2O)_2](H_2O)_{0.5}$	$P2_1/a$	16.887	12.492	6.735	—	90.88	—		4t	48
	$[(UO_2)(SO_4)(H_2O)_2]_2(H_2O)_3$	$P2_1ca$	11.227	6.790	21.186	—	—	—	Ae	4t	49
	$[(UO_2)(CrO_4)(H_2O)_2]_4(H_2O)_9$	$P2_1/c$	31.397	7.170	16.248	—	97.52	—	HT[120]	4t	50
	$[(UO_2)(CrO_4)](H_2O)_{5.5}$	$P2_1/c$	11.179	7.119	26.49	—	94.19	—		4t	51
	$[(UO_2)(CrO_4)(H_2O)_2](H_2O)$	$P2_1$	9.721	7.162	11.091	—	92.39	—	Ae	4t	50
	$[(UO_2)(SeO_4)(H_2O)_2](H_2O)_2$	$C2/c$	14.653	10.799	12.664	—	119.95	—		4t	52
	$[(UO_2)(SeO_4)](D_2O)_{1.65}(H_2O)_{0.35}$	$P2_1/c$	6.974	8.289	11.664	—	92.32	—	HT[100]	4t	53
	$[(UO_2)(SO_4)(H_2O)_2](H_2O)_{1.5}$	$C2/c$	13.70	10.79	11.91	—	110.8	—	A	4t	54
	$[(UO_2)(CrO_4)(H_2O)_2]$	$C2/m$	16.786	22.731	6.997	—	90.05	—	Ae	4t	50
U_2L_{4+z}-type structures											
	$K_3[(UO_2)_2(IO_3)_6](IO_3)(H_2O)$	$P\bar{1}$	7.061	14.569	14.705	119.55	95.27	93.21	HT[180]	4u	55
	$Rb[(UO_2)(CrO_4)(IO_3)(H_2O)]$	$P\bar{1}$	7.313	8.056	8.487	88.74	87.08	71.67	HT[180]	4v	56
	$Rb_2[(UO_2)(CrO_4)(IO_3)_2]$	$P2_1/c$	11.346	7.326	15.933	—	108.17	—	HT[180]	4w	56
	$Cs_2[(UO_2)(CrO_4)(IO_3)_2]$	$P2_1/n$	7.393	8.135	22.126	—	90.65	—	HT[180]	4w	57
	$K_2[(UO_2)(MoO_4)(IO_3)_2]$	$P2_1/c$	11.372	7.290	15.712	—	108.17	—			58
	$K_2[(UO_2)(CrO_4)(IO_3)_2]$	$P2_1/c$	11.134	7.288	15.566	—	107.98	—	HT[180]	4w	56
	$(UO_2)_2(ReO_4)_4(H_2O)_3$	$P\bar{1}$	5.277	13.100	15.476	107.18	99.13	94.11	Ae	4x	59
	$Ba_4[(UO_2)_2(As_2O_7)_3]$	$Pbc2_1$	5.601	13.344	31.751	—	—	—	SS[850]	4y	60
Chains containing clusters of element-sharing uranyl polyhedral											
Chains of $^{[L]}[(U_2L_0)L_2]$-type clusters											
	$K_6[(UO_2)_2O(MoO_4)_4]$	$P\bar{1}$	7.828	7.829	10.302	83.89	73.13	80.34	SS[850]	4z	61
	$Rb_6[(UO_2)_2O(MoO_4)_4]$	$P\bar{1}$	10.157	10.182	13.113	76.92	76.55	65.24	SS[700]	4z	62
	$Rb_6[(UO_2)_2O(WO_4)_4]$	$P\bar{1}$	10.188	13.110	18.822	97.86	96.57	103.89	SS[920]	4aa	63
	$Cs_6[(UO_2)_2(MoO_4)_3(MoO_5)]$	$P\bar{1}$	10.428	15.075	17.806	70.72	80.38	86.39	SS[950]	4aa	64
Chains of $^{[L]}[(U_2L_0)L_2]$-type cluster											
	$K_2[(UF_2O_2)(SO_4)]H_2O$	$P2_1/c$	9.263	8.672	11.019	—	101.60	—	Ae	4ab	65
	$Rb_2[(UO_2)(CrO_4)_2]$	$P\bar{1}$	8.052	10.362	13.707	102.93	106.89	94.55	HT[270]	4ac	66
	$Cs_2[(UO_2)(CrO_4)_2]$	$P\bar{1}$	7.829	8.588	9.796	74.73	71.58	74.18	HT[270]	4ac	66
Lakebogaite	$CaNa(Fe^{3+})_2[H(UO_2)_2(PO_4)_4(OH)_2](H_2O)_8$	Cc	19.644	7.096	18.703	—	115.69	—		4ac	67
	$Cs[(UO_2)Ga(PO_4)_2]$	$P\bar{1}$	7.777	8.504	8.912	66.64	70.56	84.00	HT[180]	4ac	68
	$Sr[(UO_2)(HPO_3)_2](H_2O)_2$	$P\bar{1}$	7.746	8.651	8.723	98.81	108.52	110.15	HT[200]	4ac	69
	$Na_3(H_3O)[(UO_2)(SeO_3)]_2(H_2O)$	$P\bar{1}$	9.543	9.602	11.742	66.69	84.10	63.69	HT[110]	4ad	70
	$Sr[(UO_2)(SeO_3)_2](H_2O)_2$	$P\bar{1}$	7.055	7.466	10.048	106.99	108.03	98.88	HT[180]	4ad	71
	$Sr[(UO_2)(HPO_3)_2](H_2O)_2$	$P\bar{1}$	7.746	8.651	8.723	98.81	108.52	110.15	HT[200]	4ad	69
Chains of $^{[T]}[(U_2L_2)L_2]$-type clusters											
	$Ca[(UO_2)(SeO_3)_2]$	$P\bar{1}$	5.550	6.642	11.013	104.06	93.34	110.59	HT[180]	4ae	71
	$Sr[(UO_2)(SeO_3)_2]$	$P\bar{1}$	5.672	6.763	11.262	104.69	93.71	109.49	HT[425]	4ae	72
Parsonite	$Pb_2[(UO_2)(PO_4)_2]$	$P\bar{1}$	6.842	10.383	6.670	101.27	98.17	86.38		4af	73
Hallimondite	$Pb_2[(UO_2)(AsO_4)_2](H_2O)_n$	$P\bar{1}$	7.115	10.478	6.857	101.18	95.71	86.65		4af	74
Chains of clusters uranyl polyhedra (U > 2)											
	$Rb_8[(UO_2)_4(WO_4)_4(WO_5)_2]$	$P2_1/n$	11.098	13.161	25.017	—	90.03	—	SS[920]	4ag	63
	$Cs_8[(UO_2)_4(WO_4)_4(WO_5)_2]$	$P2_1/n$	11.252	13.815	25.736	—	89.99	—	SS[920]	4ag	63
Uranopilite	$[(UO_2)_6(SO_4)O_2(OH)_6(H_2O)_6](H_2O)_8$	$P\bar{1}$	8.896	14.029	14.339	96.61	98.47	99.80		4ah	75

Note: Double lines (=) indicate major differences in the stoichiometry of the structural unit, as indicated by the corresponding header in the table; single lines (–) indicates different topologic configurations; and dotted lines (- -) separate graphical isomers.

[a] Synthesis column data. HT[T] and SS[T] correspond to hydrothermal and solid state synthesis, respectively, at maximum reported temperature T (°C); V-Cl: vapor phase chlorination; A, aqueous (Ae denotes evaporation to dryness); Ac, concentrated acid; Flx, molten flux; SDg, slow diffusion in gel.

References: (1) Wolf & Hoppe (1986); (2) Loopstra & Rietveld (1969); (3) Kovba (1972); (4) Sterns *et al.* (1986); (5) Roof *et al.* (2010a); (6) Roof *et al.* (2010a); (7) Alekseev *et al.* (2007a); (8) Forbes *et al.* (2007); (9) Shishkina *et al.* (2001); (10) Plášil *et al.* (2012b); (11) Taylor & Wilson (1974); (12) Swihart *et al.* (1993); (13) Bean *et al.* (2001b); (14) Burns & Hughes (2003); (15) Deliens & Piret (1983); (16) Ivanov *et al.* (1981); (17) Nguyen *et al.* (1981); (18) Bean *et al.* (2002); (19) Allpress & Wadsley (1964); (20) Bean *et al.* (2001c); (21) Bean & Albrecht-Schmitt (2001); (22) Mereiter (1982c); (23) Krause *et al.* (1995); (24) Pushcharovsky *et al.* (1996); (25) Tali *et al.* (1993); (26) Guesdon *et al.* (2002); (27) Krivovichev & Burns (2003h); (28) Ginderow & Cesbron (1983b); (29) Almond & Albrecht-Schmitt (2002a); (30) Fawcett *et al.* (1982); (31) Tabachenko *et al.* (1979); (32) Plášil *et al.* (2015); (33) Ling *et al.* (2010b); (34) Tanner & Mak (1999); (35) Mercier *et al.* (1985); (36) Gesing & Ruscher (2000); (37) Krivovichev & Kahlenberg (2005c); (38) Krivovichev & Kahlenberg (2005a); (39) Alekseev *et al.* (2005a); (40) Ginderow & Cesbron (1983a); (41) Koskenlinna *et al.* (1997); (42) Mistryukov & Mikhailov (1983); (43) Krivovichev & Burns (2003e); (44) Krivovichev &

TABLE 3. (CONTINUED).

Burns (2003g); (45) Krivovichev & Burns (2003c); (46) Plášil *et al.* (2013d); (47) Vlček *et al.* (2009); (48) van der Putten & Loopstra (1974); (49) Zalkin *et al.* (1978); (50) Krivovichev & Burns (2003f); (51) Serezhkin & Trunov (1981); (52) Serezhkin *et al.* (1981b); (53) Marukhnov *et al.* (2008b); (54) Brandenburg & Loopstra (1973); (55) Sykora *et al.* (2004a); (56) Sykora *et al.* (2002a); (57) Sykora *et al.* (2002b); (58) Sykora *et al.* (2002a); (59) Karimova & Burns (2007); (60) Alekseev *et al.* (2011); (61) Krivovichev & Burns (2001a); (62) Krivovichev & Burns (2002a); (63) Alekseev *et al.* (2006a); (64) Yagoubi *et al.* (2011); (65) Alcock *et al.* (1980); (66) Siidra *et al.* (2012b); (67) Mills *et al.* (2008); (68) Shvareva *et al.* (2005c); (69) Villa *et al.* (2013a); (70) Serezhkina *et al.* (2009); (71) Almond *et al.* (2002b); (72) Almond & Albrecht-Schmitt (2004); (73) Burns (2000); (74) Locock *et al.* (2005a); (75) Burns (2001b); (76) Gurzhiy *et al.* (2009).

corresponding chain. Figures 4a through 4c contain chains based on corner-sharing uranium polyhedra. The basic undecorated $[UO_5]$ chain, formed where octahedrally coordinated U^{6+} cations are successively linked by *trans* anions of the octahedron (Fig. 4a), occurs in seven structures listed in Table 3. In each of these, the U^{6+} cation occurs in relatively undistorted octahedra, in which bond lengths range from ~2.0 Å to 2.2 Å (mean ~2.1 Å); short bonds associated with the linear uranyl ion are absent. The structure of $Cs_2[(UO_2)O(MoO_4)]$ (Fig. 4b) also consists of the basic corner-sharing $[UO_5]$ chain; however, in this instance the linking vertices are in a *cis* arrangement to the centrally coordinated U^{6+} atom. This chain contains non-structural decorating polyhedra (MoO_4^{2-}) that link every third polyhedron in the chain, and it has a bond-length distribution consisting of two short (~1.8 Å) bonds located on directly opposite sides of the U^{6+} cation and four long (~2.3– 2.4 Å) bonds, typical of the uranyl ion.

The mineral adolfpateraite, $K[(UO_2)(SO_4)(OH)]$ (H_2O), as well as the isostructural compounds $X[(UO_2)(SO_4)(OH)(H_2O)]$ ($X = K$, Rb) contains the only well-characterized isolated chain of corner-sharing uranyl pentagonal bipyramids (Fig. 4c). Here (SO_4) anions link adjacent uranyl polyhedra, resulting in a zigzagged kink in the chain. The bridging anion is (OH) and the remaining equatorial ligands, not bonded to another element of the chain, are (H_2O). Figures 4d through 4g show chains based on a single-width of edge-sharing uranyl polyhedra. The structures of $[(UO_2)Cl_2(H_2O)]$ (Fig. 4d) and moctezumite, $Pb[(UO_2)O_3(Te_2O_3)]$ (Fig. 4e), each contain edge-sharing uranyl pentagonal bipyramids. In $[(UO_2)Cl_2$ $(H_2O)]$, uranyl polyhedra are bridged by $^{[2]}Cl^-$ ions. The chain is hydrous, with (H_2O) groups at the non-bridging equatorial position. The chain is electro-neutral and the structure is stabilized by H-bonds emanating from the equatorial (H_2O) groups and linking to the Cl anions on an adjacent chain. In moctezumite, one of the few anhydrous uranyl minerals, each pentagonal bipyramid in the chain is

decorated by edge-sharing $[Te^{4+}O_4]$ and corner-sharing $[Te^{4+}O_3]$ oxyanions, forming the structural unit $[(UO_2)O_3(Te_2O_3)]^{2-}$. The moctezumite chains are arranged to form pseudo-sheets that are held together by [6]-coordinate Pb^{2+} in the interstitial complex that weakly bond to the –yl oxygen atoms and the oxygen atoms of the Te^{4+} polyoxoanions.

The chain illustrated in Figure 4f occurs in the structure of $[UO_2(IO_3)_2]$ and consists of edge-sharing uranyl hexagonal bipyramids. Lone-pair stereoactive $(IO_3)^-$ groups decorate two of the equatorial edges (in *trans* configuration; *cf.* 3d) of each bipyramid. The structure is anhydrous and contains no interstitial complex; it is stabilized only by weak electrostatic interactions occurring between the I^{5+} ion and the yl O^{2-} of the adjacent chain.

Studtite, $[(UO_2)(O_2)(H_2O)_2](H_2O)_4$, and its less-hydrated form metastudtite, $[(UO_2)(O_2)(H_2O)_2]$ $(H_2O)_2$, are the only minerals known to contain the peroxide $(O_2)^{2-}$ anion. The structures of both are based on infinite chains of edge-sharing uranyl hexagonal bipyramids that are bridged by the peroxide group (Fig. 4g). The chain is hydrous and electroneutral, with two equatorial (H_2O) groups on each uranyl polyhedron. H bonds emanating from the chains that link to interstitial (H_2O) groups stabilize the structure. When viewed parallel to the (O=O) axes, a distinct kinking of the chain is observed with a $U–O_2–U$ dihedral angle of ~126°. This feature, a characteristic of the uranyl peroxo-system, has been exploited to develop a novel class of compounds, uranyl peroxo cage clusters (Burns 2011, Qiu & Burns 2013), where the curvature induced by the O_2 ligand ultimately forms spherical cage clusters with diameters ranging from ~1.4 to ~3 nm. Further, a considerable amount of work has been done to develop a more extensive catalogue of extended structures wherein the uranyl ion is coordinated by the peroxide ligand (Kubatko & Burns 2006a, Kubatko *et al.* 2007) (see below). The peroxide in studtite and metastudtite results from the alpha-radiolysis of water in uranium-rich geochemical environments (Kubatko *et al.* 2003).

The compounds $Ni(H_2O)_6[(UO_2)_2F_7)_2]$ and $Na_3(H_2O)_6[(UO_2)_2F_7]$ contain the chain shown in Figure 4h, which is the only single-width chain that contains uranyl polyhedra linked by both edge- and corner-sharing. The chain is anhydrous, with all equatorial positions of the uranyl bipyramids corresponding to F^- anions. In the structure of $Ni(H_2O)_6[(UO_2)_2F_7)_2]$, H bonds emanating from the (H_2O) of the $Ni(H_2O)_6$ interstitial complex link to the structural unit. In contrast, in the structure of $Na_3(H_2O)_6[(UO_2)_2F_7]$, the chain is directly bonded to Na in the interstitial complex, with additional stabilizing H bonding from (H_2O) groups bonded to the Na.

The chains in the structures of $Cs_2[(UO_2)_3Cl_2(IO_3)(OH)O_2)](H_2O)_2$ (Fig. 4i), $(Li(H_2O)_2)[(UO_2)_2Cl_3O(H_2O)]$ (Fig. 4j), and $Cs_{0.9}(UO_2)OCl_{0.9}$ (Fig. 4k) are all greater than one uranyl polyhedron wide and the equatorial ligands are dominated by chlorine. Each chain consists of somewhat irregularly shaped uranyl pentagonal bipyramids that link together predominantly *via* edge-sharing. The adjacency of the two large Cl^- anions (radii ~ 1.8 Å; Shannon 1976) appears to possibly facilitate the observed distortion of the uranyl polyhedra.

The two similar chains shown in Figures 4l and 4m occur in the closely related compounds $X[(UO_2)_2(IO_3)_2O_2](H_2O)$ (X = Ba, Sr, and Pb) and $X_2[(UO_2)_3(IO_3)_4O_2]$ (X = Rb, Tl, K). Both chains are anhydrous and contain fragments of more complex uranyl oxyhydrate sheets. For example, these chains are fragments of extended sheet topologies found in structures based on the sayarite topology and β-U_3O_8-type sheets, receptively. It is noteworthy that this chain is only known to exist with two electron lone-pair stereochemically active (IO_3) decorations, suggesting that the lone-pair configuration may limit polymerization in the second dimension.

Chains containing bridging ligand polyhedra

All chains present in this category contain bridging ligand polyhedra. As such, these ligand polyhedra contribute directly to the structure of the chain – if these were to be removed, the chains would no longer be infinite. Similar to the approach taken for the organization of finite clusters, we distinguish between groups of chains based on the U_xL_{y+z} form of the smallest repeat unit, where the subscript $y + z$ distinguishes the number of bridging and non-bridging ligand polyhedra, respectively.

The U_1L_{2+z}-type chain and its structures

The topologically simplest chain that contains uranyl polyhedra bridged through other ligand polyhedra is the U_1L_{2+z} chain. In this chain type, the uranyl ion is either in square (Figs. 4n–o) or pentagonal (Figs. 4p–s) bipyramidal coordination. In the former, each equatorial anion is linked to a bridging polyhedron and $z = 0$; whereas, in the latter, one of the five equatorial anions does not link to a bridging polyhedron and may link to a non-chain-forming ligand ($z = 0$ and 1). In these types, ligands can be regular tetrahedra (*e.g.*, AsO_4, MoO_4, SeO_4) or irregular, lone-electron-pair-bearing (SeO_3). The structure of the compound $[UF_2O_2(SbF_5)_3]$ contains the unique UL_2 chain type illustrated in Figure 4p. Here, all anion positions (except those in the $-yl$ positions) are occupied by F^-, and the ligand polyhedra are regular-shared SbF_6 octahedra.

The U_1L_{2+z} chain occurs in 28 known structures (including five minerals), none of which are isostructural. A greater number of phases are known to contain the pentagonal (19 compounds) than the square (nine compounds) bipyramids. Chains of this type are sufficiently versatile to allow their incorporation into crystals with diverse structures and compositions. We speculate that some of the stability of these chain types results from: (1) the low degree of cation-cation repulsion that would originate from an edge-sharing connectivity; (2) the lack of steric constraints imposed on the ligand polyhedra – either tetrahedra, triangles, or modified electron lone-pair stereoactive tetrahedra are possible; and (3) the ability of cations with various formal valences to satisfy the local bond valence requirements of the bridging anion. For instance, the bonding configuration at the bridging oxygen is $^{[X]}U^{6+}$ $-\Phi = {}^{[Y]}M^{b+}$, where X is either 6 or 7. As discussed above, the bond valence contribution to Φ from U^{6+} is either 0.44 (X = 6) or 0.53 *vu* (X = 7) and from *M* can be approximated as b/Y. Commonly observed b/Y values are 1.25 (for $As^{5+}O_4$ and $P^{5+}O_4$), 1.50 *vu* (for $S^{6+}O_4$ and $Mo^{6+}O_4$), and $4/3 = 1.33$ *vu* (for $Se^{4+}O_3$). Where X = 6, the incident bond valence sums are 1.69, 1.94, and 1.77 *vu*, respectively; where X = 7, they are 1.78, 2.03, and 1.86 *vu*, respectively. Two of these configurations, $^{[4]}S–O–^{[6]}U$ and $^{[4]}S–O–^{[7]}U$, result in bond valence sums that are sufficiently close to 2.0 (required for the most common case where $\Phi = O^{2-}$) that a stable configuration exists. The other configurations are sufficiently close to 2.0 that modest reductions in bond lengths or donation of incident bond valence from cations (or H bonds) in the interstitial complex results in stable configurations. Examples of each of these compositions are listed in Table 3. Further, Figure 4n (inset) illustrates that the U_1L_{2+z} chain can either adopt a configuration wherein an approximate mirror plane bisects the chains, or a [2]-fold axis extends along its axis. The UL_2 chain may also twist in a helical fashion, as is observed in the structure of $Na_{13-x}Tl_{3x}[(UO_2)(MoO_4)_3]_4(H_2O)_{6-x}$.
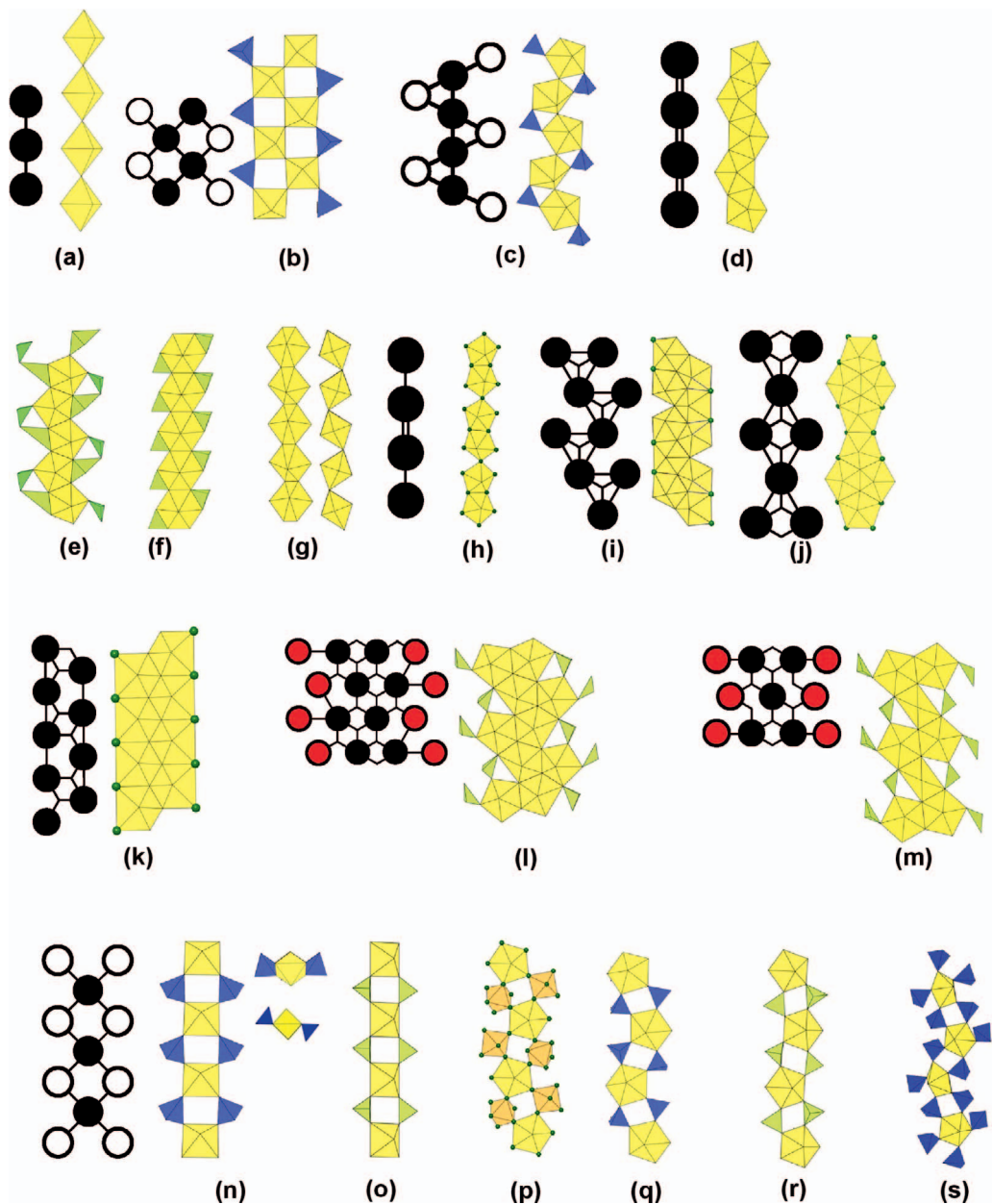
FIG. 4. Infinite chains (graphical and polyhedral representations) consisting of polyhedra of uranium and other high-valence cations that occur in the 97 compounds listed in Table 3.

The U_2L_2 chain and its structures

The U_2L_2 chain, shown in Figure 4t, is the second most common chain topology amongst all the structures listed in Table 3, occurring in 10 structures in which bridging ligands are all tetrahedra and the uranyl ion is always in pentagonal bipyramidal coordination. This chain is not observed to contain decorating tetrahedra, but it often contains (H_2O) at equatorial positions of the uranyl polyhedra. In contrast to the U_1L_x chains, the U_2L_2 chains contain tetrahedra that bridge three individual uranyl pentagonal bipyramids. The compositional variability observed in the U_2L_2 chains (Table 3) shows that
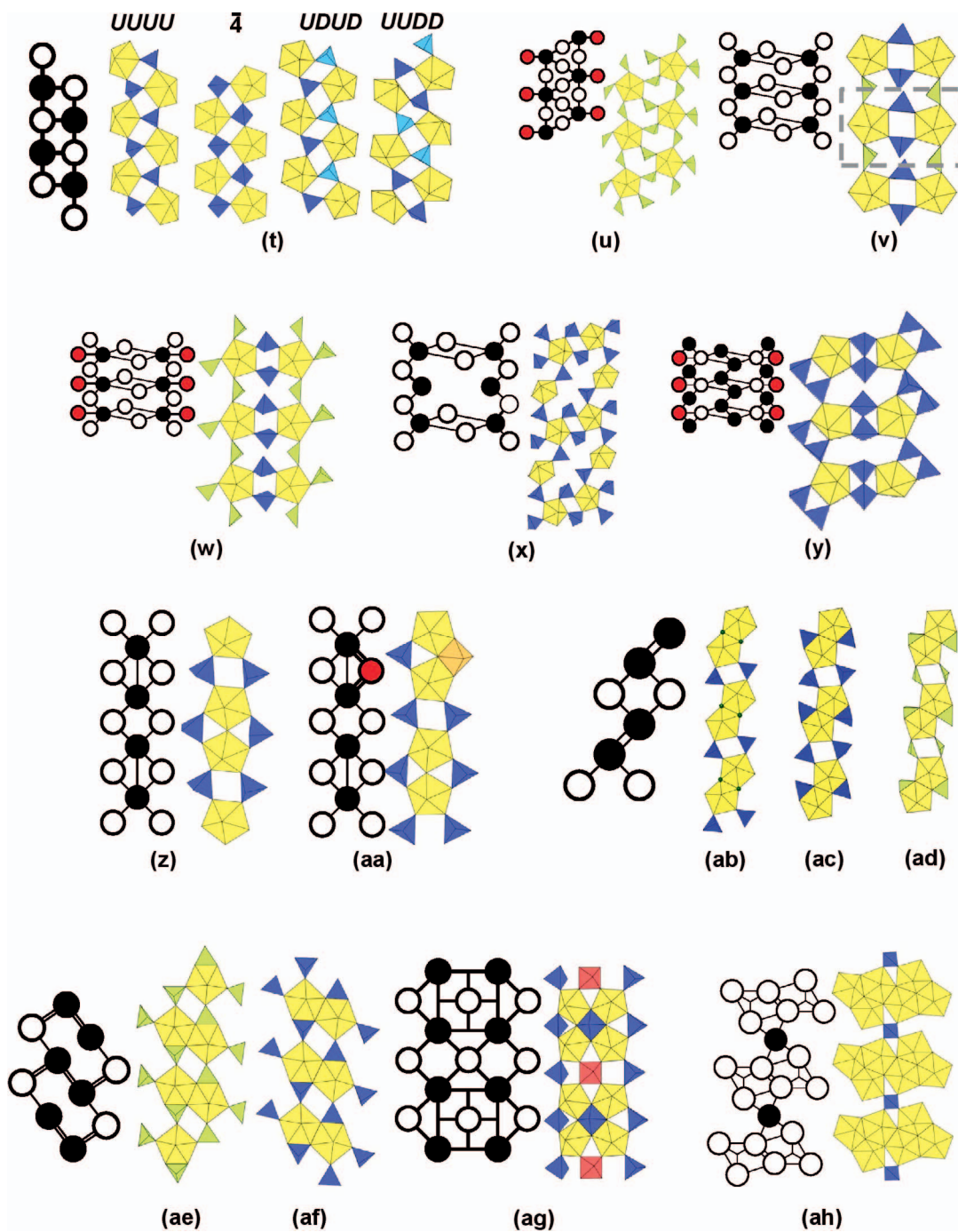
F<small>IG</small>. 4. Continued.

they are also relatively free from steric and compositional constraints and can accommodate a wide range of geometries and compositions. It is noteworthy that in all U_2L_2 chain-type structures, the interstitial complexes are devoid of cations, and hence each of these structures is stabilized by H bonds. In all the U_2L_2 structures, H bonds emanate from both the structural unit and the interstitial complex; however, in the structure of $[(UO_2)(SO_4)]$ $(H_2O)_{2.5}$, the only H present is as (H_2O) in the interstitial complex.

Four conformational variants of the U_2L_2 chains are observed in the corresponding compounds listed in Table 3; these are illustrated (in the order discussed below) in Figure 4t. The first type occurs in the structures of $[(UO_2)(SO_4)(H_2O)_{2.5}]$, $[(UO_2)(SO_4)(H_2O)_2](H_2O)_{0.5}$, $[(UO_2)(SO_4)(H_2O)_2]_2(H_2O)_3$, $[(UO_2)(CrO_4)(H_2O)_2]$, and $[(UO_2)(CrO_4)(H_2O)_2]_4$ $(H_2O)_9$ and in it the apical anions of successive ligand tetrahedra point directly out of the plane of projection (i.e., in the same direction). Hence, a (pseudo) glide plane runs along the chains axis and is related to the orientations of the tetrahedral ligands. In the second chain type, which occurs in the structures of $[(UO_2)(CrO_4)(H_2O_2](H_2O)$, $[(UO_2)(CrO_4)(H_2O)_2]_4$ $(H_2O)_9$, $[(UO_2)(CrO_4)(H_2O)_2](H_2O)_{5.5}$, $[(UO_2)(CrO_4)(H_2O)_2](H_2O)$, and $[(UO_2)(CrO_4)(H_2O)_2]_4(H_2O)_2$, the tetrahedra are oriented such that their $\bar{4}$ axes are all perpendicular to the plane of the projection. In the third chain type, which occurs only in the structure of $[(UO_2)(SeO_4)][(D_2O)_{1.65}(H_2O)_{0.35}]$, the apical anions of successive tetrahedra alternate in orientation (denoted $UDUDUD$ in Figure 4t). In the second and third chain type, a (pseudo) [2]-fold screw axis operates along the chain axis (with the repeat distance corresponding to the distance between every third uranium atom). Note that these structures differ only by the (H_2O) content of the interstitial complexes. The fourth chain occurs in the structure of $[(UO_2)(SO_4)(H_2O)_2](H_2O)_{1.5}$, and has an unusual $UUDDUUDD$ orientation pattern of successive tetrahedra.

U_2L_{4+z} chains

The double-width chains shown in Figures 4u through 4y have the general formula U_2L_{4+z} (where z denotes the number of non-chain-forming polyhedra). These chains, although having significantly different graphical representations, are dominated by vertex-sharing between uranyl polyhedra and other bridging ligand polyhedra. The structure of $K_3[(UO_2)_2(IO_3)_6(IO_3)](H_2O)$ contains a U_2L_{4+2} chain, where uranyl pentagonal bipyramids are linked by vertex-sharing with lone-pair electron stereoactive (IO_3) polyhedra (Fig. 4u). Both the U_2L_{4+2} and U_2L_2 chains

consist of uranyl pentagonal bipyramids arranged in a similar (zig-zag) manner. However, in the U_2L_{4+2} chain, each chain-forming ligand polyhedron is [2]-coordinated with respect to uranyl pentagonal bipyramids, whereas in the U_2L_2 chain the ligand polyhedra are each [3]-coordinated. Also, in comparison with the other U_2L_{4+z} chains shown (Fig. 4v–y; see below), any two adjacent bipyramids in the chain are bridged by a single ligand polyhedron.

The U_2L_{4+z}-type chains shown in Figures 4v through 4y are all based on pairs of uranyl pentagonal bipyramids that are cross-linked to each other by two strongly bonded polyhedra. This basic unit is highlighted by the grey box in Figure 4v; note the topological similarity to the finite clusters shown in Figures 3s–t; these pairs are, in turn, bridged by vertex-sharing with additional polyhedra along the chain length to form the resulting infinite chain. In the structures of $Rb[UO_2(CrO_4)(IO_3)(H_2O)]$ (Fig. 4v) and $X_2[UO_2(CrO_4)(IO_3)_2]$ (X = Rb, Cs, K) (Fig. 4w), the dimeric units are bridged by (IO_3) polyhedra. Here, the lone electron pairs associated with the bridging $(IO_3)^-$ groups are directed towards each other and the central chain axis, an usual behavior not observed in other chains that contain lps-elements (cf. 4l–m, u). In the structure of $[(UO_2)_2(ReO_4)_4(H_2O)_3]$ (Fig. 4x), these dimeric units are linked via additional monomeric uranyl pentagonal bipyramids. This structure contains no interstitial complexes and the only (H_2O) group is located at an equatorial position of a uranyl polyhedron. Lastly, in the structure of $Ba[(UO_2)_2(As_2O_7)_3]$ pairs of bipyramids are linked by pyroarsenate groups, and in this anhydrous phase, the chains (Fig. 4y) are arranged in parallel to form pseudo sheets, held together by Ba^{2+} ions.

Chains based on clusters of vertex-sharing uranyl polyhedra

There are six chain topologies that include discrete clusters of directly linked uranyl polyhedra that are further linked by bridging polyhedral ligands along one dimension to form infinite chains (Figs. 4z–4ah). We designate the basic stoichiometry of these types of chains as $^X[(U_xL_y)L_z]$, where x and y are the number of uranium atoms and ligand polyhedra in the cluster, respectively, and z is the number of bridging ligand polyhedra that are involved in linking the clusters together. The superscript X indicates whether the cluster is oriented transvers (T) or longitudinal (L) to the chain axis. Hierarchically, we organize these chains on the basis of the cluster topology, i.e., increasing values of x and y. As the cluster is entirely defined by the connectivity of uranyl polyhedra, all

ligand polyhedra within the clusters (those described by subscript y) are designated as non-bridging.

Figures 4z and 4aa show two variants of the $^{[L]}[(U_2L_2)L_2]$ chain. The former occurs in the structures of $X_6[(UO_2)_2O(MoO_4)_4]$ (X = K, Rb) and the latter occurs in Rb$_6$ [(UO$_2$)$_2$O(WO$_4$)$_4$] and Cs[(UO$_2$)$_2$(MoO$_4$)$_3$(MoO$_5$)]. Both of these chains are based on vertex-sharing dimers of uranyl pentagonal bipyramids. In both, the dimer is bridged by two tetrahedra. Further, both chains contain non-bridging ligands that link the dimeric uranyl polyhedra. This type of configuration is not observed in any other chain, possibly due to the strain resulting from the deformation of adjacent bipyramids that is required to accommodate the linking tetrahedra. In the chain shown in Figure 4aa, the uranyl polyhedra in the dimeric cluster are linked by vertex-sharing MoO$_4$ polyhedra and edge-sharing MoO$_5$ polyhedra. This configuration is topologically related to the finite cluster shown in Figure 2t.

The $^{[L]}[(U_2L_0)L_2]$-type chain (Fig. 4ab) occurs in the structure of K$_2$[(UO$_2$)F$_2$(SO$_4$)]H$_2$O; here the uranyl polyhedra are bridged by F$^-$ ions and (H$_2$O) groups are located at the non-bridging equatorial positions. Adding two edge-sharing polyhedra to the dimers results in the $^{[L]}[(U_2L_2)L_2]$-type chain shown in Figure 4ac (and 4ad). This basic chain occurs with either $L = TO_4$ (*e.g.*, CrO$_4$, PO$_4$) or $L = DO_3E$ (*e.g.*, SeO$_3$) in five synthetic compounds [X_2(UO$_2$)(CrO$_4$)$_2$ (X = K, Rb); Cs[(UO$_2$)Ga(PO$_4$)$_2$], and Sr[(UO$_2$) (HPO$_3$)$_2$](H$_2$O)$_2$)], as well as lakebogaite (CaNa (Fe^{3+})$_2$[(H(UO$_2$)$_2$(PO$_4$)$_4$(OH)$_2$](H$_2$O)$_8$). In the compounds where L = SeO$_3$ [Na$_3$(H$_3$O)[(UO$_2$)(SeO$_3$)]$_2$ (H$_2$O), Sr[(UO$_2$)(SeO$_3$)]$_2$(H$_2$O)$_2$, and Sr[(UO$_2$) (HPO$_3$)](H$_2$O)$_2$] the lone electron pairs (E) point away from the chain axis (Fig. 4ad).

Figures 4ae and 4af show $^{[T]}[(U_2L_2)L_2]$ type chains. These chains contain the same cluster observed in the longitudinal [L] chains, rotated 90°. Here the edge-sharing ligands become bridging, whereas the vertex-sharing ligands become decorating; this results in double-wide chains. This chain type occurs with L = SeO$_3E$(X[(UO$_2$)(SeO$_3$)]; X = Ca, Sr) and $L = TO_4$ tetrahedra in the structure of the minerals parsonite [Pb$_2$[(UO$_2$)(PO$_4$)$_2$] and hallmondite [Pb$_2$[(UO$_2$) (AsO$_4$)$_2$](H$_2$O)$_n$].

The complex chain shown in Figure 4ag occurs in the isostructural anhydrous compounds X_8[(UO$_2$)$_4$ (WO$_4$)$_4$(WO$_5$)$_2$] (X = Rb, Cs) and has the general stoichiometry (U_4L_3)L_3. It consists of tetrameric clusters of vertex-sharing uranyl polyhedra that coordinate a central WO$_5$ pyramid. The basic four-membered cross-shaped topology observed in these chains is also observed in the unusual sheets found in mathesiusite (Fig. 12n) and the synthetic compounds

K$_8$[(UO$_2$)$_8$(MoO$_5$)$_3$O$_6$] (Fig. 9ah) and Cs$_6$[(UO$_2$)$_4$ (W$_5$O$_{21}$)(OH)$_2$(H$_2$O)$_2$] (Fig. 12o). The chain shown in Figure 4ah has the general formula $^{[T]}[(U_6L_0)L_1]$ and is only observed in uranopilite, [(UO$_2$)$_6$(SO$_4$) O$_2$(OH)$_6$(H$_2$O)$_6$]. Here complex clusters of six edge-sharing uranyl pentagonal bipyramids are linked by a solitary sulfate tetrahedron in which all the apexes participate in linking the chain. In each cluster there are six (OH) and six (H$_2$O) groups. This complex structure is devoid of interstitial cations or (H$_2$O) molecules. As such, its stability is solely maintained by the complex array of H bonds that link adjacent chains. If the uranopilite chain was extended perpendicular to the axis, the zippeite-type sheet (see Fig. 9aa) would be generated.

STRUCTURES CONTAINING INFINITE SHEETS OF URANYL POLYHEDRA

A total of 353 compounds (47%) containing stoichiometric quantities of U^{6+} have structural units based on infinite sheets of polyhedra, making this the most commonly observed type of structural unit in uranyl compounds (Tables 4–11). These sheets contain U^{6+} (nearly always as the uranyl ion) and (commonly) other high-valence cations. The preponderance of sheet structures was also observed in previous hierarchies of Burns *et al.* (1996) and Burns (2005) where they were noted to occur in 24% and 55% of known compounds of U^{6+}, respectively. The incorporation of uranyl polyhedra into sheet structures is a consequence of the residual bond valences of the apical yl oxygen atoms being sufficiently low (~0.3 *vu*) to preclude bridging to additional uranyl polyhedra in the third dimension, whereas the residual bond valences of the equatorial anions are sufficiently high (~1.5 *vu*) that the opposite is true. Thus, successive linkages with other uranyl polyhedra and/or with polyhedra containing other high-valence cations results in infinite sheets. These commonly incorporate different chemical species and occur with remarkable compositional and topological diversity.

The current hierarchy builds upon the classification proposed by Burns *et al.* (1996) and Burns (2005), relying heavily on the concept of a sheet-anion topology. To reveal the sheet-anion topology of nearly any polyhedral sheet, all cations and (most often) yl oxygen atoms associated with uranyl polyhedra, as well as other non-bridging anions, are removed and lines are drawn to link the remaining anions, up to distances of ~3.5 Å. In doing this, for example, a uranyl pentagonal bipyramid becomes simply a pentagon. The array of lines connecting the anions defines the anion topology in three dimensions, although projection onto a two-dimensional plane is

TABLE 4. U(VI) COMPOUNDS WITH SQUARE SHEETS DOMINATED BY VERTEX-SHARING WITH {4.4.4.4} GRAPHS

MINERAL	FORMULA	SG	a (Å)	b (Å)	c (Å)	α (°)	β (°)	γ (°)	SYN[a]	FIG	REF
Vertex-sharing uranyl polyhedra											
	$K_2(UO_4)$	$I4/mmm$	4.332	4.332	13.138	—	—	—	Fx[750]	5b	1
Markcooperite	$Pb_2(U_{0.75}Te_{0.25}O_2)(TeO_6)]$	$P2_1/c$	5.722	7.748	7.889	—	90.83	—		5c	2
	$Pb_2(UO_2)(TeO_6)$	$P2_1/c$	5.742	7.789	7.928	—	90.73	—		5c	3
	$Li_2[(UO_2)O_2]$	$Pnma$	10.547	6.065	5.134	—	—	—	SS[810]	5d	4
	$Ba[(UO_2)O_2]$	$Pbcm$	5.744	8.136	8.237	—	—	—	SS[1000]	5d	5
	$Sr[(UO_2)O_2]$	$Pbcm$	5.489	7.977	8.129	—	—	—	SS[1000]	5d	6
	γ-$[(UO_2)(OH)_2]$	$P2_1/c$	5.560	5.522	6.416	—	112.71	—	HT[85]	5d	7
	$Pb[(UO_2)O_2]$	$Pbcm$	5.536	7.968	8.212	—	—	—	SS[550]	5d	8
	α-$Sr[(UO_2)O_2]$	$Pbcm$	5.493	7.983	8.128	—	—	—		5d	9
	β-$Na_2[(UO_2)O_2]$	$Pccn$	11.708	5.805	5.97	—	—	—	Rs	5e	10
	β-$[(UO_2)(OH)_2]$	$Pbca$	5.644	6.287	9.937	—	—	—	HT[290]	5f	11
Autunite-type Sheets											
	$[(UO_2)(HPO_4)](H_2O)_4$	$P4/ncc$	6.995	6.995	17.491	—	—	—	SD	5i	12
	$[(UO_2)(DAsO_4)](D_2O)_4$	$P4/ncc$	7.162	7.162	17.639	—	—	—		5i	13
Monovalent interstitial cations											
	$Li[(UO_2)(AsO_4)](D_2O)_4$	$P4/n$	7.097	7.097	9.190	—	—	—		5i	14
	$Li[(UO_2)(PO_4)](H_2O)_4$	$P4/n$	6.956	6.956	9.139	—	—	—	SDg	5i	15
	$ND_4[(UO_2)(PO_4)](D_2O)_3$	$P4/ncc$	7.022	7.022	18.091	—	—	—	AC	5i	16
	$NH_4[(UO_2)(AsO_4)](H_2O)_3$	$P4/ncc$	7.189	7.189	18.191	—	—	—	Ae	5i	17
Uramarsite	$(UO_2)_2(AsO_4)(PO_4)(NH_4)(H_3O)(H_2O)_6$	$P\bar{1}$	7.173	7.167	9.30	90.13	90.09	89.96		5i	18
	$Na[(UO_2)(AsO_4)](H_2O)_3$	$P4/ncc$	7.150	7.150	17.325	—	—	—	SDg	5i	15
	$Na[(UO_2)(PO_4)](H_2O)_3$	$P4/ncc$	6.962	6.962	17.268	—	—	—	SDg	5i	15
	$K(H_3O)[(UO_2)(AsO_4)]_2(H_2O)_6$	$P4/ncc$	7.171	7.171	18.048	—	—	—		5i	17
	$K[(UO_2)(AsO_4)](H_2O)_3$	$P4/ncc$	7.160	7.160	17.746	—	—	—	HT[200]	5i	19
	$Rb[(UO_2)(PO_4)](H_2O)_3$	$P4/ncc$	7.011	7.011	17.977	—	—	—	SDg	5i	15
	$Rb[(UO_2)(AsO_4)](H_2O)_3$	$P4/n$	7.190	7.190	17.643	—	—	—	SDg	5i	15
	$Ag[(UO_2)(PO_4)](H_2O)_3$	$P4/ncc$	6.933	6.933	16.931	—	—	—	SDg	5i	15
	$Ag[(UO_2)(AsO_4)](H_2O)_3$	$P4/ncc$	7.090	7.090	17.045	—	—	—	HT[190]	5i	15
	$Cs_2[(UO_2)(PO_4)]_2(H_2O)_5$	$P2_1/n$	9.872	9.955	17.647	—	90.40	—	SDg	5h	15
	$Cs(H_3O)[(UO_2)(AsO_4)]_2(H_2O)_5$	$P2_1/n$	14.261	7.143	17.221	—	91.11	—	SDg	5i	15
	$Tl[(UO_2)(PO_4)](H_2O)_3$	$P4/ncc$	7.019	7.019	17.98	—	—	—	SDg	5i	15
	$Tl[(UO_2)(AsO_4)](H_2O)_3$	$P4/ncc$	7.191	7.191	17.97	—	—	—	HT[190]	5i	15
Divalent interstitial cation											
Saleeite	$Mg[(UO_2)(PO_4)]_2(H_2O)_{10}$	$P2_1/c$	6.951	19.947	9.896	—	135.17	—		5i	20
	$Mg[(UO_2)(AsO_4)]_2(H_2O)_{12}$	$P\bar{1}$	7.159	7.161	11.315	81.39	81.18	88.88	SDg	5i	21
	$Mg[(UO_2)(AsO_4)]_2(H_2O)_{10}$	$P2_1/n$	7.133	20.085	7.157	—	90.59	—	SDg	5i	21
	$[((Mg_{0.81}Fe_{0.19})(H_2O)_4]$ $[(UO_2)((P_{0.67}As_{0.33})O_4)]_2$	$P2_1/n$	6.952	19.865	6.969	—	90.81	—		5i	22
	$K[(UO_2)(PO_4)](D_2O)_3$	$P4/ncc$	6.994	6.994	17.784	—	—	—	Ac	5i	23
Abernathyite	$K[(UO_2)(AsO_4)](H_2O)_3$	$P4/ncc$	7.176	7.176	18.126	—	—	—		5i	17
Autunite	$Ca[(UO_2)(PO_4)]_2(H_2O)_{11}$	$Pnma$	14.014	20.712	6.996	—	—	—		5i	24
Meta-autunite	$Ca[(UO_2)(PO_4)]_2(H_2O)_6$	$P4/nmm$	6.96	6.96	8.40	—	—	—		5i	25
	$Mn[(UO_2)(AsO_4)]_2(H_2O)_{12}$	$P\bar{1}$	7.136	7.144	11.362	81.59	81.64	88.92	SDg	5i	21
	$Mn[(UO_2)(AsO_4)]_2(H_2O)_8$	$P\bar{1}$	7.224	9.917	13.337	75.01	84.14	81.99	HT[220]	5h	21
	$Mn[(UO_2)(PO_4)]_2(H_2O)_{10}$	$I2/m$	6.966	20.377	6.978	—	91.02	—	SDg	5i	21
	$Fe[(UO_2)(AsO_4)]_2(H_2O)_8$	$P\bar{1}$	7.207	9.824	13.271	75.37	84.02	81.84	HT[220]	5i	21
Metakirch-heimerite	$(Co_{0.53}Mg_{0.25}Ni_{0.08}Zn_{0.07}Fe_{0.05}Ca_{0.03})_{1.01}$ $(UO_2)_{2.07}[(AsO_4)_{1.99}(PO_4)_{0.01}]_2H_2O_8$	$P\bar{1}$	7.210	9.771	13.252	75.39	83.94	81.88		5i	26
	$Co[(UO_2)(AsO_4)]_2(H_2O)_{12}$	$P\bar{1}$	7.155	7.159	11.291	81.49	81.41	88.89	SDg	5i	21
	$Co[(UO_2)(AsO_4)]_2(H_2O)_8$	$P\bar{1}$	7.196	9.772	13.232	75.53	84.05	81.66	HT[220]	5i	21
	$Co[(UO_2)(PO_4)]_2(H_2O)_{10}$	$P2_1/n$	6.949	19.935	6.962	—	90.44	—	SDg	5i	21
	$Ni[(UO_2)(AsO_4)]_2(H_2O)_{12}$	$P\bar{1}$	7.152	7.158	11.256	81.55	81.36	88.92	SDg	5i	21
Metarauchite	$Ni[(UO_2)_2(AsO_4)_2](H_2O)_8$	$P\bar{1}$	7.194	9.713	13.201	75.79	83.92	81.59		5i	27
	$Ni[(UO_2)(PO_4)]_2(H_2O)_{12}$	$P\bar{1}$	6.996	7.001	11.171	81.59	82.19	88.72	SDg	5i	21
	$Ni[(UO_2)(PO_4)]_2(H_2O)_{10}$	$P2_1/n$	6.951	19.822	6.971	—	90.42	—	SDg	5i	21
Zeunerite	$Cu[(UO_2)(AsO_4)]_2(H_2O)_{12}$	$P4/nnc$	7.179	7.179	20.857	—	—	—		5i	28
Metazeunerite	$Cu[(UO_2)(AsO_4)]_2(H_2O)_8$	$P4/n$	7.109	7.109	17.416	—	—	—		5i	28
Torbernite	$Cu[(UO_2)(PO_4)]_2(H_2O)_{12}$	$P4/ncc$	7.027	7.027	20.807	—	—	—		5i	28
Metatorbernite	$Cu[(UO_2)(PO_4)]_2(H_2O)_8$	$P4/n$	6.976	6.976	17.349	—	—	—		5i	28
Metalodevite	$(Zn_{0.72}Fe_{0.10}Mg_{0.06}Al_{0.05})_{0.93}(UO_2)_{2.12}$ $[(AsO_4)_{1.44}(PO_4)_{0.56}]_2(H_2O)_{8.43}$	$P\bar{1}$	7.193	9.771	13.204	75.54	81.07	81.68			56
	$Sr[(UO_2)(PO_4)]_2(H_2O)_{11}$	$Pnma$	14.042	21.008	6.997	—	—	—	SDg	5h	30
	$Sr[(UO_2)(AsO_4)]_2(H_2O)_{11}$	$Pnma$	14.378	20.961	7.170	—	—	—	SDg	5h	30
	$Sr[(UO_2)(AsO_4)]_2(H_2O)_8$	$P2/c$	7.154	7.101	18.901	—	92.67	—	HT[60]	5i	31

TABLE 4. (CONTINUED). U(VI) COMPOUNDS WITH SQUARE SHEETS DOMINATED BY VERTEX-SHARING WITH {4.4.4.4} GRAPHS

Metauranocircite	Ba[(UO$_2$)(PO$_4$)]$_2$(H$_2$O)$_6$	P2$_1$/a	9.789	9.882	16.868	—	—	89.95		5h	32
	Ba[(UO$_2$)(PO$_4$)]$_2$(H$_2$O)$_7$	P2$_1$	6.943	17.634	6.952	—	90.02	—	SDg	5i	30
Trivalent interstitial cations											
Threadgoldite	Al[(UO$_2$)(PO$_4$)]$_2$(OH)(H$_2$O)$_8$	C2/c	20.168	9.847	19.719	—	110.71	—		5h	33
Uranospathite	Al$_{0.86}$[(UO$_2$)(PO$_4$)]$_2$(H$_2$O)$_{20.42}$F$_{0.58}$	Pnn2	30.020	7.008	7.049	—	—	—		5i	34
	Al$_{0.67}$[(UO$_2$)(PO$_4$)]$_2$(H$_2$O)$_{15.5}$	P$\bar{1}$	7.002	13.712	14.024	78.42	89.68	81.86	SDg	5i	34
	K$_4$[(UO$_2$)(PO$_4$)]$_2$	P4$_2$/nmc	6.985	6.985	11.865					5k	35
	Cs$_2$[(UO$_2$)$_2$(PO$_4$)$_2$]	P2$_1$/c	6.100	9.211	9.772	—	98.17	—		5l	36

Note: Double lines (═) indicate major differences in the stoichiometry of the structural unit, as indicated by the corresponding header in the table; single lines (–) indicates different topologic configurations; and dotted lines (- -) separate graphical isomers.

[a] Synthesis column data. HT[T] and SS[T] correspond to hydrothermal and solid state synthesis, respectively, at maximum reported temperature T (°C); V-Cl: vapor phase chlorination; A, aqueous (Ae denotes evaporation to dryness); Ac, concentrated acid; Flx, molten flux; SDg, slow diffusion in gel.

References: (1) Roof *et al.* (2010a); (2) Kampf *et al.* (2010); (3) Ling *et al.* (2011); (4) Gebert *et al.* (1978); (5) Reis *et al.* (1976); (6) Loopstra & Rietveld (1969); (7) Siegel *et al.* (1972a); (8) Cremers *et al.* (1986); (9) Sawyer (1972); (10) Kovba (1971); (11) Taylor & Bannister (1972); (12) Morosin (1978); (13) Fitch *et al.* (1983); (14) Fitch *et al.* (1982); (15) Locock *et al.* (2004a); (16) Fitch & Fender (1983); (17) Ross & Evans (1964); (18) Rastsvetaeva *et al.* (2008); (19) Alekseev *et al.* (2005c); (20) Miller & Taylor (1986); (21) Locock *et al.* (2004b); (22) Yakubovich *et al.* (2008); (23) Fitch & Cole (1991); (24) Locock & Burns (2003b); (25) Makarov & Ivanov (1960); (26) Plášil *et al.* (2009); (27) Plášil *et al.* (2010a); (28) Locock & Burns (2003c); (29) Plášil *et al.* (2010b); (30) Locock *et al.* (2005b); (31) Pushcharovskii *et al.* (2003); (32) Khosrawansazedj (1982a); (33) Khosrawan-Sazedj (1982b); (34) Locock *et al.* (2005c); (35) Linde *et al.* (1980); (36) Ling *et al.* (2009); (37) Locock & Burns (2003f).

necessary for illustration. Taking this approach for many sheets, nearly all can be placed into one of several categories on the basis of which geometric shapes occur and the specifics of their arrangement, and this is how structures are grouped here (*i.e.*, sheets consisting of triangles-pentagons; triangles-squares-pentagons; triangles-squares-pentagons-hexagons; hexagons-triangles; and miscellaneous shapes). These categories are further subdivided on the basis of the connectivity of uranyl polyhedra (*i.e.*, sheets of uranyl polyhedral clusters, sheets of linked chains of uranyl polyhedra, and sheets formed by the polymerization of uranyl polyhedra). Such subdivisions are useful in that they allow more structure to be imposed upon the increasingly populous sheet category, facilitating both the comparison of known structures and the addition of new ones. We add the category of 'complex sheets' to the current hierarchy, into which those sheet structures that contain multiple linked sheets are placed.

A noteworthy exception to the sheet-anion topology classification scheme described above is the large group of sheets based on vertex-sharing clusters. For these sheets, the sheet-anion topology approach fails to effectively differentiate between the subtle topological differences that exist. Thus, these are hierarchically organized on the basis of nodal connectedness as explained below.

Sheets dominated by vertex-sharing polyhedra

Tables 4 through 6 list the 140 compositionally distinct compounds that contain sheets that are solely based on the linkage of polyhedra *via* vertex sharing (*i.e.*, with no sharing of polyhedral edges). Classifying these structures in a useful fashion is challenging, as the topological variability distinguishing each sheet is remarkably subtle and, in contrast, the chemical variability is extensive. A cursory examination of the structures listed in Tables 4–6 shows that the uranyl ion may by present as both uranyl square and pentagonal bipyramids, although the latter is significantly more common. Ligand polyhedra are predominantly tetrahedra, occurring mostly as regular tetrahedra (PO$_4^{3-}$, AsO$_4^{3-}$, MoO$_4^{2-}$, SO$_4^{2-}$, CrO$_4^{2-}$, SeO$_4^{2-}$), and less often as irregular tetrahedra containing an electron lone-pair at one vertex (*e.g.*, IO$_3$, SeO$_3$) or tetrahedra with a protonated vertex (HPO$_3$, HSeO$_3$).

Consistent with the approach taken by Burns (2005), the structures dominated by vertex-sharing, where no polyhedra of the same cation species share any vertex, are hierarchically organized on the basis of the connectedness parameter, **s**, initially proposed by Krivovichev & Burns (2003a). Krivovichev (2004) showed that sheet topologies dominated by vertex-sharing can be effectively represented with graphical nets, wherein each net consists of two node types. Black nodes represent the uranyl ion and white nodes represent the ligand polyhedra, and a single line drawn between these nodes represents a shared vertex. Krivovichev (2004) showed that it is possible to represent any topology in this manner. The resulting graphs will contain rings of linked nodes. Such graphs

TABLE 5. U(VI) COMPOUNDS WITH STRUCTURES CONTAINING SHEETS DOMINATED BY VERTEX-SHARING

RINGS	FORMULA	SG	a (Å)	b (Å)	c (Å)	α (°)	β (°)	γ (°)		SYN[a]	FIG	REF
{5.3.5.3}{5.3.5.4} topology												
[4₁]	β-Cs₂[(UO₂)₂(MoO₄)₃]	$P4_2/n$	10.137	10.137	16.283	—	—	—		SS[850]	5n	1
[4₁]	Cs₂[(UO₂)₂(SO₄)₃]	$P\overline{4}\,2_1m$	9.62	9.62	8.13	—	—	—		A	5n	2
[4₁]	Cs₂[(UO₂)₂(CrO₄)₃]	$P\overline{4}\,2_1m$	9.957	9.957	8.021	—	—	—			5n	3
[4₁]	Mg[(UO₂)(AsO₄)]₂(H₂O)₄	$C2/m$	18.207	7.062	6.661	—	99.65	—		HT[180]	5n	4
Derived from the {3.6.3.6} parent graph												
[6₁4₁]	K₂[(UO₂)(HPO₃)₂](H₂O)₂	$P2_1$	7.598	6.938	10.617	—	110.84	—	I1/2		5q	5
[6₁4₁]	K(H₅O₂)[(UO₂)₂(SeO₄)₃(H₂O)]	$P2_1/c$	11.456	10.231	14.809	—	101.90	—			5q	6
[6₁4₁]	Na₂[(UO₂)(MoO₄)₂]	$P2_12_12_1$	7.229	11.324	12.013	—	—	—	I1/2	SS[850]	5q	7
[6₁4₂]	Cu₂[(UO₂)₃((S,Cr)O₄)₅]m(H₂O)₁₇	$Pbca$	18.059	19.989	20.555	—	—	—			5s	8
[6₁4₂]	Rb₄[(UO₂)₃(SeO₄)₅](H₂O)	$Pbnm$	11.371	15.069	19.209	—	—	—	I3/5	Ae	5s	9
[6₁4₃]	Cs₂[(UO₂)₂(HPO₃)₃](H₂O)	$P2_1/c$	10.705	11.851	12.643	—	101.59	—	I2/3	HT[200]	5u	10
[6₁4₃]	Rb₂(UO₂)₂(HPO₃)₃	$P2_1/n$	11.165	11.331	12.157	—	109.38	—	I2/3	HT[200]	5u	10
[6₁4₆]	Mg₂[(UO₂)₃(CrO₄)₅](H₂O)₁₇	$Pbca$	19.921	21.053	18.497	—	—	—	I3/5b	HT[120]	5w	11
[6₁4₆]	Ca₂[(UO₂)₃(CrO₄)₅](H₂O)₁₉	$P2_1/m$	11.036	17.536	11.506	—	118.18	—	I3/5b	HT[120]	5w	11
[6₁4₆]	Cu₂[(UO₂)₃((SCr)O₄)₅](H₂O)₁₇	$Pbca$	18.059	19.989	20.555	—	—	—	I3/5b	SS[900]	5w	12
[6₁4₆]	Zn₂[(UO₂)₃(SeO₄)₅](H₂O)₁₇	$Pbca$	18.429	19.979	20.690	—	—	—	I3/5b	A	5w	13
[6₁4₆]	α-Mg₂[(UO₂)₃(SeO₄)₅](H₂O)₁₆	$C2/c$	19.544	10.478	18.02	—	91.35	—	I3/5b	Ae	5w	14
[6₁4₆]	Co₂[(UO₂)₃(SeO₄)₅](H₂O)₁₆	$P\overline{1}$	10.458	11.032	17.893	89.45	90.28	61.76	I3/5b	HT[180]	5w	15
[6₁4₆]	Zn₂[(UO₂)₃(SeO₄)₅](H₂O)₁₆	$P\overline{1}$	10.438	11.063	17.895	89.19	89.85	61.72	I3/5b	A	5w	15
[6₁4₆]	K₄[(UO₂)₃(CrO₄)₅](H₂O)₈	$P2_1/c$	18.804	21.241		—	89.98	—	I3/5a	Ae	5w	16
[6₁4₆]	Cu₂{(UO₂)₃[(S,Cr)O₄]₅}(H₂O)₁₇	$Pbca$	18.059	20.000	20.555	—	—	—	I3/5a	Aq	5w	51
[5₂4₇]	K₆[(UO₂)₄(CrO₄)₇](H₂O)₆	$P2_12_12$	10.958	22.582	7.955	—	—	—	I4/7	HT[180]	5y	17
[8₁]	Cs₂[(UO₂)(SeO₄)₂H₂O]H₂O	$Pna2_1$	14.367	11.682	7.826	—	—	—	I1/2b	IS[110]	5aa	18
[8₁]	Mg[(UO₂)(SO₄)₂](H₂O)₁₁	$C2/c$	11.334	7.715	21.709	—	102.22	—	I1/2b	Rs	5aa	19
[8₁]	[(UO₂)(SO₄)₂]H₂(H₂O)₅	$C2/c$	11.008	8.242	15.619	—	113.71	—	I1/2b	Ae	5aa	20
[8₁]	K₂[(UO₂)(SO₄)₂](H₂O)₂	$Pnma$	13.806	11.577	7.292	—	—	—	I1/2b		5aa	21
[8₁]	Rb₂[(UO₂)(SO₄)₂(H₂O)](H₂O)	$Pna2_1$	13.451	11.479	7.410	—	—	—	I1/2b	A	5aa	22
[8₁]	Rb₂[(UO₂)(SeO₄)₂(H₂O)](H₂O)	$Pna2_1$	13.677	11.871	7.639	—	—	—	I1/2b	Ae	5aa	9
[8₁]	K₂[(UO₂)(SO₄)₂(H₂O)₂]	$Pna2_1$	13.773	7.288	11.556	—	—	—	I1/2b		5aa	23
[8₁]	Rb₂[(UO₂)(SeO₄)₂(D₂O)₂]	$Pna2_1$	13.654	11.863	7.625	—	—	—	I1/2b	HT[100]	5aa	24
[8₁]	Fe[(UO₂)(SO₄)₂](H₂O)₁₁ [b]	$C2/c$	11.320	7.729	21.815	—	102.40	—	I1/2b		5aa	25
[8₁]	UO₂(IO₃)₂(H₂O)(HIO₃)₂	$Pbcn$	8.335	7.659	20.899	—	—	—	I1/2b	HT[200]	5ab	26
[8₁]	UO₂(IO₃)₂(H₂O)	$Pbcn$	8.452	7.707	12.271	—	—	—	I1/2b	HT[425]	5ab	27
[8₁]	K[(UO₂)(IO₃)₃]	$Pbca$	11.495	7.229	25.394	—	—	—	I1/2b	HT[180]	5ad	28
[8₁4₂]	K₂[(UO₂)₂(CrO₄)₃(H₂O)₂](H₂O)₄	$P2_1/c$	10.742	14.529	14.139	—	108.14	—	I2/3e	Ae	5af	16
[8₁4₂]	Rb₂[(UO₂)₂(CrO₄)₃(H₂O)₂](H₂O)₄	$P2_1/c$	10.695	14.684	14.125	—	108.39	—			5af	29
[8₁4₃]	Na₂[(UO₂)(MoO₄)₂](H₂O)₄	$P2_1/n$	8.902	11.515	13.815	—	107.74	—	I1/2d	HT[120]	5ah	30
[8₁4₃]	Cs₂[(UO₂)(MoO₄)₂]	$Pbca$	11.762	14.081	14.323	—	—	—	I1/2d	SS[600]	5ah	31
[8₁4₃]	Cs₂[(UO₂)(MoO₄)₂](H₂O)	$P2_1/c$	8.222	11.099	13.999	—	95.16	—	I1/2d	HT[120]	5ah	31
[8₁4₃]	K₂[(UO₂)(MoO₄)₂]	$P2_1/c$	12.269	13.468	12.857	—	95.08	—	I1/2d	A[HT]	5ah	32
[8₁4₃]	Rb₂[(UO₂)(MoO₄)₂]	$P2_1/c$	12.302	13.638	13.508	—	94.98	—	I1/2d	SS[700]	5ah	33
[8₁4₃]	K₂[(UO₂)(MoO₄)₂](H₂O)	$P2_1/c$	7.893	10.907	13.558	—	98.70	—	I1/2d	HT[150]	5ah	7
[8₁4₃]	Rb₂[(UO₂)(MoO₄)₂](H₂O)	$P2_1/c$	7.967	10.956	13.679	—	96.69	—	I1/2d	Aq/Ac[120–180]	5ah	34
[8₁4₃]	Tl₂[(UO₂)(CrO₄)₂]	$Pca2_1$	10.703	13.425	13.936	—	—	—	I1/2d	HT[220]	5ah	35
[8₁4₃]	Tl₂[(UO₂)(MoO₄)₂]	$Pca2_1$	10.977	14.004	14.041	—	—	—	I1/2d	SS[600]	5ah	35
[8₁4₃]	Cs[(UO₂)(HSeO₃)(SeO₃)]	$P2_1/c$	13.853	10.615	12.592	—	101.09	—	I1/2d	HT[180]	5ah	36
[8₁4₃]	Tl[(UO₂)(HSeO₃)(SeO₃)]	$P2_1/n$	8.364	10.346	9.834	—	97.27	—	I1/2d	HT[180]	5ah	36
[8₁4₃]	Na₂[(UO₂)(SeO₄)₂](H₂O)₄	$P2_1/c$	8.650	11.003	13.879	—	108.08	—	I1/2d		5ah	37
[8₁4₃]	((H₅O₂)(H₃O)(H₂O)]((UO₂)(SeO₄)₂)	$P2_1/n$	8.311	11.079	13.227	—	103.88	—	I1/2d	Ae	5ah	38
[8₁4₃]	K[(UO₂)(HSeO₃)(SeO₃)]	$P2_1/n$	8.416	10.144	9.691	—	97.56	—	I1/2d	HT[180]	5ai	36
[8₁4₃]	Rb[(UO₂)(HSeO₃)(SeO₃)]	$P2_1/n$	8.417	10.258	9.854	—	96.83	—	I1/2d	HT[180]	5ai	36
[8₁4₃]	(NH₄)₂UO₂(SeO₃)₂(H₂O)₀.₅	$P2_1/c$	7.193	10.368	13.823	—	91.47	—	I1/2d	HT[97]	5ai	39
[8₁4₃]	(NH₄)[(UO₂)(HSeO₃)(SeO₃)]	$P2_1/n$	8.348	10.326	9.929	—	97.06	—	I1/2d	HT[97]	5ai	40
[8₁4₃]	Cs[(UO₂)(SeO₃)(HSeO₃)](H₂O)₃	$P2_1/n$	8.673	10.452	13.235	—	105.15	—	I1/2d	HT[180]	5ai	41
[8₁4₃]	Na[(UO₂)(SeO₃)(HSeO₃)](H₂O)₄	$P2_1/n$	8.803	10.461	13.131	—	105.05	—	I1/2d	Ae	5ai	42
[8₁4₃]	Cs[(UO₂)(HPO₃)(HPO₃)]	$P\overline{1}$	7.975	10.564	10.677	94.15	95.88	90.41	I1/2d	Ae	5ai	10
[8₁4₃]	(H₃O)[(UO₂)(SeO₄)(SeO₂(OH)]	$P2_1/n$	8.668	10.655	9.846	—	97.88	—	I1/2d	A	5aj	43
[8₁4₇]	K₂.₅(NO₃)₀.₅[(UO₂)₂(SeO₄)₃(H₂O)](H₂O)₄	$C2/c$	20.290	10.380	21.436	—	103.45	—			5al	44
[8₁4₇]	K(H₃O)[(UO₂)₂(SeO₄)₃(H₂O)](H₂O)₆	$P2_1/n$	14.715	10.156	15.833	—	114.42	—	I2/3	A	5al	45
[8₂4₃]	Ag₂[(UO₂)(SeO₃)₂]	$P2_1/n$	5.856	6.505	21.164	—	96.79	—	I1/2	HT[180]	5an	36
[12₁4₁]	(NH₄)₂[(UO₂)(SO₄)₂(H₂O)](H₂O)	$P2_1/c$	7.783	7.403	20.918	—	102.25	—	I1/2b		5ap	46
[12₁4₁]	K₂(H₅O₂)(H₃O)[(UO₂)₂(SeO₄)₄(H₂O)₂](H₂O)₄	$C2/c$	17.879	8.152	17.872	—	—	—			5ap	47
[12₁4₁]	K₃(H₃O)[(UO₂)₂(SeO₄)₄(H₂O)₂](H₂O)₅	$P2_1/c$	17.838	8.148	23.696	—	131.622	—			5ap	47
[12₁4₁]	(H₃O)₂[(UO₂)(SeO₄)₂](H₂O)₂	$P2_1/c$	7.867	7.536	21.386	—	101.48	—	I1/2c	Ae	5ap	48
[12₁4₅]	(H₃O)₂[(UO₂)₂(SeO₄)₃(H₂O)₂](H₂O)₃.₅	$P2_1/m$	11.940	13.645	13.727	—	109.44	—	I2/3i	Ae	5ar	49
[12₁4₅]	Rb₂[(UO₂)₂(SeO₄)₃(H₂O)₂](H₂O)₄	$P\overline{1}$	8.426	11.864	13.328	102.61	107.25	102.51	I2/3i	Ae	5ar	9
[12₁4₅]	K₃(H₃O)[(UO₂)₄(SeO₄)₆(H₂O)₄](H₂O)₅	$P2_1/m$	12.001	13.613	13.753	—	109.187	—			5ar	44
	[UF₄O(SbF₅)₂]	$P2_1/c$	7.864	14.704	9.980	—	99.8	—			5as	50

TABLE 5. (CONTINUED).

Note: Double lines (=) indicate major differences in the stoichiometry of the structural unit, as indicated by the corresponding header in the table; single lines (–) indicates different topologic configurations; and dotted lines (—) separate graphical isomers.

[a] Synthesis column data. HT[T] and SS[T] correspond to hydrothermal and solid state synthesis, respectively, at maximum reported temperature T (°C); V-Cl: vapor phase chlorination; A, aqueous (Ae denotes evaporation to dryness); Ac, concentrated acid; Flx, molten flux; SDg, slow diffusion in gel.

[b] Mineral: Leydetite.

References: (1) Krivovichev *et al.* (2002a); (2) Ross & Evans (1960); (3) Siidra *et al.* (2013); (4) Bachet *et al.* (1991); (5) Mistryukov & Mikhailov (1985); (6) Gurzhiy *et al.* (2012); (7) Krivovichev *et al.* (2002b); (8) Krivovichev & Burns (2004b); (9) Krivovichev & Kahlenberg (2005d); (10) Villa *et al.* (2012); (11) Krivovichev & Burns (2003f); (12) Strobel & Schleid (2004); (13) Krivovichev & Kahlenberg (2005e); (14) Krivovichev & Kahlenberg (2004); (15) Krivovichev & Kahlenberg (2005f); (16) Krivovichev & Burns (2003g); (17) Sykora *et al.* (2004c); (18) Mikhailov *et al.* (2001b); (19) Serezhkin *et al.* (1981a); (20) Alcock *et al.* (1982); (21) Niinisto (1979); (22) Serezhkina *et al.* (2004); (23) Alekseev *et al.* (2006c); (24) Serezhkin *et al.* (2010); (25) Plášil *et al.* (2013e); (26) Ling & Albrecht-Schmitt (2007); (27) Bean *et al.* (2001b); (28) Shvareva *et al.* (2005a); (29) Verevkin *et al.* (2010); (30) Krivovichev & Burns (2003c); (31) Krivovichev & Burns (2005); (32) Sadikov *et al.* (1988); (33) Krivovichev & Burns (2002a); (34) Khrustalev *et al.* (2000); (35) Krivovichev *et al.* (2005i); (36) Almond & Albrecht-Schmitt (2002b); (37) Mikhailov *et al.* (2001a); (38) Krivovichev (2008b); (39) Koskenlinna *et al.* (1997); (40) Koskenlinna & Valkonen (1996); (41) Burns & Ibers (2009); (42) Marukhnov *et al.* (2008a); (43) Krivovichev (2009); (44) Gurzhiy *et al.* (2014); (45) Ling *et al.* (2010b); (46) Niinisto *et al.* (1978); (47) Gurzhiy *et al.* (2011); (48) Krivovichev (2008a); (49) Krivovichev & Kahlenberg (2005b); (50) Bougon *et al.* (1979); Krivovichev & Burns (2004c).

can be characterized by three parameters: (1) a connectedness vector (**s**), which indicates the coordination number of each node; (2) the *U/L* ratio, which indicates the relative ratio of uranyl to ligand polyhedra in the sheet; and (3) the ratio of ring sizes given as A_xB_y, which indicates the relative frequency (x:y) of which rings of size A and B occur in the sheet. The parameters U/L and A_xB_y are independent of each other; however, a graph with a given *U/L* ratio may correspond to multiple A_xB_y values, as shown by the compounds listed in Table 6.

Taking this approach, the complexity of the initial 136 structures is distilled down to 19 different structure topologies, each of which is relatable to one of three parent graph topologies. The $\mathbf{s} = \{4.4.4.4\}$ parent graph consists solely of square [4]-membered rings (*i.e.*, $A_x = 4_1$), wherein each node is [4]-coordinated (Fig. 5a, g). The $\mathbf{s} = \{5.3.5.3\}\{5.3.5.4\}$

TABLE 6. U(VI) COMPOUNDS WITH STRUCTURES CONTAINING MISCELLANEOUS SHEETS BASED ON VERTEX-SHARING

FORMULA	SG	a (Å)	b (Å)	c (Å)	α (°)	β (°)	γ (°)	SYN[a]	FIG	REF
$K_2[(UO_2)As_2O_7]$	*Pmmn*	12.601	13.242	5.621	—	—	—	SS[800]	6a	1
$Cs_2[(UO_2)(P_2O_7)]$	*Pmmn*	12.670	12.807	6.1522	—	—	—		6a	2
$Na_6[(UO_2)_2(AsO_4)_2(As_2O_7)]$	$P\bar{1}$	10.996	11.633	14.057	108.63	91.27	97.4	SS[1053]	6b	3
$Ag_6[(UO_2)_2(AsO_4)_2(As_2O_7)]$	$P\bar{1}$	11.218	11.729	14.146	108.69	91.94	97.63	SS[1053]	6b	4
$Ag_6[(UO_2)_2(As_2O_7)(As_4O_{13})]$	$P2_1/n$	8.963	27.576	9.207	—	105.04	—	SS[1053]	6c	5
α-$K[(UO_2)(P_3O_9)]$	$P2_1/m$	8.497	15.115	14.789	—	91.91	—	SS[850]	6d	6
$K[(UO2)Te_2O_5(OH)]$	*Cmcm*	7.999	8.742	11.441	—	—	—	HT[180]	6e	7
$Pb[(UO_2)(SeO_3)_2]$	$Pmc2_1$	11.991	5.781	11.253	—	—	—	HT[180]	6f	8
$Pb_2[(UO_2)(TeO_3)_3]$	$P2_1/n$	11.605	13.389	6.981	—	91.23	—		6g	9

Note: Double lines (=) indicate major differences in the stoichiometry of the structural unit, as indicated by the corresponding header in the table; single lines (–) indicates different topologic configurations; and dotted lines (- -) separate graphical isomers.

[a] Synthesis column data. HT[T] and SS[T] correspond to hydrothermal and solid state synthesis, respectively, at maximum reported temperature T (°C); V-Cl: vapor phase chlorination; A, aqueous (Ae denotes evaporation to dryness); Ac, concentrated acid; Flx, molten flux; SDg, slow diffusion in gel.

References: (1) Alekseev *et al.* (2007b); (2) Linde *et al.* (1981); (3) Alekseev *et al.* (2009b); (4) Alekseev *et al.* (2009b); (5) Alekseev *et al.* (2009b); (6) Alekseev *et al.* (2008a); (7) Almond & Albrecht-Schmitt (2002a); (8) Almond & Albrecht-Schmitt (2002b); (9) Brandstatter (1981).

TABLE 7. U(VI) COMPOUNDS WITH SHEET ANION TOPOLOGIES CONSISTING OF TRIANGLES AND PENTAGONS

MINERAL	FORMULA	SG	a (Å)	b (Å)	c (Å)	α (°)	β (°)	γ (°)	FIG	SYN[a]	REF
TrPt sheets formed by clusters											
	$(H_3O)_2[(UO_2)_3O(OH)_3(SeO_4)_2]$	$R32$	9.567	9.567	22.703	—	—	120	7b		1
TrPt sheets of linked parallel chains											
	$K[(UO_2)(SO_4)(OH)]$	$Pbca$	8.445	10.806	13.541	—	—	—	7d	HT[145]	2
	$Ba[(UO_2)F(PO_4)]$	$P2_1/c$	6.667	8.266	10.795	—	92.06	—	7e	HT[190]	3
	$K[(UO_2)F(HPO_4)](H_2O)$	$P2_1/n$	6.789	8.702	12.020	—	94.09	—	7e	HT[200]	4
	$Rb[(UO_2)(SO_4)F]$	$Pca2_1$	25.393	6.735	11.496	—	—	—	7f		5
Infinite TrPt sheets											
Protasite	$Ba[(UO_2)_3O_3(OH)_2](H_2O)_3$	Pn	12.295	7.221	6.956	—	90.40	—	7h		6
Billietite	$Ba[(UO_2)_3O_2(OH)_3]_2(H_2O)_4$	$Pbn2_1$	12.072	30.167	7.146	—	—	—	7h		6
Becquerelite	$Ca[(UO_2)_3O_2(OH)_3]_2(H_2O)_8$	$Pn2_1a$	13.853	12.393	14.929	—	—	—	7h		7
	$Sr_{1.27}[(UO_2)_3O_{3.54}(OH)_{1.46}](H_2O)_3$	$P3$	7.020	7.020	6.992	—	—	120	7h	HT[160]	7
	$Cs_3[(UO_2)_{12}O_7(OH)_{13}](H_2O)_3$	$R3$	14.124	14.124	22.407	—	—	120	7h	HT[160]	8
	$Na_2[(UO_2)_3O_3(OH)_2]$	$P2_1/n$	7.048	11.413	12.027	—	—	—	7h		9
Richetite	$(Fe,Mg)_1Pb_{8.57}[(UO_2)_{18}O_{18}(OH)_{12}]_2(H_2O)_{41}$	$P1$	20.939	12.100	16.345	103.87	115.37	90.27	7h		10
Agrinierite	$K_2(Ca_{0.65}Sr_{0.35})[(UO_2)_3O_3(OH)_2]_2(H_2O)_5$	$F2mm$	14.094	14.127	24.106	—	—	—	7h		11
Masuyite	$Pb[(UO_2)_3O_3(OH)_2](H_2O)_3$	Pn	12.241	7.008	6.983	—	90.40	—	7h		12
Compreignacite	$K_2[(UO_2)_3O_2(OH)_3]_2(H_2O)_7$	$Pnnm$	14.859	7.175	12.187	—	—	—	7h		13
	$\alpha\text{-}U_3O_8$	$C2mm$	6.716	11.96	4.147	—	—	—	7h		14
Billietite	$Ba[(UO_2)_3O_4(OH)](H_2O)_8$	$Pbn2_1$	12.094	30.211	7.156	—	—	—	7h		15
	$Cs_3[(UO_2)_3O_2(OH)_3]_2Cl(H_2O)_3$	$Im2m$	15.471	7.239	12.064	—	—	—	7h		16
	$Mg[(UO_2)(SO_4)_2](H_2O)_{11}$	$C2/c$	11.334	7.715	21.709	—	102.22	—	7i		17
	$[(UO_2)(H_2SO_4)_2](H_2O)_5$	$C2/c$	11.008	8.242	15.619	—	113.71	—	7i	Ac	18
	$K_2[(UO_2)(SO_4)_2](H_2O)_2$	$Pnma$	13.806	11.577	7.292	—	—	—	7i		19
	$Na[(UO_2)_4O_2(OH)_5](H_2O)_2$	$P\bar{1}$	8.075	8.463	11.218	80.39	87.49	71.31	7k	HT[150]	20
Fourmarierite	$Pb[(UO_2)_4O_3(OH)_4](H_2O)_4$	$Bb2_1m$	13.986	16.400	14.293	—	—	—	7m		21
Metaschoepite	$[(UO_2)_4O(OH)_6](H_2O)_5$	$Pbcn$	14.686	13.979	16.706	—	—	—	7m		22
Schoepite	$[(UO_2)_8O_2(OH)_{12}](H_2O)_{12}$	$P2_1ca$	14.337	16.813	14.731	—	—	—	7m		23
Vanden-driesscheite	$Pb_{1.57}[(UO_2)_{10}O_6(OH)_{11}](H_2O)_{11}$	$Pbca$	14.117	41.378	14.535	—	—	—	7o		24
	$\alpha\text{-}Cs_2[(UO_2)_2O_3]$	$C2/m$	14.528	4.264	7.605	—	112.93	—	7q	SS[600]	25

Note: Double lines (═) indicate major differences in the stoichiometry of the structural unit, as indicated by the corresponding header in the table; single lines (–) indicates different topologic configurations; and dotted lines (--) separate graphical isomers.

[a] Synthesis column data. HT[T] and SS[T] correspond to hydrothermal and solid state synthesis, respectively, at maximum reported temperature T (°C); V-Cl: vapor phase chlorination; A, aqueous (Ae denotes evaporation to dryness); Ac, concentrated acid; Flx, molten flux; SDg, slow diffusion in gel.

References: (1) Mit'kovskaya *et al.* (2003); (2) Forbes *et al.* (2007); (3) Ling *et al.* (2009); (4) Ok *et al.* (2006); (5) Mikhailov *et al.* (2002a); (6) Pagoaga *et al.* (1987); (7) Burns & Li (2002); (8) Hill & Burns (1999); (9) Li & Burns (2001b); (10) Burns (1998c); (11) Cahill & Burns (2000); (12) Burns & Hanchar (1999); (13) Burns (1998b); (14) Loopstra, (1977); (15) Finch *et al.* (2006); (16) Li *et al.* (2001a); (17) Serezhkin *et al.* (1981a); (18) Alcock *et al.* (1982); (19) Niinisto (1979); (20) Burns & Deely (2002); (21) Piret (1985); (22) Weller *et al.* (2000); (23) Finch *et al.* (1996); (24) Burns (1997); (25) van Egmond (1976).

[4₁, $U/L = 2/3$] parent graph (Fig. 5m) contains two nodal ring types, with the coordination numbers of the nodes being {5.3.5.3} and {5.3.5.4}. The $\mathbf{s} = \{3.6.3.6\}$ [4₁, $U/L = 1/2$] parent graph topology (Fig. 5o) is not observed in any known phase; however, by selectively deleting linkages, all other sheet topologies observed in compounds and minerals listed in Table 5 and illustrated in Figures 5p through 5as can be derived.

Sheets related to the {4.4.4.4} parent graph. There are 65 compounds corresponding to this graph type, all containing U^{6+} in [6]-coordination. Of these, all but $K_2[UO_4]$ contain uranyl square bipyramids. There are two basic variants of this graph. First, octahedral polyhedra may link directly to each other to form the sheet (Fig. 5a–f). This sheet is in the 11 compounds (one mineral) listed in Table 4. These octahedra may all be uranyl polyhedra, or may alternate with different chemical species (*e.g.*, markcooperite and $Pb_2[(UO_2)(TeO_6)]$). Amongst the structures with only uranium polyhedra, considerable positional variability is observed. The edges of the vacant squares are geometrically perfect in the structure of $K_2[UO_4]$ (Fig. 5b), whereas they are slightly distorted in the structures of $Ba[UO_4]$, $Sr[UO_4]$, $Pb[UO_4]$, $\gamma\text{-}[(UO_2)(OH)_2]$, and $Li_2[(UO_2)O_2]$ (Fig. 5d). Diamond-shape vacancies occur where uranyl polyhedra have either rotated about the axis of the uranyl ion ($\beta\text{-}Na_2[(UO_4)]$) (Fig. 5e) or adopt a sheared distortion ($\beta\text{-}[(UO_2)(OH_2)]$) (Fig. 5f) relative to the undistorted sheet. In the two compounds lacking an interstitial cation (γ- and β-$[(UO_2)(OH_2)]$), the uranyl polyhedra are bridged by (OH) groups and the sheets are stabilized by H bonds.

The well-known and mineralogically important autunite-type sheet occurs where the uranyl square

bipyramid is bridged to four ligand polyhedra (Fig. 5g–i), such that the U/L ratio is always 1/1. In a review article, Locock (2007) listed a total of 109 inorganic compounds that contain the autunite-type sheet (or compounds in which it can be confidently inferred). Of these, 33 are transuranium compounds (not addressed here), 40 are minerals (though not all are currently approved by the International Mineralogical Association), and 36 are other synthetic, inorganic compounds. At the current time, the number of synthetic compounds has increased to 38, and of the 40 proposed minerals, 15 have well-characterized crystal structures and are included in Table 4; these constitute the 53 compounds listed in Table 4. Autunite-type minerals are commonly associated with regions of high uranium concentration (*i.e.*, U deposits or contaminated sites) and can be significant in impacting the mobility of U in vadose zones. The low solubility of these phases retards the movement of uranium from areas of high contamination and such compounds can be readily precipitated by bacteria (Basnakova *et al*. 1998, Macaskie *et al*. 2000, Martinez *et al*. 2007).

In all autunite-group minerals, the uranyl square bipyramids are linked by vertex-sharing with either AsO_4 (24 species) or PO_4 (29 species) tetrahedra. The sheets are separated by an interlayer region consisting of H_2O groups and/or monovalent (17 compounds), divalent (30 compounds), or trivalent (five compounds) cations. The sheets are linked by a complex network of H bonds and bonds to the interlayer cations, the precise geometry of which varies from compound to compound, as does the alignment of adjacent sheets. The ideal autunite sheet has tetragonal symmetry; however, the space group symmetry of the minerals varies, depending on the ligand tetrahedra (*i.e.*, PO_4 *versus* AsO_4), composition of the interlayer (cation species and hydration state), and the temperature at which the structural data were collected. Figures 5h and 5i contrast the orthogonal and sheared forms of autunite sheets. Examination of Table 5 shows that the sheared form of the autunite sheet occurs commonly in autunite phases.

Locock (2007) discussed trends in the autunite-type phases on the basis of the formal valence of the interlayer cation, and Table 5 is structured accordingly. A comprehensive discussion of the crystal-chemical factors that influence these trends exceeds the scope of the current work, and interested readers are referred to Locock (2007) and references therein.

The sheets of polyhedra in the compounds $K_4[(UO_2)(PO_4)_2]$ (Fig. 5k) and $Cs_2[(UO_2)_2(PO_4)_2$ (Fig. 5l) correspond to the graphical representation shown in Figure 5j. This graph is derived from the autunite topology by deleting half of the uranyl ions. Due to the general orthogonal nature of the structures,

they appear similar to the autunite sheets, and hence are included in this category. However, it is important to note that this graph can also be derived from the {3.6.3.6} parent graph and that it is graphically isomeric with the [8₁] graphs shown in Figures 5z–ab.

Sheets related to the {5.3.5.3}{5.3.5.4} parent graph. Table 5 lists four structures that contain this graph type. The {5.3.5.3}{5.3.5.4} graph and its corresponding structures show the highest possible degrees of connectivity involving only sharing of vertices, with each equatorial anion of the uranyl pentagonal bipyramid bridging to a ligand tetrahedron, and ¾ of the ligand tetrahedra linking to three uranyl polyhedra, and the remaining ¼ of the ligand tetrahedra linked to four uranyl polyhedra. The sheets in three structures are anhydrous, and their interlayers contain Cs. $Cs_2[(UO_2)_2(SO_4)_3]$ and $Cs_2[(UO_2)_2(CrO_4)_3]$ are isostructural, differing only in the composition of the tetrahedral species. Here the sheets are aligned, corresponding to a *c*-parameter repeat distance of ∼8 Å. In the compound β-$Cs_2[(UO_2)_2(MoO_4)_3]$, adjacent sheets are related by an inversion center, resulting in a doubling of the *c* cell parameter.

Sheets related to the {3.6.3.6} parent graph. Krivovichev (2004) lists 34 derivative graphs of the {3.6.3.6} parent with $U:L$ ratios of 1/2, 2/3, 4/3, 13/18, 3/8, 5/8, 3/5, and 1/1. The graphs are enumerated with the designator $I\ x/y\ n$, where I indicates isolated uranyl polyhedra (referred to as 'islands'), x/y corresponds to the U/L ratio in the sheet, and n distinguishes different graph topologies. For the most part, the sheet topologies observed in the compounds listed in Table 6 coincide with the 34 initial graphs proposed by Krivovichev (2004), and hence the appropriate 'n' designator is maintained. However, there are an infinite number of possible {3.6.3.6} offspring graphs that can be derived if the size of the unit cell is allowed to vary, and correspondingly, additions to this class correspond to new sheet topologies. Where this occurs, the 'n' designator is omitted.

Burns (2005) lists 29 structures with topologies derived from the {3.6.3.6} parent graph. There are 62 structures currently; of these, 38, six, and nine correspond to $U:L$ ratios of 1/2, 2/3, and 3/5, respectively. Only the structure of $K_6[(UO_2)_4(CrO_4)_7](H_2O)_6$ contains sheets with a U/L ratio (4/7) not previously observed. The ring compositions facilitate comparison between the various structures, and Table 5 lists compounds in order of the size and relative frequency of the largest ring.

Structures derived from the {3.6.3.6} parent show considerable variability in their water content. Of the 66 structures listed in Table 5, 35 contain anhydrous sheets. Of these, 21 contain hydrous interlayers. Only 11 of these compounds are anhydrous, and were

TABLE 8. U(VI) COMPOUNDS WITH SHEET ANION TOPOLOGIES CONSISTING OF TRIANGLES, SQUARES, AND PENTAGONS

MINERAL	FORMULA	SG	a (Å)	b (Å)	c (Å)	α (°)	β (°)	γ (°)	FIG	SYNᵃ	REF
Uranophane Group											
	Na[(UO$_2$)(BO$_3$)]	Pcam	10.712	5.780	6.862	—	—	—	8b		1
	Li[(UO$_2$)(BO$_3$)]	P2$_1$/c	5.767	10.574	6.835	—	105.04	—	8b		2
α-uranophane	Ca[(UO$_2$)(SiO$_3$OH)]$_2$(H$_2$O)$_5$	P2$_1$	15.909	7.002	6.665	—	97.27	—	8c		3
Boltwoodite	(K$_{0.56}$Na)$_{0.42}$[(UO$_2$)(SiO$_3$OH)](H$_2$O)$_{1.48}$	P2$_1$/m	7.077	7.059	6.648	—	104.98	—	8c		4
	Cs[(UO$_2$)(SiO$_3$OH)]	P2$_1$/m	7.476	7.087	6.666	—	104.16	—	8c	HT[200]	5
Cuprosklodowskite	Cu[(UO$_2$)(SiO$_3$OH)]$_2$(H$_2$O)$_6$	P$\overline{1}$	7.052	9.267	6.655	109.23	89.84	110.01	8c		6
Sklodowskite	Mg[(UO$_2$)(SiO$_3$OH)]$_2$(H$_2$O)$_6$	C2/m	17.382	7.047	6.610	—	105.9	—	8c		7
Kasolite	Pb[(UO$_2$)(SiO$_4$)](H$_2$O)	P2$_1$/c	6.704	6.932	13.252	—	104.22	—	8c		8
	Mg[(UO$_2$)(AsO$_3$)$_{0.7}$(AsO$_4$)$_{0.3}$]$_2$(H$_2$O)$_7$	C2/m	18.194	7.071	6.670	—	99.70	—	8c		9
	Mg[(UO$_2$)(AsO$_4$)]$_2$(H$_2$O)$_4$	C2/m	18.207	7.062	6.661	—	99.65	—	8c		10
Oursinite	Co$_{0.8}$Mg$_{0.2}$[(UO$_2$)(SiO$_3$OH)]$_2$(H$_2$O)$_6$	Cmca	7.049	17.550	12.734	—	—	—	8d		11
β-uranophane	Ca[(UO$_2$)(SiO$_3$OH)]$_4$(H$_2$O)$_5$	P2$_1$/a	13.966	15.443	6.632	—	91.38	—	8e		12
Ulrichite	CaCu[(UO$_2$)(PO$_4$)$_2$](H$_2$O)$_4$	P2$_1$/c	12.784	6.996	13.007	—	91.92	—	8f		13
	(Ca$_{1.81}$(UO$_2$)$_{0.19}$][(UO$_2$)(HPO$_3$)$_4$](H$_2$O)$_5$	C2	22.865	6.618	7.031	—	94.76	—	8f		14
Umohoite	[(UO$_2$)(MoO$_4$)(H$_2$O)](H$_2$O)	P$\overline{1}$	6.375	7.529	14.628	82.64	85.95	89.91	8g		15
	Li$_4$[(UO$_2$)$_2$(W$_2$O$_{10}$)]	Cmc2$_1$	7.382	14.049	10.189	—	—	—	8g		16
	K$_2$[(UO$_2$)$_2$O$_3$]	P2$_1$	6.931	7.690	6.984	—	109.69	—	8h	Flx[800]	17
	[(UO$_2$)$_3$(CuO$_4$)]	P$\overline{1}$	6.516	7.614	5.615	109.46	125.18	89.99	8i	SS[750]	18
Schmitterite	[(UO$_2$)(TeO$_3$)]	Pca2$_1$	10.161	5.363	7.862	—	—	—	8j		19
	K[(UO$_2$)(NbO$_4$)]	Pcab	7.579	11.321	15.259	—	—	—	8k		20
	γ-Rb(NbUO$_6$)(H$_2$O)$_{0.84}$	Pcab	7.614	11.219	16.510	—	—	—	8k	SS[1360]	21
	Li(NbUO$_6$)	P2$_1$/c	10.309	6.441	7.560	—	100.652	—	8k	HT[350]	22
	[H$_2$(UO$_2$)$_3$O$_4$]	P$\overline{1}$	6.802	7.417	5.556	108.5	125.5	88.2	8l		23
	K$_2$[(UO$_2$)(W$_2$O$_8$)]	Pmcn	7.588	8.616	13.946	—	—	—	8m		24
	Na$_2$[(UO$_2$)(W$_2$O$_8$)]	P$\overline{1}$	6.648	7.531	8.487	89.95	86.19	73.29	8m		25
	α-Ag$_2$[(UO$_2$)(W$_2$O$_8$)]	P2$_1$/c	8.426	7.489	12.927	—	95.44	—	8m		25
	β-Ag$_2$[(UO$_2$)(W$_2$O$_8$)]	Pnma	8.642	7.561	12.451	—	—	—	8m		25
Sheets of clusters of uranyl polyhedra											
Iriginite	[(UO$_2$)(Mo$_2$O$_7$)(H$_2$O)$_2$](H$_2$O)	Pbcm	6.705	12.731	11.524	—	—	—	9b		26
	[(UO$_2$)(Mo$_2$O$_7$)(H$_2$O)$_2$]	C2/c	35.071	6.717	11.513	—	90.07	—	9b		27
	[Ca(UO$_2$)(Mo$_4$O$_7$)$_2$]	P$\overline{1}$	13.239	6.651	8.236	—	90.38	120.16	9b		28
	K(UO$_2$)(OH)(CrO$_4$)(H$_2$O)$_{1.5}$	P2$_1$/c	13.292	9.477	13.137	—	104.12	—	9d	Rs	29
	Cs[UO$_2$(OH)(SeO$_4$)](H$_2$O)	P2$_1$/c	8.455	11.536	9.557	—	113.27	—	9e	HT[220]	30
	Cs(UO$_2$)F(HPO$_4$)(H$_2$O)$_{0.5}$	Pca2$_1$	25.656	6.039	9.207	—	—	—	9f	HT[200]	31
Vandenbrandeite	[Cu(UO$_2$)(OH)$_4$]	P$\overline{1}$	7.855	5.449	6.089	91.44	101.90	89.2	9h		32
Uranosphaerite	[Bi(UO$_2$)O$_2$OH]	P2$_1$/n	7.559	7.811	7.693	—	92.88	—	9j		33
Francevillite	Ba$_{0.96}$Pb$_{0.04}$[(UO$_2$)$_2$(V$_2$O$_8$)$_2$](H$_2$O)$_5$	Pcan	10.419	8.510	16.763	—	—	—	9j		34
	Ba[(VUO$_6$)$_2$]	P2$_1$/c	6.499	8.380	10.424	—	104.75	—	9j	SS[780]	35
Curienite	Pb[(UO$_2$)$_2$(V$_2$O$_8$)](H$_2$O)$_5$	Pcan	10.419	8.494	16.405	—	—	—	9j		36
Carnotite (syn.)	K$_2$[(UO$_2$)$_2$(V$_2$O$_8$)]	P2$_1$/a	10.47	8.41	6.59	—	103.83	—	9j	Flx	37
Sengierite	Cu[(UO$_2$)(VO$_4$)](OH)(H$_2$O)$_3$	P2$_1$/a	10.599	8.093	10.085	—	103.42	—	9j		38
	Ni[(UO$_2$)$_2$(V$_2$O$_8$)](H$_2$O)$_4$	Pnam	10.6	8.25	15.12	—	—	—	9j		39
	Cs$_2$[(UO$_2$)$_2$(V$_2$O$_8$)]	P2$_1$/a	10.521	8.437	7.308	—	106.08	—	9j	SS[700]	40
	Cs[(UO$_2$)(NbO$_4$)]	P2$_1$/c	7.430	8.700	10.668	—	105.08	—	9j	SS[1200]	41
	K$_2$[(UO$_2$)$_2$(Cr$_2$O$_8$)]	P2$_1$/c	6.548	8.355	10.420	—	105.04	—	9j	HT[230]	42
	Rb$_2$[(UO$_2$)$_2$(Cr$_2$O$_8$)]	P2$_1$/c	6.868	8.359	10.463	—	106.00	—	9j	HT[220]	42
	Cs$_2$[(UO$_2$)$_2$(Cr$_2$O$_8$)]	P2$_1$/c	7.264	8.380	10.510	—	106.39	—	9j	HT[220]	42
	Ba[(UO$_2$)$_2$(TiO$_4$)]	P2$_1$/c	6.446	8.599	10.253	—	75.94	—	9j	SS[750]	43
	(NH$_4$)$_2$[(UO$_2$)$_2$(V$_2$O$_8$)]	P2$_1$/c	6.894	8.384	10.473	—	106.07	—	9j	HT[180]	44
	Mg$_2$[(UO$_2$)$_2$(Cr$_2$O$_8$)](H$_2$O)$_4$	Pnam	10.583	15.134	8.1425	—	—	—	9j	HT[230]	42
Metatyuyamunite	Ca[(UO$_2$)$_2$(VO$_4$)$_2$](H$_2$O)$_5$	Pbcn	8.575	10.584	16.856	—	—	—	9j		45

TABLE 8 (CONTINUED). U(VI) COMPOUNDS WITH SHEET ANION TOPOLOGIES CONSISTING OF TRIANGLES, SQUARES, AND PENTAGONS

MINERAL	FORMULA	SG	a (Å)	b (Å)	c (Å)	α (°)	β (°)	γ (°)	FIG	SYN[a]	REF
Sheets formed by chains of uranium polyhedra											
	$Cs_4 [(UO_2)_3O(MoO_4)_2(MoO_5)]$	$P1$	7.510	7.897	9.774	79.28	81.27	87.25	9l	SS[850]	46
	$Ag [(UO_2)(HTeO_5)]$	$Pbca$	7.085	11.986	13.913	—	—	—	9n	HT[220]	47
	$K_2 [(UO_2)_3(TeO_3)_2O_2]$	$P\bar{1}$	6.799	7.012	7.897	101.85	102.97	100.08	9p	SS[800]	48
	$Rb_2 [(UO_2)_3(TeO_3)_2O_2]$	$P\bar{1}$	7.010	7.074	8.085	105.51	101.76	99.46	9p	SS[800]	48
	$Cs_2 [(UO_2)_3(TeO_3)_2O_2]$	$P\bar{1}$	7.001	7.519	8.433	109.30	100.57	99.50	9p	SS[800]	48
	$Na_6 [(UO_2)_5(VO_4)_2O_5]$	$P2_1/c$	12.584	24.360	7.050	—	100.61	—	9r	Flx[775]	49
	$\beta\text{-}Rb_6 [(UO_2)5(VO4)_2O_5]$	$P2_1/n$	7.164	14.079	24.965	—	90.23	—	9r	SS[1200]	50
	$K_4 [(UO_2)_5(TeO_3)_2O_5]$	$P\bar{1}$	6.851	7.106	11.314	99.64	93.59	100.51	9s	Flx[800]	51
	$\alpha\text{-}Rb_6 [(UO_2)_5(VO_4)_2O_5]$	$C2/c$	24.887	7.099	14.376	—	103.92	—	9t	SS[650]	52
	$Ba_5Ca [(UO_2)_8(AsO_4)_4O_8]$	$P2_1/c$	12.073	12.838	13.472	—	116.97	—	10v	SS[1150]	53
	$CsNa_3 [(UO_2)_4O_4(Mo_2O_8)]$	$P\bar{1}$	6.466	6.906	11.381	84.33	77.91	80.23	9w	SS[950]	54
	$Ag_{10} [(UO_2)_8O_8(Mo_5O_{20})]$	$C2/c$	24.672	23.401	6.793	—	94.99	—	9y	SS[650]	55
	$K_2Na_8 (UO_2)_8(Mo_4O_{24})[(S,Mo)O_4]$	$C2/c$	24.282	12.117	13.6174	—	106.33	—	9y		56
	$Na_{10} [(UO_2)_8(W_5O_{20})O_8]$	$C2/c$	24.359	23.506	6.807	—	94.85	—	9y	SS[650]	52
Zippeite	$K_3(H_2O)_3 [(UO_2)_4(SO_4)_2O_3(OH)]$	$C2$	8.752	13.919	17.697	—	104.18	—	9aa		57
"Na zippeite"	$Na_5(H_2O)_{12} [(UO_2)_8(SO_4)_4O_5(OH)_3]$	$P2_1/n$	17.643	14.627	17.692	—	104.46	—	9aa	HT[100–220]	57
"Mg zippeite"	$Mg(H_2O)_{3.5} [(UO_2)_2(SO_4)O_2]$	$C2/m$	8.651	14.194	17.721	—	104.13	—	9aa	HT[100–220]	57
Magnesiozippeite	$Mg [(UO_2)_2O_2(SO_4)] (H_2O)_{3.5}$	$C2/m$	8.701	14.25	8.843	—	104.41	—	9aa		58
"Zn zippeite"	$Zn(H2O)_{3.5} [(UO_2)_2(SO_4)O_2]$	$C2/m$	8.644	14.166	17.701	—	104.04	—	9aa	HT[100–220]	57
"Co zippeite"	$Co(H2O)_{3.5} [(UO_2)_2(SO_4)O_2]$	$C2/m$	8.650	14.252	17.742	—	104.09	—	9aa	HT[100–220]	57
Marécottite	$Mg_3(H_2O)_{18} [(UO_2)_4O_3(OH)(SO_4)_2]_2 (H_2O)_{10}$	$P\bar{1}$	10.815	11.249	13.851	66.22	72.41	69.95	9aa		59
	$(NH_4)_4(H_2O) [(UO_2)_2(SO_4)O_2]_2$	$C2/m$	8.699	14.166	17.85	—	104.12	—	9aa	HT[100–220]	57
	$(NH_4)_2 [(UO_2)_2(SO_4)O_2]$	$Cmca$	14.252	8.775	17.186	—	—	—	9aa	HT[100–220]	57
	$Mg_2(H_2O)_{11} [(UO_2)_2(SO_4)O_2]_2$	$P2_1/c$	8.646	17.200	18.464	—	102.119	—	9aa	HT[100–220]	57
	$K_{0.5}Zn_{0.75} [(UO_2)_2(SO_4)O_2] (H_2O)_3$	$C2/c$	8.650	14.180	17.709	—	104.14	—	9aa	HT[150]	60
	$K_{0.5}Mn_{0.75} [(UO_2)_2(SO_4)O_2] (H_2O)_3$	$C2/c$	8.661	14.375	17.705	—	104.12	—	9aa	HT[150]	60
	$K_{0.5}Co_{0.75} [(UO_2)_2(SO_4)O_2] (H_2O)_3$	$C2/c$	8.651	14.188	17.713	—	104.14	—	9aa	HT[150]	60
	$K_{0.5}Ni_{0.75} [(UO_2)_2(SO_4)O_2] (H_2O)_3$	$C2/c$	8.662	14.095	17.770	—	104.18	—	9aa	HT[150]	60
Nat. Zippeite	$K_{1.85}H_{0.15} [(UO_2)_4O_2(SO_4)_2 (OH)_2] (H_2O)_4$	$C2/m$	8.780	13.990	8.863	—	104.52	—	9aa		61
Sejkoraite-(Y)	$(Y_{1.98}Dy_{0.24})H_{0.34} [(UO_2)_8O_7(OH)(SO_4)_4] (H_2O)_{26}$	$P\bar{1}$	14.074	17.417	17.706	75.93	128.00	74.42	9aa		62
	$K_2(UO_2)_2(MoO_4)O_2$	$P2_1/c$	8.249	15.337	8.351	—	104.75	—	9aa	Flx[950]	63
Rabejacite	$Ca_2 [(UO_2)_4O_4(SO_4)_2] (H_2O)_8$	$P\bar{1}$	8.743	8.309	8.869	77.86	104.64	82.94	9aa		64
	$Zn [(UO_2)_2(SO_4)(OH)_4] (H_2O)_{1.5}$	$B112/m$	8.654	17.714	14.182	—	—	103.92	9aa		65
	$Rb_2 [(UO_2)_2(MoO_4)O_2]$	$P2_1/c$	8.542	15.360	8.436	—	104.28	—	9ad	SS[1000]	66

TABLE 8 (CONTINUED). U(VI) COMPOUNDS WITH SHEET ANION TOPOLOGIES CONSISTING OF
TRIANGLES, SQUARES, AND PENTAGONS

MINERAL	FORMULA	SG	a (Å)	b (Å)	c (Å)	α (°)	β (°)	γ (°)	FIG	SYN[a]	REF
Sheets of uranyl polyhedra											
	$K_2 [(UO_2)_2(WO_5)O]$	$P2_1/n$	8.083	28.724	9.012	—	102.14	—	9af	SS[650]	52
	$Rb_2 [(UO_2)_2(WO_5)O]$	$P2_1/n$	8.234	28.740	9.378	—	104.59	—	9af	SS[650]	52
	$Tl_2 [(UO_2)_2O(MoO_5)]$	$P2_1/n$	8.253	28.508	9.156	—	104.12	—	9af	SS[650]	67
	$Cs_2 [(UO_2)_2(WO_6)]$	$P2_1/n$	8.611	28.910	9.499	—	107.73	—	9af	SS[600-1000]	68
	$K_8 [(UO_2)_8(MoO_5)_3O_6]$	$P4/n$	23.488	23.488	6.786	—	—	—	9ah	SS[950}	63
	$Cs_9 [(UO_2)_8O_4(NbO_5)(Nb_2O_5)_2]$	$P2_1/c$	16.729	14.933	20.155	—	110.59	—	9aj	SS[1400]	69
Sayrite	$Pb_2 [(UO_2)_5O_6(OH)_2] (H_2O)_4$	$P2_1/c$	10.704	6.96	14.533	—	116.81	—	9al		70
	$Na_6 [(UO_2)_5(VO_4)_2O_5]$	$P2_1/c$	12.548	24.360	7.050	—	101.61	—	9al		49
	$K_6 [(UO_2)_5(VO_4)_2O_5]$	$P2_1/c$	6.856	24.797	7.135	—	98.79	—	9al	SS[775]	49
	$KNa_3 [(UO_2)_5O_8(SO_4)]$	$Pbca$	13.286	13.726	19.712	—	—	—	9al	SS[700]	88
	$K_2 [(UO_2)_5O_8(UO_2)_2]$	$Pbam$	6.945	19.533	7.215	—	—	—	9al	SS	71
Wölsendorfite	$Pb_{6.16}Ba_{0.36} [(UO_2)_{14}O_{19}(OH)_4] (H_2O)_{12}$	$Cmcm$	14.131	13.885	55.969	—	—	—	9an		72
	$\beta\text{-}U_3O_8$	$Cmcm$	7.069	11.445	8.303	—	—	—	9ap		73
Ianthinite	$[U_2^{4+}(UO_2)_4O_6(OH)_4(H_2O)_4] (H_2O)_5$	$P2_1cn$	7.178	11.473	30.39	—	—	—	9ap		74
Spriggite	$Pb_3 [(UO_2)_6O_8(OH)_2] (H_2O)_3$	$C2/c$	28.355	11.990	13.998	—	104.248	—	9ap		75
	$[U^{5+}(H_2O)_2(UO_2)_2O_4(OH)] (H_2O)_4$	$Immm$	7.176	11.400	15.310	—	—	—	9ap	HT[120]	76
Wyartite	$CaU^{5+}(UO_2)_2(CO_3)O_4(OH) (H_2O)_7$	$P2_12_12_1$	11.271	7.106	20.807	—	—	—	9aq		77
Wyartite-Dehyd.	$Ca [(CO_3)[U^{5+}(U^{6+}O_2)_2O_4(OH)] (H_2O)_3$	$Pmnc$	11.261	7.087	16.836	—	—	—	9aq		78
	$K [(UO_2)_2(UO_4)(OH)(NO_3)_2] (H_2O)$	$Pbca$	7.268	17.119	21.551	—	—	—	9ar	HT[220]	79
	$Ba [(UO_2)_2(UO_4)(OH)(NO_3)_2] (H_2O)_2$	$Pbca$	7.262	17.097	21.549	—	—	—	9ar	HT[220]	79
	$Cs_7 [(UO_2)_8O_4]_2ClO_8]$	$Pmmn$	21.458	11.773	7.495	—	—	—	9as	SS[725]	80
	$Rb_7 [(UO_2)_8(VO_4)_2ClO_8]$	$Pmcn$	21.427	11.814	14.203	—	—	—	9as	SS[600]	80
	$Cs_4 [(UO_2)_5O_7]$	$Pbcn$	18.776	7.070	14.958	—	—	—	9au	SS[600]	81
	$Rb_4 [(UO_2)_5O_7]$	$Pbcn$	18.676	7.049	14.121	—	—	—	9au	SS[1300]	82
	$Rb_8U_9O_{31}$	$Pbna$	6.993	14.288	34.062	—	—	—	9aw		83
	$K_5 [(UO_2)_{10}O_8(OH)_9] (H_2O)$	Pn	13.179	20.895	13.431	—	106.3216	—	9ay	HT[225]	84
	$Ca [(UO_2)_4O_3(OH)_4] (H_2O)_2$	$P\bar{1}$	8.0556	8.4212	10.958	78.878	87.922	72.2877	9ba	HT[200]	85
Curite	$Pb_3 [(UO_2)_8O_8(OH)_6] (H_2O)_{23}$	$Pnam$	12.548	13.013	8.389	—	—	—	9bc		86
	$Sr_{2.82}(H_2O)_2 [(UO_2)_4O_{3.82}(OH)_{3.18}]_2$	$Pnam$	12.314	12.961	8.405	—	—	—	9bc	HT[185]	87

Note: Double lines (═) indicate major differences in the stoichiometry of the structural unit, as indicated by the corresponding header in the table; single lines (–) indicates different topologic configurations; and dotted lines (- -) separate graphical isomers.

[a] Synthesis column data. HT[T] and SS[T] correspond to hydrothermal and solid state synthesis, respectively, at maximum reported temperature T (°C); V-Cl: vapor phase chlorination; A, aqueous (Ae denotes evaporation to dryness); Ac, concentrated acid; Flx, molten flux; SDg, slow diffusion in gel.

References: (1) Gasperin (1988); (2) Gasperin (1990); (3) Ginderow (1988); (4) Burns (1998a); (5) Burns (1999b); (6) Rosenzweig & Ryan (1975); (7) Ryan & Rosenzweig (1977); (8) Rosenzweig & Ryan (1977a); (9) Piret & Piretmeunier (1994); (10) Bachet *et al.* (1991); (11) Kubatko & Burns (2006c); (12) Viswanathan & Harneit (1986); (13) Kolitsch & Giester (2001); (14) Villa *et al.* (2013b); (15) Krivovichev & Burns (2000); (16) Alekseev *et al.* (2007c); (17) Saine (1989); (18) Dickens *et al.* (1993); (19) Meunier & Galy (1973); (20) Gasperin (1987b); (21) Alekseev *et al.* (2005b); (22) Surble *et al.* (2006); (23) Siegel *et al.* (1972b); (24) Obbade *et al.* (2003a); (25) Krivovichev & Burns (2003i); (26) Krivovichev & Burns (2000); (27) Krivovichev & Burns (2002c); (28) Lee & Jaulmes (1987); (29) Serezhkina *et al.* (1990); (30) Serezhkina *et al.* (2010); (31) Ok *et al.* (2006); (32) Rosenzweig & Ryan (1977b); (33) Hughes *et al.* (2003); (34) Mereiter (1986b); (35) Alekseev *et al.* (2004); (36) Borene & Cesbron (1971); (37) Appleman & Evans (1965); (38) Piret *et al.* (1980); (39) Borene & Cesbron (1970); (40) Dickens *et al.* (1992); (411) Gasperin (1987d); (42) Locock *et al.* (2004c); (43) Wallwork *et al.* (2006); (44) Rivenet *et al.* (2007); (45) Burciaga-Valencia *et al.* (2010); (46) Krivovichev & Burns (2002b); (47) Ling *et al.* (2011); (48) Woodward *et al.* (2004); (49) Dion *et al.* (2000); (50) Obbade *et al.* (2003b); (51) Woodward & Albrecht-Schmitt (2005); (52) Obbade *et al.* (2003a); (53) Alekseev *et al.* (2011); (54) Nazarchuk *et al.* (2009); (55) Krivovichev & Burns (2003d); (56) Krivovichev (2014); (57) Burns *et al.* (2003); (58) Plášil *et al.* (2013c); (59) Brugger *et al.* (2003); (60) Peeters *et al.* (2008); (61) Plášil *et al.* (2011b); (62) Plášil *et al.* (2011a); (63) Obbade *et al.* (2003c); (64) Plášil *et al.* (2014a); (65) Spitsyn *et al.* (1982); (66) Alekseev *et al.* (2007e); (67) Krivovichev & Burns (2003b); (68) Alekseev *et al.* (2006d); (69) Saad *et al.* (2008); (70) Piret *et al.* (1983); (71) Kovba (1972); (72) Burns (1999c); (73) Loopstra (1970); (74) Burns *et al.* (1997b); (75) Brugger *et al.* (2004); (76) Belai *et al.* (2008); (77) Burns & Finch (1999); (78) Hawthorne *et al.* (2006); (79) Unruh *et al.* (2010); (80) Duribreux *et al.* (2003); (81) van Egmond (1976); (82) Saad *et al.* (2009); (83) Yagoubi *et al.* (2005); (84) Burns & Hill (2000b); (85) Glatz *et al.* (2002); (86) Li & Burns (2000a); (87) Burns & Hill (2000a); (88) Krivovichev (2008c).

TABLE 9. U(VI) COMPOUNDS WITH SHEET ANION TOPOLOGIES CONSISTING OF TRIANGLES, SQUARES, PENTAGONS AND HEXAGONS

MINERAL	FORMULA	SG	a (Å)	b (Å)	c (Å)	α (°)	β (°)	γ (°)	SYN[a]	FIG	REF
Phosphuranylite	$KCa[(H_3O)_3(UO_2)_7(PO_4)_2O_2]_2(H_2O)_8$	$Cmcm$	15.899	13.740	17.300	—	—	—		10b	1
Upalite	$Al[(UO_2)_3(PO_4)_2O(OH)](H_2O)_7$	$P2_1/a$	13.704	16.820	9.332	—	111.5	—		10b	2
Francoisite-Nd	$Nd[(UO_2)_3(PO_4)_2O(OH)](H_2O)_6$	$P2_1/c$	9.298	15.605	13.668	—	112.77	—		10b	3
Dewindtite	$Pb_3[(UO_2)_3O_2(PO_4)_2]_2(H_2O)_{12}$	$Bmmb$	16.031	17.264	13.605	—	—	—		10b	4
Dumontite	$Pb_2[(UO_2)_3(PO_4)_2O_2](H_2O)_5$	$P2_1/m$	8.118	16.819	6.983	—	109.03	—		10c	5
Hügelite	$Pb_2[(UO_2)_3(AsO_4)_2](H_2O)_5$	$P2_1/m$	31.066	17.303	7.043	—	96.49	—		10c	6
Vanmeersscheite	$U(OH)_4[(UO_2)_3(PO_4)_2(OH)_2](H_2O)_4$	$P2_1mn$	17.06	16.760	7.023	—	—	—		10c	7
Phurcalite	$Ca_2[(UO_2)_3(PO_4)_2O_2](H_2O)_7$	$Pbca$	17.415	16.035	13.598	—	—	—		10d	8
Phuralumite	$Al_2[(UO_2)_3(PO_4)_2(OH)_2](OH)_4(H_2O)_{10}$	$P2_1/a$	13.836	20.918	9.428	—	112.44	—		10e	9
Althupite	$AlTh(UO_2)[(UO_2)_3(PO_4)_2O(OH)]_2(OH)_3(H_2O)_{15}$	$P\bar{1}$	10.953	18.567	13.504	72.64	68.2	84.21		10e	10
Bergenite	$Ca_2Ba_4[(UO_2)_3O_2(PO_4)_2]_3(H_2O)_{16}$	$P2_1/c$	10.092	17.245	17.355	—	113.68	—		10f	11
Fontanite	$Ca[(UO_2)_3(CO_3)_2O_2](H_2O)_6$	$P2_1/n$	6.968	17.276	15.377	—	90.06	—		10g	12
Marthozite	$Cu[(UO_2)_3(SeO_3)_2O_2](H_2O)_8$	$Pbn2_1$	6.988	16.454	17.223	—	—	—		10h	13
Guilleminite	$Ba[(UO_2)_3(SeO_3)_2O_2](H_2O)_3$	$P2_1nm$	7.084	7.293	16.881	—	—	—		10h	14
Larisaite	$Na(H_3O)[(UO_2)_3(SeO_3)_2O_2](H_2O)_4$	$P11m$	6.981	7.646	17.249	—	—	90.04		10h	15
	$Sr[(UO_2)_3(SeO_3)_2O_2](H_2O)_4$	$C2/m$	17.014	7.064	7.108	—	100.54	—	SCW[425]	10i	16
Johannite	$Cu[(UO_2)_2(SO_4)_2(OH)_2](H_2O)_8$	$P\bar{1}$	8.903	9.499	6.812	109.87	112.01	100.40		10j	17
	$Sr[(UO_2)_2(CrO_4)_2(OH)_2](H_2O)_8$	$P\bar{1}$	8.923	9.965	11.602	106.63	99.09	97.26	Rs	10j	18
	$(Hg_5O_2(OH)_4)[(UO_2)_2(AsO_4)_2]$	$P\bar{1}$	6.823	6.879	9.596	109.46	104.84	93.87	HT[200]	10j	19
	$Rb_{1.08}[(UO_2)F(HPO_4)]$	$Cmc2_1$	17.719	6.877	12.139	—	—	—	HT[200]	10k	20
Deliensite	$Fe[(UO_2)_2(SO_4)_2(OH)_2](H_2O)_7$	$Pnn2$	15.851	16.248	6.894	—	—	—		10l	21
	$Cs[(UO_2)(OH)(SeO_4)](H_2O)_{1.5}$	$P2_1/m$	7.214	14.494	8.927	—	112.71	—		10m	22
Roubaultite	$[Cu_2(UO_2)_3(CO_3)_2O_2(OH)_2](H_2O)_4$	$P\bar{1}$	7.767	6.924	7.850	92.16	90.89	93.48		10o	23
	$Cs_2[(UO_2)_4(Co(H_2O)_2)_2(HPO_4)_4(PO_4)]$	$C2/c$	18.055	10.748	15.350	—	99.24	—	HT[195]	10q	24

Note: Double lines (=) indicate major differences in the stoichiometry of the structural unit, as indicated by the corresponding header in the table; single lines (–) indicates different topologic configurations; and dotted lines (- -) separate graphical isomers.
[a] Synthesis column data. HT[T] and SS[T] correspond to hydrothermal and solid state synthesis, respectively, at maximum reported temperature T (°C); V-Cl: vapor phase chlorination; A, aqueous (Ae denotes evaporation to dryness); Ac, concentrated acid; Flx, molten flux; SDg, slow diffusion in gel.
References: (1) Demartin *et al.* (1991); (2) Piret & Declercq (1983); (3) Piret *et al.* (1988); (4) Piret *et al.* (1990); (5) Piret & Piretmeunier (1988); (6) Locock & Burns (2003f); (7) Piret & Deliens (1982); (8) Atencio *et al.* (1991); (9) Piret *et al.* (1979); (10) Piret & Deliens (1987); (11) Locock & Burns (2003a); (12) Hughes & Burns (2003a); (13) Cooper & Hawthorne (2001); (14) Cooper & Hawthorne (1995); (15) Chukanov *et al.* (2004); (16) Almond & Albrecht-Schmitt (2004); (17) Mereiter (1982a); (18) Serezhkin *et al.* (1982); (19) Yu *et al.* (2009); (20) Ok *et al.* (2006); (21) Plášil *et al.* (2012a); (22) Serezhkina *et al.* (2010); (23) Ginderow & Cesbron (1985); (24) Shvareva & Albrecht-Schmitt (2006).

synthesized at elevated temperatures (*i.e.*, > 200 °C). There is no obvious correlation between the interlayer composition and the ring size within the sheet, suggesting that the interlayer cations, where they are present, do not serve to 'template' the sheet topology.

The topological differences that distinguish the vertex-sharing sheets are subtle. Correspondingly, a detailed discussion of each type adds little to our understanding of these structures. Instead, a series of generalized observations are presented. In the {3.6.3.6} parent graphs, all the U^{6+} is present as uranyl ions. In the 62 structures based on the {3.6.3.6} parent graph the following ligands occur: SeO_4 (15 structures), SeO_3 (10), PO_4 (2), SO_4 (7), CrO_4 (8), HPO_3 (4), MoO_4 (10), and IO_3 (2). Trends between ligand speciation and sheet topology are ambiguous. For instance, (SeO_4) tetrahedra occur in seven structure topologies, (CrO_4) tetrahedra occur in four, and (SeO_3) distorted tetrahedra occur in four. In contrast, (MoO_4) tetrahedra all occur in sheets with the I1/2d (Fig. 5ag) topology (except for one) and (SO_4) tetrahedra are all in sheets with the I1/2b (Fig. 5z) topology.

Structures with a *U:L* stoichiometry of 1:2 are the most common (as observed in Burns 2005), with major types of graphical arrangements being I1/2b (Fig. 5aa) and I1/2d (Fig. 5ah–aj); these correspond to 13 and 21 compounds, respectively. Krivovichev & Kahlenberg (2004) list at least 12 different topologies of 1:2 graphs. Of these, only three contain eight-membered rings of nodes, and two are I1/2b and I1/2d.

In some cases, the arrangement of uranyl bipyramids, irrespective of the ligand tetrahedra, may be related to the topologies of other known sheets. For example, $Rb_4[(UO_2)_3(SeO_4)_5(H_2O)]$ (Fig. 5s) consists of uranyl pentagonal bipyramids that are linked by either four or five tetrahedra *via* vertex-sharing. Removing the tetrahedra and connecting the bipyramids results in the α-U_3O_8 topology (Fig. 5h). Similarly, the sheet topology shown in Figure 5aa,

TABLE 10. U(VI) COMPOUNDS WITH SHEET ANION TOPOLOGIES WITH TRIANGLES AND HEXAGONS

MINERAL	FORMULA	SG	a (Å)	b (Å)	c (Å)	α (°)	β (°)	γ (°)	SYN[a]	FIG	REF
Rutherfordine	$[UO_2CO_3]$	$Imm2$	4.840	9.273	4.298	—	—	—	—	11b	1
	$[(UO_2)(SeO_3)]$	$P2_1/m$	5.408	9.278	4.2545	—	93.45	—	Flx[950]	11c	2
Widenmannite	$Pb_{1.85}[(OH)_{1.7}(H_2O)_{0.15}][(UO_2)(CO_3)_2]$	$Pmmn$	4.977	9.387	8.9597	—	—	—	—	11e	3
	$[(UO_2)(B_2O_3)O]$	$C2/c$	12.504	4.183	10.453	—	122.18	—	SS[1423]	11g	4
	$[(UO_2)(B_2O_3)O)]$	$C2$	10.461	4.186	5.6251	—	109.77	—	AF[190]	11g	5
Tr₇Hx₁-type sheets											
Isolated sheets											
	$K_{11}[(UO_2)_6(B_{24}O_{36})F_{22}][H_2BO_3]$	$P6_3/m$	11.091	11.091	26.577	—	—	120	HT[220]	11i	6
	$Na[(UO_2)(B_9O_{15})(OH)F(H_2O)]$	Cc	11.185	6.401	14.191	—	104.63	—	HT[220]	11j,k	6
	$K[(UO_2)_2(B_{10}O_{15})(OH)_5]$	$C2/c$	6.464	11.115	25.419	—	96.37	—	HT[190]	11j,k	7
	$Tl[(UO_2)(B_5O_8)(OH)F]$	$P1$	6.416	6.466	7.136	103.28	92.05	119.58	HT[220]	11j,k	6
	$K[(UO_2)_2B_{10}O_{16}(OH)_8]$	$C2/c$	6.464	11.115	25.419	—	96.37	—		11j,k	7
	$K[(UO_2)(B_5O_8)(OH)F]$	$P2_1/n$	6.443	13.439	10.799	—	90.63	—	HT[220]	11l,m	6
	$Rb[(UO_2)(B_5O_8)(OH)F]$	Cc	11.144	6.483	13.874	—	95.46	—	HT[220]	11n,o	6
Double sheets											
	$(UO_2)_2(B_{13}O_{20}(OH)_3)(H_2O)_{1.25}$	$P\bar{1}$	6.473	10.798	19.665	85.71	82.66	89.29	HT[190]	11p,q	5
	$\alpha\text{-}(UO_2)_2(B_9O_{14}(OH)_4)$	$P2_1$	6.453	21.254	6.455	—	119.87	—		11r,t	5
	$Rb[(UO_2)_2B_{10}O_{16}(OH)_3(H_2O)_{0.7}]$	$P2_1/m$	6.406	26.028	6.457	—	119.72	—		11r,u	7
	$\beta\text{-}(UO_2)_2(B_9O_{14}(OH)_4)$	$P\bar{1}$	6.417	6.449	11.018	97.60	92.37	119.48		11v,w	5
	$K_2[(UO_2)_2B_{12}O_{19}(OH)_4](H_2O)_{0.3}$	$P3_112$	6.442	6.442	47.457	—	—	120		11x,y	7
	$Rb_2[(UO_2)_2B_{13}O_{20}(OH)_5]$	$P2_1/n$	6.445	11.097	33.997	—	92.26	—		11x,y	7
Linked sheet											
	$Na[(UO_2)(B_6O_{10})(OH)](H_2O)_2$	Cc	6.391	11.139	15.987	—	92.77	—	HT[200]	11n,z	8

Note: Double lines (=) indicate major differences in the stoichiometry of the structural unit, as indicated by the corresponding header in the table; single lines (–) indicates different topologic configurations; and dotted lines (- -) separate graphical isomers.

[a] Synthesis column data. HT[T] and SS[T] correspond to hydrothermal and solid state synthesis, respectively, at maximum reported temperature T (°C); V-Cl: vapor phase chlorination; A, aqueous (Ae denotes evaporation to dryness); Ac, concentrated acid; Flx, molten flux; SDg, slow diffusion in gel.

References: (1) Finch *et al.* (1999); (2) Loopstra & Brandenburg (1978); (3) Plášil *et al.* (2014c); (4) Gasperin (1987a); (5) Wang *et al.* (2010c); (6) Wang *et al.* (2011a); (7) Wang *et al.* (2010b); (8) Wang *et al.* (2010a).

which occurs in nine compounds (Table 5), equates to the α-U_3O_8 topology with the pentagonal chains removed, and the topologically identical sheet shown in Figure 5ap differs only in the orientation of the bipyramids.

Various sheets contain features that are noteworthy. The sheet in $(H_3O)[(UO_2)(SeO_4)(SeO_2OH)](H_2O)_6$ (Fig. 5aj) is the only vertex-sharing sheet known that contains two types of ligand polyhedra, SeO_4 tetrahedra and SeO_3H tetrahedra, wherein the lone electron pair in the latter occupies the fourth tetrahedral apex. The compound $[UF_4O(SbF_5)_2]$ contains the only sheet in this class with octahedral ligands (Fig. 5as). Here, the shared polyhedral elements correspond to F anions. The compound $K[(UO_2)(IO_3)_3]$ (Fig. 5ad) contains a sheet topology closely related to the I1/2b graphs in Figure 5aa–ab but is the only sheet of this group that contains a decorative (*i.e.*, non-structural) ligand that does not bridge two distinct uranyl polyhedra.

Miscellaneous sheets based on vertex-sharing polyhedra

Table 6 and Figure 6 list and illustrate, respectively, nine compounds (seven sheet topologies) that contain sheets based predominantly on the sharing of

vertices, but with topologies that cannot be derived from either of the three parent graphs discussed above. All of these contain isolated uranyl polyhedra that are linked to the remainder of the structural unit *via* vertex-sharing. Hence, the structures in this category can be arranged with increasing topological complexity of the linkages of non-uranyl polyhedra.

The isostructural compounds $K_2[(UO_2)(As_2O_7)]$ and $Cs_2[(UO_2)(P_2O_7)]$ contain the sheet shown in Figure 6a. This contains uranyl square bipyramids linked through pyroarsenate or pyrophosphate tetrahedral dimers. This sheet can be derived from the autunite sheet topology by replacing the normally observed ($T\Phi_4$) groups with ($T_2\Phi_7$) groups.

The isostructural compounds $Na_6[(UO_2)_2(AsO_4)_2(As_2O_7)]$ and $Ag_6[(UO_2)_2(AsO_4)_2(As_2O_7)]$ contain the sheet illustrated in Figure 6b. These consist of uranyl pentagonal bipyramids linked *via* vertex-sharing with monomeric and dimeric tetrahedral groups. The compound $Ag_6[(UO_2)_2(AsO_4)(As_4O_{13})]$ contains uranyl pentagonal bipyramids that are linked to form sheets by ($T\Phi_4$) tetrahedra occurring as both dimers of polyhedra and vertex-sharing tetramers of tetrahedra (Fig. 6c). Both the dimeric and tetrameric units link four isolated uranyl polyhedra. Similarly, the structure of $K[(UO_2)(P_3O_9)]$ contains uranyl pentago-

TABLE 11. U(VI) COMPOUNDS CONTAINING SHEETS WITH MISCELLANEOUS TOPOLOGIES

MINERAL	FORMULA	SG	a (Å)	b (Å)	c (Å)	α(°)	β (°)	γ (°)	FIG	SYN[a]	REF
Miscellaneous sheets with hexagons											
	α-UO_3	$C2mm$	3.961	6.860	4.166	—	—	—	12b		1
	α-$(UO_2)(OH)_4$	$Cmca$	4.242	10.302	6.868	—	—	—	12b	HT[290]	2
	$Bi_2[(UO_2)O_2]O_2$	$C2$	6.872	4.009	9.690	—	90.16	—	12b	SS[800]	3
	α-$Cs_2(U_2O_7)(D_2O)_{0.444}$	$C2/m$	14.531	4.274	7.601	—	113.02	—	12b	SS[600]	4
	$Ca[(UO_2)O_2]$	$R\bar{3}m$	6.268	6.268	6.268	36.04	36.04	36.04	12b	SS[1000]	5
	α-$Cd[(UO_2)O_2]$	$R\bar{3}m$	6.233	6.233	6.233	36.12	36.12	36.12	12b	HT[520]	6
	$(Na_2U_2O_7)_{0.5}$	$R\bar{3}m$	6.34	6.34	6.34	36.11	36.11	36.11	12b		7
	$K_2[(UO_2)_2O_3]$	$R\bar{3}m$	3.96	3.96	19.82	—	—	120	12b	Flx[1520]	8
	$[(UO_2)TiNb_2O_8]$	$Fddd$	7.28	12.62	16.02	—	—	—	12d		9
	$[(UO_2)Nb_3O_8]$	$Fddd$	7.38	12.78	15.96	—	—	—	12d		10
	$Cs(UO_2)(VO_3)_3$	$P2_1/a$	11.904	6.821	12.095	—	106.99	—	12d	SS[300–650]	11
	$[(UO_2)(Sb_2O_4)]$	$C2/m$	13.49	4.003	5.142	—	104.17	—	12f	HT[180]	12
	$Ag_4[(UO_2)_4(IO_3)_2(IO_4)_2O_2]$	$P2_1/n$	15.040	8.051	18.332	—	100.74	—	12h	HT[650]	13
	$Cs_4[(UO_2)_2(V_2O_7)O_2]$	$Pmmn$	8.483	13.426	7.137	—	—	—	12i	SS[980]	14
Sheets with miscellaneous sheet-anion topologies											
	$K[(UO_2)(CrO_4)(NO_3)]$	$P2_1/c$	9.881	7.215	14.226	—	124.85	—	12j	SS[270]	15
	$Rb[(UO_2)(CrO_4)(NO_3)]$	$P2_1/c$	9.804	7.359	14.269	—	122.05	—	12j	SS[270]	15
	$Tl_3((UO_2)_2[Te_2O_5(OH)](Te_2O_6)\}(H_2O)_2$	$Pbam$	10.062	23.024	7.939	—	—	—	12k	HT[180]	16
	$[(UO_2)(Se_2O_5)]$	$P\bar{1}$	9.405	11.574	6.698	93.01	93.66	109.69	12l	HT[447]	17
	$Ag_6[(UO_2)_3O(MoO_4)_5]$	$C2/c$	16.451	11.324	12.742	—	100.01	—	12m	SS[650]	18
Mathesiusite	$K_5[(UO_2)_4(SO_4)_4(VO_5)](H_2O)_4$	$P4/n$	14.970	14.970	6.817	—	—	—	12n		19
	$Cs_8[(UO_2)_4(OH)_2(H_2O)_2]$	$I4cm$	15.959	15.959	14.215	—	—	—	12o	HT[180]	20
	$Rb(UO_2(SeO_4)F)(H_2O)$	$Pnma$	8.475	13.523	13.529	—	—	—	12p	Ae	21
	$NH_4[(UO_2)F(SeO_4)](H_2O)$	$Pnma$	8.450	13.483	13.569	—	—	—	12p		22
Haiweeite	$Ca[(UO_2)_2Si_5O_{12}(OH)_2](H_2O)_3$	$Cmcm$	7.125	17.937	18.342	—	—	—	12q		23
Bijvoetite	$[M^{3+}(H_2O)_{25}(UO_2)_{16}O_8(OH)_8(CO_3)_{16}](H_2O)_{14}$	$B2_1$	21.234	12.958	44.911	—	—	—	12r		24
	$K_2[(UO_2)_3F_8(H_2O)](H_2O)_3$	$C2cm$	8.39	14.12	13.66	—	—	—	12s		25
	$Rb_2[U_2O_7]$	$P2_1/c$	7.323	8.004	6.950	—	108.81	—	12t	SS[750]	26
	β-$Cs_2[(UO_2)_2O_3)]$	$C2/m$	14.615	4.319	7.465	—	113.78	—	12u	SS[600]	27
	$Na_5[(UO_2)_3(O_2)_4(OH)_3](H_2O)_{13}$	$Cmca$	23.632	15.886	13.952	—	—	—	12v		28
	$Na_{5.5}[(UO2)_3(H_{0.5}PO_4)(PO_4)_5]$	$P1$	6.675	6.922	10.732	83.96	82.29	89.44	12w		29
	$Na_7(U^{IV}O_2)(U^{V}O)(U^{V/VI}O_2)_2Si_4O_{16}$	$P\bar{1}$	6.793	6.969	11.916	95.47	98.37	90.69	12w		30

Note: Double lines (=) indicate major differences in the stoichiometry of the structural unit, as indicated by the corresponding header in the table; single lines (–) indicates different topologic configurations; and dotted lines (- -) separate graphical isomers.
[a] Synthesis column data. HT[T] and SS[T] correspond to hydrothermal and solid state synthesis, respectively, at maximum reported temperature T (°C); V-Cl: vapor phase chlorination; A, aqueous (Ae denotes evaporation to dryness); Ac, concentrated acid; Flx, molten flux; SDg, slow diffusion in gel.
References: (1) Loopstra & Cordfunke (1966); (2) Taylor (1971); (3) Koster *et al*. (1975); (4) Mijlhoff *et al*. (1993); (5) Loopstra & Rietveld (1969); (6) Yamashita *et al*. (1981); (7) Kovba *et al*. (1958); (8) Jove *et al*. (1988); (9) Chevalier & Gasperin (1969); (10) Chevalier & Gasperin (1968); (11) Duribreux *et al*. (1999); (12) Sykora *et al*. (2004b); (13) Bean *et al*. (2001a); (14) Obbade *et al*. (2004b); (15) Siidra *et al*. (2012a); (16) Almond & Albrecht-Schmitt (2002a); (17) Trombe *et al*. (1985); (18) Krivovichev & Burns (2002d); (19) Plášil *et al*. (2014d); (20) Sykora & Albrecht-Schmitt (2004); (21) Serezhkina *et al*. (2011); (22) Blatov *et al*. (1989); (23) Plášil; *et al*. (2013a); (24) Li *et al*. (2000); (25) Dao *et al*. (1979); (26) Yagoubi *et al*. (2005); (27) van Egmond (1976); (28) Kubatko & Burns (2006a); (29) Gorbunova *et al*. (1980); (30) Lee *et al*. (2010).

nal bipyramids that are linked by five-membered chains of vertex-sharing tetrahedra (Fig. 6d). Each chain links four separate uranyl pentagonal bipyramids, three by monodentate and one by bidentate connections. The structure of $K[(UO_2)(Te_2O_5)(OH)]$ contains uranyl square bipyramids that are linked to infinite chains of very irregular vertex-sharing ($Te\Phi_4$) tetrahedra (Fig. 6e). The structure of $Pb[(UO_2)(SeO_3)_2]$ contains uranyl pentagonal bipyramids edge-sharing with lone-pair electron stereoactive (SeO_3) groups (Fig. 6f). Although this edge-sharing, in the strict sense, violates the rules for inclusion into this class, it is listed here because the $[(UO_2)(SeO_3)]$ edge-sharing clusters are linked exclusively by vertex-sharing. These $U=L$ clusters link to form infinite, parallel chains; these chains are in turn linked to each other *via* vertex-sharing with additional SeO_3 groups. The structure of $Pb[(UO_2)(TeO_3)]$ exhibits a similar structure (Fig. 6g). Here, irregular lone-pair electron stereoactive (TeO_3) polyhedra link uranyl pentagonal bipyramids to form the observed sheet. For each bipyramid, two of the equatorial anions are shared with (TeO_3) groups and three additional (TeO_3) groups link to the equatorial anions *via* vertex-sharing.
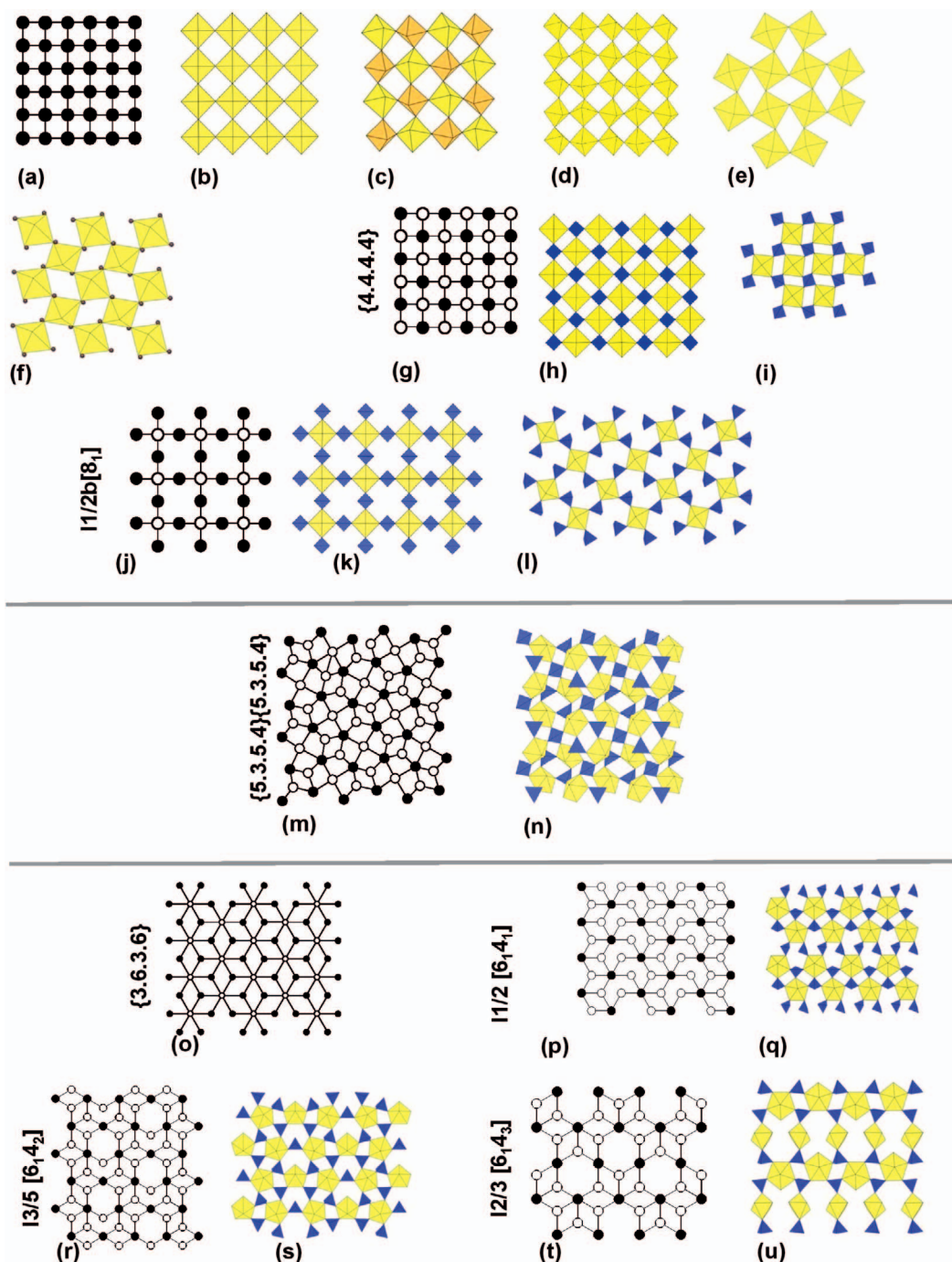
FIG. 5. Sheets dominated by vertex-sharing between uranyl and other ligand polyhedra (containing high-valence cations) found in the synthetic compounds and minerals listed in Tables 4 and 5. Graphic representations (and nomenclature) are according to the guidelines of Krivovichev (2004).

(v) (w) (x) (y)

(z) (aa) (ab)

(ac) (ad)

(ae) (af)

(ag) (ah)
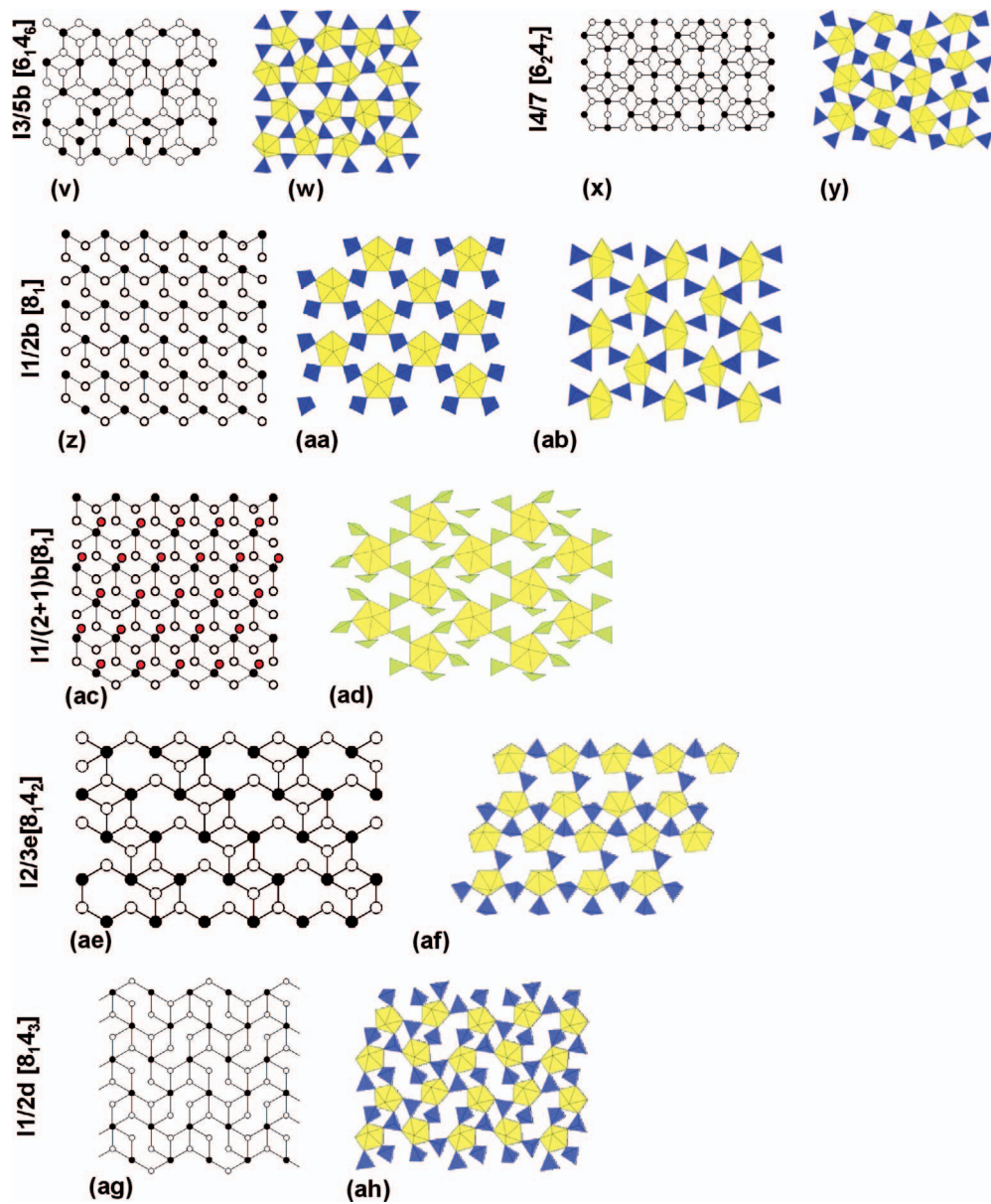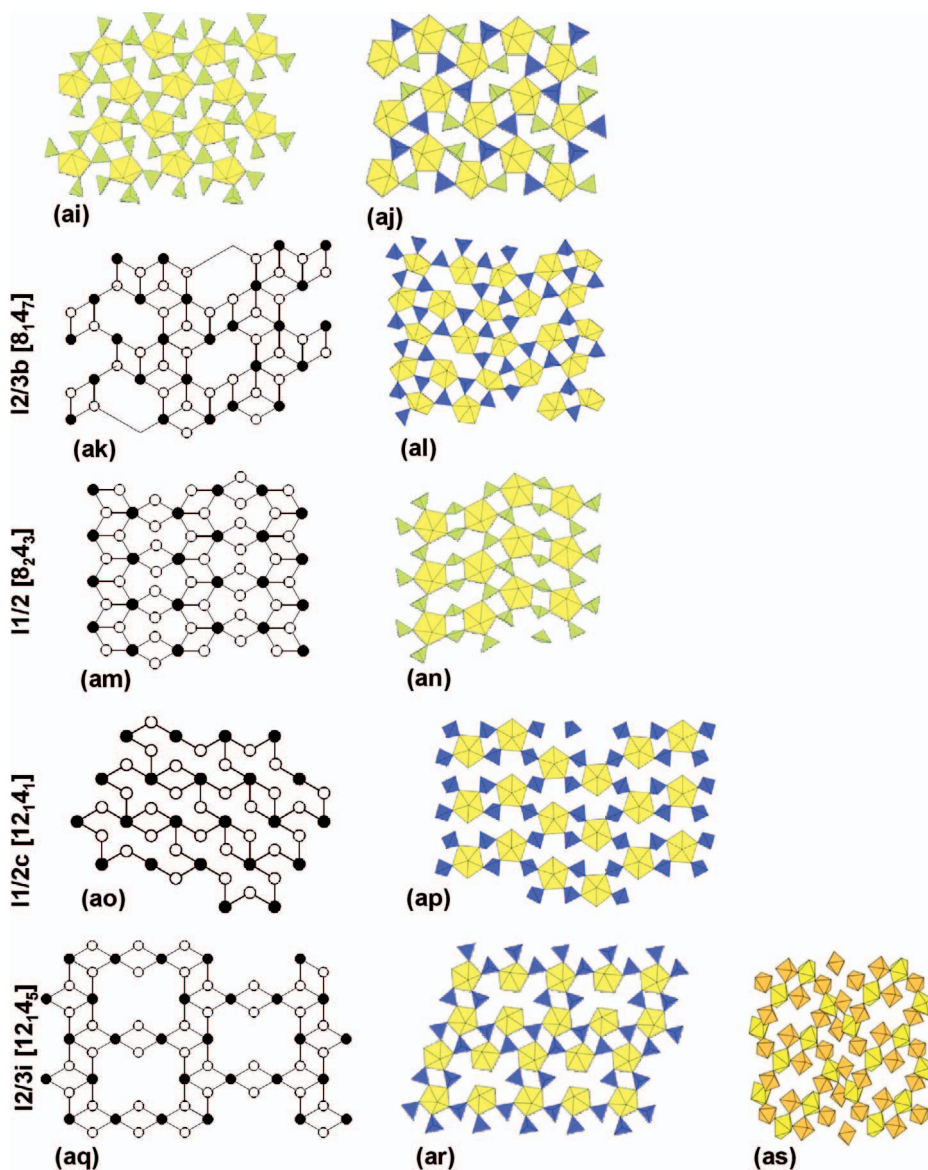
Fɪɢ. 5. Continued.

FIG. 5. Continued.

Topologically complex sheets classified by sheet-anion topologies

The remaining sheets structures are grouped on the basis of their sheet-anion topologies.

Sheet anion topologies containing triangles and pentagons (TrPt sheets)

Table 7 lists the 27 compounds (seven topologies) that contain sheets with anion topologies based solely on triangles and pentagons.

TrPt sheets based on clusters of uranyl polyhedra

$(H_3O)[(UO_2)_3O(OH)_3(SeO_4)_2]$ *anion topology (Fig. 7a–b).* This structure consists of isolated clusters of three edge-sharing uranyl pentagonal bipyramids that are similar to the finite cluster illustrated in Figure 3z. These clusters are linked by vertex-sharing with the tetrahedra to form sheets in which the non-bridging anions of the tetrahedra are oriented such that half point out of the plane of projection while the others point in the opposite direction. In the structure,
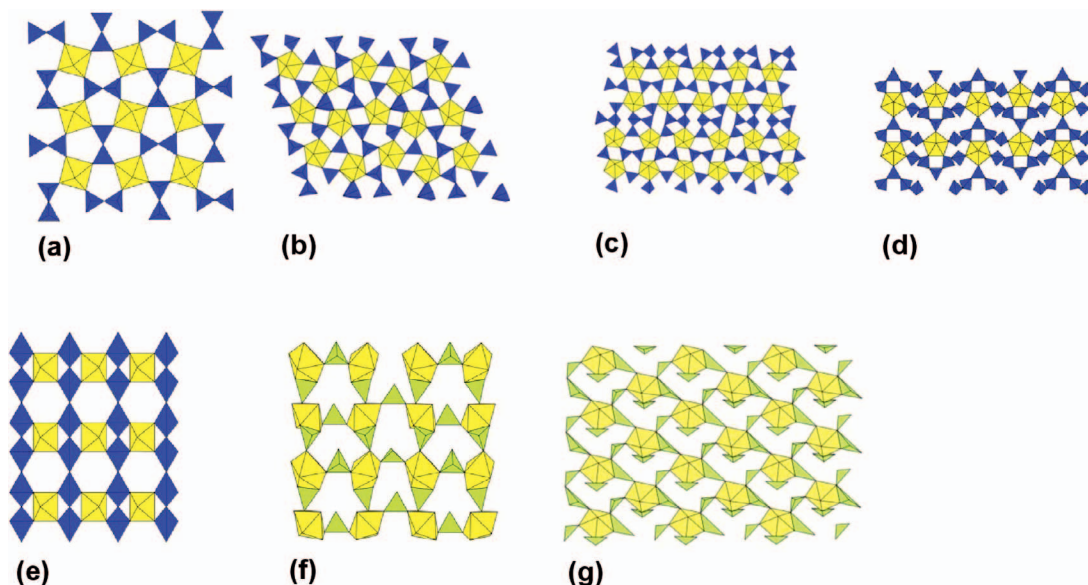
FIG. 6. Sheets with topologies that are dominated by vertex-sharing between uranyl and other ligand polyhedra (containing high-valence cations) found in the synthetic compounds and minerals listed in Table 6. In contrast to those shown in Figure 5, these cannot be represented by the scheme proposed by Krivovichev (2004).

adjacent sheets are linked *via* H bonds emanating from the $(H_3O)^+$ cations in the interlayer.

TrPt sheets based on chains of uranyl polyhedra

$K[(UO_2)(SO_4)(OH)]$ *anion topology (Fig. 7c–f).* This sheet anion topology consists of chains of edge-sharing pentagons separated by edge-sharing dimers of triangles. The polyhedral representation of the corresponding sheet shows that half of the pentagons are occupied by uranyl ions and half of the triangles are occupied by (SO_4) tetrahedra, such that infinite vertex-sharing chains of uranyl polyhedra result. These chains are linked to form the sheet by vertex-sharing with the sulfate tetrahedra. On the basis of tetrahedral orientation, there are three different graphical isomers that occur (Fig. 7d–f), where the orientation of tetrahedra is differentiated by color (light blue: up, dark blue: down). In the structure of $K[(UO_2)(SO_4)(OH)]$, the uranyl pentagonal bipyramids are linked by (OH) groups, whereas in the structures of $Ba[(UO_2)F(PO_4)]$, $K[(UO_2)F(HPO_4)$, and $Rb[(UO_2)(SO_4)F]$ they are linked by F anions. Low-valence cations in the interlayer of each of these structures link adjacent sheets.

TrPt sheets based on sheets of uranyl polyhedra

Protasite anion topology (Fig. 7g–h). The protasite sheet-anion topology is shown in Figure 7g and is the basis of the sheets in eight minerals as well as eight synthetic phases. The polyhedral representation of the protasite sheet (Fig. 7h) shows that each pentagon is populated by a uranyl ion, whereas all the triangles are vacant. The triangles are isolated from each other in the sheet, in contrast to other sheets in the class, and are all orientated in the same direction. A wide range of interlayer constituents occur in phases with the protasite topology (*e.g.*, Na^+, Ca^{2+}, K^+, Cs^+, Ba^{2+}, and Pb^{2+}); some phases contain interstitial (H_2O) groups. The net charge of the sheet is variable owing to adjustments of the number of (OH) groups, with four different arrangements of hydroxyl ions observed for the protasite topology. If the infinite chains of parallel, edge-sharing uranyl bipyramids in protasite are removed, the remaining, isolated bipyramids can be connected through vertex-sharing by tetrahedra to generate the topology observed in Figure 7i, which is known to occur in the three compounds listed.

$Na[(UO_2)_4O_2(OH)_5](H_2O)_2$ *anion topology (Fig. 7j–k).* Two synthetic compounds adopt this anion topology, $Na[(UO_2)_4O_2(OH)_5]$ and $[(UO_2)_4O(OH)_6]$ $(H_2O)_{12}$, which shows variability in hydroxyl content. The polyhedral representation shows that, as for the protasite topology, all pentagons are occupied by uranyl ions, with the triangles vacant. Here, the triangles occur as vertex-sharing dimers that resemble 'bowties', all of which are in the same orientation.
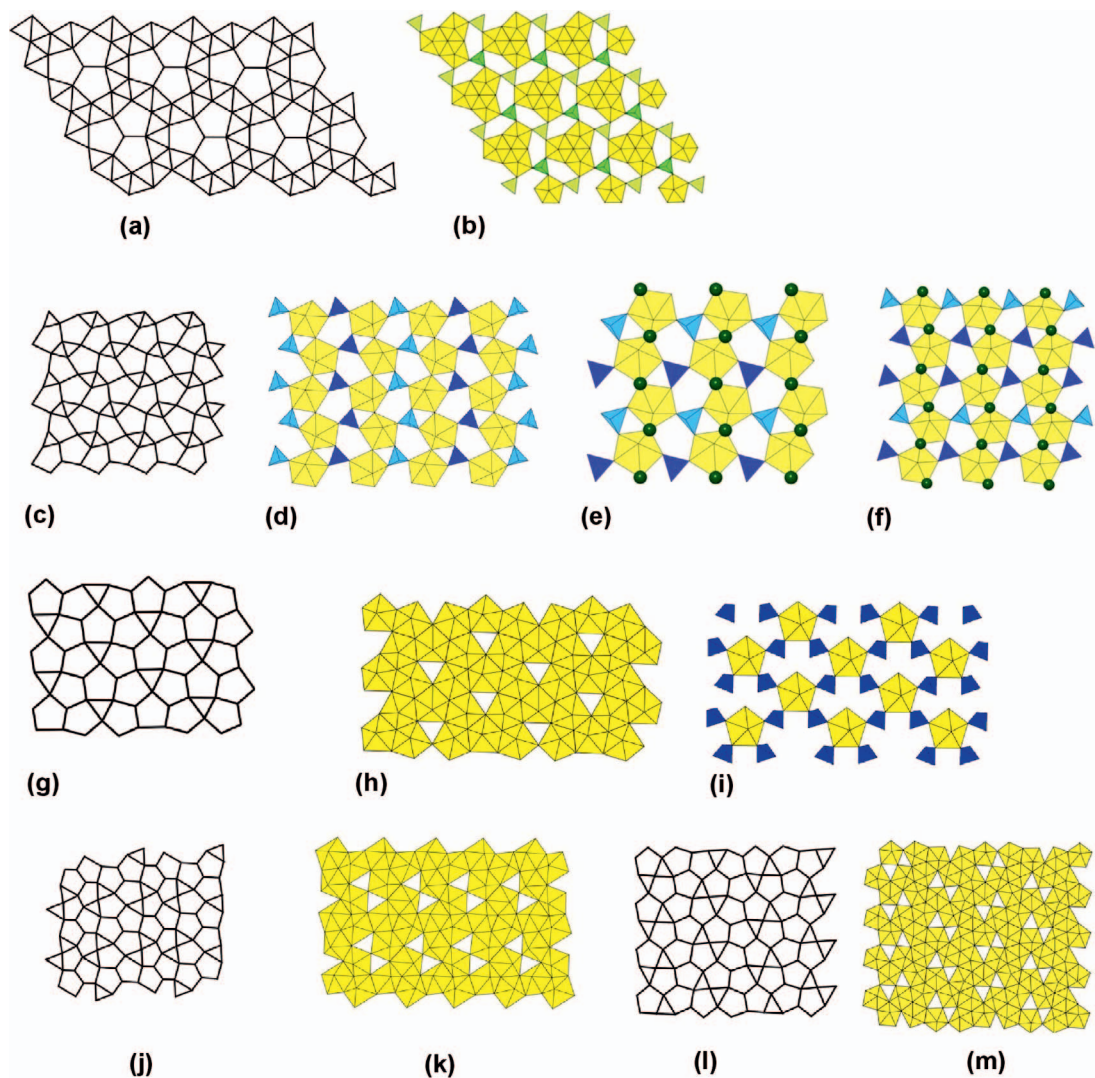
FIG. 7. Sheet-anion topologies, and corresponding polyhedral representations, consisting of triangles and pentagons (*TrPt*-sheets). The corresponding synthetic compounds and minerals are listed in Table 7.

Fourmarierite anion topology (Fig. 7l–m). Sheets based on the fourmarierite anion topology occur in three minerals: fourmarierite $[Pb[(UO_2)_4O_3(OH)_4](H_2O)_4]$, schoepite $[[(UO_2)_8O_2(OH)_{12}](H_2O)_{12}]$, and metaschoepite $[[(UO_2)_4O_3(OH)_6](H_2O)_5]$. In the fourmarierite sheet, each pentagon of the corresponding anion topology is occupied by a uranyl ion, whereas all the triangles are vacant. The triangles share vertices, forming bowtie-like pairs that are in two orientations. The (OH) content of the sheet varies; in fourmarierite the sheet carries a net negative charge requiring the presence of Pb^{2+} in the interlayer, but it is electro-

neutral in both schoepite and metaschoepite and only (H_2O) is located in the interlayer in each case. Li & Burns (2000b) reported a synthetic phase compositionally intermediate between fourmarierite and schoepite (*i.e.*, significant variability in interstitial Pb and H_2O content), suggesting the possibility of a solid-solution series between the three phases with the general formula $Pb_{(1-x)}[(UO_2)_4O_{(3-2x)}](H_2O)_4$.

Vandendrisschiete anion topology (Fig. 7n–o). Vandendrisschite, $Pb_{1.57}[(UO_3)_{10}O_6(OH)_{11}](H_2O)_{11}$, contains sheets with an underlying anion topology that is the most complex observed for simple combinations

(n)

(o)

(p)

(q)
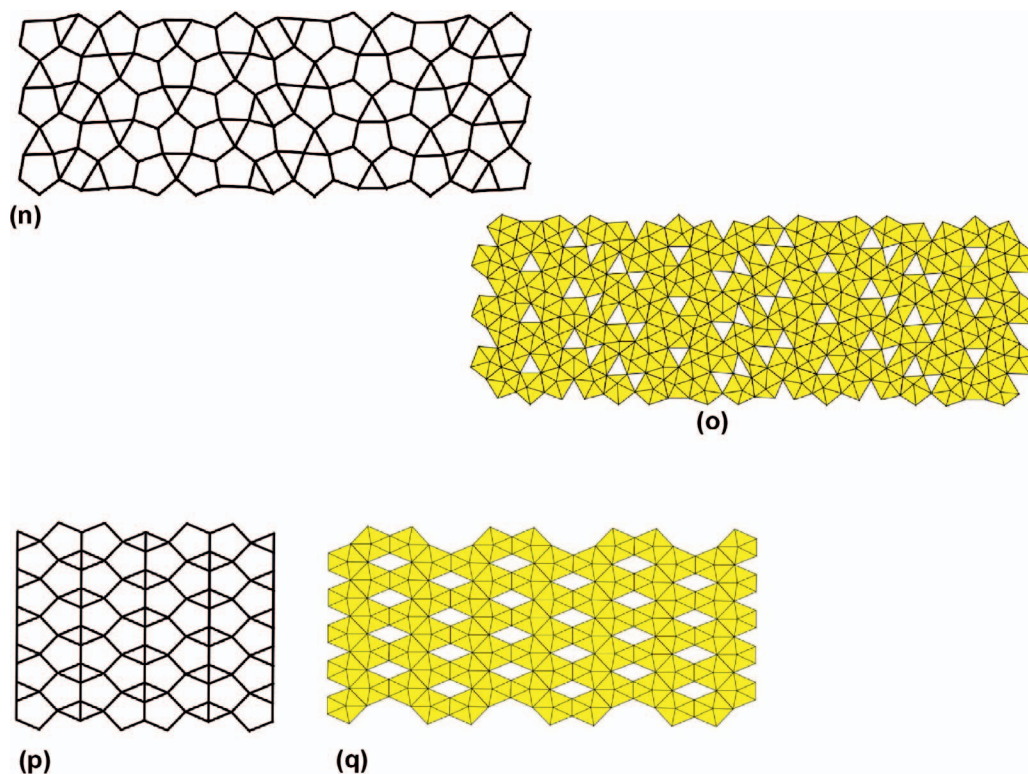
FIG. 7. Continued.

of pentagons and triangles (Fig. 7n). The primitive *b*-cell parameter in the plane of the sheet is ~41 Å. All of the pentagons in the anion topology are occupied by uranyl ions in the corresponding sheet, whereas the triangles are vacant. Triangles occur both as isolated units and as vertex-sharing dimers resembling bowties. Despite the apparent complexity of this sheet, Burns (1997) demonstrated that the vandendrisscchiete topology consists of modules of the protasite (*i.e.*, α-U_3O_8) topology in two different orientations.

α-$Cs_2[(UO_2)_2O_3]$ anion topology (Fig. 7p–q). All pentagons of the anion topology are occupied by uranyl ions in the corresponding sheet, and all triangles are vacant. The sheet consists of infinite chains of edge-sharing uranyl pentagonal bipyramids that are topologically similar to those observed in zippeite-group sheets. These chains link *via* edge-sharing to form the bulk sheet, and adjacent sheets are linked *via* Cs^+ in the interlayer.

Sheet anion topologies containing triangles, squares, and pentagons (TrSqPt sheets)

A total of 112 compounds (29 minerals) are based on 26 unique sheet-anion topologies containing

triangles, squares, and pentagons, as listed in Table 8. Such *TrSqPt* sheets are the most common sheet-anion topology known. The corresponding phases are illustrated in Figures 8 and 9.

Uranophane anion topology. The uranophane sheet anion topology is shown in Figure 8a; it consists of chains of edge-sharing pentagons that are separated by chains of edge-sharing triangles and squares. There are 27 chemically distinct compounds that contain sheets based upon this anion topology: 17 synthetic and 10 minerals. For simplicity, we divide this group on the basis of the occupancy of the anion topology; specifically, into those in which the triangles are occupied and the squares are vacant, those in which the squares are occupied and the triangles are vacant, and those in which the triangles and the squares are both vacant.

Uranophane sheet-anion topologies with occupied triangles. The triangles in the sheet-anion topology are either occupied by triangular BO_3 groups, or by the face of a tetrahedron. Structures where triangles are present, $Na[(UO_2)(BO_3)]$ and $Li[(UO_2)(BO_3)]$ (Fig. 8b), are anhydrous, with the sheets linked by the large monovalent cation in the interlayer. The crystal
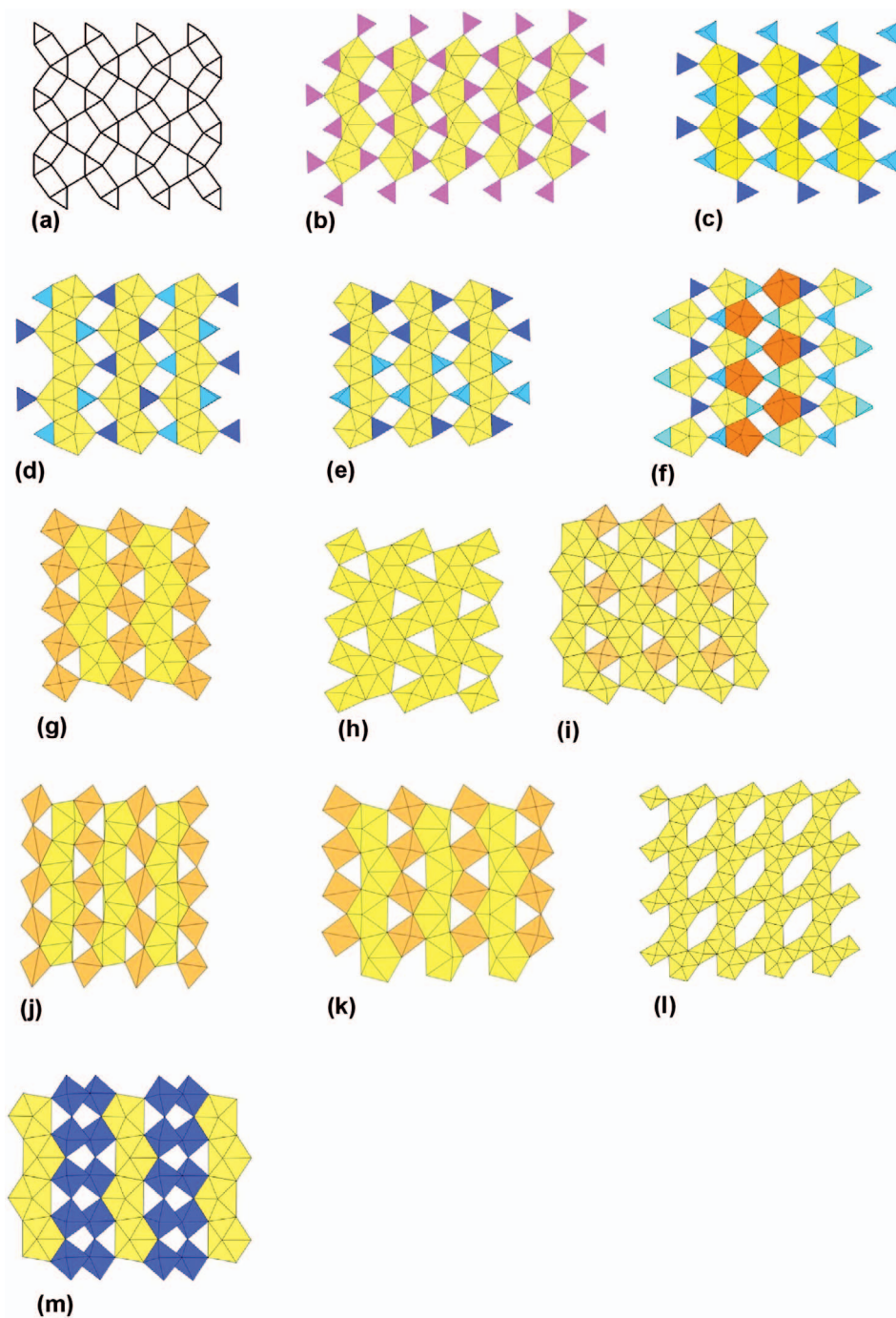
FIG. 8. Sheets based on the uranophane-type topology consisting of polyhedra of uranyl and other high-valence cations. In addition to the parallel, edge-sharing chains of pentagons, these sheets contain either triangles or squares. The corresponding compounds are listed in Table 8.

chemistry of the uranophane-type sheets containing tetrahedra is much more complex. In structures where the tetrahedrally coordinated cation is Si^{4+} (α-, β-uranophane, boltwoodite, curposklowdoskite, sklodowskite, oursinite, kasolite), the tetrahedron contains an (OH) group as the apical anion, except in the case of kasolite. The H-bond network was resolved for oursinite, $[(Co_{0.8}Mg_{0.2})[(UO_2)(SiO_3OH)]_2(H_2O)_6]$ by Kubatko & Burns (2006c), who proposed that the H bond emanating from the tetrahedral hydroxyl links to a yl oxygen atom of the same chain, and that the H bonds emanating from the interstitial (H_2O) link to the chain *via* the yl oxygen as well. Several tetrahedron-bearing phases with uranophane topology sheets do not contain an (OH) group in the tetrahedron, such as kasolite, $Pb[(UO_2)(SiO_4)](H_2O)$, seelite, $Mg[(UO_2)(AsO_3)_{0.7}(AsO_4)_{0.3}]_2(H_2O)_7$, and ulrichite, $CaCu[(UO_2)(PO_4)_2](H_2O)_4$. It is possible to substitute various tetrahedral cations (*e.g.*, AsO_4, PO_4) into the uranophane sheet, but this group remains dominated by uranyl silicates, although a series of uranyl phosphates with framework structures containing uranophane topology sheets has recently emerged (see below). Graphical isomerism commonly arises in sheets based upon the uranophane topology *via* the orientation of the tetrahedra in the sheet, either up or down relative to the plane of the page. Table 8 lists these structures arranged on the basis of their tetrahedral orientation and Figure 8 distinguishes tetrahedral orientation by coloring the 'up' and 'down' tetrahedra differently. Three variants are observed: α-uranophane (Fig. 8c), β-uranophane (Fig. 8d), and oursinite (Fig. 8e). Ulrichite (Fig. 8f) also displays a unique pattern of tetrahedral orientation, in addition to every second pentagon of the anion topology being occupied by irregular CaO_8 coordination polyhedra.

Uranophane anion topologies with occupied squares. These compounds contain sheets in which the triangles of the corresponding anion topology are vacant, but the squares are occupied. Note that polyhedra corresponding to the topological squares share vertices with each other, as well as edges with two different uranyl pentagonal bipyramids. Five different populations of the squares of the anion topology are observed: (1) octahedrally coordinated cations in umhoite, $[[(UO_2)(MoO_4)(H_2O)](H_2O)_{1.45}]$, and $Li_4[(UO_2)_2(W_2O_{10})]$ (Fig. 8g); (2) uranyl square bipyramids in $K_2[(UO_2)_2O_3]$ (Fig. 8h); (3) both uranyl square bipyramids and regular Cu-octahedra in $[(UO_2)(CuO_4)]$ (Fig. 8i); (4) polyhedra distorted by lone-pair stereoactive electrons in schmitterite $[(UO_2)(TeO_3)]$ (Fig. 8j); and (5) [5]-sided, distorted pyramids in $K[(UO_2)(NbO_4)]$, γ-$Rb(NbUO_6)(H_2O)$, and $Li[(UO_2)(NbO_4)]$ (Fig. 8k). Anhydrous schmitterite and $[(UO_2)(CuO_4)]$ contain electroneutral sheets

and no interstitial cations. In schmitterite, adjacent sheets are held together solely by van der Waals forces. Schmitterite is the only uranyl tellurite to adopt the uranophane topology. In $[(UO_2)(CuO_4)]$, the sheets are bonded directly to one another through the apical anions of Jahn-Teller distorted CuO_6 octahedra, which are also oxygen atoms of the uranyl ions. Structures with the formulae $X_2[(UO_2)(W_2O_8)]$ (X = K, Na, Ag) contain the sheet illustrated in Figure 8m. This sheet is related to the uranophane-type sheets shown in Figures 8j–l, wherein the single chain of vertex-sharing octahedra is replaced by a double chain.

Uranophane topologies with vacant squares and triangles. The only sheet based upon the uranophane anion topology in which both the topological triangles and (half of the) squares are empty is in $[H_2(UO_2)_3O_4]$ (Fig. 8l), which also contains no interlayer cations.

TrSqPt sheets of clusters of uranyl polyhedra

Iriginite anion topology (Fig. 9a–b). This sheet anion topology occurs in iriginite $[(UO_2)(Mo_2O_7)_2](H_2O)$, as well as synthetic $[(UO_2)(Mo_2O_7)(H_2O)_2]$ and $[Ca(UO_2)(Mo_4O_7)_2]$. In the latter compound, the pentagons of the topology are populated by both Ca and uranyl ions. The resulting sheet consists of monomers of uranyl pentagonal bipyramids bridged by edge-sharing dimers of octahedra, with (H_2O) groups at the non-bridging apices of the octahedra. All examples of sheets based on this topology are electroneutral. In iriginite, the sheets are linked through (H_2O) groups in the interlayer. In $[(UO_2)(Mo_2O_7)(H_2O)_2]$, the sheets are held together solely by H bonds emanating from the (H_2O) groups within the sheet, as there are no interlayer constituents. In $[Ca(UO_2)(Mo_4O_7)_2]$ the sheets are directly bonded to each other. In iriginite, the sheets stack with an *ABAB* order (*i.e.*, every second sheet is directly on top of each other with respect to the **c**-axis), consistent with a short repeat distance of 12.7 Å. In the synthetic phase the sheets stack with an *ABCDEFA* sequence, giving the significantly longer repeat distance of 35.1 Å.

$Cs[(UO_2)F(HPO_4)](H_2O)_{0.5}$ anion topology (Fig. 9c–f). This sheet-anion topology contains groups of six edge-sharing pentagons, with groups of triangles and squares between them. The polyhedral representation of the corresponding sheet shows that half of the pentagons are occupied by uranyl ions, giving edge-sharing dimers. The triangles correspond to faces of tetrahedra, and the squares are vacant. The dimers of uranyl pentagonal bipyramids are interconnected by six vertex-sharing tetrahedra that link to the uranyl ions at the equatorial positions. Each tetrahedron is coordinated by three different uranyl polyhedra. On the basis of the orientation of the apical (non-bridging)
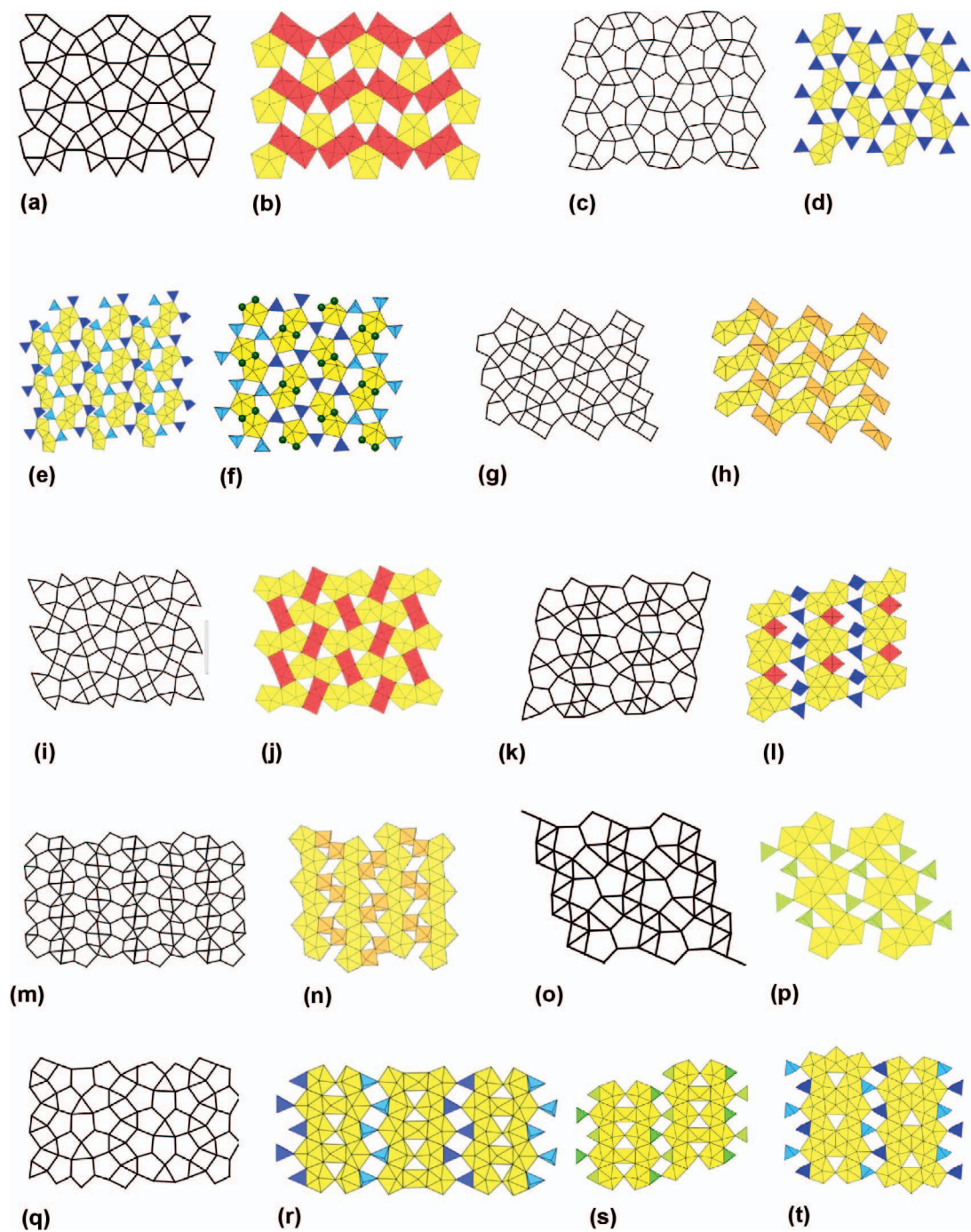
FIG. 9. Sheet-anion topologies, and corresponding polyhedral representations, consisting of triangles, squares, and pentagons (*TrSqPt* sheets). The corresponding synthetic compounds and minerals are listed in Table 8.
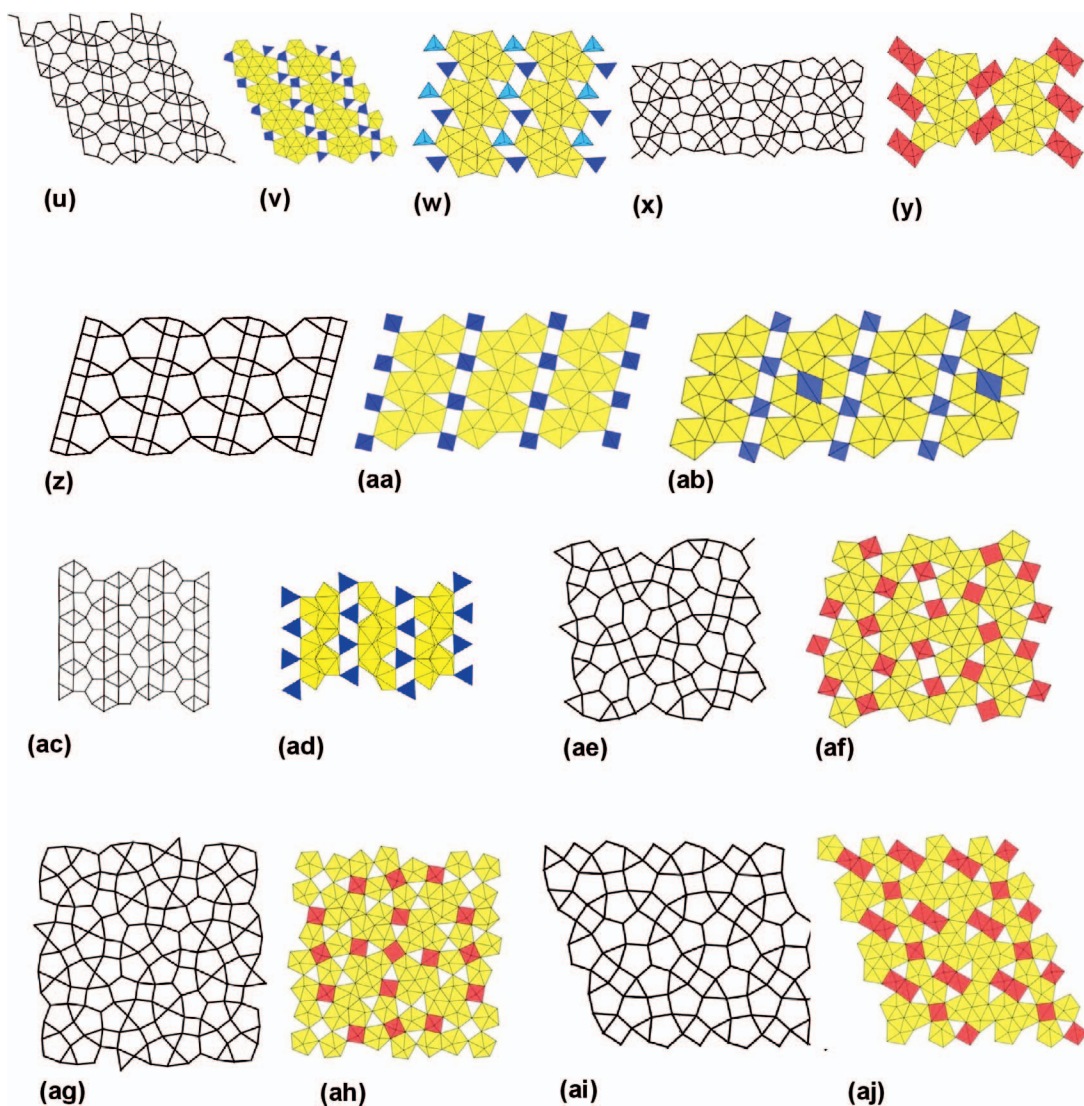
FIG. 9. Continued.

tetrahedral anion, three graphical isomers are observed (Fig. 9d–f). The uranyl dimers are either bridged *via* pairs of F anions, as in $Cs[(UO_2)F(HPO_4)](H_2O)_{0.5}$, or pairs of hydroxyl anions, as in $Cs[(UO_2)(OH)(SeO_4)]$ (H_2O) and $K[(UO_2)(OH)(CrO_4)](H_2O)$.

Vandenbrandeite anion topology (Fig. 9g–h). This sheet anion topology is only known from vandebrandeite, $[Cu(UO_2)(OH)_4]$. The corresponding sheet consists of dimers of edge-sharing uranyl polyhedra linked *via* dimers of edge-sharing CuO_5 square pyramids with apical anions oriented in opposing directions. This sheet is electroneutral and adjacent

sheets are directly linked by the yl oxygen atoms of the uranyl ions that are apical ligands of the CuO_5 square bipyramids of the adjacent sheet.

Francevillite anion topology (Fig. 9i–j). The francevillite anion topology consists of edge-sharing dimers of pentagons and edge-sharing dimers of squares. In the corresponding sheet, all of the pentagons are occupied by uranyl ions. In the structure of uranosphaerite, $[Bi(UO_2)(OH)]$, the squares are occupied by irregular $(Bi\Phi_4)$ polyhedra. Note that this sheet is the only francevillite-type sheet to contain an (OH) group, which is located at the vertex-shared

(ak)

(al)

(am)

(an)

(ao)

(ap)

(aq)

(ar)

(as)
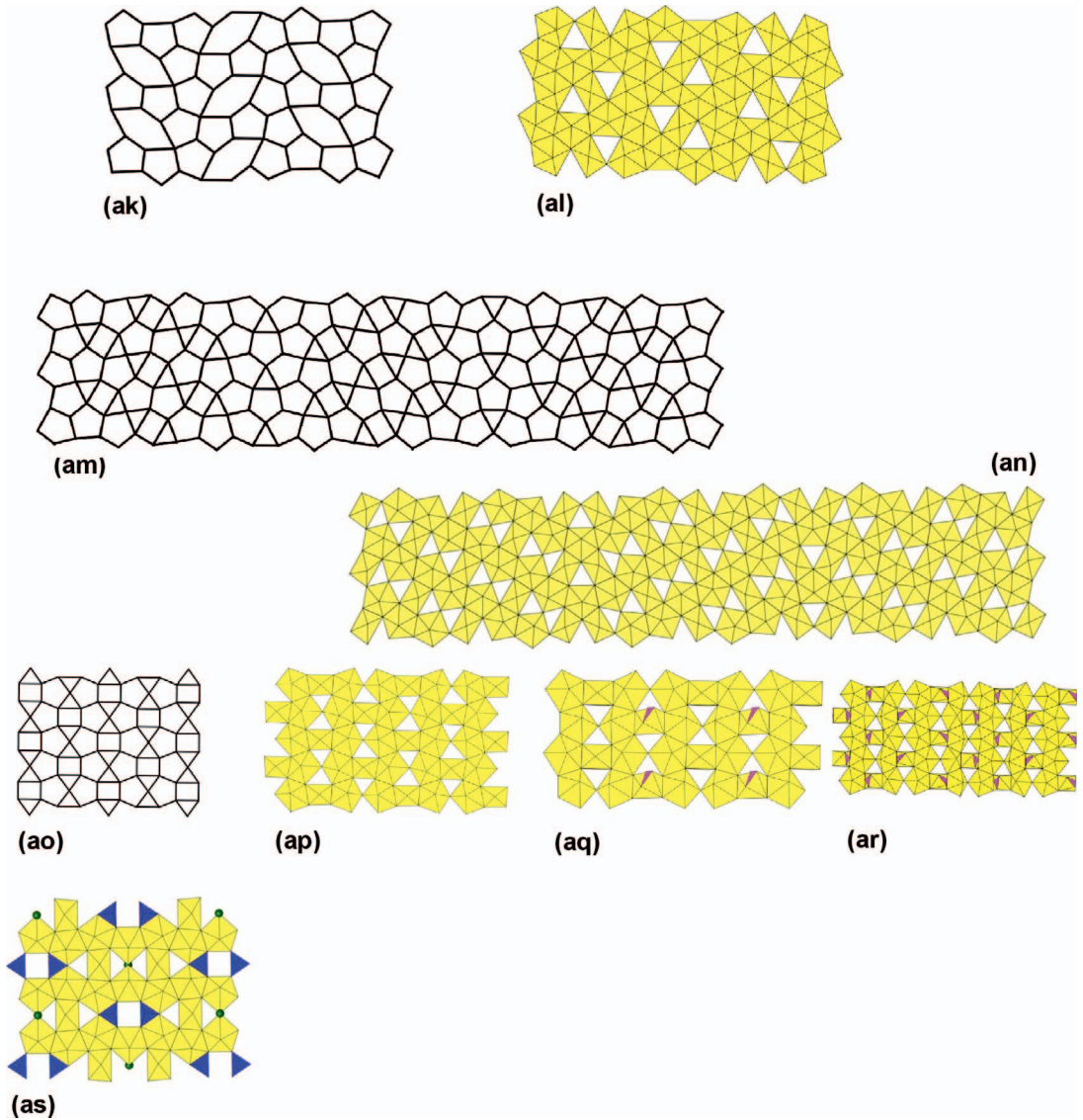
F$_{IG}$. 9. Continued.

anion position between the uranyl dimers. In the remaining francevillite-type phases, the squares are occupied by the basal plane of square pyramids of (VO_5), $(Cr^{5+}O_5)$, (NbO_5), or (TiO_5). As in vanden-brandeite, the apical anions of these polymeric dimers are oriented in opposing directions. Only (VO_5) groups occur within this sheet in minerals. There are four differently oriented triangles in this topology, all of which are vacant. The francevillite-type sheet is observed in five minerals and 11 synthetic phases. In each, the sheets are anhydrous and, with few

exceptions (e.g., sengierite, metatyuyamunite, and $Mg_2[(UO_2)(Cr_2O_8)](H_2O)_4)$, so is the interstitial complex; hence the sheets are linked solely by cations in the interlayer. These cations may be either large and of low valence, or octahedrally coordinated metals (e.g., Mg^{2+} or Ni^{2+}).

Sheets formed by infinite chains of uranium polyhedra

$Cs_4[(UO_2)_3O(MoO_4)_2(MoO_5)]$ *anion topology (Fig. 9k–l)*. This sheet-anion topology occurs only in
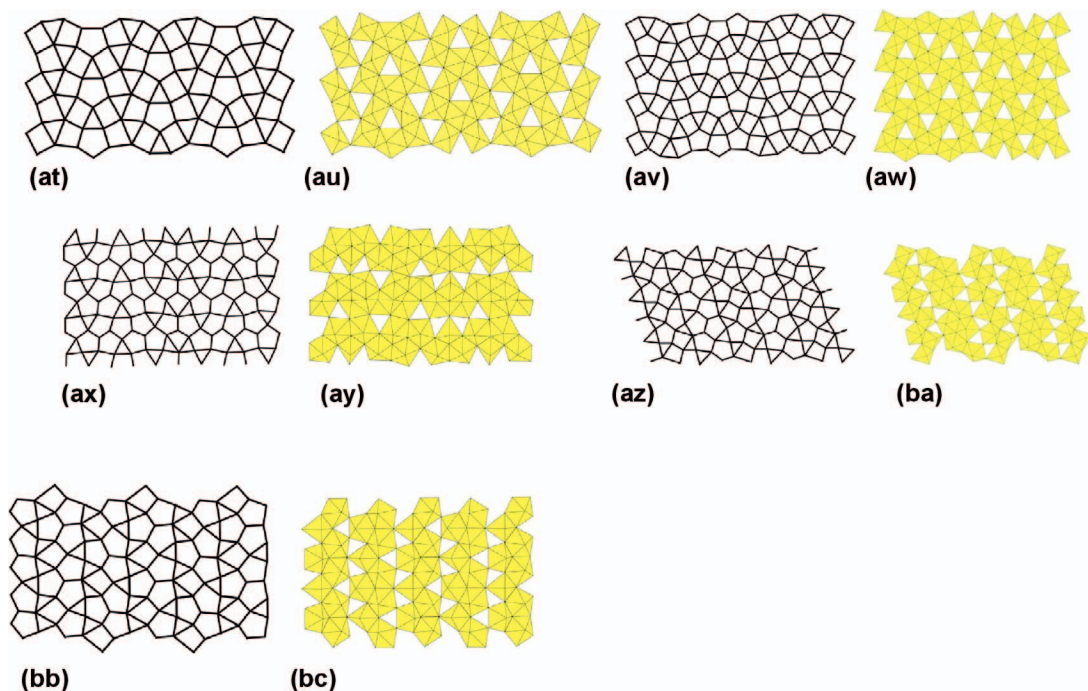
FIG. 9. Continued.

the structure of the synthetic phase $Cs_4[(UO_2)_3O(MoO_4)_2(MoO_5)]$. In the corresponding sheet, trimers of edge-sharing uranyl pentagonal bipyramids are linked *via* vertex-sharing to form infinite chains. MoO_5 pyramids link to adjacent trimers by edge-sharing. The resulting chains are linked to form infinite sheets *via* vertex-sharing MoO_4 tetrahedra. This anhydrous phase contains only Cs^+ in the interlayer.

Ag[(UO₂)(HTeO₅)] anion topology (Fig. 9m–n). This sheet anion topology exists only in the synthetic phase $Ag[(UO_2)(HTeO_5)]$. The topology contains uranophane-type chains of pentagons, all of which are occupied by uranyl ions in the corresponding sheet. These chains are linked by dimers of edge-sharing octahedra. These octahedra share one edge with one chain and two vertices with the other. The apical oxygen positions of the octahedra each contain a hydroxyl group. The Ag^+ cation in the interlayer links the sheets together.

K₂[(UO₂)₃(TeO₃)₂O₂] anion topology (Fig. 9o–p). Sheets of this topology occur in the three isostructural compounds $X_2[(UO_2)_3(TeO_3)_2O_2]$ (X = K, Rb, Cs). The anion topology has chains of edge-sharing pentagons and squares linked together to form infinite sheets that are separated by infinite chains of edge-sharing triangles. The polyhedral representations of the corresponding sheets show that the squares and pentagons are occupied by uranyl square and pentag-

onal bipyramids, respectively. Chains of edge-sharing uranyl pentagonal and square bipyramids are linked together *via* vertex-sharing tetrahedra. This same chain (Fig. 4m) exists as an isolated unit in the three compounds $X_2[(UO_2)_3(IO_3)_4O_2]$ (X = Rb^+, Tl^+, K^+). In the sheet structure, basal planes of lone-pair stereo-active electron-bearing tetrahedra occupy ¼ of the triangles. No graphical isomerism with regard to the orientation of tetrahedra is observed in these phases, although this appears likely to be discovered in future compounds. Each phase is anhydrous, and the sheets are linked solely by the monovalent cations located in the interlayer.

Na₆[(UO₂)₅(VO₄)₂O₅] anion topology (Fig. 9q–s). This sheet topology occurs in three synthetic phases: $Na_6[(UO_2)_5(VO_4)_2O_5]$, β-$Rb_6[(UO_2)_5(VO_4)_2O_5]$, and $K_4[(UO_2)_5(TeO_3)_2O_5]$ (Table 8). It consists of fragments of the β-U_3O_8 topology linked by chains of edge-sharing triangles and squares (similar to those observed in the uranophane topology). The polyhedral representation of the corresponding sheets shows that the squares and pentagons are occupied by uranyl ions, the triangles are occupied by the basal plane of tetrahedra (either VO_4 or TeO_3), and the squares are vacant. The resulting sheet consists of chains of edge-sharing uranyl pentagonal bipyramids that are fragments of the β-U_3O_8 sheet topology. Two graphical isomers can be distinguished. The compounds corre-

sponding to Figure 9r contain regular tetrahedra, whereas those corresponding to Figure 9s contains irregular tetrahedra with a lone-electron pair at one of the tetrahedral vertices. Considering the orientation of tetrahedra between any two uranyl chains, these sheets can be distinguished further; the sheet in Figure 9r shows that these are all oriented in the same direction, whereas that in Figure 9s shows these to alternate. All phases containing this sheet (regardless of tetrahedral orientation) are anhydrous and are held together solely by monovalent interstitial cations.

α-Rb[(UO$_2$)$_5$(VO$_4$)$_2$O$_5$] *sheet-anion topology (Fig. 9t)*. This sheet-anion topology is nearly identical to the Na$_6$[(UO$_2$)$_5$(VO$_4$)$_2$O$_5$] topology, differing only in one significant way. The central chain of uranyl polyhedra corresponds to a fragment of the protasite (or α-U$_3$O$_8$) sheet (Fig. 7h). Hence, there are fewer squares and more pentagons than in the Na$_6$[(UO$_2$)$_5$(VO$_4$)$_2$O$_5$] sheet-anion topology.

(Ba$_5$Ca)[(UO$_2$)$_8$(AsO$_4$)$_4$O$_8$] sheet-anion topology (Fig. 9u–w). This anion topology occurs only in CsNa$_3$[(UO$_2$)$_4$O$_4$(Mo$_2$O$_8$)] and Ba$_5$Ca[(UO$_2$)$_8$(AsO$_4$)$_4$O$_8$]. The sheet-anion topology consists of infinite chains of edge-sharing pentagons separated by parallel chains of edge-sharing triangles and squares. The polyhedral representation of the corresponding sheet shows that all pentagons are occupied by uranyl ions and some triangles correspond to bridging tetrahedra; the squares are vacant. The orientation of the linking tetrahedra differs such that two graphical isomers result (Fig. 9v and 9w). The phases are anhydrous, and the sheets are held together solely by the cations in the interlayer.

Ag$_{10}$[(UO$_2$)$_8$O$_8$(Mo$_5$O$_{20}$)] anion topology (Fig. 9x–y). Chains of pentagons are separated by complex chains of edge-sharing squares and triangles. Sheets with this anion topology occur in the isostructural compounds X_{10}(UO$_2$)$_8$O$_8$(Mo$_5$O$_{20}$)] ($X =$ Ag, Na). The polyhedral representation shows all pentagons of the topology are occupied by uranyl ions and the squares are occupied by (MoO$_5$) five-sided pyramids, all of which have apices directed in the same orientation. Adjacent sheets are linked by monovalent cations in the interlayer; additionally, an isolated tetrahedron exists between every second group of sheets.

Zippeite anion topology (Fig. 9z–ab). The zippeite anion topology consists of zig-zag chains of edge-sharing pentagons that are separated by infinite chains of squares and triangles. There are 18 compositionally distinct phases that contain sheets that are based on this topology (five minerals), and in all of these the pentagons are occupied by uranyl ions, the triangles remain vacant, and half of the squares are occupied by sulfate tetrahedra. The sulfate tetrahedra link to four unique bipyramids (Fig. 9aa). The hydroxyl content of the zippeite sheet varies, as the ligands shared between uranyl ions can be either O or OH. Interstitial cations and a network of H bonds emanating from interstitial (H$_2$O) groups link the sheets. Only the phase (NH$_4$)[(UO$_2$)$_2$(SO$_4$)O$_2$] lacks (H$_2$O) in the interlayer. The synthetic zippeite-like compound K$_{0.5}$Zn$_{0.75}$ [(UO$_2$)$_2$(SO$_4$)O$_2$](H$_2$O)$_3$ is unusual in that it contains Zn in octahedral coordination (in the interlayer) as well as in irregular tetrahedral coordination. Two of the tetrahedral apices are yl oxygen atoms of uranyl ions in the sheet (Fig. 9ab).

Rb$_2$[(UO$_2$)$_2$(MoO$_4$)O$_2$] sheet-anion topology (Fig. 9ac–ad). This sheet topology contains the same arrangement of chains of pentagons as the zippeite anion topology. Here the chains are again linked by vertex-sharing with tetrahedra, but only three tetrahedral vertices participate, with the fourth being oriented towards the interlayer.

TrSqPt sheets of connected uranyl polyhedra

The 28 compounds in this class all contain sheets of uranyl polyhedra, polymerized either by edge-sharing or vertex-sharing to form infinite sheets. Although such sheets may contain additional high-valence cations, removing these from the polyhedral representation would not interrupt the two-dimensional continuity of the sheet structure.

K$_2$[(UO$_2$)$_2$(WO$_5$)O] anion topology (Fig. 9ae–af). This anion topology contains clusters of eight edge-sharing pentagons, each of which is connected to four identical clusters by vertex-sharing. Between these clusters, topological squares and triangles occur. In the polyhedral representation of the corresponding sheet, the pentagons are occupied by uranyl ions, the triangles are vacant, and the squares are occupied by the basal plane of [5]-sided pyramids of MoO$_5$ or WO$_5$. Squares in this topology exist in three different local environments: one shares three edges with three bipyramids, another shares one edge and two vertices with three bipyramids, and the third shares two edges with bipyramids and two edges with squares (these are vacant). The sheets are linked only *via* cations located in the interlayer.

K$_8$[(UO$_2$)$_8$(MoO$_5$)$_3$O$_6$] anion topology (Fig. 9ag–ah). This sheet topology consists of a complex array of pentagons that are linked by either edge- or vertex-sharing, with triangles and squares between the pentagons. In the polyhedral representation of the corresponding populated sheet, each pentagon contains a uranyl ion, and ¾ of the squares correspond to the basal plane of a [5]-sided MoO$_5$ pyramid. The sheet contains squares in two distinct types of local environments; one sharing four edges with adjacent pentagons and another sharing three edges with

pentagons and one edge with a triangle. Half of the former square types are occupied, whereas all of the latter square types are occupied. The sheets are linked solely through K^+ cations located in the interstitial complex.

$Cs_9[(UO_2)_8O_4(NbO_5)(Nb_2O_8)]$ (Fig. 9ai–aj). This sheet anion topology occurs only in $Cs_9[(UO_2)_8O_4(NbO_5)(Nb_2O_8)]$. Similar to the sheet discussed in the previous section, the topology consists of a complex arrangement of edge- and vertex-sharing pentagons, with squares and triangles located between the pentagons. Squares occur as monomeric units, where they share all four edges with pentagons, or as dimeric, edge-sharing units. Each dimer shares three edges with uranyl bipyramids and three edges with vacant triangles. Each pentagon contains a uranyl ion and each square contains a NbO_5 [5]-sided pyramid. Where these are present as edge-sharing dimers, the apical anions point in opposing directions. The sheets are held together solely by the Cs cations.

Sayarite anion topology (Fig. 9ak–al). In the sayrite sheet, each square and pentagon of the corresponding anion topology is occupied by a uranyl ion, and the triangles are vacant. This sheet is known from sayerite, $Pb_2[(UO_2)_5O_6(OH)_2](H_2O)$, and the synthetic compounds $K_6[(UO_2)_5(VO_4)_2O_5]$ and $K_2[(UO_2)_5O_8](UO_2)_2$. In sayerite, (OH) groups are present in the sheet and (H_2O) molecules are in the interlayer; along with Pb^{2+}, these serve to link the adjacent sheets. In $K_6[(UO_2)_5(VO_4)_2O_5]$, only K is located in the interlayer, however in $K_2(UO_2)_2[(UO_2)_5O_8]$ the interlayer contains uranyl ions with irregular [7]-fold coordination.

Wölsendorfite anion topology (Fig. 9am–an). Despite its relatively simply composition, wolsendorfite contains the most topologically complex sheet of uranyl polyhedra known. The primitive repeat distance of ~56 Å is the largest cell parameter of any uranyl mineral. The complex wolsendorfite sheet-anion topology is composed of fragments of the simpler protasite (α-U_3O_8) and β-U_3O_8 topologies (Burns 1999c). In the corresponding sheet, all of the triangles remain vacant, occurring as either vertex-sharing dimers or as monomers. All pentagons and squares are populated by uranyl ions. The interstitial complex consists of divalent cations (Pb^{2+} and Ba^{2+}) as well as H_2O groups.

β-U_3O_8-sheet topology (Fig. 9ao–as). The β-U_3O_8-sheet-anion topology consists of infinite chains of edge-sharing pentagons that are similar to those in uranophane-type phases. However, in β-U_3O_8, these chains are linked by vertex-sharing such that triangles and squares occur between the chains. The polyhedral representation of the corresponding sheet shows that in β-U_3O_8 each pentagon and each square are occupied by uranium ions, whereas the triangles are empty. The basic β-U_3O_8-type sheet occurs in four minerals (wyartite, dehydrated wyartite, ianthinite, and spriggite) and one synthetic phase (β-U_3O_8). β-U_3O_8 contains U in multiple valence states.

In spriggite, all of the U is hexavalent, and in the sheet, both the squares and pentagons of the β-U_3O_8 sheet topology are occupied by uranyl ions (Fig 9ap). Wyartite (and its dehydrated analogue) is the only mineral reported to contain stoichiometric amounts of pentavalent uranium, although synthetic U^{5+} phases are well known (Burns & Finch 1999). Pentavalent uranium is unstable relative to the tetravalent and hexavalent oxidation states under most aqueous conditions, and most synthetic compounds containing it were produced in the absence of water (Lee *et al.* 2010, Chen *et al.* 2012). The polyhedral sheet in wyartite retains the basic β-U_3O_8 sheet topology, wherein the chains of pentagons are occupied by $U^{6+}O_7$ uranyl pentagonal bipyramids and the squares are occupied by irregular $U^{5+}O_7$ polyhedra (Fig 9aq). The (CO_3) groups share edges with the U^{5+} polyhedra and extend into the interlayer. Adjacent sheets are linked *via* the Ca cations and H bonding from (H_2O) groups present in the interlayer.

Ianthinite is reported to contain both hexavalent and tetravalent uranium. However, Burns (2005) suggested that the initial refinement reported in Burns *et al.* (1997b) may have lacked the precision needed to completely distinguish between U^{4+} and U^{5+}, hence pentavalent uranium may also be present. Several attempts to acquire superior diffraction data have been unsuccessful owing to the quality of available crystals. The U^{6+} occurs as uranyl pentagonal bipyramids, whereas the U^{4+} occurs as distorted octahedra, occupying the square spaces in the sheet-anion topology (Fig. 9ar).

The isostructural synthetic phases $K[(UO_2)_2(UO_4)(OH)(NO_3)_2](H_2O)$ and $Ba[(UO_2)_4(UO_4)_2(OH)_2(NO_3)_4](H_2O)_2$ also contain sheets based on the β-U_3O_8 anion topology. In these phases, the pentagons of the topology are occupied by uranyl ions, but the squares are occupied by U^{6+} showing an unusual tetraoxido core configuration (Fig. 9ar). In the tetraoxido polyhedron, the central U^{6+} cation is coordinated to four equatorial anions at relatively short bond lengths (~1.95–2.0 Å); in addition, two bidentate (NO_3) groups are located at either end of the coordination polyhedron with bond lengths ~2.5–2.7 Å.

The two phases $Cs_7[(UO_2)_8(VO_4)_2ClO_8]$ and $Rb_7[(UO_2)_8(VO_4)_2ClO_8]$ contain sheets with novel populations of the β-U_3O_8 anion topology (Fig. 9as). In these sheets, half of the squares of the topology are vacant and half the triangles are populated by the basal

planes of $(VO_4)^{3-}$ tetrahedra. The pentagonal chains are linked together *via* Cl anions.

$Cs_4[(UO_2)_5O_7]$ *sheet topology (Fig. 9at–au)*. This sheet consists of uranyl square and pentagonal bipyramids linked by the sharing of equatorial edges and vertices, and occurs in $X_4[(UO_2)O_7]$ ($X = Cs$, Rb). The edge-sharing polyhedra form complex infinite chains. These are linked by vertex-sharing, such that chains of vacant triangles are present, as well as isolated triangles. The interstitial complex consists only of Cs.

$Rb_8[(UO_2)_9O_{31}]$ *anion topology (Fig. 9av–aw)*. This sheet is topologically very similar to that observed in $Cs_4[(UO_2)_5O_7]$ with infinite chains of equatorial edge-sharing uranyl square and pentagonal bipyramids. The distinction is the width of the chains, which are doubled with respect to that of $Cs_4[(UO_2)_5O_7]$. The topology contains both isolated triangles located inside these infinite chains as well as infinite chains of vertex-sharing triangles that are present between the chains of uranyl polyhedra. In this anhydrous phase, the adjacent sheets are linked together *via* Rb cations in the interlayer.

The following three sheet anion topologies consist of infinite chains containing both edge-sharing squares and pentagons. In each corresponding phase, these are populated by uranyl ions in pentagonal bipyramidal and irregular square bipyramidal coordination, respectively. The exact arrangement of these differs subtly, such that the anion topologies are also different. The individual chains link together by (predominantly) vertex-sharing to form the observed infinite sheets. In each case, linear arrangements of vertex-sharing triangles exist in the topologies between the chains. These are either of finite length [*e.g.*, $K_5[(UO_2)_{10}O_8(OH)_9](H_2O)$] or infinite length [*e.g.*, $Ca[(UO_2)_4O_3$-Plášil$(OH)_4](H_2O)$ and curite].

$K_5[(UO_2)_{10}O_8(OH)_9](H_2O)$ *anion topology (Fig. 9ax–ay)*. In this sheet-anion topology, squares and pentagons occur with a ratio of 1:6, and there is only one type of chain of pentagons. These chains are connected by sharing vertices and edges to form the topology, and all are populated by uranyl ions to form the sheet. Between the resulting chains of uranyl pentagonal bipyramids, triangles occur as isolated units, as well as four-membered and six-membered truncated groups. The interlayer is occupied by K^+ cations as well as (H_2O).

$Ca[(UO_2)_4O_3(OH)_4](H_2O)_2$ *anion topology (Fig. 9az–ba)*. In this sheet-anion topology, two types of infinite chains occur, one consisting of edge-sharing pentagons and distorted squares (with a 2:1 ratio, respectively), the other consisting of only edge-sharing pentagons. These chains alternate and are linked only by edge sharing to form the topology. The pentagons

are populated by uranyl ions, giving chains of uranyl polyhedra, between which infinite chains of vertex-sharing triangles are observed. Calcium cations and (H_2O) groups are present in the interlayer and attach adjacent sheets.

Curite, $Pb_3[(UO_2)_8O_8(OH)_6](H_2O)_3$, *sheet-anion topology (Fig. 9bb–bc)*. The curite sheet-anion topology occurs in both curite and the synthetic Sr-substituted analogue. Curite contains infinite chains of equatorial edge-sharing pentagonal bipyramids and highly distorted square bipyramids (in a ratio of 3:1); these are linked only by vertex-sharing such that infinite chains of vertex-sharing triangles exist between them. The general formula $Pb_{3+x}(H_2O)_2[(UO_2)_4O_{4+x}(OH)_{3-x}]_2$ was proposed by Li & Burns (2000a) for curite, suggesting that the variability in interstitial Pb^{2+} is balanced by variability in hydroxyl content of the interlayer.

Sheet anion topologies containing triangles, squares, pentagons, and hexagons (TrSqPtHx sheets)

There are 24 compounds (18 minerals) based on sheet-anion topologies containing triangles, squares, pentagons, and hexagons. These are listed in Table 9 and illustrated in Figure 10. All except for one, $Cs_2[(UO_2)_4(Co(H_2O)_2)_2(HPO_4)(PO_4)]$, are topologically related to the phosphuranylite sheet topology, with the significant differences being in how the phosphuranylite-type chains link to form the observed sheet.

Phosphuranylite anion topology

The phosphuranylite sheet-anion topology (Fig. 10a) is the basis of the sheets in the 24 compositionally distinct phases listed in Table 9. This topology contains two types of infinite chains of polygons. The first consists of dimers of edge-sharing pentagons that are further linked by edge-sharing hexagons, and the second consists of edge-sharing triangles and squares which form a zig-zag pattern. The phosphuranylite anion topology is formed by successive linked edges of these two chain types. The sheets that result from the population of this anion topology (Fig. 10b–l) occur in two general types of graphical isomers, both of which have vacant squares. The first type is observed in the 16 phosphuranylite-group minerals (and one related synthetic compound) (Figs. 10b–i). Both the pentagons and hexagons of the anion topology are occupied by uranyl ions. The triangles are occupied by either (1) faces of PO_4 or (more rarely) AsO_4 tetrahedra, (2) triangular CO_3 groups (Fig. 10g), or (3) the basal plane of irregular tetrahedra containing stereoactive lone-electron pair-bearing-cation oxyanions such as SeO_3 (Fig. 10h–i).

The second type is observed in three minerals and four synthetic compounds, and corresponds to the sheets illustrated in Figures 10j–l. In these compounds, the hexagons of the anion topology are vacant, resulting in isolated, edge-sharing dimers of uranyl pentagonal bipyramids that are bridged by vertex-sharing tetrahedra. In both modes of anion topology population, graphical isomerism results from differences in the orientation of the apical non-bridging anions (or lone-electron pairs in the case of $Se^{4+}O_3$ polyhedra) of the tetrahedra. In phases containing uranyl hexagonal bipyramids and tetrahedral ligands (*i.e.*, PO_4 or AsO_4), there are five graphical isomers (Figs. 10b–f). In phases with irregular tetrahedra with lone-electron pairs, there are two graphical isomers (Figs. 10h–i). The uranyl selenite minerals (marthozite, guilleminite, and larisaite) have sheets that correspond to one graphical isomer, in which tetrahedra on either side of any uranyl hexagonal bipyramid are oriented in a similar manner. In the synthetic uranyl selenate phase, $Sr[(UO_2)_3(SeO_3)_2O_2](H_2O)_4$, a different isomer occurs, wherein the tetrahedra on either side of a hexagonal bipyramid are oriented differently. The orientations of tetrahedral apices are distinguished in the corresponding Figures by color shading.

Phosphuranylite group minerals (and synthetic compounds) contain complex interlayers. All of these include (H_2O) and (at least) one species of cation. Althupite is noteworthy as it contains Al, Th, and (UO_2^{2+}) in the interlayer. The Al^{3+} is present in dimers of octahedra that are linked by edge-sharing to two ThO_9 polyhedra. The two (ThO_9) polyhedra link to adjacent sheets by sharing vertices with uranyl pentagonal bipyramids (*via* the yl oxygen atom) and PO_4 tetrahedra. Each interstitial uranyl pentagonal bipyramid shares vertices with two different PO_4 tetrahedra. Phosphuranylite and vanmeersscheite contain uranyl square bipyramids in the interlayer, and they are amongst the rare examples of compounds containing uranyl ions in all three common coordinations. In phosphuranylite, the four equatorial anions of the interlayer uranyl square bipyramid link to vertices of phosphate tetrahedra, two of which are on each adjacent sheet. In vanmeersscheite, only two equatorial vertices of the uranyl square bipyramid are linked to the vertices of phosphate tetrahedra on adjacent sheets. Each of phosphuranylite, vanmeersscheite, and althupite could be grouped with open three-dimensional frameworks, owing to the strong bonds that serve to link adjacent sheets. This statement also applies to upalite in which the apices of PO_4 tetrahedra on adjacent sheets are linked by AlO_6 octahedra.

The sheets observed in johannite $Sr[(UO_2)_2(CrO_4)_2(OH)_2](H_2O)_8$ and $[Hg_5O_2(OH)_4][(UO_2)$ $(AsO_4)_2]$ can be derived directly from the phurcalite-type sheet by removing the uranyl ions from the hexagonal bipyramids and replacing the tetrahedra (Fig. 10j). The graphical isomers in the sheets present in $Rb_{1.08}[(UO_2)F(PO_3(OH))]$ (Fig. 10k), deliensite (Fig. 10l), and $Cs[(UO_2)(OH)(SeO_4)](H_2O)_{1.5}$ (Fig. 10m) are unique. In the former, all the tetrahedra are similarly oriented, whereas in the latter two, the improper four-fold tetrahedral axis is orientated orthogonal to the plane of the sheet. However, close inspection of the sheets in Figures 10l and 10m reveal differences in the orientation of the tetrahedra.

Burns (2005) noted that the absence of the hexagonally coordinated uranyl ion in $Sr[(UO_2)_2(CrO_4)_2(OH)_2](H_2O)_8$ and $Cu[(UO_2)_2(SO_4)_2(OH)_2](H_2O)_8$ may be promoted by what would be short $^{[2+6]}U^{6+}$–Cr^{6+} and $^{[2+6]}U^{6+}$–S^{6+} distances. However, recently three additional phosphuranylite-types phases with vacant anion topology hexagons have been reported (deliensite, $[Hg_5O_2(OH)_4](UO_2)(AsO_4)_2$, and $Rb_{1.08}[(UO_2)F(PO_3(OH))]$, none of which contain hexavalent tetrahedral cations, suggesting that other factors contribute to differentiating between the two types of phosphyranylite sheets.

Roubaultite anion topology (Fig. 10n–o). The roubaultite anion topology consists of the same infinite chains of edge-sharing pentagon dimers linked by edge-sharing hexagons that is observed in the graphical isomers of the phosphuranylite-types phases. However, in roubaultite, these are separated by chains of edge-sharing squares that are flanked by trimers of edge-sharing triangles. The polyhedral representation of the corresponding sheet shows that all the pentagons and hexagons are occupied by uranyl ions, and one of the triangles (per trimer) is occupied by (CO_3) groups. This results in chains that are identical to those in fontanite. The squares are occupied by ($Cu\Phi_6$) octahedra, resulting in *trans* edge-sharing ($Cu\Phi_4$) chains. The infinite chains of octahedra share vertices with those of the uranyl pentagonal bipyramids and with the (CO_3) triangles; these two features are further linked by (CO_3) groups, which occupy one triangle per flanking trimer of triangles. Adjacent sheets in roubaultite are linked only by H bonds to interlayer (H_2O) groups.

$Cs_2[(UO_2)_4(Co(H_2O)_2)_2(HPO_4)(PO_4)]$ anion topology (Fig. 10p–q). In this sheet topology, each of the triangles are occupied by (PO_4) tetrahedra, where the pentagons and hexagons are occupied by the uranyl ion. All the squares remain vacant. The polyhedral representation shows that the sheets consist of a centrally located hexagonal bipyramid that is edge-sharing with the pentagonal bipyramids, and three (PO_4) tetrahedra that are linked by vertex-sharing through the tetrahedra. CuO_6 octahedra are linked to the surface of the sheet
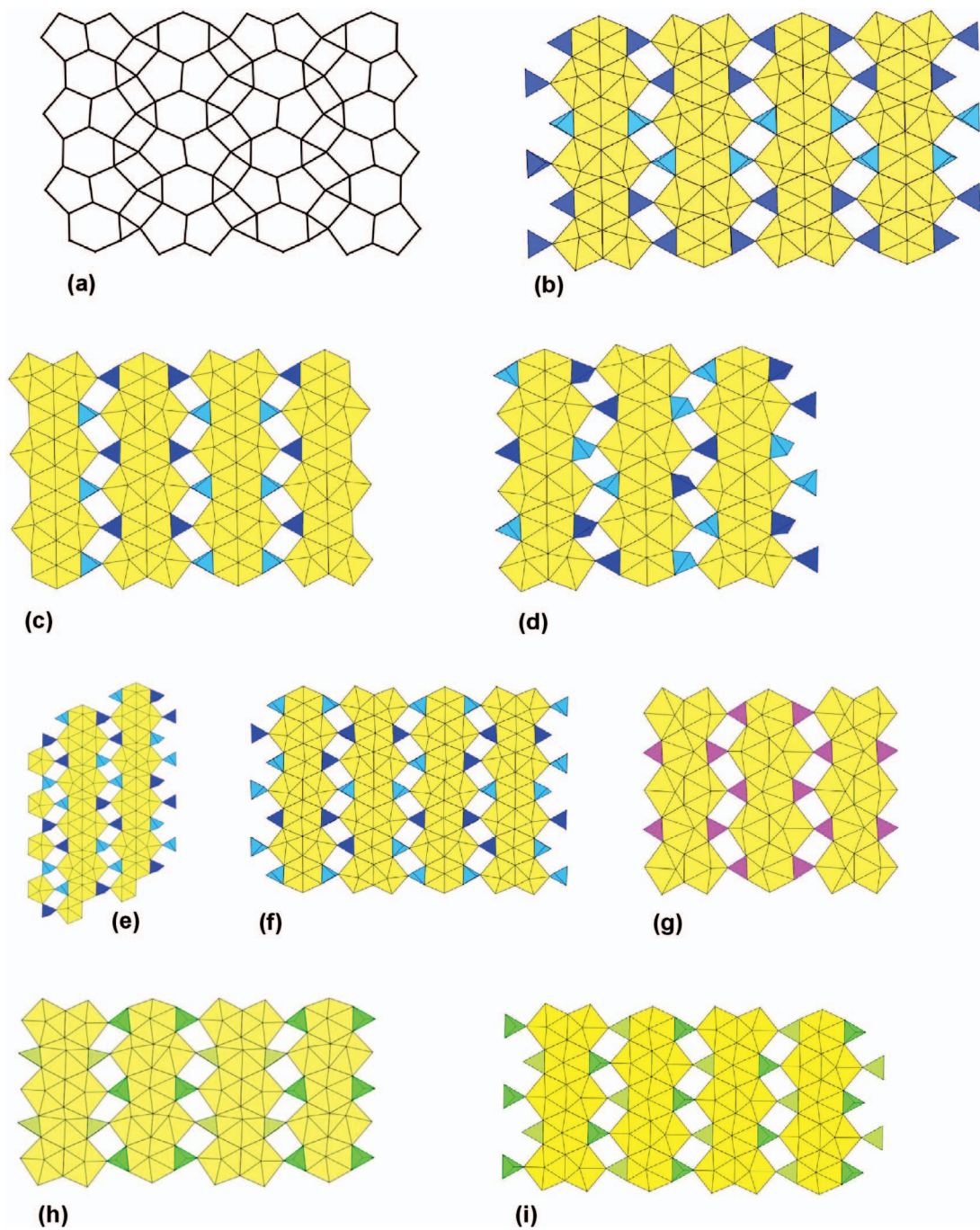
FIG. 10. Sheet-anion topologies, and corresponding polyhedral representations, consisting of triangles, squares, pentagons, and hexagons (*TrSqPtHx* sheets). The corresponding synthetic compounds and minerals are listed in Table 9.

Fig. 10. Continued.

Sheet topologies containing triangles and hexagons (TrHx sheets)
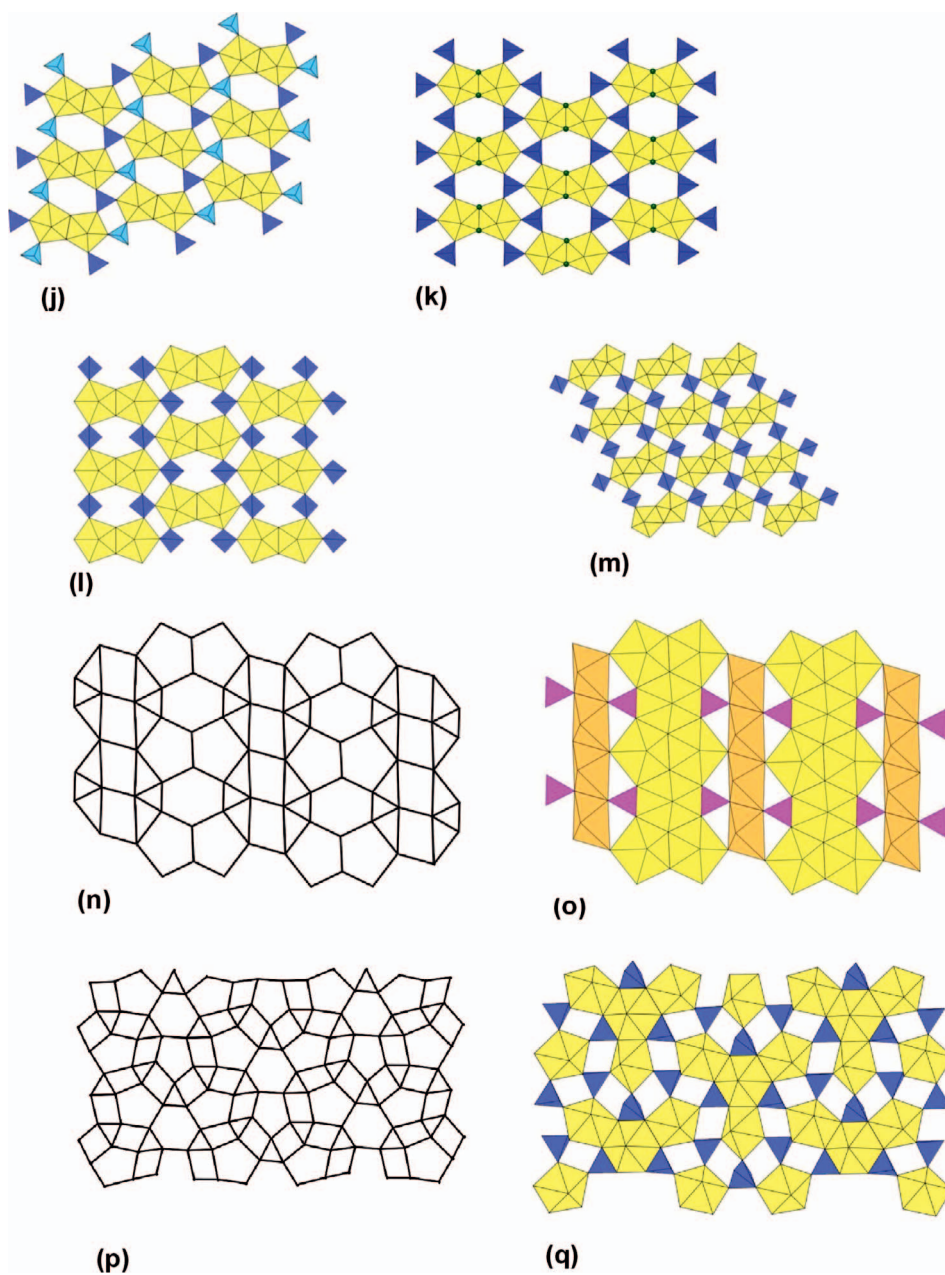
(not shown) and the sheets are stabilized by the presence of (H$_2$O) and Cs in the interlayer.

The hierarchy of Burns (2005) did not include *TrHx sheets*, as only three structures would have been eligible for consideration at that time, and these were simply grouped with miscellaneous sheets. Now, 19 structures corresponding to four sheet anion topologies (and multiple graphical isomers) that are based solely on triangles and hexagons are known. These are listed in Table 10 and illustrated in Figure 11.
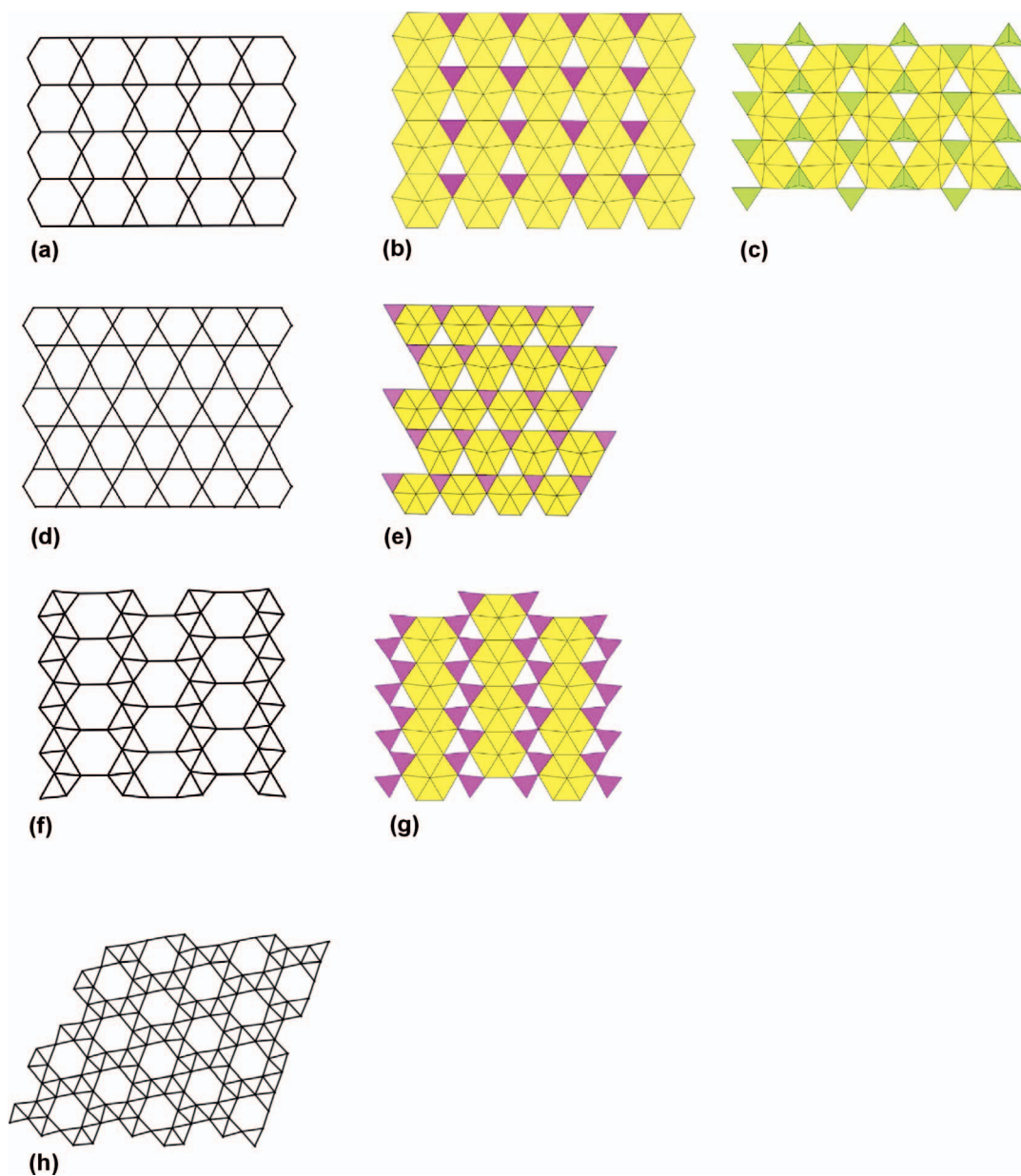
Fig. 11. Sheet-anion topologies, and corresponding polyhedral representations, consisting of triangles and hexagons (*TrHx sheets*). The corresponding synthetic compounds and minerals are listed in Table 10.

The rutherfordine [(UO$_2$)(CO$_3$)] anion topology (Fig. 11a–c). The corresponding sheet-anion topology consists of parallel chains of edge-sharing hexagons separated by dimers of edge-sharing triangles. These dimers of vertex-sharing triangles link such that they form infinite chains between the hexagons. In the polyhedral representation of the corresponding sheet, each of the hexagons is occupied by a uranyl ion, and half of the triangles (one per dimer) are occupied by a (CO$_3$) group, such that all the (CO$_3$) triangles are oriented in the same direction with respect to the plane of projection. The sheet is electroneutral and there are no interlayer species, with sheets linked only by van der Waals bonds.
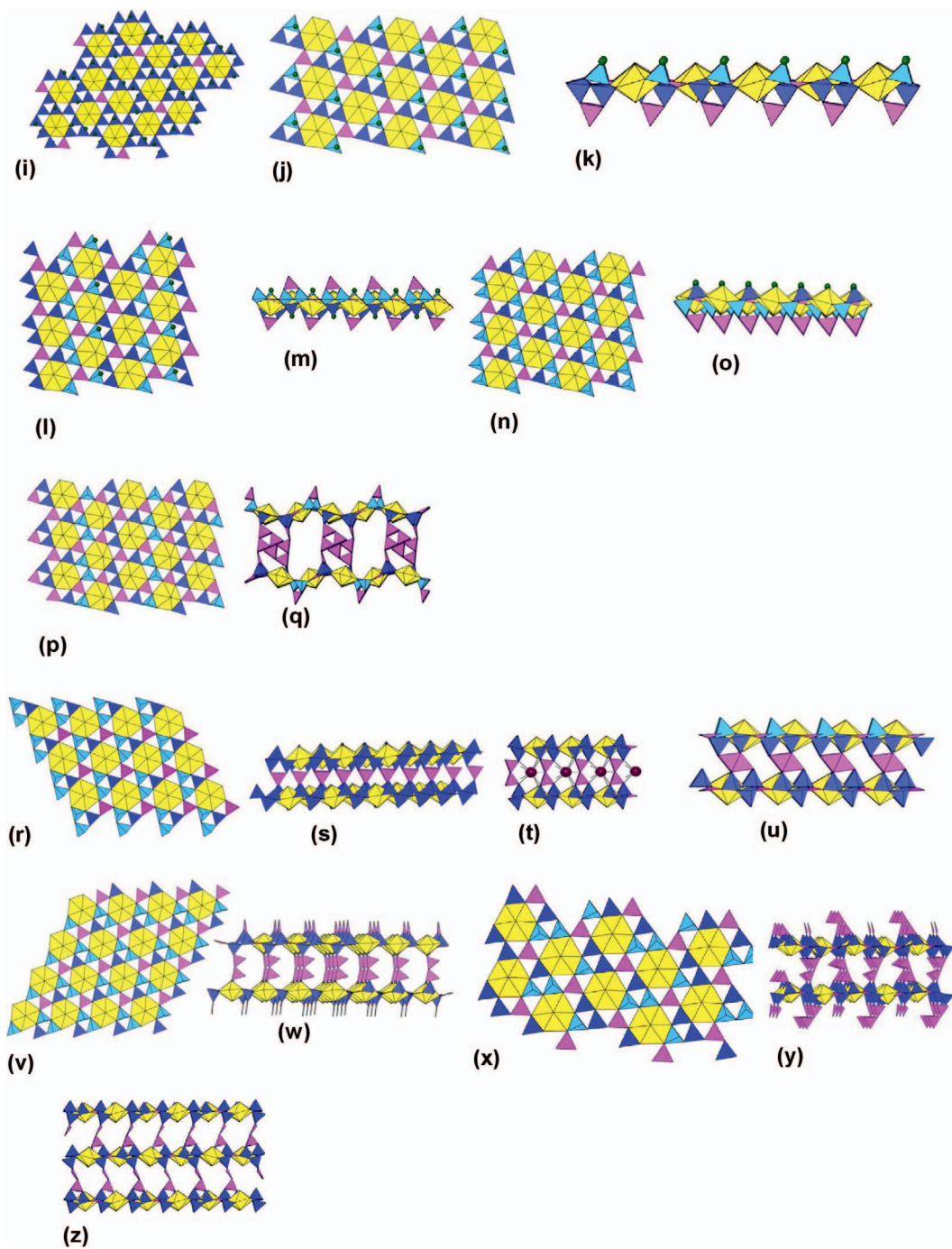
FIG. 11. Continued.

The sheets in $[(UO_2)(SeO_3)]$ (Fig. 11c) are also based on the rutherfordine anion topology. The hexagons are occupied by uranyl ions in the same manner as in rutherfordine, and triangles are occupied by the basal plane of $(Se^{4+}O_3)$ tetrahedra, with the fourth vertex corresponding to the lone-electron pair. In each edge-sharing dimer of triangles, only one of these is occupied. Here the occupied triangles are oriented in two directions. Further, all of the triangles pointing either up or down in the sheet are oriented such that the apex (electron lone-pair) portion of the tetrahedron is oriented in the same direction. These sheets are also electroneutral, and are held together only by van der Waal bonds.

$Pb_{1.85}[(OH)_{1.7}(H_2O)_{0.15}][(UO_2)(CO_3)_2]$ *anion topology (Fig. 11d–e)*. This anion topology is similar to that observed in rutherfordine. Here each of the six hexagonal vertices is shared with another hexagon, and each hexagon shares edges with six triangles. In the polyhedral representation of the corresponding sheet, each hexagon is occupied by a uranyl ion, and half of the triangles (those oriented in the same direction) are occupied by (CO_3) groups. The $UO_2:CO_3$ ratio of this phase is 1:2 and therefore these sheets carry a charge of -2. This charge is balanced by a complex arrangement of variable amounts of Pb^{2+}, (OH), and (H_2O) in the interlayer, which also serve to link the sheets.

$[(UO_2)(B_2O_3)O]$ *anion topology (Fig. 11f–g)*. This anion topology consists of infinite chains of edge-sharing hexagons that are separated by infinite chains of zig-zagging, edge-sharing triangles. In the populated topology, each hexagon is occupied by a uranyl ion, and half the triangles are occupied by (BO_3) groups. This sheet is electroneutral, and adjacent sheets are held together solely by van der Waal interactions. Table 10 lists two reports of the same chemical compound. The first, by Gasperin (1987a), crystallizes in space group $C2/c$, while the more recent, reported by Wang *et al.* (2010c), crystallizes in the uncommon (chiral) space group $C2$.

$Na[(UO_2)(B_6O_{19}(OH)](H_2O)_2$ *anion topology (Hx_1Tr_7 sheets) (Fig. 11h–y)*. There are 15 species containing sheets with this anion topology (Table 10), corresponding to at least seven graphical isomers, as illustrated throughout Figure 11. It contains isolated hexagons that are surrounded by a complex network of edge-sharing triangles. Each hexagon is surrounded by a total of 18 edge-sharing triangles, with a hexagon: triangle ratio of 1:7. In the polyhedral representation of the corresponding sheet each hexagon is occupied by a uranyl ion and half of the triangles are occupied by either flat, triangular (BO_3) groups, or by the basal face of BO_4 tetrahedra; the other half remain vacant. Extensive graphical isomerism is observed in these sheets, resulting from variations of the location of BO_3

and BO_4 polyhedra as well as the orientation of the apical non-bridging anions of the BO_4 tetrahedra. With only two exceptions (discussed below), each of these sheets have $BO_3:BO_4$ ratios of 1:3, although decorating (non-sheet) polyhedra may also be present, where they extend into the interlayer. Compounds that crystallize in centrosymmetric space groups contain enantiomorphic sets of any given Hx_1Tr_7 sheet. All of the uranyl borate phases that adopt the Hx_1Tr_7 sheet were synthesized in fluxes of boric acid at $\sim200\ °C$, resulting in the complex topological arrangement of BO_x polyhedra.

The Tr_1Hx_7 sheets exist in the compounds as isolated (seven compounds; Fig. 11i–o), double (five compounds; Fig. 11r–y), or infinitely linked sheets forming open frameworks (one compound; Fig. 11z). Amongst those containing isolated sheets, K_{11} $[(UO_2)_6(B_{24}O_{36})F_{22}][BO(OH)_2]$ has the unusual $BO_3:$ BO_4 ratio of 1:11 and contains an additional isolated $BO(OH)_2$ triangle in the interlayer that does not bond directly to either of the adjacent structural sheets. The remaining five compounds with isolated Tr_1Hx_7 sheets have the ratio $BO_3:BO_4 = 1:3$, and correspond to three graphical isomers. In each sheet, BO_4 tetrahedra occur as vertex-sharing [3]-member ring trimers, wherein the apical anion of two tetrahedra points in one direction, and the third points in the opposite direction. The apical anions of the pair of commonly oriented tetrahedra are bridged by (BO_3) triangles, and the apical anion of the third tetrahedron is typically fluorine.

Seven compounds occur with Tr_1Hx_7 double sheets linked by complex networks of BO_3 triangles (Figs. 11p–z). In each, the Tr_1Hx_7 sheet occurs with a $BO_3:BO_4$ ratio of 1:3. The same [3]-membered ring trimers of BO_4 groups are observed in all compounds except $[(UO_2)B_{13}O_{20}(OH)_3](H_2O)_{1.25}$ (Fig. 11p, q), in which they occur as linear trimers. No halogen anions occur in these compounds, and all apical anions are either O^{2-} or $(OH)^-$. The adjacent double sheets are linked into the overall structure by a complex network of H bonds that emanate from adjacent sheets and by the presence of interstitial cations in the cases of $K_2[(UO_2)_2B_{12}O_{19}(OH)_4](H_2O)_{0.3}$ and $Rb_2[(UO_2)_2$ $B_{13}O_{20}(OH)_5]$. Interestingly, $Rb[(UO_2)_2B_{10}O_{16}$ $(OH)_3](H_2O)_{0.7}$ contains Rb cations located between the linked sheets and not in the interlayer between adjacent double sheets. In the structure of $Na[(UO_2)$ $(B_6O_{19})(OH)](H_2O)_2$ each adjacent Tr_1Hz_7 sheet is link by vertex-sharing BO_3 groups and by interstitial Na. This linkage results in an open three-dimensional framework structure.

Miscellaneous sheet-anion topologies

Of the known compounds that contain infinite sheets of uranyl polyhedra, 31 do not fit into the

above-presented categories (Table 11). Fourteen are based on sheet anion topologies that contain hexagons. The remaining 17 are based on sheet anion topologies that contain shapes other than the triangles, squares, pentagons, and hexagons used to classify the previous ~250 sheet-based structures. Many of these sheets are based on sufficiently complex topologies that the sheet anion topology approach is ineffective; thus, these are not presented for each of the sheets discussed below.

Miscellaneous sheet topologies with hexagons

α-UO$_3$ *anion topology (Fig. 12a–b).* The α-UO$_3$ sheet anion topology consists solely of hexagons that tile the plane to completion. In α-UO$_3$, each of these is occupied by a uranium atom. The published structure of α-UO$_3$ reports U–O bond lengths that are all in excess of 2 Å, and hence they do not contain uranyl ions. The α-UO$_3$ sheets are linked directly *via* bridging anions, and thus this structure can also be described as a closed framework formed by condensed sheets. However, the eight additional structures that contain the α-UO$_3$ sheet (Table 11) all have U–O bond length distributions characteristic of uranyl compounds; sheets in these phases are separated by an interlayer that is occupied by (OH) emanating from the sheet (*e.g.*, α-[(UO$_2$)(OH)$_2$]) or by mono- or divalent cations.

[(UO$_2$)Nb$_3$O$_8$] anion topology (Fig. 12c–d). This sheet-anion topology consists of hexagons, squares, and triangles. Each hexagon shares its six edges with squares and six vertices with triangles, forming discrete $Hx_1Tr_6Sq_6$ clusters. In the polyhedral representation of the corresponding sheet (Fig. 12d), each hexagon is occupied by a uranyl ion and each square is occupied by either distorted [5]-sided pyramids [(NbO$_5$) or (VO$_5$)] or octahedra (NbO$_6$ or TiO$_6$); the triangles are always vacant. The resulting clusters of polyhedra are linked into sheets. In the three compounds containing these sheets, the manner in which adjacent sheets are linked varies considerably. In [(UO$_2$)(TiNb$_2$O$_8$)], the squares of the sheet-anion topology are occupied by both octahedra and tetrahedra. There are no interlayer cations and adjacent sheets are bridged directly *via* apical anions of the NbO$_5$ and TiO$_6$ polyhedra. In [(UO$_2$)(NbO$_5$)], all niobium is octahedrally coordinated. Adjacent sheets are bridged *via* the apical anions of the octahedra in different sheets. In Cs[(UO$_2$)(VO$_3$)$_3$], two types of linkages occur; Cs$^+$ is present as an interlayer cation between half of the sheets, and successive *sheet-Cs-sheet* blocks are linked only by van der Waals bonding.

[(UO$_2$)(Sb$_2$O$_4$)] anion topology (Fig. 12e–f). This sheet-anion topology consists of infinite chains of edge-sharing hexagons that are separated by infinite chains of squares, and it is known from one compound. In the polyhedral sheet the hexagons are all occupied by uranyl ions, and the squares are occupied by highly irregular SbO$_4$ polyhedra (Fig. 12f). The stereoactive lone electron pair associated with the Sb^{3+} cations projects away from the basal plane of four oxygen atoms that form the square outline. The adjacent sheets are held together *via* van der Waals bonding amplified by the presence of the lone electron pairs.

Ag$_4$[(UO$_2$)$_4$(IO$_3$)$_2$(IO$_4$)$_2$O$_2$] anion topology (Fig. 12g–h). This sheet-anion topology contains infinite chains of edge-sharing hexagons (similar to those observed in the rutherfordine, Fig. 11a–b, and [(UO$_2$)(Sb$_2$O$_4$)], Fig. 12e–f, anion topologies). Pentagons are attached to these hexagons on either side, and the topology is completed by triangles and squares. The hexagons and pentagons of the anion topology are all populated by uranyl ions, producing chains that are linked together *via* IO$_4$ and IO$_3$ polyhedra. The distorted (IO$_4$) polyhedra attach to the edge of the chains of bipyramids and the (IO$_3$) polyhedra link adjacent chains *via* vertex-sharing. Ag$^+$ cations occupy the interlayer.

Cs$_4$[(UO$_2$)$_2$(V$_2$O$_7$)O$_2$] sheets (Fig. 12i). This structure consists of sheets of uranyl square bipyramids that are linked *via* vertex-sharing to form infinite UΦ_5-type chains, similar to those found as isolated chains in the $X_{2–5}$[(UO$_2$)O$_3$]-type compounds listed in Table 3. These parallel chains are linked by vertex-sharing with dimeric tetrahedral pyrovanadate (V$_2$O$_7$)$^{4-}$ groups.

Miscellaneous sheet topologies lacking hexagons

Structures gathered here contain sheets with geometrical shapes other than triangles, squares, pentagons, and hexagons. There are 16 structures in this category (including bijvoetite and haiweeite) that correspond to 13 unique sheet anion topologies.

K[(UO$_2$)(CrO$_4$)(NO$_3$)] sheet (Fig. 12j). This unusual topology is observed in the isostructural compounds K[(UO$_2$)(CrO$_4$)(NO$_3$)] and Rb[(UO$_2$)(CrO$_4$)(NO$_3$)]. The sheets are formed of uranyl pentagonal bipyramids, each of which is vertex-sharing with three CrO$_4$ tetrahedra. Each tetrahedron is [3]-coordinated by uranyl polyhedra. The remaining equatorial edge of each uranyl polyhedron is shared with a (NO$_3$) triangle. The (NO$_3$) triangle contains one non-bridging ligand. The sheets are linked by Rb$^+$ or K$^+$ cations in the interlayer.

Tl$_3${(UO$_2$)$_2$[Te$_2$O$_5$(OH)](Te$_2$O$_6$)}2H$_2$O sheet (Fig. 12k). This compound contains sheets of uranyl pentagonal bipyramids that are isolated from other bipyramids within the sheet. Infinite chains of vertex-sharing, highly distorted (Te$^{4+}\Phi_4$) pyramids are also
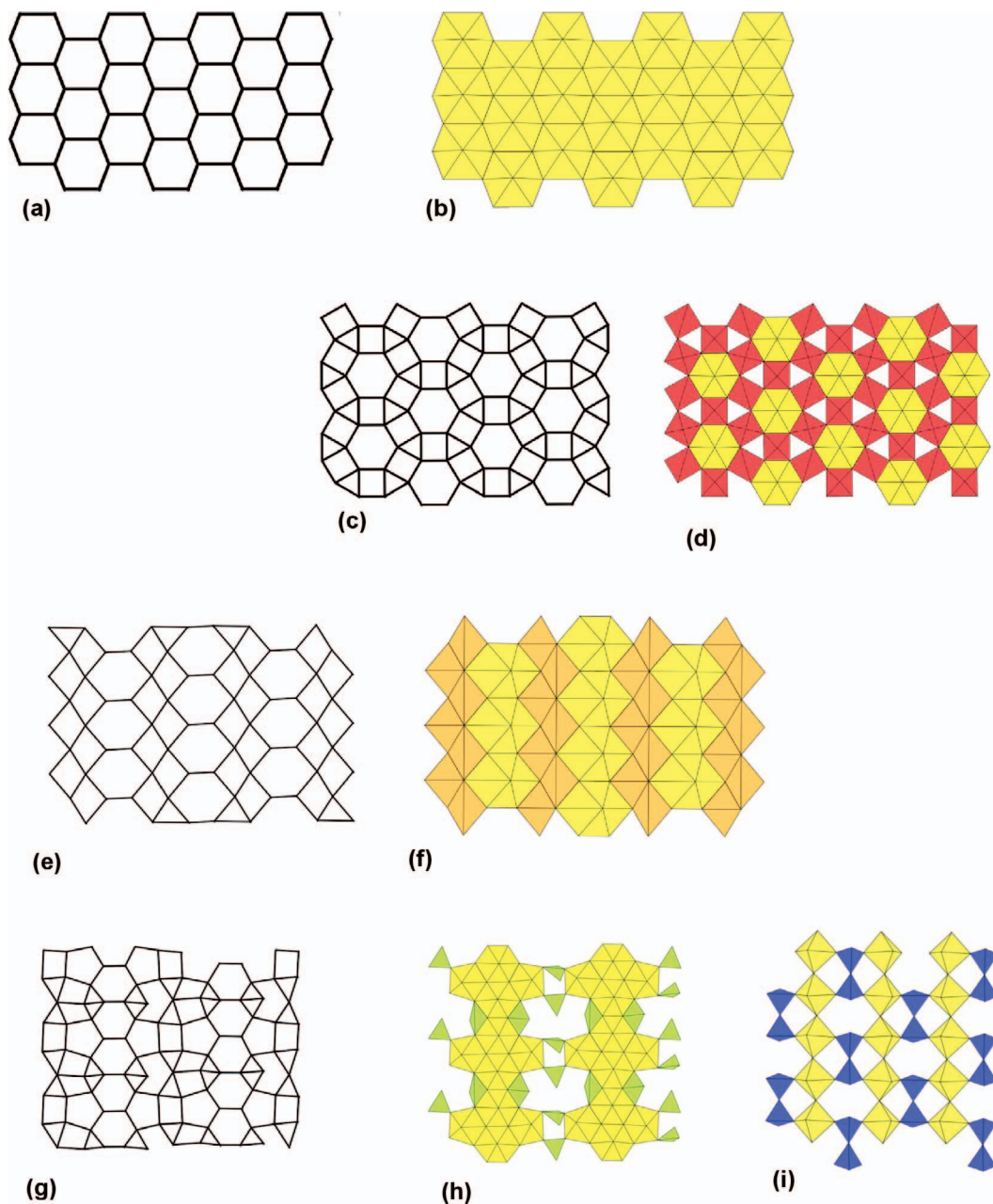
FIG. 12. Sheets with miscellaneous anion topologies and corresponding polyhedral representations. (a–i) Sheets with anion topologies containing hexagons. (j–v) Sheet-anion topologies lacking hexagons. The corresponding synthetic compounds and minerals are listed in Table 11.

present. Uranyl pentagonal bipyramids link to these chains by both edge- and vertex-sharing of equatorial anions. In the interlayer, Tl^+ cations serve to link adjacent sheets.

$[(UO_2)(Se_2O_5)]$ *topology (Fig. 12l)*. This sheet is based on dimers of edge-sharing uranyl pentagonal bipyramids. These are arranged in a similar configuration to that observed in the sheets shown in Figure

FIG. 12. Continued.

(w)
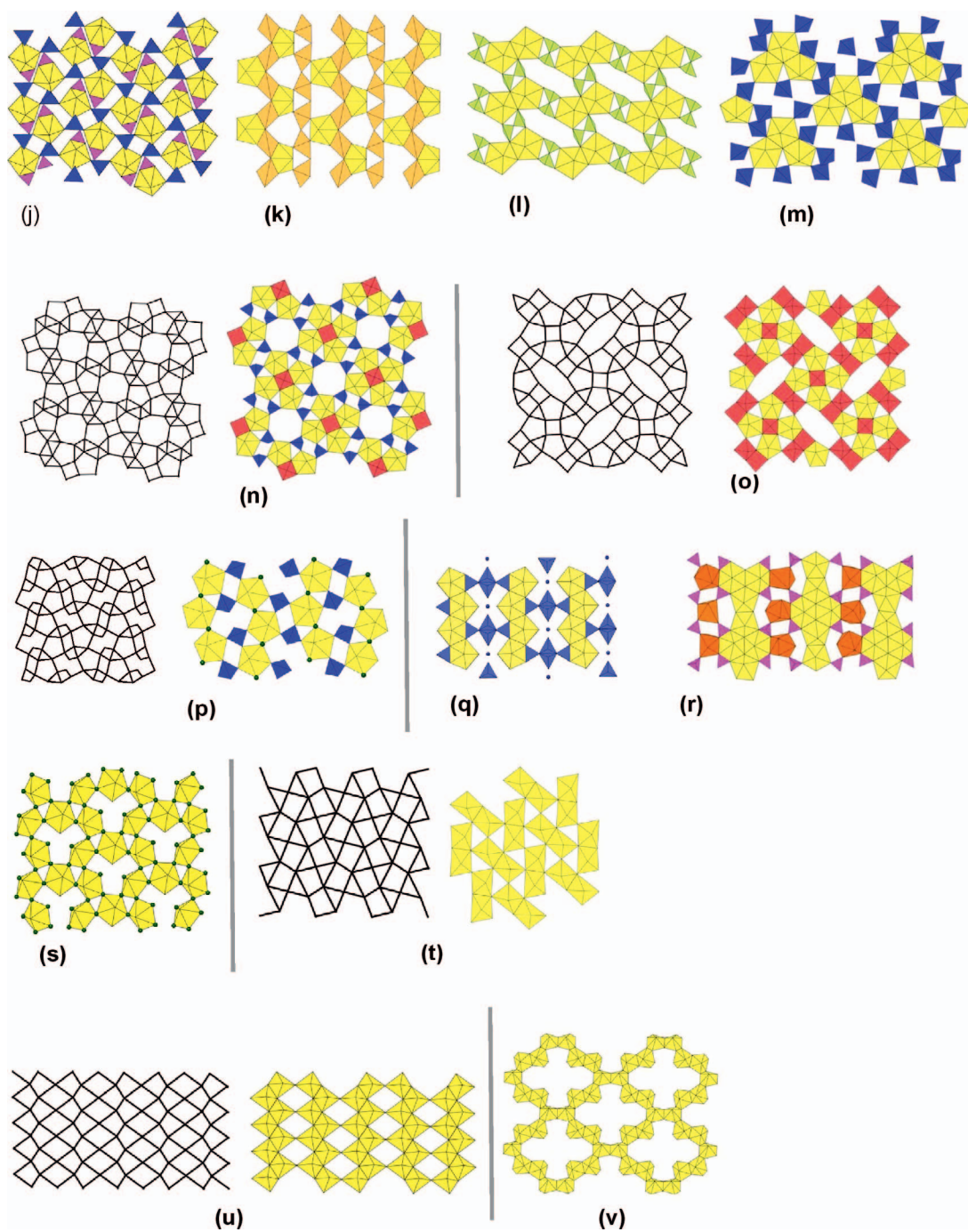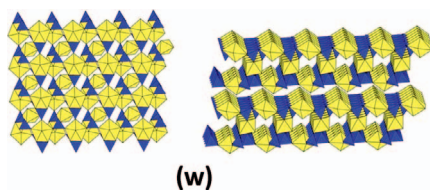
Fig. 12. Continued.

10j–m, but the manner in which these are linked is very different. Here, vertex-sharing (Se_2O_5) groups link the uranyl dimers lengthwise and widthwise through vertex-sharing. The structure is anhydrous and lacks interstitial cations; the electroneutral sheets are linked by electrostatic interactions associated with the lone electron pair emanating from the (Se_2O_5) groups.

$Ag_6[(UO_2)_3O(MoO_4)_5]$ topology (Fig. 12m). This sheet consists of edge-sharing trimers of uranyl pentagonal bipyramids linked by $(MoO_4)^{2-}$ tetrahedra via vertex-sharing. Each trimer is linked to nine tetrahedra, eight of which are directly involved in bridging adjacent trimers, whereas the remaining tetrahedron shares two vertices with each pentagonal trimer. Each bridging tetrahedron links two distinct clusters in the sheets, and two tetrahedral coordination environments are observed: one type links only two polyhedra, and in the other type one vertex is bonded to two uranium centers and the other bonds to only one. The structure is anhydrous, and interstitial Ag^+ cations link adjacent sheets.

Mathesiusite and $Cs_6[(UO_2)_4(W_5O_{21}(OH)_2)](H_2O_2)$ sheet topologies (Fig. 12n–o). These sheet topologies are very similar. Both are based on edge-sharing Sq_1Pt_4 'iron cross' configurations observed in other chain [(e.g., $X_8[(UO_2)_4(WO_4)_4(WO_5)_2]$ (X = Rb, Cs); Fig. 4ag] and sheet [$Cs_9[(UO_2)_8O_4(NbO_5)(Nb_2O_8)_2]$; Fig. 9ai) compounds. In both, the square is occupied by the basal plane of five-sided pyramids of VO_5 and WO_5 groups, respectively. However, the two structures differ in how these Sq_1Pt_4 are linked to form infinite sheets. In mathesiusite-type sheets, they are linked by vertex-sharing (SO_4) tetrahedra. Each sulfate tetrahedron coordinates three unique uranyl polyhedra, two from the same cross structure, and one from a different cross. In each polyhedron, the three equatorial anions that are not linked to the centrally coordinated [5]-sided pyramid each link to a (SO_4) group. In mathesiusite, the iron crosses are arranged to form an oblique [2]-dimensional net. By contrast, topologically identical crosses in the sheet of $Cs_6[(UO_2)_4(W_5O_{21}(OH))](H_2O_2)$ are linked by edge-sharing dimers of WO_5 [5]-sided pyramids, consisting of opposite-oriented apical anions. These dimers each

link two cross configurations to form the complex sheet, resulting in a face-centered [2]-dimensional net. In both compounds, a network of monovalent cations (K^+ or Cs^+) and (H_2O) link adjacent sheets.

$[(UO_2)(SeO_4)F](H_2O)$ (Fig. 12p). This sheet occurs in the isostructural compounds $X[(UO_2)(SeO_4)F]$ (H_2O) (where X = Rb^+, NH_4^+). It consists of uranyl pentagonal bipyramids that are vertex-linked to form infinite parallel chains. These chains are linked, forming infinite sheets, via vertex-sharing tetrahedra such that each tetrahedron is bridged to three individual uranyl pentagonal bipyramids. Both Rb and (H_2O) are present in the interlayer.

Haiweeite, $Ca[(UO_2)_2Si_5O_{12}(OH)_2](H_2O)_3$ (Fig. 12q). The structure of haiweeite contains uranophane-type chains of edge-sharing uranyl pentagonal bipyramids with edge-sharing (SiO_4) tetrahedra. However, the linkages between these chains differs sharply from that of the uranophane group. In haiweeite, a complex network of (SiO_4) tetrahedra links these chains of uranyl pentagonal bipyramids and silicate tetrahedra, whereas in the uranophane group, the chains are linked directly by sharing vertices. Refining the configuration of this tetrahedral network, however, has required several attempts over the past two decades. Rastsvetaeva et al. (1997) reported the first structure of haiweeite (with a cell corresponding to: a 14.263(2) Å, b 17.988(3) Å, c 18.395(2) Å, $P2_12_12_1$) and showed that it contains a new type of uranyl silicate sheet. Burns (2001a) proposed a revised orthorhombic structure (cell: a 7.125 Å, b 17.973 Å, c 18.342 Å, $Cmcm$) and showed that the uranophane type chains were linked by 'crankshaft'-like chains of vertex-sharing silicate tetrahedra. Several of the Si positions were designated as partially occupied. Recently, Plášil et al. (2013a) argued that these partially occupied Si sites occur because the cell of Burns (2001a) corresponds to an averaged structure. These authors proposed an updated orthorhombic cell (a 18.3000(5) Å, b 14.2331(3) Å, c 17.9192(5) Å, $Pbcn$) after observing weak reflections corresponding to a doubling of the a-parameter reported by Burns (2001a). In the doubled cell of Plášil et al. (2013a), all Si, U, and Ca positions are fully occupied, resulting in continuous chains of vertex-sharing (SiO_4) tetrahedra

that link the uranophane-type chains to produce the observed sheets. Both Ca and (H_2O) are present in the interlayer and link adjacent sheets.

Bijvoetite, $[M^{3+}(H_2O)_{25}(UO_2)_{16}O_8(OH)_8(CO_3)_{16}]$ $(H_2O)_{14}$ *(Fig. 12r).* The complex sheet of bijvoetite consists of infinite chains of edge-sharing uranyl pentagonal and hexagonal uranyl bipyramids, as well as trivalent-cation polyhedra and carbonate groups. Each hexagonal bipyramid shares edges with two triangular (CO_3) groups. The infinite chains are linked by irregularly coordinated cation positions that are occupied by variable amounts of rare-earth elements, Y^{3+}, and Nd^{3+}. The sheet is extensively hydrated, with two (OH) groups occupying the equatorial positions of each uranyl pentagonal bipyramid and (H_2O) groups linked directly to the large M^{3+} cation sites. The interlayer contains many (H_2O) molecules, resulting in a complex network of H bonding that ultimately serves to stabilize the adjacent sheets. Bijvoetite is a rare example of a mineral that contains uranyl carbonate sheets (in addition to rutherfordine, fontanite, and wyartite), as most uranyl carbonates contain the isolated uranyl triscarbonato [*i.e.,* $(UO_2)(CO_3)_3$] cluster.

$K_2[(UO_2)_3F_8(H_2O)](H_2O)_3$ (Fig. 12s). This sheet consists of edge-sharing uranyl pentagonal bipyramids linked by F^- anions to form [6]-membered rings of polyhedra. In each ring, five of the six uranyl pentagonal bipyramids contain only F^- at the equatorial positions. Those of the remaining bipyramid, however, contain $F_4(H_2O)$, with the (H_2O) extending towards the center of the ring. Successive rings are themselves linked by vertex-sharing to form the observed sheet. Potassium cations and (H_2O) groups occupy the interlayer and link the adjacent sheets.

$Rb_2[U_2O_7]$ anion topology (Fig. 12t). This sheet-anion topology is the only one known that consists solely of squares and triangles. The squares occur as edge-sharing dimers that are linked together through vertex-sharing. These occur in two different orientations, angled at approximately 45° relative to each other. Between these are isolated triangles. In the polyhedral representation of the corresponding sheet, each square is occupied by a uranyl ion and each triangle is vacant. Only Rb is present in the interlayer to link adjacent sheets.

β-$Cs_2[(UO_2)_2O_3]$ anion topology (Fig. 12u). This sheet-anion topology consists of two types of squares. The first is relatively large, with a fairly regular geometry, and the second is distorted with one edge slightly shortened. The irregular squares form parallel, zig-zag chains by edge-sharing, whereas the regular squares form parallel chains by vertex-sharing. In the polyhedral representation of the corresponding sheet, the irregular squares are occupied by uranyl ions

resulting in distorted uranyl square bipyramids that are very similar to those in the sheets illustrated in Figures 9ba and bc. Cesium cations are located in the interlayer.

$Na_5[(UO_2)_3(O_2)_4(OH)_3](H_2O)_{13}$ anion topology (Fig. 12v). The sheet observed in the compound $Na_5[(UO_2)_3(O_2)_4(OH)_3](H_2O)_{13}$ consists solely of edge-sharing uranyl di-peroxo hexagonal bipyramids. These polyhedra are linked by hydroxyl bridges to form dimers of the type observed in Figure 3p. Successive dimers link *via* peroxo bridges to form the complete sheet. A complex network of Na and (H_2O) in the interstitial region stabilizes the adjacent sheets.

Lastly, the structure of $Na_{5.5}[(UO_2)_3(H_{0.5}PO_4)$ $(PO_4)_3]$ contains the sheet topology shown in Figure 12w. Here, UL-L_2 clusters link successively to form a uranophane-type sheet wherein every second pentagon is vacant. A uranyl square bipyramid serves to link doublets of these sheets together. Sodium, present in the region between these doublets, then serves to stabilize the structure.

STRUCTURES BASED ON FRAMEWORKS OF URANIUM POLYHEDRA

Framework structures are those in which relatively strong bonds (*i.e.,* >0.2 *vu*) are directed throughout the structure in all three dimensions. A framework may contain only vertex-sharing uranium (usually uranyl) polyhedra or may include an assortment of other high-valence polyhedral species. There are 186 known compounds (and only 13 minerals) with stoichiometric quantities of U^{6+} that are classified here as frameworks. In Burns (2005), 56 framework structures are listed in categories based primarily on the chemical composition of ligand polyhedra, hence frameworks of: (1) uranium polyhedra; (2) uranium polyhedra with silicate tetrahedra; (3) uranium polyhedra with phosphate, arsenate, or vanadate tetrahedra; (4) uranium polyhedra with molybdate tetrahedra; and (5) miscellaneous frameworks. The nearly four-fold increase in framework structures now requires a more sophisticated approach to classification, in part because compositionally based subdivisions hinder useful comparison of common structural features. Here, structures are divided into classes that emphasize common topological features that link to form the complete framework. Hence, frameworks are grouped as: (1) only uranium polyhedra; (2) *UL*-clusters; (3) linked chains (parallel and interpenetrating); (4) strongly linked sheets; (5) cation-cation interactions; and (6) miscellaneous topologies. We attempt to order these structures on the basis of their increasing connectivity of uranium polyhedra. For example, Table 18 lists the frameworks containing cation-cation

TABLE 12. U(VI) COMPOUNDS CONTAINING FRAMEWORKS BASED ON ELEMENT-SHARING URANYL POLYHEDRA

MINERAL	FORMULA	SG	a (Å)	b (Å)	c (Å)	α (°)	β (°)	γ (°)	SYN[a]	FIG	REF
Vertex-sharing uranium polyhedra only											
	δ-UO_3	$Pm\overline{3}m$	4.165	4.165	4.165	—	—	—	HT[375]	13a	1
	$K_9[BiU_6O_{24}]$	$Pm\overline{3}m$	8.631	8.631	8.631	—	—	—	SS[1200]	13b	2
	$K_6Ba_2[CaU_6O_{24}]$	$Im\overline{3}m$	8.680	8.680	8.680	—	—	—	SS[1200]	13c	3
	$BaK_4[U_3O_{12}]$	$Im\overline{3}m$	8.723	8.723	8.723	—	—	—	Flx[1050]	13c	4
	Ba_2CaUO_6	$P2_1/n$	6.162	6.119	8.698	—	90.10	—	SS[1300]	13c	5
	$Ba_2[MgUO_6]$	$Fm\overline{3}m$	8.379	8.379	8.379	—	—	—		13d	6
	$Sr_2[CoUO_6]$	$P2_1/n$	5.792	5.803	8.179	—	90.15	—	SS[1150]	13d	7
	$Sr_2[ZnUO_6]$	$P2_1/n$	5.832	5.812	8.200	—	89.96	—	SS[950]	13d	8
	$Sr_2[NiUO_6]$	$P2_1/n$	5.781	5.775	8.156	—	89.84	—	SS[950]	13d	8
	$Sr_2[FeUO_6]$	$P2_1/n$	5.799	5.782	8.167	—	89.83	—	SS[950]	13d	8
	$Sr_2[MnUO_6]$	$P2_1/n$	5.897	5.854	8.278	—	90.01	—	SS[950]	13d	8
	$Sr_2[MgUO_6]$	$P2_1/n$	5.802	5.796	8.187	—	89.99	—	SS[1150]	13d	9
	$Sr_2[CdUO_6]$	$P2_1/n$	6.049	5.929	8.429	—	89.88	—	SS[900]	13d	9
	$Ba_2[CaUO_6]$	$I4/mmm$	5.779	5.779	8.810	—	—	—	SS[1050]	13d	10
	$Ba_2[NiUO_6]$	$Fm\overline{3}m$	8.335	8.335	8.335	—	—	—	SS[1150]	13d	10
	$Ba_2[ZnUO_6]$	$Fm\overline{3}m$	8.383	8.383	8.383	—	—	—	SS[1050]	13d	10
	$Pb_2[MgUO_6]$	$P2_1/n$	5.846	5.834	8.249	—	90.06	—	SS[1050]	13d	11
	$Pb_2[CaUO_6]$	$P2_1/n$	6.059	5.974	8.526	—	89.92	—	SS[1050]	13d	11
	$Pb_2[CdUO_6]$	$P2_1/n$	5.989	6.033	8.514	—	89.90	—	SS[850]	13d	11
	$(Sr_{0.5}Ba_{0.5})_2Sr(UO_6)$	$P2_1/n$	6.169	6.167	8.734	—	89.07	—	SS[1500]	13d	9
	Ba_2SrUO_6	$Fm\overline{3}m$	8.938	8.938	8.938	—	—	—	SS[1400]	13d	12
	$[CoUO_4]$	$Imma$	6.497	6.952	6.497	—	—	—		13e	13
	$[CuUO_4]$	$P2_1/n$	5.475	4.957	6.569	—	118.87	—	HT	13e	14
	$[Rh_2UO_6]$	$P4_2/mnm$	4.744	4.744	9.360	—	—	—		13e	15
	β-$Cd(UO_2)O_2$	$Cmmm$	7.023	6.849	3.514	—	—	—	SS[850]	13e	16
	$Mn(UO_2)O_2$	$Imma$	6.647	6.984	6.75	—	—	—		13e	17
	$Cs[TaUO_6]$	$Fd\overline{3}m$	10.785	10.785	10.785	—	—	—	SS[1050]	13f	18
	$Cs[SbUO_6]$	$Fd\overline{3}m$	10.729	10.729	10.729	—	—	—	SS[1050]	13f	18
Vertex- and edge-sharing uranium polyhedra											
	β-UO_3	$P2_1$	10.34	14.33	3.910	—	99.03	—	SS[500]	13g	19
	γ-UO_3	$Fddd$	9.787	19.932	9.705	—	—	—		13h	20
	$[(UO_2)F_2(H_2O)](H_2O)_{0.571}$	$C2/c$	13.843	9.801	24.970	—	104.47	—	HT[150]	13i	21
Edge-sharing polyhedra only											
Vorlanite	$[(Ca_{1.06}U_{0.94})O_4]$	$Fm\overline{3}m$	5.381	5.381	5.381	—	—	—		13k	22

Note: Double lines (═) indicate major differences in the stoichiometry of the structural unit, as indicated by the corresponding header in the table; single lines (–) indicates different topologic configurations; and dotted lines (- -) separate graphical isomers.

[a] Synthesis column data. HT[T] and SS[T] correspond to hydrothermal and solid state synthesis, respectively, at maximum reported temperature T (°C); V-Cl: vapor phase chlorination; A, aqueous (Ae denotes evaporation to dryness); Ac, concentrated acid; Flx, molten flux; SDg, slow diffusion in gel.

References: (1) Weller *et al.* (1988); (2) Gasperin *et al.* (1991); (3) Saine (1987); (4) Roof *et al.* (2010b); (5) Fu *et al.* (2008); (6) Padel *et al.* (1972); (7) Pinacca *et al.* (2005); (8) Pinacca *et al.* (2007); (9) Chernorukov *et al.* (2010); (10) Roof *et al.* (2010c); (11) Knyazev *et al.* (2011); (12) Reynolds *et al.* (2013); (13) Bertaut *et al.* (1962); (14) Siegel & Hoekstra (1968); (15) Omaly & Badaud (1972); (16) Yamashita *et al.* (1981); (17) Bacmann & Bertaut (1966); (18) Knyazev & Kuznetsova (2009); (19) Debets (1966); (20) Loopstra *et al.* (1977); (21) Mikhailov *et al.* (2002b); (22) Galuskin *et al* (2011).

interactions, and these are further subdivided into CCI structures wherein uranium polyhedra form chains, sheets, and true infinite frameworks.

Frameworks of vertex-sharing uranium polyhedra

There are 32 compounds (one mineral, vorlanite) corresponding to nine structure types with framework structures that are based on vertex-sharing uranium polyhedra; these are listed in Table 12 and illustrated in Figure 13. These are sub-divided into frameworks formed of (1) only vertex-sharing (28 compounds), (2)

both vertex and edge sharing (three compounds), and (3) only edge-sharing (one compound). These phases are either composed solely of uranium polyhedra (*e.g.*, δ-UO_3), or have additional cations existing in a coordination environment that is identical to U^{6+} (shown in red) (*e.g.*, $K_9[BiU_6O_{24}]$). Although all contain U^{6+}, most lack uranyl ions.

Many structures are [3]-dimensional arrays of vertex-sharing octahedra (Table 12) in which each octahedral vertex bridges to an additional octahedron. This creates [12]-coordinated voids, which may (or
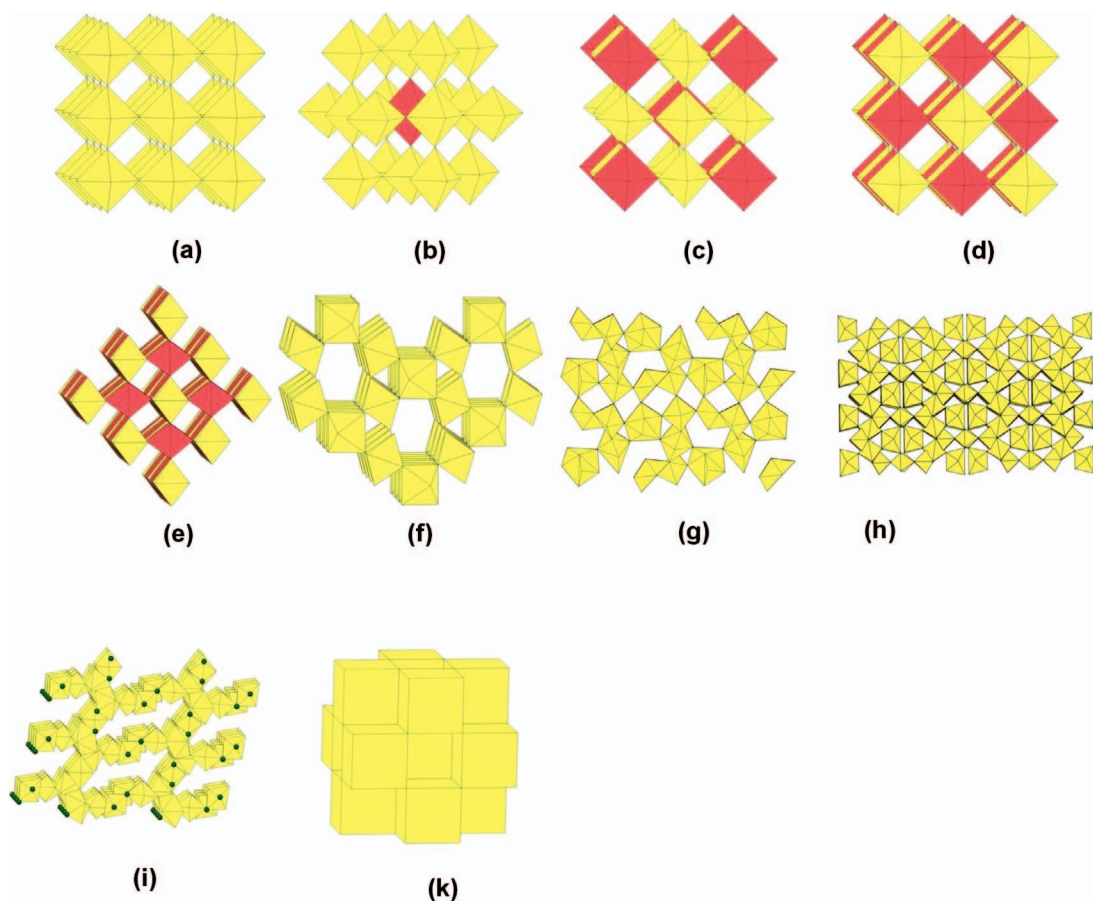
FIG. 13. Framework structures formed by element-sharing uranium polyhedra. The corresponding synthetic compounds and minerals are listed in Table 12.

may not) be occupied by additional cations of the interstitial complex. In the simplest of these, the structure of δ-UO_3 (Fig. 13a), uranium octahedra are regular (no uranyl ion) and the voids are vacant. The structure of $K_9[BiU_6O_{24}]$ is the same basic topology (Fig. 13b) with three departures: (1) two-thirds of the octahedral positions are uranyl square bipyramids, and the remaining one-third are octahedrally coordinated U^{6+}; (2) one-seventh of the UO_6 octahedra are instead occupied by BiO_6 octahedra that are located at the body center of the isometric cell; and (3) the octahedral environment next to the –yl oxygen atom contains a [12]-coordinated K^+ cation. The structures of $(Ba_2K_6)[CaU_6O_{24}]$ and $(BaK_4)[U_3O_{12}]$ (Fig. 13c) have the same topology as the δ-UO_3 framework, with two-fifths of the octahedral positions occupied by low-valence cations (*i.e.*, K, Ba) in octahedral coordina-tion. Similarly, the 16 compounds corresponding to Figure 13d have the basic δ-UO_3 topology with no

uranyl ions present. In these structures, half of the octahedra are occupied by a divalent cation (*e.g.*, Mg^{2+}, Co^{2+}, Zn^{2+}, Fe^{2+}, *etc.*), and each [12]-coordinated void is occupied by two large divalent cations (*e.g.*, Sr^{2+}, Ba^{2+}, Pb^{2+}). The size difference between these two cations is overcome by inducing a shearing distortion and rotation of the uranium octahedra. The irregular polyhedra coordinating the large divalent cations are, in turn, linked together by edge-sharing, thus forming interpenetrating chains.

The five compounds corresponding to Figure 13e are isostructural with the rock-forming rutile-group minerals. The structure contains infinite parallel chains of *trans*-edge-sharing $(M,U)O_4$ octahedra. Adjacent chains are linked by shared vertices such that the chains are oriented at right angles with respect to one another. This arrangement forms the very compact framework shown in Figure 13e. There are three sequences of octahedral occupancy observed in the

(MO_4)-type chains of the rutile-type phases. In [$CdUO_4$], [$MnUO_4$], and [$CoUO_4$], all the octahedrally coordinated cations in any particular chain are of the same species; two chains are observed, MO_4 (where M is either Cd, Mn, or Co) and UO_4. The structures of [$CuUO_4$] and [Rh_2UO_4] both contain only one type of chain. In [$CuUO_4$] Cu and U alternate, and in [Rh_2UO_4], the sequence Rh-Rh-U-Rh-Rh-U occurs. In all but one of the rutile-type structures, the axis of the uranyl ion is oriented perpendicular to the plane formed by the sharing of the *trans* octahedral edges. The compound [$CuUO_4$] is unusual in that both the axis of the uranyl ion and the elongated Cu–O bonds (of the Jahn-Teller distorted octahedra) are in the edge-sharing plane.

The isostructural compounds Cs[$TaUO_6$] and Cs[$SbUO_6$] consist of infinite UO_4-type chains of uranium octahedra linked by vertex sharing to form a complex network of linked parallel chains that form irregularly shaped channels occupied by Cs^+ cations of the interstitial complex (Fig. 13f). The structure refinements for each of these compounds indicate that the elemental pairs of either Ta^{5+}–U^{6+} or Sb–U^{6+} are disordered over the octahedra with a 1:1 ratio. In both compounds, octahedra are formed by six equidistant bonds, with no uranyl ions.

There are three compounds with frameworks that are based on both edge- and vertex-sharing uranium polyhedra. The structures of β-UO_3 (Fig. 13g) and γ-UO_3 (Fig. 13h) both consist of vertex- and edge-sharing uranyl bipyramids that form very complex topologies. In the structure of [(UO_2)F_2(H_2O)], uranyl pentagonal bipyramids occur as edge-sharing dimers that are bridged by pairs of F^- anions, or as single polyhedra with only H_2O groups at the equatorial positions. The dimers and monomers are linked by vertex-sharing to result in the complex [3]-dimensional topology shown in Figure 13i.

The structure of vorlanite, [($Ca_{1.06}U_{0.94}$)O_4], is the only framework structure that is based solely on edge-sharing uranium polyhedra (Fig. 13k). Vorlanite has the fluorite structure that also occurs for uraninite, UO_2. Calcium and U^{6+} are disordered over [8]-coordinated cubic sites. Galuskin *et al.* (2011) noted that the black color of vorlanite is uncharacteristic of phases with hexavalent uranium, and that there is a marked discrepancy between the crystallographic symmetry ($fm\overline{3}3m$) and crystal morphology ($\overline{3}m$), suggestive of pseudomorphism. In the refined structure the U–O bond length is ~2.3 Å, but high refined displacement factors for the uranium site, in combination with Raman spectra, correspond to shorter body diagonals (1.98 Å), and suggest disorder of uranyl ions. Galuskin *et al.* (2011) also showed that when vorlanite is heated above 750 °C the structure

transforms into rhombohedral $CaUO_4$ with an ordered distribution of Ca and U. Such a phase could form in high-temperature skarns and undergo a phase transition to vorlanite upon cooling, with the transformation perhaps aided by the α-decay of uranium.

Frameworks based on UL_x clusters with only vertex-sharing

In addition to forming the complex array of [2]-dimensional sheets illustrated in Figure 5, the UL_x-type clusters polymerize into topologically complex frameworks. The majority of these structures contain a single species of tetrahedrally coordinated (*e.g.*, SiΦ$_4$, SΦ$_4$, PΦ$_4$, GeΦ$_4$), or less commonly octahedrally coordinated (*e.g.*, MgΦ$_6$, AlΦ$_6$) ligands. Burns (2005) lists only 15 compounds in this category, whereas there are currently 46.

All the structures included in this category (Table 13) contain uranyl polyhedra that are in either square or pentagonal bipyramidal coordination. Uranyl polyhedra are never element-sharing with other uranyl polyhedra in these structures, but adjacent ligand polyhedra can be vertex-sharing. These structures are organized on the basis of the ligand-ligand connections into groups wherein tetrahedra exist as monomers (*i.e.*, bridged only to non-tetrahedral species), dimers, trimers, infinite chains, or complex sheets.

The framework structures grouped here involve linkages of clusters in the [2]-dimensional sheets listed in Tables 4–5. The graphical connectedness approach was an efficient tool in the hierarchical organization of these [2]-dimensional sheets (Krivovichev 2004); however, it is difficult to extend this approach to higher dimensionality because (1) there is a non-unique choice of nodal 'rings', and (2) it is difficult to represent [3]-dimensional connectivity with a [2]-dimensional projection. However, if we consider each uranyl bipyramid and each tetrahedron as a framework node, it is straightforward to calculate the average coordination number, which informs on the degree of connectedness in a [3]-dimensional framework and facilitates comparison. These values are presented in Table 13 for each structure in the form $A_iB_jN_k$. Here, the structures are reduced to a three-dimensional graphical representation, wherein each polyhedron is represented by a connection node, and each polyhedron-polyhedron linkage (vertex-sharing) is represented by a connecting line. The number of connecting lines for each node is tabulated and corresponds to the values of $A, B, \ldots N$. The relative frequency in which similar nodal configurations occur is represented by the subscripts i, j, k; note that the coordination number of the high-valence cations (*i.e.*, tetrahedral, octahedral) is disregarded. Such an approach facilitates the

organization of complex, three-dimensional structures based on the complexity of the connecting network. As example, in the structure of $K_5[(UO_2)(Si_4O_{12}(OH))]$, each uranyl square bipyramid bridges to four SiO_4 tetrahedra *via* the equatorial anions, and each tetrahedron links to two additional tetrahedra and a uranyl polyhedron; the former occurs three times as often as the latter. Hence, we designate this connectivity 4_33_1. The structures in Table 13 are ranked on the bases of increasing coordination number and occurrence in the structure.

The connectedness data in Table 13 show that nearly all of these compounds contain tetrahedral ligands in which all four apices link to additional polyhedra. This is in contrast to the analogous sheets of polymerized *UL* clusters, wherein few sheets (only those corresponding to the {5.3.5.4}{5.3.5.3} parent graph) contain [4]-coordinated nodes corresponding to tetrahedral ligands. In both sheets and frameworks of *UL* clusters, the coordination of the uranyl nodes typically varies between four and five. This shows that the primary difference in connectivity between the *UL* sheets and *UL* frameworks is the increased coordination of the tetrahedral ligands, and not of the uranyl ion. Structures with the {4_1} nodal designation are the most common, corresponding to 19 out of the 46 compounds listed in Table 13. In these compounds, all polyhedra are located at [4]-coordinated nodes. For most, uranyl is present in square bipyramidal coordination, whereas in only $Na_2[(UO_2)(SiO_4)]$, $[(UO_2)(MoO_4)(H_2O)_2]$, $(NH_4)_2[(UO_2)_6(MoO_4)_7(H_2O)_2]$, and $Rb_2[(UO_2)_6(MoO_4)_7(H_2O)_2]$, U^{6+} occurs in pentagonal bipyramidal coordination.

There are 31 compounds in which tetrahedra are present as monomers (23 compounds), dimers (five compounds), linear trimers (two compounds), or linear tetramers (one compound). The frameworks with monomers (Fig. 14a–v) either result from the linking of vertex-sharing sheets (topologically similar to those illustrated in Table 5) or by other modes of linkage. Those of the first type (Figs. 14k–v) contain *UL* clusters linked into sheets of vertex-sharing uranyl and ligand polyhedra, with adjacent sheets linked by uranyl bipyramids that act as pillars. The uranyl ions between the sheets are typically oriented approximately perpendicular to those in the sheets. Throughout Figure 14 dotted grey boxes outline the sheet portion of the structure for clarity. This type of construction frequently results in the formation of open channel spaces that contain interstitial cations and (H_2O).

The isostructural compounds $Mg[(UO_2)_3(MoO_4)_4(H_2O)_8]$ and $Zn[(UO_2)_3(MoO_4)_4(H_2O)_8]$ are the only *UL*-based frameworks with octahedral ligands ($Mg\Phi_6$ and $Zn\Phi_6$). Their structures contain sheets of *UL* clusters that are linked by pillars to form channels, with the octahedra on the sides of the channels (Fig. 14p).

Structures that do not contain sheets or pillars are illustrated in Figure 14a–j, where individual *UL* clusters are linked to form a relatively dense network of polyhedra. The compound $Ca[(UO_2)_6(MoO_4)_7(H_2O)_2]H_2O_{7.6}$ is unique here in that it consists of channels [occupied by $Ca(H_2O)_x$ complexes] through the structure defined by vertex-sharing *UL* clusters. The compound $Na_8[(UO_2)_6(TeO_3)_{10}]$ is the only uranyl tellurate with a framework of this type. It is also the only vertex-sharing framework to contain ligands with lone-pair stereoactive electrons.

The structures based on dimers, trimers, and tetramers of ligand tetrahedra are illustrated in Figures 14s–x. The structures of $X[(UO_2)_3(Si_2O_7)_2]F$ ($X = K_3Cs_4$, $NaRb_6$; Fig. 14s) and $Cs_6[(UO_2)_3(Ge_2O_7)_2](H_2O)_4$ (Fig. 14t) are both based on uranyl polyhedra linked by dimers of tetrahedra. The structure results from the intersection of identical sheets of vertex-sharing polyhedra (grey boxes), forming channels throughout the structure. The compound $[(UO_2)(S_2O_7)]$ is also based on dimers of tetrahedra and occurs in two distinct polymorphs (Figs. 14t–u). These two frameworks have the same nodal connectivity, but crystallize with different symmetries at different temperatures of hydrothermal syntheses (175 *versus* 300 °C).

There are five compounds in which vertex-sharing tetrahedral ligands form infinite chains that link uranyl bipyramids into frameworks. In each structure, the tetrahedral chains are oriented parallel to each other, and these are linked *via* edge-sharing with uranyl polyhedra. The compounds $Cs_2[(UO_2)(Si_2O_6)]$ and $X_2[(UO_2)(Si_2O_6)](H_2O)_{0.5}$ ($X = Rb^+$, Cs^+) are nearly isostructural (differing only by the presence of H_2O in the interlayers) and contain tetrahedra linked to form infinite helical crankshaft-type chains with repeat distances corresponding to eight (SiO_4) units (Fig. 14y). In the structure of $[(UO_2)H(PO_3)_3]$, phosphate tetrahedra are linked to form similar helical crankshaft type chains (Fig. 14z) with a repeat distance of six tetrahedra. The structure of β-$K[(UO_2)(P_3O_9)]$ also contains helical chains, repeating every six tetrahedra (Fig. 14aa). These chains link to uranyl pentagonal bipyramids, resulting in a structure with discrete channels occupied by K^+.

Seven structures (six structure types) contain isolated rings of vertex-sharing tetrahedra. In the structure of $Cs_8U(UO_2)_3(Ge_3O_9)_3(H_2O)_3$, [3]-membered rings of germanate tetrahedra link successive uranyl square bipyramids to form the elaborate chain structure shown in Figure 14ab. These chains are linked by irregular polyhedra containing U^{4+}. Four-membered rings are the most common type of vertex-

TABLE 13. U(VI) COMPOUNDS CONTAINING FRAMEWORK STRUCTURES BASED ON VERTEX-SHARING

	FORMULA	SG	a (Å)	b (Å)	c (Å)	α (°)	β (°)	γ (°)	SYN[a]	FIG	REF
Isolated tetrahedra											
4_1	β-Li[(UO$_2$)(AsO$_4$)]	$P\bar{1}$	5.051	5.303	10.101	90.31	97.49	105.08	SS[820]	14a	1
4_1	Ca[(UO$_2$)$_6$(MoO$_4$)$_7$(H$_2$O)$_2$](H$_2$O)$_{7.6}$	$C222_1$	11.369	20.031	23.833	—	—	—	HT	14b	2
4_1	Na$_2$[UO$_2$SiO$_4$]	$I4_1/acd$	12.718	12.718	13.376	—	—	—		14c	3
$5_1 3_1$	Na$_8$[(UO$_2$)$_6$(TeO$_3$)$_{10}$]	$I2_13$	16.897	16.897	16.897	—	—	—	HT[180]	14d	4
	Ba[(UO$_2$)(SeO$_3$)$_2$]	$P2_1/c$	7.307	8.124	13.651	—	100.38	—		14e	5
$5_1 2_1 3_1$	[(UO$_2$)(HSO$_4$)$_2$]	$P2_1/n$	7.798	8.154	12.858	—	103.70	—	HT[300]	14f	6
	Tl$_2$[(UO$_2$)$_2$(MnO$_4$)$_3$]	$Pna21$	20.130	8.281	9.705	—	—	—	SS[600]	14f	36
$5_1 5_2 5_1$	[(UO$_2$(H$_2$PO$_2$)$_2$)(H$_3$PO$_2$)]	$P2_12_12_1$	7.157	7.236	17.554	—	—	—	Ac[4]	14g	7
$5_2 4_1 3_2$	Cs$_2$[(UO$_2$)$_2$(MoO$_4$)$_3$]	$Pna2_1$	20.430	8.555	9.855	—	—	—	HT[180]	14h	8
$5_2 4_1 3_2$	Rb$_2$[(UO$_2$)$_2$(MoO$_4$)$_3$]	$Pna2_1$	20.214	8.374	9.746	—	—	—	SS[700]	14h	9
$5_2 4_1 3_2$	Tl$_2$[(UO$_2$)$_2$(MoO$_4$)$_3$]	$Pna2_1$	20.129	8.281	9.705	—	—	—	SS[600]	14h	10
	Na$_2$[(UO$_2$)$_2$(SeO$_4$)$_3$(H$_2$O)$_2$](H$_2$O)$_{6.5}$	$P2_1/c$	19.736	10.821	21.358	—	103.43	—	A	14i	11
$7_1 5_1 3_4$	Cs$_2$[(UO$_2$)(U^{IV})(HPO$_4$)$_2$(HPO$_3$)$_2$]	$P\bar{1}$	6.857	11.119	12.039	63.86	77.48	79.33	HT[200]	14j	12
-with 'sheet' and 'pillar' structures											
4_1	α-[(UO$_2$)(MoO$_4$)(H$_2$O)$_2$]	$P2_1/c$	13.612	11.005	10.854	—	113.05	—		14k	13
$5_2 4_5$	Sr[(UO$_2$)$_6$(MoO$_4$)$_7$(H$_2$O)$_{19}$]	$C222_1$	11.166	20.281	24.061	—	—	—		14l	14
$5_1 4_3$	(NH$_4$)$_2$[(UO$_2$)$_6$(MoO$_4$)$_7$(H$_2$O)$_2$]	$Pbcm$	13.970	10.747	25.607	—	—	—	HT[180]	14m	15
$5_1 4_3$	Rb$_2$[(UO$_2$)$_6$(MoO$_4$)$_7$(H$_2$O)$_2$]	$Pbcm$	13.961	10.752	25.579	—	—	—	HT[230]	14m	9
$5_1 4_3$	Cs$_2$[(UO$_2$)$_6$(MoO$_4$)$_7$(H$_2$O)$_2$]	$Pbcm$	13.990	10.808	25.671	—	—	—	HT[230]	14m	15
$5_2 4_1 3_2$	Ba[(UO$_2$)$_3$(MoO$_4$)$_4$(H$_2$O)$_4$]	$Pbca$	17.797	11.975	23.33	—	—	—		14n	16
$5_1 4_1 3_3$	(H$_3$O)$_2$[(UO$_2$)$_2$(SeO$_4$)$_3$(H$_2$O)]	$P2_1/c$	10.612	14.772	13.714	—	96.99	—	A	14o	11
$5_1 4_3 2_1$	Mg[(UO$_2$)$_3$(MoO$_4$)$_4$(H$_2$O)$_8$]	$Cmc2_1$	17.105	13.786	10.908	—	—	—		14p	18
$5_1 4_3 2_1$	Zn[(UO$_2$)$_3$(MoO$_4$)$_4$(H$_2$O)$_8$]	$Cmc2_1$	17.056	13.786	10.919	—	—	—		14p	18
$5_5 4_4 3_3$	(NH$_4$)$_4$[(UO$_2$)$_5$(MoO$_4$)$_7$](H$_2$O)$_5$	$P6_1$	11.407	11.407	70.659	—	—	120	HT[180]	14q	19
$5_2 4_5 0_1$	Mg[(UO$_2$)$_6$(MoO$_4$)$_7$](H$_2$O)$_{14}$	$C222_1$	11.313	20.163	23.877	—	—	—		14r	20
Dimers of vertex-sharing tetrahedra											
4_1	K$_3$Cs$_4$[(UO$_2$)$_3$(Si$_2$O$_7$)$_2$]F	$Cmc2_1$	7.809	22.282	14.086	—	—	—	Flx[750]	14s	21
4_1	NaRb$_6$[(UO$_2$)$_3$(Si$_2$O$_7$)$_2$]F	$Pnnm$	11.143	13.515	7.887	—	—	—	Flx[750]	14s	21
4_1	Cs$_6$[(UO$_2$)$_3$(Ge$_2$O$_7$)$_2$](H$_2$O)$_4$	$P2_1/n$	7.641	10.328	18.855	—	92.94	—	HT[585]	14t	22
$5_1 4_1 3_1$	[(UO$_2$)(S$_2$O$_7$)]	$P\bar{1}$	6.478	6.842	8.001	87.31	78.37	75.34	HT[175]	14u	6
$5_1 4_1 3_1$	[(UO$_2$)(S$_2$O$_7$)]	$Pca2_1$	10.802	8.147	16.556	—	—	—	HT[300]	14v	6
Linear trimers of vertex-sharing tetrahedra											
4_1	α-K[(UO$_2$)$_2$(P$_3$O$_{10}$)]	$Pbcn$	10.632	10.325	11.209	—	—	—	SS[850]	14w	23
4_1	Rb[(UO$_2$)$_2$(As$_3$O$_{10}$)]	$Pbcn$	10.558	11.037	11.464	—	—	—	SS[820]	14w	24
Linear tetramers of vertex-sharing tetrahedra											
$4_3 3_1$	K$_5$[(UO$_2$)$_2$(Si$_4$O$_{12}$)(OH)]	$Pbcm$	13.127	12.264	22.233	—	—	—	HT[750]	14x	25
Chains of vertex-sharing tetrahedra											
4_1	Cs$_2$[(UO$_2$)(Si$_2$O$_6$)]	$Ibca$	15.137	15.295	16.401	—	—	—	HT[750]	14y	26
4_1	Rb$_2$[(UO$_2$)(Si$_2$O$_6$)](H$_2$O)$_{0.5}$	$Pbca$	14.627	15.145	16.645	—	—	—	HT[245]	14y	27
4_1	Cs$_2$[(UO$_2$)(Si$_2$O$_6$)](H$_2$O)$_{0.5}$	$Pbca$	15.047	15.427	16.732	—	—	—	HT[245]	14y	27
$5_2 4_5 3_1$	[(UO$_2$)H(PO$_3$)$_3$]	$P112_1/b$	9.811	20.814	8.695	—	—	94.09		14z	28
$3_1 4_4 5_1$	β-K[(UO$_2$)(P$_3$O$_9$)]	$P2_1/n$	14.842	8.607	14.951	—	95.83	—	SS[850]	14aa	23
Rings of vertex-sharing tetrahedra											
$4_4 6_1$	Cs$_8$U(UO$_2$)$_3$(Ge$_3$O$_9$)$_3$(H$_2$O)$_3$	$P6_3/m$	14.885	14.885	11.032	—	—	120	HT[585]	14ab	29
4_1	Cs$_2$[(UO$_2$)(Ge$_2$O$_6$)](H$_2$O)	$P2_1/n$	7.916	21.595	12.466	—	96.96	—	HT[220]	14ac	30
4_1	RbNa[(UO$_2$)(Si$_2$O$_6$)(H$_2$O)]	$P\bar{1}$	7.367	7.869	8.177	78.02	75.01	83.74	HT[230]	14ad	31
4_1	Cs$_2$[(UO$_2$)(Ge$_2$O$_6$)](H$_2$O)	$P2_1/n$	7.916	21.595	12.466	—	96.96	—	HT[220]	14ae	30
4_1	Rb$_2$[(UO$_2$)(Si$_2$O$_6$)](H$_2$O)	$P2_1/n$	7.699	20.974	12.050	—	97.92	—	HT[245]	14ae	27
$5_1 4_4$	Rb$_2$[(UO$_2$)$_3$(P$_2$O$_7$)(P$_4$O$_{12}$)]	$P2_1/n$	6.791	16.155	19.856	—	97.48	—	SS[820]	14af	24
$5_1 4_2 6_1$	Cs[(UO$_2$)(PO$_3$)$_3$]	$P2_1/n$	6.988	10.838	13.309	—	104.25	—		14ag	32
Sheets of vertex-sharing tetrahedra											
4_1	KNa$_3$[(UO$_2$)$_2$(Si$_4$O$_{10}$)$_2$](H$_2$O)$_4$	$C2$	1.278	1.362	0.825	—	119.24	—		14ah	33
4_1	Na$_4$[(UO$_2$)$_2$(Si$_4$O$_{10}$)$_2$](H$_2$O)$_4$	$C2/m$	1.277	1.361	0.824	—	119.25	—		14ah	34
4_1	Cs$_2$[(UO$_2$)Si$_{10}$O$_{22}$]	$P2_1/c$	12.251	8.0518	23.379	—	90.01	—	HT[750]	14ai	35

Note: Double lines (═) indicate major differences in the stoichiometry of the structural unit, as indicated by the corresponding header in the table; single lines (–) indicates different topologic configurations; and dotted lines (- -) separate graphical isomers.

[a] Synthesis column data. HT[T] and SS[T] correspond to hydrothermal and solid state synthesis, respectively, at maximum reported temperature T (℃); V-Cl: vapor phase chlorination; A, aqueous (Ae denotes evaporation to dryness); Ac, concentrated acid; Flx, molten flux; SDg, slow diffusion in gel.

References: (1) Alekseev *et al.* (2008b); (2) Nazarchuk *et al.* (2005a); (3) Shashkin *et al.* (1974); (4) Almond *et al.* (2002a); (5) Almond *et al.* (2002b); (6) Betke & Wickleder (2012); (7) Tanner & Mak (1999); (8) Krivovichev *et al.* (2002a); (9) Krivovichev & Burns (2002a); (10) Nazarchuk *et al.* (2005b); (11) Baeva *et al.* (2006); (12) Villa *et al.* (2012); (13) Serezhkin *et al.* (1980a); (14) Tabachenko *et al.* (1984a); (15) Krivovichev & Burns (2001b); (16) Tabachenko *et al.* (1984b); (17) Ling *et al.* (2010b); (18) Tabachenko *et al.* (1983); (19) Krivovichev *et al.* (2003); (20) Tabachenko *et al.* (1984c); (21) Lee *et al.* (2009); (22) Lin *et al.* (2009); (23) Alekseev *et al.* (2008a); (24) Alekseev *et al.* (2009c); (25) Chen *et al.* (2005b); (26) Chen *et al.* (2005a); (27) Huang *et al.* (2003); (28) Sarin *et al.* (1983); (29) Nguyen *et al.* (2011); (30) Ling *et al.* (2010a); (31) Wang *et al.* (2002); (32) Linde *et al.* (1978); (33) Burns *et al.* (2000); (34) Li & Burns (2001b); (35) Liu *et al.* (2011); (36) Nazarchuk *et al.* (2005c).

sharing tetrahedral rings observed in the structures listed in Table 13, with the tetrahedral cations either Si (three structures), Ge (one structure), or P (one structure). These occur in $Cs_2[(UO_2)(Ge_2O_6)](H_2O)$ (Fig. 14ac), $RbNa[(UO_2)(Si_2O_6)(H_2O)]$ (Fig. 14ad), $Cs_2[(UO_2)(Ge_2O_6)]H_2O$ (and isostructural $Rb_2[(UO_2)(Si_2O_6)]H_2O$) (Fig. 14ae), and $Rb_2[(UO_2)_3(P_2O_7)(P_4O_{12})]$ (Fig. 14af). In the ring, the basal planes of the linked tetrahedra lie along approximately the same plane, and with respect to the orientation of apical tetrahedra, all the [4]-membered rings adopt a [X-X-Y-Y] pattern, where X and Y designate apical tetrahedral anions with similar orientations. The latter structure also contains pyrophosphate (P_2O_7) dimers. The compound $Cs[(UO_2)(PO_3)_3]$ (Fig. 14ag) is the only one to contain [6]-membered rings of phosphate tetrahedra. In it each ring is distorted and links directly to six unique uranyl polyhedra to form the framework structure.

The structures of three compounds contain tetrahedra that link to form topologically complex infinite sheets, with uranyl square bipyramids between the sheets that link them together to create the framework. These structures could be considered as 'inverted' sheet structures, wherein uranyl cations are the relatively weakly bonded (by comparison to the strong Si–O bonds) interstitial cations. In the isostructural compounds $X[(UO_2)_2(Si_4O_{10})_2](H_2O)_4$ (X = KNa_3, K_4), sheets consist of [4]- and [8]-membered rings of tetrahedra that link to form two-dimensional sheets (Fig. 14ah). In $Cs_2[(UO_2)(Si_{10}O_{22})]$, sheets consist of arrangements of [5]- and [6]-membered rings of tetrahedra showing remarkable topological complexity (Fig. 14ai). These rings are stacked to form complex three-dimensional sheets with empty channels. The channels in the tetrahedral sheets are too narrow (3.5–5.5 Å) to contain the large Cs^+ (r = ~1.6 Å) interstitial cations that are instead located between the uranyl square bipyramids.

Frameworks based on UL clusters with edge-sharing

Table 14 lists 12 compounds with framework structures based on infinite (UL) clusters that contain edge-sharing polyhedra. There are two sub-classes of structures: (1) those containing the UL-L_3 cluster (Fig. 15a), wherein a central uranyl pentagonal bipyramid shares one edge and three vertices with tetrahedral ligand polyhedra; and (2) those containing the L_2-$LUUL$-L_2 cluster (Fig 15b), wherein uranyl pentagonal bipyramids occur as an edge-sharing dimer, each of which shares one edge and two vertices with tetrahedral ligand polyhedra.

The five structures that contain UL-L_3 clusters are listed in Table 14. All of these contain $T_2\Phi_7$ groups

that are either pyrophosphate, pyroarsenate, or pyrovanadate. The structure of $Na_2[(UO_2)(P_2O_7)]$ is topologically similar to the structure of the uranophane-group phases. Every second uranyl polyhedron in the uranophane chain is absent and the 'sheets' are directly linked *via* pyrophosphate groups (Fig. 15d). In the structures of $Na_2[(UO_2)(P_2O_7)]$ (Fig. 15d), $Ba_3[(UO_2)_2(AsO_4)_2(AsO_7)$ (Fig. 15e), and $Pb[(UO_2)(V_2O_7)]$ (Fig. 15f) the uranyl ion occurs only in UL-L_2 clusters, and the frameworks result from the dense interconnectivity of only these cluster types. The structures of $Li_2[(UO_2)_3(P_2O_7)_2]$ (Fig. 15g) and $Ba_3[(UO_2)_2(HPO_4)_2(PO_4)_2]$ (Fig. 15h), however, contain the uranyl ion in two cluster topologies. In addition to the UL-L_2 cluster, the uranyl ion also occurs in square bipyramidal coordination where the four equatorial anions belong to tetrahedra (*i.e.*, UL_4 cluster; Fig. 15c). These two cluster types link together to form the resulting framework.

There are seven structures that contain the more complex L_2-$LUUL$-L_2 cluster type. Only two of these, $Cs[(UO_2)Ga(PO_4)_2]$ (Fig. 15i) and $Cs_4[(UO_2)_2(GaOH)_2(PO_4)_4](H_2O)$ (Fig. 15j), contain a single uranyl cluster. Both structures are built from two topologically distinct chain types. Common to both phases are the infinite chains resulting from the polymerization of the cluster L_2-$L[U{=}U]L$-L_2 (of the type observed in Fig. 3ac). $Cs[(UO_2)Ga(PO_4)_2]$ also contains chains of vertex-sharing $[GeO_6]$ octahedra, with overall $[GeO_5]$ stoichiometry. In both compounds, the two chains are linked together directly at high angles. The compound $Rb_2[(UO_2)U^{4+}(PO_4)_2(HPO_3)_2](H_2O)$ contains both U^{6+} and U^{4+} (Fig. 15k). Here, the U^{6+} occupies the uranyl pentagonal bipyramids in the L_2-$L[U{=}U]L$-L_2 clusters, whereas the U^{4+} is [7]-coordinated and is vertex-sharing with four phosphate tetrahedra and two phosphonate groups. The frameworks observed in $Cs_{3.14}[(UO_2)_3CuH_{3.86}(PO_4)_5](H_2O)$ (Fig. 15l), α-$Li[(UO_2)(AsO_4)]$, α-$Li[(UO_2)(PO_4)]$ (Fig. 15m), and $Rb_4[(UO_2)_6(P_2O_7)_4(H_2O)]$ (Fig. 15n) consist of both L_2-$L[UU]L$-L_2 and UL_4 clusters. The two clusters share vertices to form the dense frameworks observed in the compounds.

Frameworks of parallel chains of uranium polyhedra

The 18 compounds listed in Table 15 contain framework structures based on infinite chains of element-sharing uranium polyhedra. These chains are oriented such that their lengths are parallel and they are linked together to form the complete framework by either the direct sharing of polyhedral elements or by additional high-valence polyhedra present between the chains. Many of these chains are topologically related
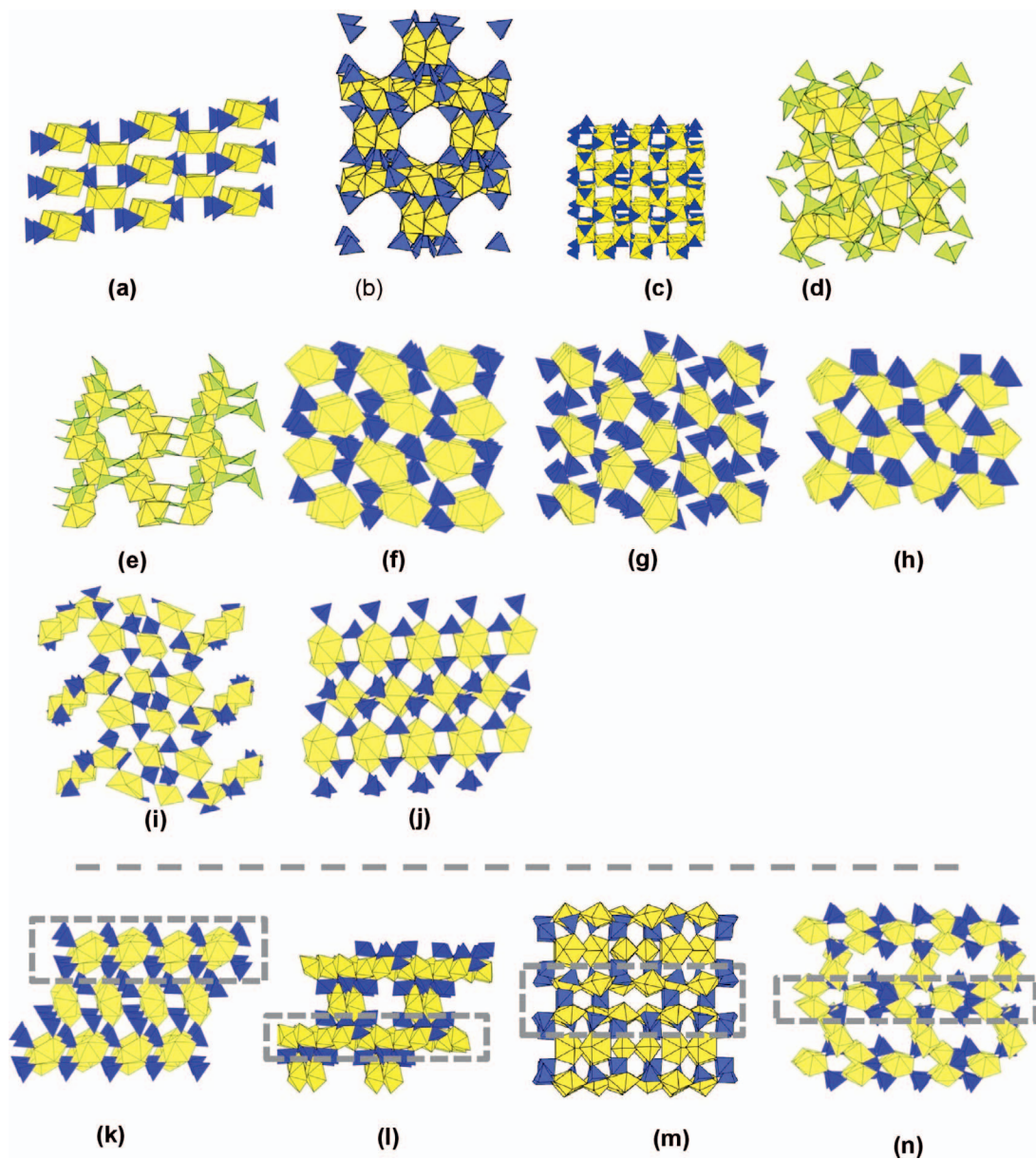
FIG. 14. Framework structures dominated by vertex-sharing between uranyl and other ligand polyhedra (containing high-valence cations) found in the compounds listed in Tables 13.

to those observed in the compounds and minerals listed in Table 3.

The structures of $Cs_2[(UO_2)(VO_2)_2(PO_4)_2](H_2O)_{0.59}$ (Fig. 16a), $Ni_7B_4[(UO_{16}]$, and $Cs_{11}Eu_4[(UO_2)_2(P_2O_7)_6(PO_4)]$ consist of infinite chains of uranyl square bipyramids linked by two ligand tetrahedra (UL_2 chains, Fig. 4n). These chains are not directly linked together in the structure, but instead are strongly bonded to the complex network of octahedra that constitutes the rest of the structural unit. The structure of $Cs_2[(UO_2)(VO_2)_2(PO_4)_2](H_2O)_{0.59}$ contains UL_2 chains (where L = PO_4 tetrahedra) as well as vertex-sharing (VO_5) pyramids. The axes of these two chain types are perpendicular to one another. The structure of $[Ni_7$
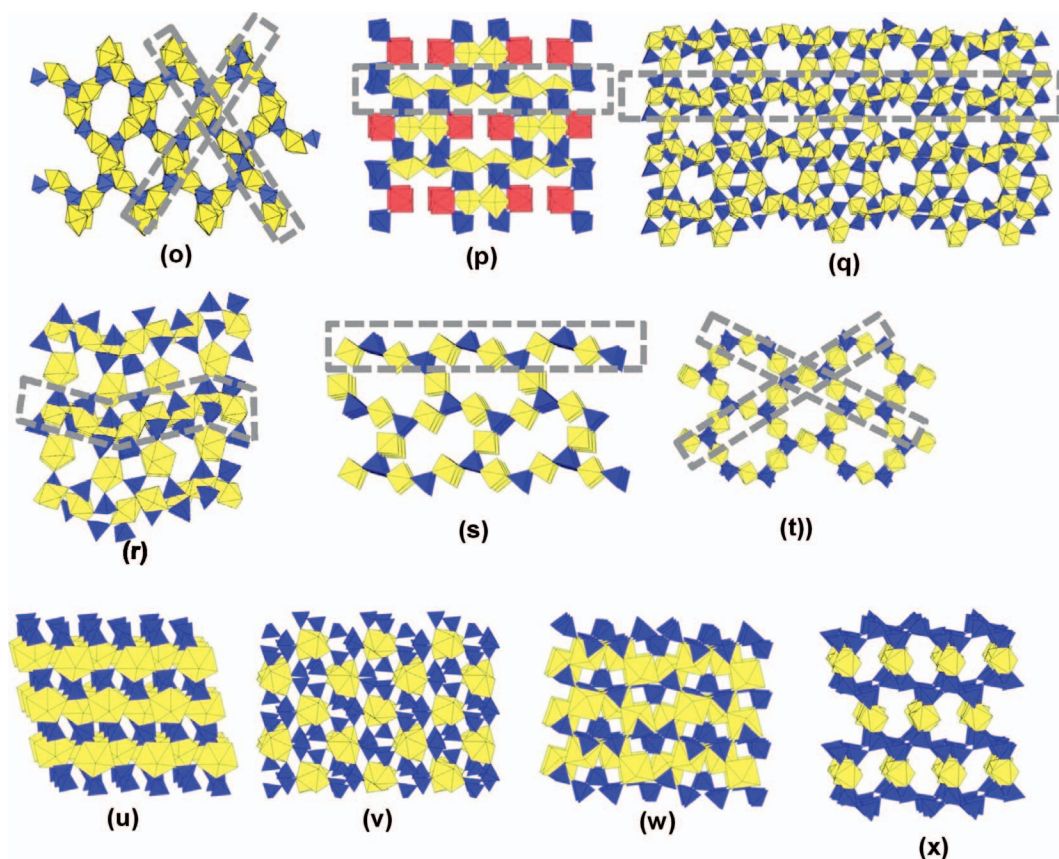
FIG. 14. Continued.

B$_4$UO$_{16}$] contains similar UL_2 chains, wherein uranyl square bipyramids are linked by (BO$_4$) tetrahedra. These chains exist in a dense framework of edge-sharing (NiO$_6$) octahedra and (BO$_3$) triangles, separated by ~4 Å and ~10 Å along the **z**- and **y**-axes, respectively. Further, if viewed in slices parallel to the (100) plane, these chains are linked to edge-sharing (NiO$_6$) octahedra that are arranged in ribbon-like fragments of gibbsite-type sheets (Fig. 16b). In the structure of Cs$_{11}$Eu$_4$[(UO$_2$)$_2$(P$_2$O$_7$)$_6$(PO$_4$)], uranyl square bipyramids are linked by pyrophosphate (P$_2$O$_7$) groups to form infinite chains (Fig. 16c) that are linked to a network of irregular EuO$_7$ polyhedra and phosphate tetrahedra to form the framework. Unlike the other structures in this category, the uranyl chains are in two different orientations, one with long axes along [010] and stacked along [100], the other being oriented along [100] and stacked along [010].

There are four compounds with structures in which parallel chains link to form discrete parallel channels in the structure. The structures of Li$_5$[(UO$_2$)$_{13}$(AsO$_4$)$_9$(As$_2$O$_7$)] (Fig. 16d) and Li$_6$[(UO$_2$)$_{12}$(PO$_4$)$_8$(P$_4$O$_{13}$)] (Fig. 16e) both contain uranophane-type chains of edge-sharing uranyl pentagonal bipyramids. Dimeric T$_2$O$_7$ tetrahedral units link these chains together into groups of four, defining infinite tubes that extend through the structure. In both structures, these discrete tubes are linked to a complex arrangement of UL-type clusters to form the resulting framework.

The structures of Ag[(UO$_2$)$_2$(I$_2$O$_7$)](H$_2$O) (Fig. 16f), Ag$_2$[(UO$_2$)$_3$(GeO$_4$)$_2$](H$_2$O)$_2$ (Fig. 16g), and K[NbUO$_6$] (Fig. 16h–i) all contain uranophane-type chains of edge-sharing uranyl pentagonal bipyramids. In the structures of Ag[(UO$_2$)$_2$(HGe$_2$O$_7$)](H$_2$O) and Ag$_2$[(UO$_2$)$_3$(GeO$_4$)$_2$](H$_2$O) the chains or bipyramids are linked by dimeric [Ge$_2$Φ$_7$] groups that replace the typically observed isolated [SiO$_3$(OH)] tetrahedra in uranophane-type structures. The manner in which the chains link together in the structures differs considerably. In the former and latter structures, respectively, the tetrahedral dimers are oriented perpendicular and
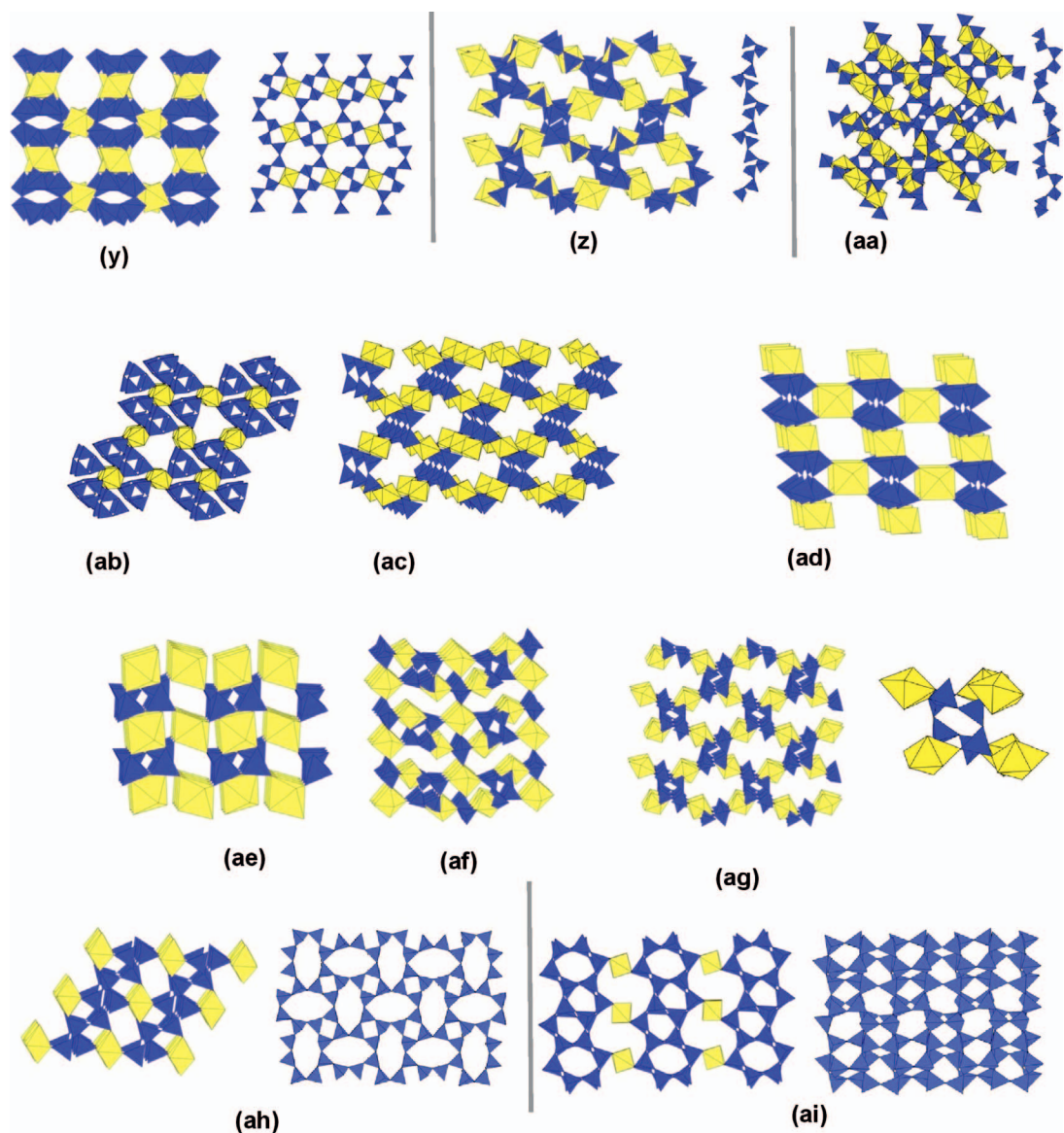
FIG. 14. Continued.

parallel to the axis of the uranyl chains, and the resulting channels consists of four and six individual chain units.

The structure of K[NbUO$_6$] (Fig. 16h) is based on edge-sharing chains of uranyl pentagonal bipyramids, and chains of dimers of Nb$_2$O$_{10}$ edge-sharing octahedra are stacked by vertex-sharing. These two chains are parallel and are linked by polyhedral edge-sharing, resulting in the sheet shown in Figure 16h. These sheets stack to form the structures corresponding to

Figures 16i–j. There are six compounds that are structurally related to K[NbUO$_6$], differing only in the symmetric relationship between the two chains. In the structures of K[NbUO$_6$], Cs$_{0.07}$Na$_{0.92}$[NbUO$_6$], Tl[Nb$_2$U$_2$O$_{11.5}$], and Rb$_{0.5}$[NbUO$_2$] (Fig. 16i), chains are arranged asymmetrically without a mirror plane. In the structures of Cs$_{0.75}$K$_{0.25}$[NbUO$_6$] and Cs$_{0.5}$ [NbUO$_6$] (Fig. 16j), the chains are arranged with a mirror plane bisecting the Nb$_2$O$_{10}$ chain. In the structure of Li$_2$(UO$_2$)(WO$_4$)$_2$ (Fig. 16k) the edge-

TABLE 14. U(VI) COMPOUNDS CONTAINING FRAMEWORK STRUCTURES WITH EDGE-SHARING URANYL CLUSTERS

FORMULA	SG	a (Å)	b (Å)	c (Å)	α (°)	β (°)	γ (°)	SYN[a]	FIG	REF
Isolated edge-sharing uranyl/ligand clusters										
UL-L₃ clusters										
$Na_2[(UO_2)(P_2O_7)]$	$Pna2_1$	13.259	8.127	6.973	—	—	—		15d	1
$Ba_3[(UO_2)_2(AsO_4)_2(As_2O_7)]$	$C2/c$	19.246	9.536	9.619	—	95.59	—	SS[850]	15e	2
$Pb[(UO_2)(V_2O_7)]$	$P2_1/n$	6.921	9.652	11.788	—	91.74	—	SS[680]	15f	3
$Li_2[(UO_2)_3(P_2O_7)_2]$	$P\bar{1}$	5.312	6.696	12.542	94.53	99.06	110.19	SS[820]	15g	4
$Ba_3[(UO_2)_2(HPO_4)_2(PO_4)_2]$	$P2_1/c$	9.506	8.699	10.544	—	97.31	–	HT[190]	15h	5
L₂-LUUL-L₂ clusters										
$Cs[(UO_2)Ga(PO_4)_2]$	$P\bar{1}$	7.777	8.504	8.912	66.64	70.56	84.00	HT[180]	15i	6
$Cs_4[(UO_2)_2(GaOH)_2(PO_4)_4](H_2O)$	$P2_1/c$	18.872	9.511	14.007	—	109.65	—	HT[180]	15j	6
$Rb_2[(UO_2)_2U(PO_4)_2(HPO_3)_2](H_2O)$	$C2/c$	16.242	10.505	11.094	—	98.75	—	HT[200]	15k	7
$Cs_{3.14}[(UO_2)_3CuH_{3.86}(PO_4)_5](H_2O)$	$Pbcm$	7.587	19.957	17.973	—	—	—	HT[195]	15l	8
α-$Li[(UO_2)(AsO_4)]$	$P\bar{1}$	5.129	10.105	11.080	107.70	102.53	104.74	SS[820]	15m	4
α-$Li[(UO_2)(PO_4)]$	$P\bar{1}$	5.027	9.879	10.892	108.28	102.99	104.13	SS[820]	15m	4
$Rb_4[(UO_2)_6(P_2O_7)_4(H_2O)]$	$P2_1/c$	9.672	12.951	32.231	—	90.12	—	SS[820]	15n	9

Note: Double lines (=) indicate major differences in the stoichiometry of the structural unit, as indicated by the corresponding header in the table; single lines (–) indicates different topologic configurations; and dotted lines (- -) separate graphical isomers.

[a] Synthesis column data. HT[T] and SS[T] correspond to hydrothermal and solid state synthesis, respectively, at maximum reported temperature T (°C); V-Cl: vapor phase chlorination; A, aqueous (Ae denotes evaporation to dryness); Ac, concentrated acid; Flx, molten flux; SDg, slow diffusion in gel.

References: (1) Linde *et al.* (1984); (2) Alekseev *et al.* (2011); (3) Obbade *et al.* (2004c); (4) Alekseev *et al.* (2008b); (5) Ling *et al.* (2009); (6) Shvareva *et al.* (2005c); (7) Villa *et al.* (2012); (8) Shvareva & Albrecht-Schmitt (2006); (9) Alekseev *et al.* (2009c).

sharing chains of uranyl pentagonal bipyramids are between infinite sheets of vertex-sharing (WO_6) octahedra.

The structure of holfertite, $[(UO_2)_{1.77}TiCa_{0.25}O_{3.61}(OH)_{0.67}](H_2O)_3$ (Fig. 16l), contains chains with disordered cations (Sokolova *et al.* 2005). In the structure, uranyl square bipyramids are arranged into infinite chains with shared *trans* equatorial edges. These chains are flanked on either side by infinite chains of edge-sharing $Ti\Phi_5$ trigonal bipyramids. The two types of chains are arranged to form wide ($\sim$12 Å) channels, each defined by six chains, that are occupied by a complex array of positionally disordered Ca^{2+} and (H_2O) groups.

The structures of $X_3[(U_2O_4)(Ge_2O_7)]$ ($X = $ Cs, Rb) and $[(UO_2)(B_3Al_4O_{11}(OH))]$ consist of chains of uranyl polyhedra linked together in a relatively dense framework. The isostructural compounds $Cs_3(U_2O_4)(Ge_2O_7)$ and $Rb_3(U_2O_4)(Ge_2O_7)$ both consist of $[MO_5]$-type chains of vertex-sharing uranyl square bipyramids. Dimeric (T_2O_7) tetrahedral ligands link successive uranyl polyhedra in each chain and the chains are kinked (Fig. 16m). The tetrahedral dimers also link the adjacent chains. The structure of $[(UO_2)(B_3Al_4O_{11}(OH)]$ is illustrated in Figure 16n, and a slice projected along ($\bar{2}01$) shows the complex nature of the chain of uranyl polyhedra that exists within the framework. Uranyl tris-boranato units (analogous to the tris-carbonato complexes illustrated

in Fig. 3g) are linked together by a common edge-sharing (BO_3) unit. A chain consisting of *trans* edge-sharing $Al\Phi_6$ octahedra is located between the chains of uranyl bipyramids, and the apical anions of successive octahedra are linked by (BO_4) tetrahedra and (BO_3) triangles. The two chains are linked to form an infinite sheet by sharing oxygen atoms of the (BO_3) groups, and $Al\Phi_6$ octahedra located between the hexagonal bipyramids also serve to link the chains together. The resulting framework arises by stacking these infinitely.

Frameworks of interpenetrating chains of uranyl polyhedra

Fifteen structures (corresponding to six structure types) are grouped here based on the cross-linking of chains (Table 16). In each, the chain topology has been encountered previously. The topologically simplest of these is $Cs_3[(UO_2)_2(PO_4)O_2]$, which consists of infinite chains formed by the sharing of *trans* vertices of uranyl square bipyramids (Fig. 17a). A (PO_4) tetrahedron bridges alternating polyhedra in the chain. These tetrahedra link adjacent chains such that their chain lengths are orientated at right angles to each other. The Cs cations occupy interstitial voids.

Twelve compounds listed in Table 16 are based on interpenetrating uranophane-type chains. Each chain consists of edge-sharing uranyl pentagonal bipyramids
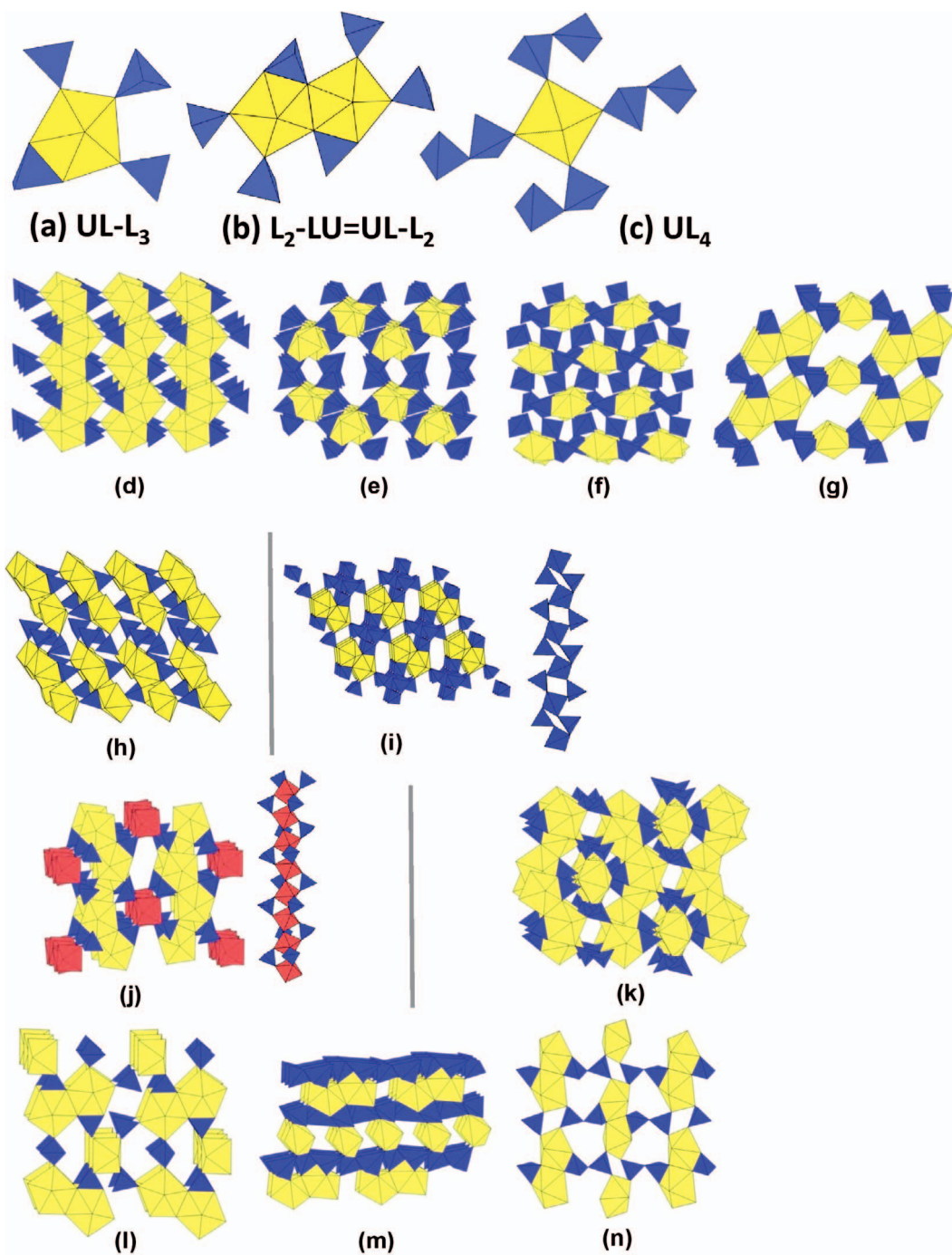
FIG. 15. Framework structures dominated by the polymerization of discrete clusters containing edge-sharing polyhedra found in the compounds listed in Table 14.

TABLE 15. U(VI) COMPOUNDS CONTAINING FRAMEWORK STRUCTURES BASED ON PARALLEL CHAINS OF URANIUM POLYHEDRA

MINERAL	FORMULA	SG	a (Å)	b (Å)	c (Å)	α (°)	β (°)	γ (°)	SYN[a]	FIG	REF
Isolated chains of uranyl polyhedra											
	$Cs_2[(UO_2)_2(VO_2)_2(PO_4)_2](H_2O)_{0.59}$	$Cmc2_1$	20.712	6.856	10.549	—	—	—	HT[190]	16a	1
	$Ni_7B_4[UO_{16}]$	$Pmnn$	5.861	20.200	4.501	—	—	—	SS[1373]	16b	2
	$Cs_{11}Eu_4[(UO_2)_2(P_2O_7)_6(PO_4)]$	$P4_2/mbc$	13.628	13.628	29.958	—	—	—		16c	3
Parallel chains forming discrete channels											
	$Li_5[(UO_2)_{13}(AsO_4)_9(As_2O_7)]$	$P\bar{1}$	7.141	13.959	31.925	82.85	88.69	79.77	SS[820]	16d	4
	$Li_6[(UO_2)_{12}(PO_4)_8(P_4O_{13})]$	$C2/m$	26.963	7.063	19.639	—	126.89	—	SS[820]	16e	4
	$Ag[(UO_2)_2(HGe_2O_7)_2(H_2O)]$	$Ama2$	7.124	10.771	14.024	—	—	—	HT[220]	16f	5
	$Ag_2[(UO_2)_3(GeO_4)_2](H_2O)_2$	$Pnma$	10.046	7.469	17.776	—	—	—	HT[220]	16g	5
	$K[NbUO_6]$	$Pnma$	10.307	7.588	13.403	—	—	—	SS[1300]	16i	6
	$Cs_{0.077}Na_{0.923}[NbUO_6]$	$Pnma$	10.272	7.628	13.451	—	—	—	SS[1300]	16i	6
	$TlNb_2[U_2O_{11.5}]$	$Pmnb$	7.713	10.329	13.947	—	—	—	Flx[1150]	16i	7
	$Rb_{0.5}[NbUO_{5.75}]$	$Pnma$	10.432	7.681	13.853	—	—	—	SS[1300]	16i	6
	$(Cs_{0.75}K_{0.25})(NbTi)U_2O_{11}$	$Amam$	7.630	10.923	13.609	—	—	—	SS[1573]	16j	8
	$Cs_{0.5}[NbUO_{5.75}]$	$Cmcm$	13.952	10.607	7.748	—	—	—	SS[1300]	16j	6
	$Li_2[(UO_2)(WO_4)_2]$	$Pbcn$	7.937	12.786	7.425	—	—	—	SS[920]	16k	9
Holfertite	$(UO_2)_{1.77}TiCa_{0.25}O_{3.61}(OH)_{0.67}(H_2O)_3$	$P3$	10.824	10.824	7.549	—	—	120	—	16l	10
Directly linked chains – no channels											
	$Cs_3[(U_2O_4)(Ge_2O_7)]$	$P2_1/n$	7.642	10.328	18.854	—	101.31	—	HT[585]	16m	11
	$Rb_3[(U_2O_4)(Ge_2O_7)]$	$P2_1/n$	6.976	12.228	15.399	—	100.56	—	HT[585]	16m	11
	$(UO_2)(B_3Al_4O_{11}(OH))$	$P2_1/m$	9.362	5.601	10.511	—	110.75	—	HT[650]	16n	12

Note: Double lines (=) indicate major differences in the stoichiometry of the structural unit, as indicated by the corresponding header in the table; single lines (–) indicates different topologic configurations; and dotted lines (- -) separate graphical isomers.
[a] Synthesis column data. HT[T] and SS[T] correspond to hydrothermal and solid state synthesis, respectively, at maximum reported temperature T (°C); V-Cl: vapor phase chlorination; A, aqueous (Ae denotes evaporation to dryness); Ac, concentrated acid; Flx, molten flux; SDg, slow diffusion in gel.
References: (1) Shvareva *et al.* (2005b); (2) Gasperin (1989); (3) Pobedina & Ilyukhin (1997); (4) Alekseev *et al.* (2009a); (5) Ling *et al.* (2010a); (6) Surble *et al.* (2006); (7) Gasperin (1987b); (8) Gasperin (1986); (9) Obbade *et al.* (2004d); (10) Sokolova *et al.* (2005); (11) Lin & Lii (2008); (12) Wu *et al.* (2012).

in combination with tetrahedra [(SiO_4), (GeO_4), (VO_4), (PO_4), (AsO_4)] that share edges with uranyl polyhedra, alternating along the sides of the chain. The compounds have these chains in approximately perpendicular arrangements. The mechanism by which they are linked varies. In the topologically simplest case, that of soddyite, $[(UO_2)_2(SiO_4)(H_2O)_2]$, the chains link directly through the sharing of tetrahedral edges (Fig. 17b). In structures of the other seven compounds, sheets of polyhedra exist between cross-linked chains. Two types of sheets (sheet *A*/sheet *B*; Fig. 17), both of which are topologically related to autunite-type sheets, are observed: sheet *A* contains a 'doubling' of tetrahedra at half the tetrahedral positions; sheet *B* has half the uranyl square bipyramids missing. Structures corresponding to the illustrations in Figures 17c–e can be described by modular combinations of these types of chains; the colored arrows indicate the location of the corresponding sheet in the structure. The structures of $Li_2[(UO_2)_3(VO_4)_2O]$ and $Li_2[(UO_2)_3(PO_4)_2O]$ (Fig. 17c) are based on the sequence $A\{^LU_{ph}\}A–\{^TU_{ph}\}–A\{^LU_{ph}\}A$ (where $^TU_{ph}$ and $^LU_{ph}$ indicate uranophane-type chains oriented in and perpendicular to the plane of the page, respectively). Similarly, the structures of $Li[(UO_2)_4(PO_4)_3]$, $Li[(UO_2)_4(AsO_4)_3]$, and $Na(UO_2)_4(VO_4)_3$ (Fig. 17d)

correspond to $B\{^LU_{ph}\}B–\{^TU_{ph}\}–B\{^LU_{ph}\}B$, and the structures of $Li_3[(UO_2)_7(PO_4)_5O]$, $Li_3[(UO_2)_7(AsO_4)_5O]$, $Ag_3[(UO_2)_7(VO_4)_5O]$, and $Li_3[(UO_2)_7(VO_4)_5O]$ (Fig. 17e) correspond to $A\{^LU_{ph}\}B–\{^TU_{ph}\}–A\{^LU_{ph}\}B$. Lastly, two structures in this class are based on phosphuranylite-type chains. In the structures of $[(UO_2)_3(PO_4)O(OH)(H_2O)_2](H_2O)$ and nielsborite, $K[(UO_2)_3(AsO_4)(OH)_4(H_2O)]$, these chains link directly, analogous to the simple uranophane-type chain framework case above (Fig. 17f).

Frameworks of sheets

Within the framework category overall, structures have been organized on the basis of the increasing connectivity of uranium polyhedra, *i.e.*, frameworks of element-sharing polyhedra, clusters of polyhedra, chains, and sheets of polyhedra. We now turn our attention to the last group, specifically frameworks built from sheets. Sheets dominated by uranium polyhedra can be connected into a framework through polyhedra containing high-valence cations located between the sheets, or directly by sharing polyhedral vertices. Previously, we placed such structures into the category corresponding to the appropriate sheet topology, rather than grouping them with frameworks.
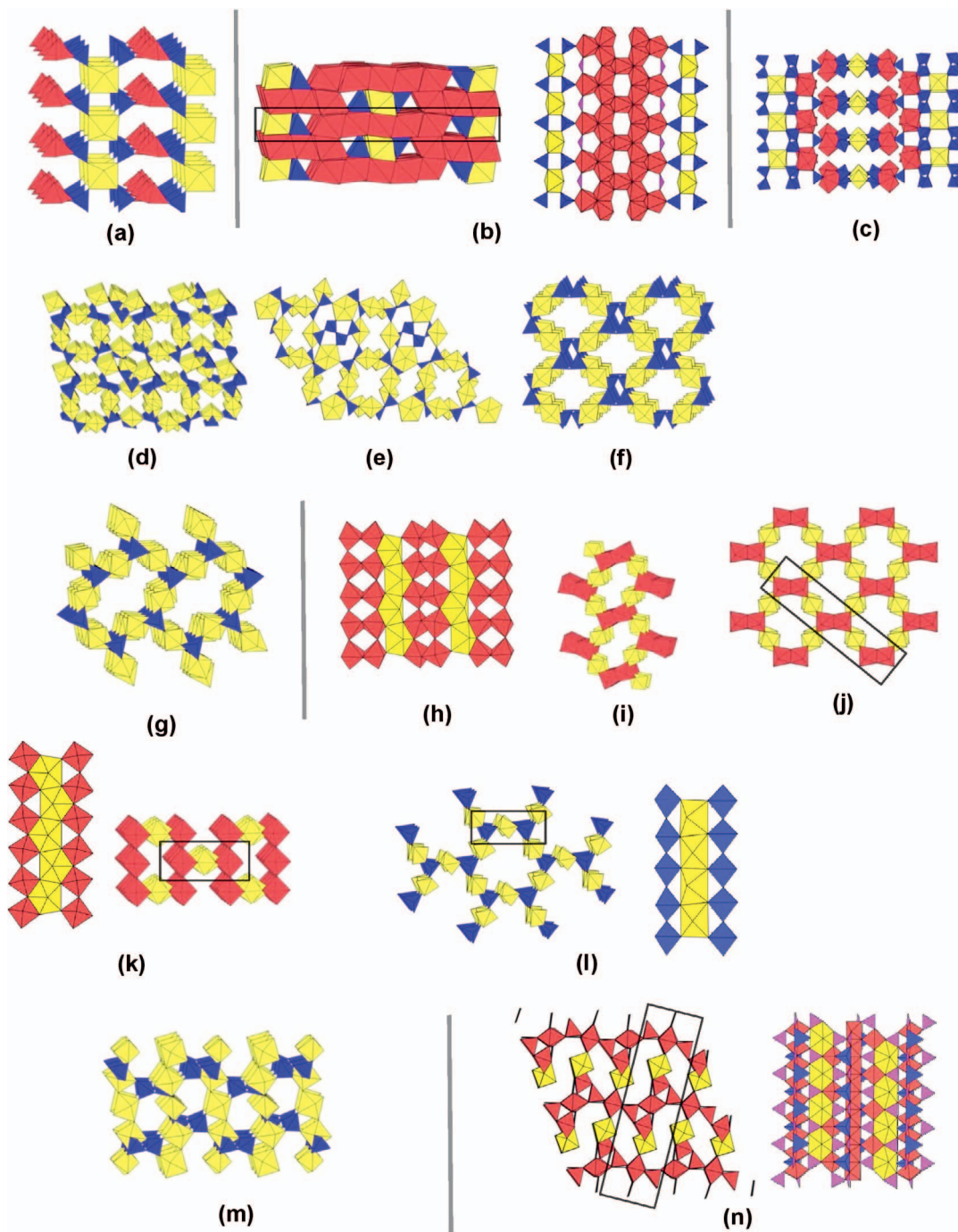
FIG. 16. Framework structures dominated by the interconnection of parallel chains of uranium polyhedra found in the compounds listed in Table 15.

TABLE 16. U(VI) COMPOUNDS CONTAINING FRAMEWORKS BASED ON INTERPENETRATING CHAINS

MINERAL	FORMULA	SG	a (Å)	b (Å)	c (Å)	α (°)	β (°)	γ (°)	SYN[a]	FIG	REF
Structures containing [6]UO5 chains											
	$Cs_3[(UO_2)_2(PO_4)_2O_2]$	C2/c	13.626	8.108	12.983	—	114.61	—	Flx[750]	17a	1
Structures containing uranophane-type chains											
Soddyite	$[(UO_2)_2(SiO_4)(H_2O)_2]$	Fddd	8.334	11.212	18.668	—	—	—		17b	2
	$[(UO_2)_2(GeO_4)(H_2O)_2]$	Fddd	8.179	11.515	19.397	—	—	—	A[80]	17b	3
	$Na_2[(UO_2)_2(SiO_4)F_2]$	I4₁/amd	6.975	6.975	18.31	—	—	—		17b	4
	$Li_2[(UO_2)_3(VO_4)_2O]$	I4₁/amd	7.330	7.330	24.653	—	—	—	SS[1000]	17c	5
	$Li_2[(UO_2)_3(PO_4)_2O]$	I4₁/amd	7.111	7.111	25.041	—	—	—	SS[1100]	17c	6
	$Li[(UO_2)_4(PO_4)_3]$	P2₁/c	9.883	9.891	17.487	—	106.19	—	SS[1100]	17d	6
	$Li[(UO_2)_4(AsO_4)_3]$	I4₁/amd	7.160	7.160	33.775	—	—	—	SS[820]	17d	7
	$Na[(UO_2)_4(VO_4)_3]$	I4₁/amd	7.227	7.227	34.079	—	—	—	SS[920]	17d	8
	$Li_3[(UO_2)_7(PO_4)_5O]$	$P\bar{4}2_1m$	9.931	9.931	14.574	—	—	—	SS[1100]	17e	6
	$Li_3[(UO_2)_7(AsO_4)_5O]$	$P\bar{4}$	7.216	7.216	14.654	—	—	—	SS[820]	17e	7
	$Ag_3[(UO_2)_7(VO_4)_5O]$	$P\bar{4}m2$	7.237	7.237	14.797	—	—	—	SS[900]	17e	9
	$Li_3[(UO_2)_7(VO_4)_5O]$	$P\bar{4}m2$	7.279	7.279	14.514	—	—	—	SS[950]	17e	9
Structures containing phosphuranyllite-type chains											
Nielsbohrite	$K[(UO_2)_3(AsO_4)_4(OH)_4(H_2O)]$	Cccm	8.193	11.430	13.500	—	—	—		17f	10
	$[(UO_2)_3(PO_4)O(OH)(H_2O)_2](H_2O)$	P4₂/mbc	14.015	14.015	13.083	—	—	—	HT[185]	17f	11

Note: Double lines (═) indicate major differences in the stoichiometry of the structural unit, as indicated by the corresponding header in the table; single lines (–) indicates different topologic configurations; and dotted lines (--) separate graphical isomers.
[a] Synthesis column data. HT[T] and SS[T] correspond to hydrothermal and solid state synthesis, respectively, at maximum reported temperature T (℃); V-Cl: vapor phase chlorination; A, aqueous (Ae denotes evaporation to dryness); Ac, concentrated acid; Flx, molten flux; SDg, slow diffusion in gel.
References: (1) Yagoubi *et al* (2013); (2) Demartin *et al*. (1992); (3) Legros & Jeannin (1975); (4) Blaton *et al*. (1999); (5) Obbade *et al*. (2007); (6) Renard *et al*. (2009); (7) Alekseev *et al*. (2009a); (8) Obbade *et al*. (2004a); (9) Obbade *et al*. (2009); (10) Walenta *et al*. (2009); (11) Burns *et al*. (2004).

We maintain this approach here, such that framework structures created by the linkage of sheets are presented in the appropriate sheet category. However, as the known number of these structures has increased significantly recently (currently 36), it is also useful to present them as a distinct type of framework, to facilitate comparison with structures sharing similar topological elements. As such, those compounds with frameworks consisting of strongly connected sheets are also listed in Table 17.

Frameworks of sheets linked by non-sheet (interstitial) polyhedra

Infinite sheets based on uranium polyhedra (and other high valence cations) may be linked directly by element-sharing with polyhedra located between the sheets. There are 22 known compounds that satisfy this criterion. Linkages with these non-sheet cations are strong (>0.2 *vu*), and they are usually included in the defined structural unit, as they stabilize the structure. Their presence between the sheets therefore results in a framework of linked sheets. Table 17 lists the 22 compounds in this class, the majority of which are based on sheets with previously encountered topologies; 12, six, and two compounds are based on the linkage of uranophane, phosphuranylite, and β-U_3O_8

type sheets, respectively. The remaining two compounds contain sheets that are novel.

Linked uranophane-type sheets. In sklodowskite, $(MgΦ_6)$ octahedra, along with a network of H bonds from (H_2O) groups, link the apices of $(SiΦ_4)$ tetrahedra from adjacent sheets (Fig. 18a). Eight compounds have framework structures corresponding to that shown in Figure 18b. In it, uranyl pentagonal bipyramids link uranophane-type sheets through vertex-sharing with $(TΦ_4)$ units of the sheets. Variable amounts of (H_2O) are between the sheets, and low-valence cations are also often present that balance the net charge of the framework. The structure of $(UO_2)[(UO_2)(AsO_4)]_2$ $(H_2O)_5$ is also based on uranophane-type sheets, but here they display an unusual, highly zig-zagged configuration (Fig. 18c).

In the structure of weeksite, $K_2[(UO_2)_2(Si_5O_{13})]·$ $4H_2O$ (Fig. 18d), chains of edge-sharing pentagonal bipyramids are linked by chains and sheets of vertex-sharing (SiO_4) tetrahedra. The sheets consist of [6]- and [14]-membered (TO_4) rings that are oriented perpendicular to the approximate plane formed by the equatorial anions of the bipyramids. Hence, these sheets both serve to link the pentagonal chains into sheets and to directly link adjacent sheets together. The weeksite structure of Jackson & Burns (2001) was solved in an orthorhombic space group (*Cmmb*) and showed several Si positions with partial vacancy. A

SHEET A   **SHEET B**
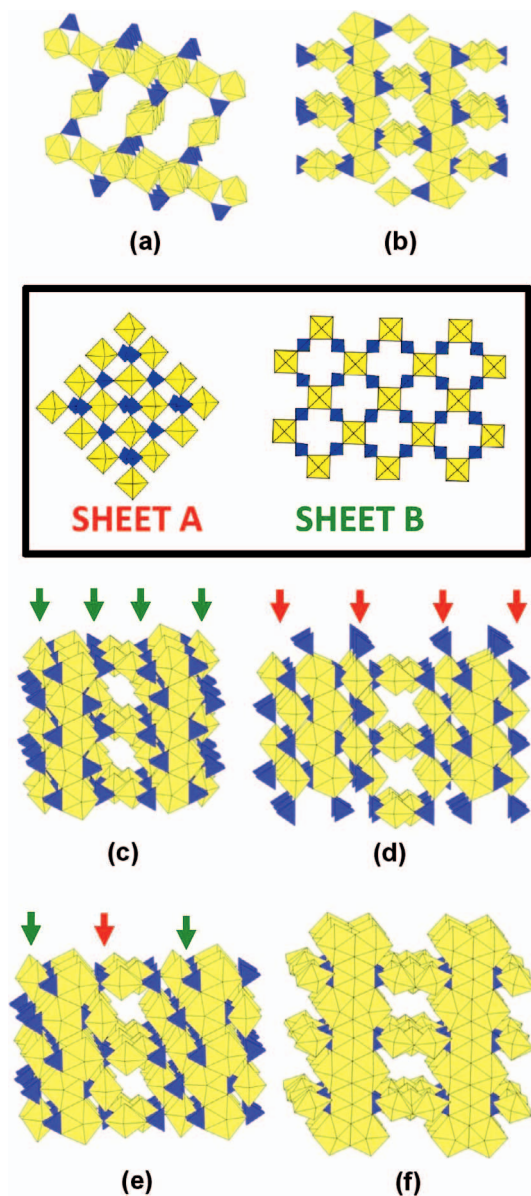
FIG. 17. Framework structures dominated by the interconnection of interpenetrating chains of uranium polyhedra found in the compounds listed in Table 16.

more recent investigation of weeksite from the same locality (Fejfarová *et al.* 2012), however, suggests that the true symmetry is monoclinic (*C2/m*) with twinned crystals. It has also been suggested that the recently discovered mineral coutinhoite, $Th_xBa_{1-2x}(H_2O)_y$ $[(UO_2)_2(Si_5O_{13})](H_2O)_3$ (Atencio *et al.* 2004) is isostructural with weeksite, but a detailed structure has yet to appear in the literature.

The compound $[La(UO_2)(V_2O_7)][(UO_2)(VO_4)]$ (Fig. 18e) contains a complex, REE-bearing structure based on sheet topological related to uranophane. Uranophane-type sheets, wherein half of the pentagons are occupied by irregular, [9]-coordinated $La^{3+}O_8$ polyhedra (La^{3+} is illustrated as green spheres), are directly linked by vertex-sharing dimers of V_2O_7 tetrahedra to form doublets. In between these doublets are sheets with the basic α-uranophane topology. Both types of sheets are bridged by vertex-sharing with La-polyhedra.

Linked phosphuranylite-type sheets. These frameworks are connected in a manner similar to those formed by the linkage of uranophane-type sheets. Specifically, apical anions of the tetrahedra of adjacent sheets are bonded to various cations located between the sheets. In phosphuranylite (Fig. 18f), uranyl pentagonal bipyramids with their equatorial planes oriented at right angles to the plane of the sheets are the bridges. In the structure of upalite, $(AlΦ_6)$ octahedra provide linkages between the sheets (Fig. 18g). Half of these octahedra share vertices with both adjacent sheets, whereas the others are interstitial and are not linked to either sheet. The sheets in francoisite-Nd (Fig. 18h) are linked by irregular (NdO_9) polyhedra. Each (NdO_9) polyhedron shares vertices with one (PO_4) tetrahedron and one yl oxygen atom (in each sheet). In the structure of vanmeerscheiteite (Fig. 18i), $U[(UO_2)_3(PO_4)_4(OH)_6(PO_4)_2](H_2O)_7$, distorted U^{6+} octahedra (without a uranyl ion) share apical vertices with (PO_4) tetrahedra to link adjacent sheets together. In the structures of phuralumite (Fig. 18j) and althupite (Fig. 18k), adjacent sheets are linked by complex clusters of polyhedra (illustrated in the inset). In the former, a [4]-membered cluster of edge- and vertex-sharing aluminum octahedra and tetrahedra occurs, whereas in the latter, two (AlO_6) and two $(Th^{4+}O_9)$ polyhedra form a complex cluster that links adjacent sheets.

There are two compounds with structures based on the linkage of sheets with the β-U_3O_8 topology. In the structure of $(NH_4)_3[(UO_2)_{10}O_{10}(OH)][(UO_4)(H_2O)_2]$ $(H_2O)_2$, β-U_3O_8-type sheets are linked by uranyl hexagonal bipyramids located between the sheets (Fig. 18l). Four of the equatorial edges of the hexagonal bipyramid are linked to $(O_{yl}–O_{eq})$ edges of four different in-sheet pentagonal bipyramids (two in the sheet above and two in the sheet below), such that a CCI configuration occurs. The (NH_4) is present in interstitial positions in the framework, located between the sheets (Fig 18l). Similarly, the structure of $[Ni(H_2O)_4]_3[U(OH)(H_2O)][(UO_2)_8O_{12}(OH)_3]$ contains β-U_3O_8-types sheets that are linked by $(NiΦ_6)$ octahedra that share vertices with the yl oxygen atoms of the sheet (Fig. 18m).

TABLE 17. U(VI) COMPOUNDS CONTAINING FRAMEWORKS OF SHEETS

MINERAL	FORMULA	SG	a (Å)	b (Å)	c (Å)	α (°)	β (°)	γ (°)	SYN[a]	FIG	REF
I. FRAMEWORKS OF SHEETS LINKED BY INTERSTITIAL POLYHEDRA											
Linked uranophane-type sheets											
Sklodowskite	$[Mg(UO_2)(SiO_5(OH))_2](H_2O)_7$	$C2/m$	17.382	7.047	6.610	—	105.9	—		18a	1
	$[(UO_2)_3(PO_4)_2](H_2O)_4$	$Pnma$	7.063	17.022	13.172	—	—	—	HT[140]	18b	2
	$(UO_2)[(UO_2)_3(AsO_4)_2](H_2O)_2$	$P2/c$	11.238	7.152	21.941	—	104.58	—	HT[230]	18b	3
	$Cs_2(UO_2)[(UO_2)_3(AsO_4)_2]_4(H_2O)_2$	$Cmc2_1$	15.157	14.079	13.439	—	—	—	HT[180]	18b	4
	$Rb_2(UO_2)[(UO_2)_3(PO_4)_2]_4(H_2O)_2$	$Fm11$	15.72	13.839	13.051	90.39	—	—	HT[200]	18b	5
	$Rb_2(UO_2)[(UO_2)_3(AsO_4)_2]_4(H_2O)_{4.5}$	$C2/m$	13.462	15.846	14.007	—	92.31	—	HT[180]	18b	4
	$K_2(UO_2)[(UO_2)_3(PO_4)_2]_4(H_2O)_2$	$Fm11$	15.257	13.831	13.007	91.76	—	—	HT[200]	18b	5
	$Tl_2(UO_2)[(UO_2)_3(PO_4)_2]_4(H_2O)_2$	Cm	12.979	15.164	9.338	—	132.31	—	HT[220]	18b	6
	$(UO_2)[(UO_2)_3(VO_4)_2](H_2O)_5$	$Cmcm$	17.978	13.561	7.163	—	—	—	HT[60]	18b	7
	$(UO_2)[(UO_2)_3(AsO_4)_2](H_2O)_5$	$Pca2_1$	20.133	11.695	7.154	—	—	—	HT[230]	18c	3
Weeksite	$K_{1.24}Ba_{0.25}Ca_{0.12}[(UO_2)_2(Si_5O_{13})](H_2O)_{4.03}$	$Cmma$	14.248	14.209	35.869	—	—	—		18d	8
	$[La(UO_2)(V_2O_7)(UO_2)(VO_4)]$	$P2_12_12_1$	6.947	7.093	25.746	—	—	—		18e	9
Linked phosphuranylite-type sheets											
Phosphuranylite	$KCa[(H_3O)_3(UO_2)][(UO_2)_3(PO_4)_2O_2]_2(H_2O)_8$	$Cmcm$	15.899	13.740	17.300	—	—	—		18f	10
Upalite	$Al[(UO_2)_3O(OH)(PO_4)_2](H_2O)_7$	$P2_1/a$	13.704	16.820	9.332	—	111.5	—		18g	11
Francoisite-Nd	$Nd[(UO_2)_3(PO_4)_2O(OH)](H_2O)_6$	$P2_1/a$	9.298	15.605	13.668	—	112.77	—		18h	12
Vanmeerscheite	$U(UO_2)_3(PO_4)_4(OH)_6(H_2O)_4$	$P2_1mn$	17.06	16.760	7.023	—	—	—		18i	13
Phuralumite	$Al_2[(UO_2)_3(PO_4)_2(OH)]_2(OH)_4(H_2O)_{10}$	$P2_1/a$	13.836	20.918	9.428	—	112.44	—		18j	14
Althupite	$AlTh(UO_2)[(UO_2)_3(PO_4)_2O(OH)]_2(OH)_3(H_2O)_{15}$	$P\overline{1}$	10.953	18.567	13.504	72.64	68.20	84.21		18k	15
Linked β-U_3O_8 sheets											
	$(NH_4)_2[(UO_2)_{10}O_{10}(OH)][(UO_4)(H_2O)_2](H_2O)_2$	$C2/c$	11.627	21.161	14.706	—	103.93	—	HT[220]	18l	16
	$(Ni(H_2O)_4)_3[U(OH)(H_2O)(UO_2)_8O_{12}(OH)_3]$	$P\overline{1}$	8.627	10.566	12.091	110.59	102.96	105.50	HT[180]	18m	17
Other types of linked sheets											
	$Ba_4[(UO_2)_7(UO_4)(AsO_4)_2O_7]$	$Pmna$	15.535	7.042	14.094	—	—	—	SS[1150]	18n	18
	$Cs_2Na_8[(UO_2)_8O_8(Mo_5O_{20})]$	$Ibam$	6.846	23.386	12.337	—	—	—	SS[950]	18o	19
II. FRAMEWORKS DIRECTLY LINKED SHEETS											
-not linked by cation-cation interactions											
	α-UO_3	$C2mm$	3.961	6.860	4.166	—	—	—	SS[800]	18p	20
	α-U_3O_8	$C222$	6.716	11.96	4.147	—	—	—		18q	21
	MgB_2UO_7	$Pcam$	9.747	8.311	7.911	—	—	—	SS[1473]	18r	22
	$UTiNb_2O_{10}$	$Fddd$	7.28	12.62	16.02	—	—	—		18t	23
	UNb_3O_{10}	$Fddd$	7.38	12.78	15.96	—	—	—		18u	24
	$Ag[(UO_2)_2(HGe_2O_7)](H_2O)$	$Ama2$	7.124	10.771	14.024	—	—	—	HT[220]	18v	25
	$(UO_2)_2(V_2O_7)$	$P2_1/c$	5.649	13.184	7.284	—	119.75	—		18w	26
	$[U^{4+}(UO_2)(PO_4)_2]$	$P\overline{1}$	8.821	9.217	5.477	102.62	97.75	102.46		18x	27
-linked by cation-cation interactions											
	β-U_3O_8	$Cmcm$	7.069	11.445	8.303	—	—	—		19i	28
	$[H_2U_3O_{10}]$	$P\overline{1}$	6.802	7.417	5.556	108.5	125.5	88.2		19g	29
	$[CuU_3O_{10}]$	$P\overline{1}$	6.516	7.614	5.615	109.464	125.18	89.99		19h	30
	$[Ca(UO_2)_2(BO_3)_2]$	$C2$	16.512	8.169	6.582	—	96.97	—	SS[1373]	19k	31
	$[Pb_3(UO_2)_{11}O_{14}]$	$Pmmn$	28.459	8.379	6.765	—	—	—		19j	32
	$[Sr_3(UO_2)_{11}O_{14}]$	$Pmmn$	28.508	8.381	6.733	—	—	—		19j	33

Note: Double lines ($=$) indicate major differences in the stoichiometry of the structural unit, as indicated by the corresponding header in the table; single lines (–) indicates different topologic configurations; and dotted lines (- -) separate graphical isomers.

[a] Synthesis column data. HT[T] and SS[T] correspond to hydrothermal and solid state synthesis, respectively, at maximum reported temperature T (℃); V-Cl: vapor phase chlorination; A, aqueous (Ae denotes evaporation to dryness); Ac, concentrated acid; Flx, molten flux; SDg, slow diffusion in gel.

References: (1) Ryan & Rosenzweig (1977); (2) Locock & Burns (2002a); (3) Locock & Burns (2003d); (4) Locock & Burns (2003e); (5) Locock & Burns (2002b); (6) Locock & Burns (2004); (7) Saadi *et al.* (2000); (8) Jackson & Burns (2001); (9) Mer *et al.* (2012); (10) Demartin *et al.* (1991); (11) Piret *et al.* (1983); (12) Piret *et al.* (1988); (13) Piret & Deliens (1982); (14) Piret *et al.* (1979); (15) Piret & Deliens (1987); (16) Li *et al.* (2001a); (17) Rivenet *et al.* (2009); (18) Wu *et al.* (2009); (19) Nazarchuk *et al.* (2009); (20) Loopstra & Cordfunke (1966); (21) Loopstra (1977); (22) Gasperin (1987e); (23) Chevalier & Gasperin (1969); (24) Chevalier & Gasperin (1968); (25) Ling *et al.* (2010a); (26) Tancret *et al.* (1995); (27) Benard *et al.* (1994); (28) Loopstra (1970); (29) Siegel *et al.* (1972b); (30) Dickens *et al.* (1993); (31) Gasperin (1987c); (32) Ijdo (1993a); (33) Cordfunke *et al.* (1991).

The structure of $Ba_4[(UO_2)_7(UO_4)(AsO_4)_2O_7]$ is the only example in this class that has a sheet-anion topology that is not observed in structures based on discrete sheets (Fig. 18n). In this sheet, half of the squares of the corresponding anion topology are occupied by uranyl ions, giving square bipyramids with the uranyl ions oriented in the plane of the sheet with CCIs present. Each of the equatorial anions of the uranyl square bipyramids are shared with a (AsO_4) tetrahedron, which bridges to the adjacent sheet. The structure of $Cs_2Na_8[(UO_2)_8O_8(Mo_5O_{20})]$ (Fig. 18o) contains sheets with the same anion topology as in
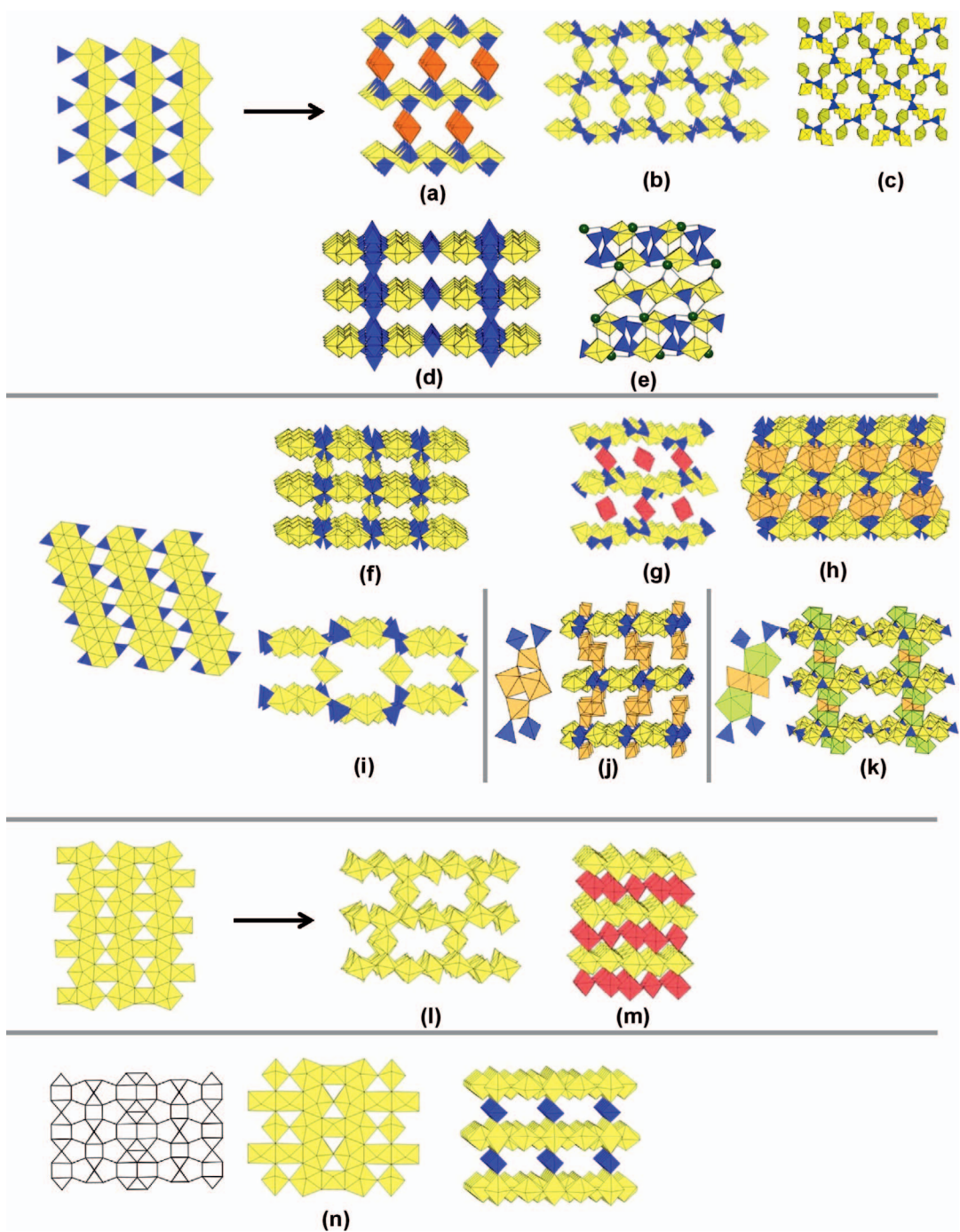
FIG. 18. Framework structures dominated by sheets connected by: (a–m) high valence cations in the interstitial region and (n–t) direct sharing of polyhedral elements. The corresponding compounds are listed in Table 17.
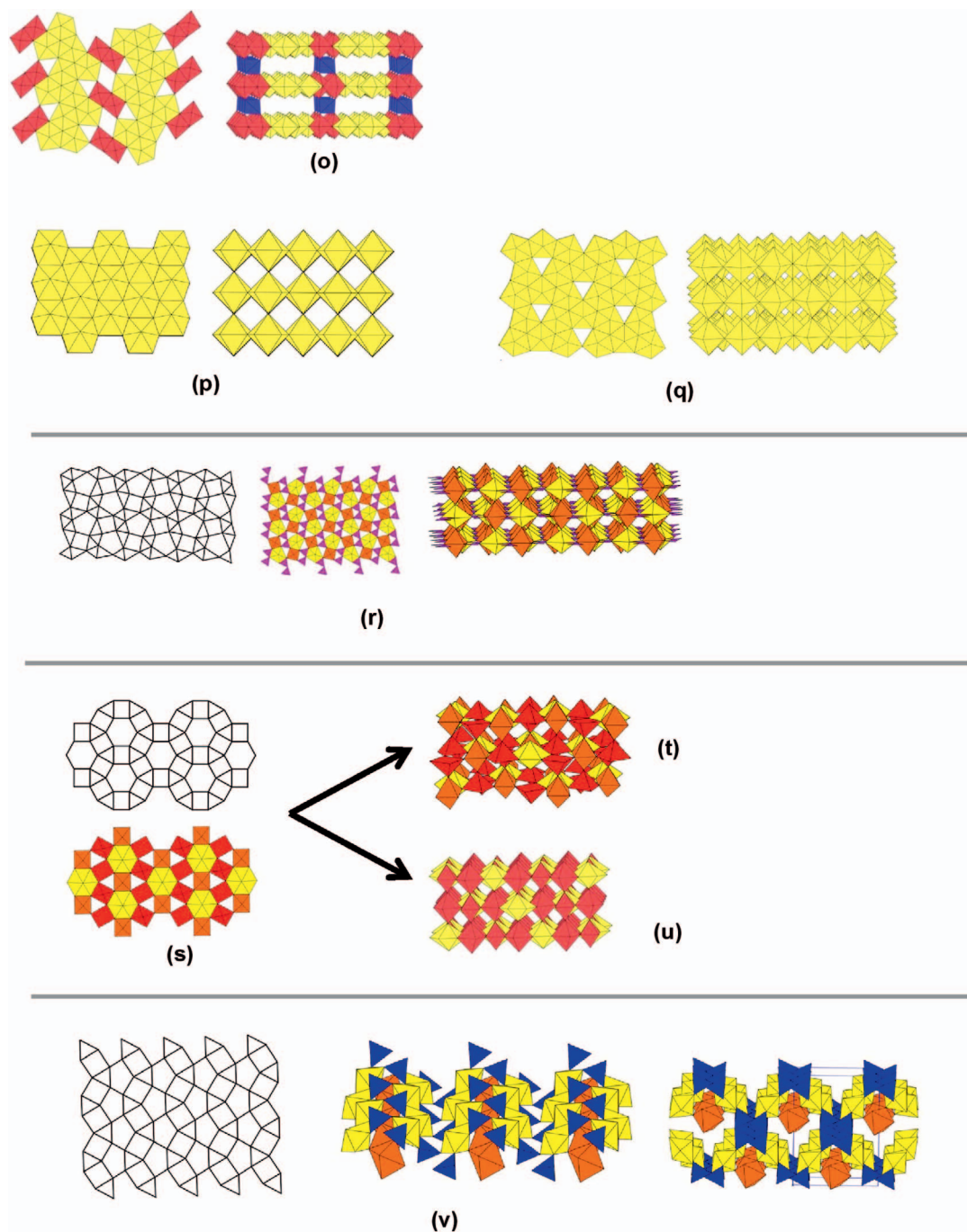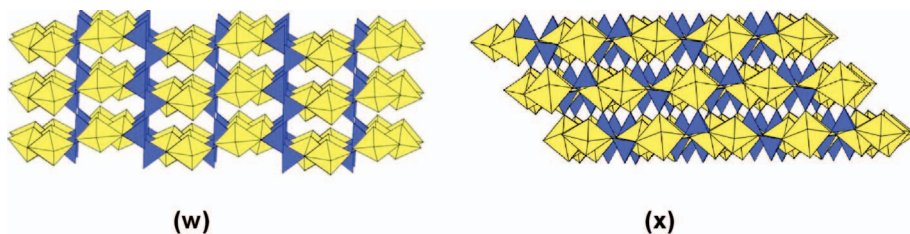
FIG. 18. Continued.

$X_{10}[(UO_2)_8O_8(Mo_5O_{20})]$ ($X = $ Ag, Na) (Fig. 9y), but otherwise their structures are significantly different. In $Cs_2Na_8[(UO_2)_8O_8(Mo_5O_{20})]$, the squares in the corresponding sheet-anion topology are occupied by (MoO_6) octahedra. (MoO_4) tetrahedra also are located between the sheets, where they bridge the two (MoO_6) octahedral apices. The remaining two tetrahedral vertices link in the same fashion to an adjacent sheet. In contrast, in $X_{10}[(UO_2)_8O_8(Mo_5O_{20})]$ the squares in the sheet-anion topology are occupied by [5]-sided (MoO_5), distorted square pyramids. Although (MoO_4) tetrahedra again occupy the region between the sheets, these are not directly element-sharing with the proximal sheets, and they occur only between every second set of sheets.

Frameworks of directly linked sheets

The 14 compounds in this category (Table 17) have frameworks of sheets of uranyl polyhedra that are predominantly linked through equatorial edges. In six of these, cation-cation interactions are involved in the linkage of adjacent sheets. As such, these compounds are also listed in Table 18 and illustrated in Figure 19.

The structures of α-UO_3 (Fig. 18p) and α-U_3O_8 (Fig. 18q) are based on directly linked sheets of uranium (mostly uranyl) polyhedra. In α-UO_3, sheets consist only of closely packed hexagonal bipyramids that are stacked directly on top of each other and that are linked *via* bridging of the apical anions. If the structure is viewed perpendicular to the plane of the sheets, infinite chains of vertex-sharing hexagonal bipyramids are visible. In contrast, the sheets in α-U_3O_8 consist only of pentagonal bipyramids and vacant triangles, each oriented in the same direction. These sheets are stacked directly on top of each other such that the apical anions of each pentagonal bipyramid link to two others, resulting in triangular channels and orthogonal-to-sheet chains of vertex-sharing pentagonal bipyramids.

The structure of $[MgB_2(UO_2)O_5]$ contains a sheet with an anion topology consisting of triangles, squares, and pentagons (Fig. 18r) that is not observed in any

phase as a discrete sheet. The pentagons and squares of the anion topology are occupied by uranyl ions and (MgO_6) octahedra, respectively, whereas half of the triangles are occupied by (BO_3) groups. The sheets are stacked such that the apical anion of the (MgO_6) octahedron is also a yl oxygen atom belonging to the adjacent sheet.

The compounds $[UTiNb_2O_{10}]$ and $[UNb_3O_{10}]$ (Fig. 18s–u) contain directly connected sheets with the topology shown in Figure 18s. These compounds are nearly isostructural, with the local bond topology differing only slightly. In the structure of $[UTiNb_2O_{10}]$, Nb^{5+} and Ti^{4+} occur in [5]-sided pyramids (which alternate with respect to the direction of the apical anions) and regular octahedra, respectively. These two polyhedra (each in different, but adjacent, sheets) share an apical anion, forming the framework structure. In this structure, the yl oxygen atoms do not bond to any additional cation. In contrast, in the structure of $[UNb_3O_{10}]$, Nb^{5+} is present only in octahedral coordination, and adjacent sheets are bridged *via* apical anions of octahedra and yl oxygen atoms (with the configuration $U^{6+} = O_{yl}-Nb^{5+}$). This highly unusual linkage appears to be responsible for the considerably elongated $U–O_{yl}$ bond lengths of 1.87 Å in this compound.

The structure of $Ag[(UO_2)_2(HGe_2O_7)](H_2O)$ contains sheets with a corrugated uranophane-type topology (Fig. 18v). Dimeric groups of vertex-sharing $Ge_2O_6(OH)$ tetrahedra replace the typically observed $SiO_3(OH)$ polyhedra of the uranophane sheet and act to bridge adjacent sheets. The corrugated topology facilitates inclusion of infinite chains of face-sharing (AgO_6) octahedra. These chains, however, link only to one of the two adjacent sheets. The structure of $[(UO_2)_2V_2O_7]$ (Fig. 18w) and the mixed-valence compound $U^{4+}(UO_2)(PO_4)_2$ (Fig. 18x) both consists of directly linked uranophane-type sheets. In the former compound, the separate sheets are linked by vertex-sharing dimers of (V_2O_7) tetrahedra, resulting in narrow, open channels throughout the structure. In the latter compound, U^{4+} occupies half of the pentagonal polyhedra, and these link directly to the

TABLE 18. U(VI) COMPOUNDS CONTAINING FRAMEWORK STRUCTURES WITH CATION–CATION INTERACTIONS

FORMULA	SG	a (Å)	b (Å)	c (Å)	α (°)	β (°)	γ (°)	D_c/R_c	SYN[a]	FIG	REF
Chains											
α-[(UO$_2$)(SeO$_4$)]	$P2_1/c$	6.909	5.525	13.318	—	103.79	—	I / I	HT[200]	19a	1
β-[(UO$_2$)(SO$_4$)]	$P2_1/c$	6.760	5.711	12.824	—	102.91	—	I / I	SS[500]	19a	1
[(UO$_2$)(MoO$_4$)]	$P2_1/c$	7.202	5.484	13.599	—	104.54	—	I / I		19a	2
(UO$_2$)Cl$_2$	$Pnma$	5.725	8.409	8.720	—	—	—	I / I	V-Cl	19b	3
Cs[(UO$_2$)$_3$(HIO$_6$)$_2$(H$_2$O)(OH)O](H$_2$O)$_{1.5}$	Cc	13.096	10.071	11.039	—	102.60	—	I / I		19c	4
Sheets											
Na$_2$Li$_8$[(UO$_2$)$_{11}$O$_{12}$(WO$_5$)$_2$]	$P\bar{1}$	6.946	11.207	12.054	99.53	106.21	90.22	I / III	SS[950]	19d	5
Sr$_5$(UO$_2$)$_{20}$(UO$_6$)$_2$O$_{16}$(OH)$_6$(H$_2$O)$_6$ [b]	$C222_1$	11.668	21.065	14.373	—	—	—	I / III	SS[920]	19e	6
Li$_2$[(UO$_2$)$_4$(WO$_4$)$_4$O]	$C2/c$	14.019	6.312	22.296	—	98.86	—	I / II	SS[920]	19f	7
[H$_2$U$_3$O$_{10}$] [c]	$P\bar{1}$	6.802	7.417	5.556	108.5	125.5	88.2	I / II	HT[350]	19g	8
[CuU$_3$O$_{10}$] [c]	$P\bar{1}$	6.516	7.614	5.615	109.46	125.18	89.99	I / II	SS[750]	19h	9
[Pb$_3$U$_{11}$O$_{36}$] [c]	$Pmmn$	28.459	8.379	6.765	—	—	—	I / II	SS[790]	19i	10
[Sr$_3$U$_{11}$O$_{36}$] [c]	$Pmmn$	28.508	8.381	6.733	—	—	—	I / II	SS[1000]	19i	11
[Ca(UO$_2$)$_2$(BO$_3$)$_2$] [c]	$C2$	16.512	8.169	6.582	—	96.97	—			19j	12
Complex Frameworks											
Li$_4$[(UO$_2$)$_{10}$O$_{10}$(Mo$_2$O$_8$)]	$P2_1/c$	7.943	19.989	10.079	—	90.58	—	II / I	SS[870]	19k	13
(NH$_4$)[(UO$_6$)$_2$(UO$_2$)$_9$(GeO$_4$)(GeO$_3$(OH))]	$P\bar{3}_1c$	10.253	10.253	17.397	—	—	120	I / I	HT[220]	19l	14
Ba[(UO$_6$)$_2$(UO$_2$)$_9$(GeO$_4$)$_2$]	$P\bar{3}_1c$	10.201	10.201	17.157	—	—	120	I / I	HT[220]	19l	14
K[(UO$_6$)$_2$(UO$_2$)$_9$(GeO$_4$)(GeO$_3$(OH))]	$P\bar{3}_1c$	10.226	10.226	17.150	—	—	120	I / I	HT[220]	19l	14
Li$_3$[(UO$_6$)$_2$(UO$_2$)$_9$(GeO$_4$)(GeO$_3$(OH))]	$P\bar{3}_1c$	10.267	10.267	17.056	—	—	120	I / I	HT[220]	19l	14
(Pb$_2$(H$_2$O))[(UO$_2$)$_{10}$UO$_{12}$(OH)$_6$(H$_2$O)$_2$]	$C2/c$	13.281	10.223	26.100	—	103.20	—	I / I	HT[220]	19m	15
Cs(UO$_2$)$_9$U$_3$O$_{16}$(OH)$_5$	$R\bar{3}c$	11.395	11.395	43.722	—	—	120	I / II	HT[220]	19n	6

Note: Double lines (=) indicate major differences in the stoichiometry of the structural unit, as indicated by the corresponding header in the table; single lines (–) indicates different topologic configurations; and dotted lines (- -) separate graphical isomers.

[a] Synthesis column data. HT[T] and SS[T] correspond to hydrothermal and solid state synthesis, respectively, at maximum reported temperature T (°C); V-Cl: vapor phase chlorination; A, aqueous (Ae denotes evaporation to dryness); Ac, concentrated acid; Flx, molten flux; SDg, slow diffusion in gel.

Could also be considered as frameworks of (b) indirectly linked sheets and (c) condensed sheets.

References: (1) Brandenburg & Loopstra (1978); (2) Serezhkin *et al*. (1980b); (3) Taylor & Wilson (1973); (4) Sullens *et al*. (2004); (5) Alekseev *et al*. (2006b); (6) Kubatko & Burns (2006b); (7) Obbade *et al*. (2004d); (8) Siegel *et al*. (1972b); (9) Dickens *et al*. (1993); (10) Ijdo (1993a); (11) Cordfunke *et al*. (1991); (12) Gasperin (1987c); (13) Alekseev *et al*. (2007d); (14) Morrison *et al*. (2011); (15) Li & Burns (2000c).

(PO$_4$) groups of the adjacent sheet to stabilize the structure.

The remaining compounds listed in Table 17 all contain cation-cation interactions that directly contribute to the linking of the adjacent sheets. A detailed discussion of these compounds is thus deferred to the following section, which focuses on the more detailed topological consequences of the CCI configuration.

Frameworks containing cation-cation interactions

Crystalline uranyl compounds containing cation-cation interactions are relatively rare. A so-called cation-cation interaction (CCI) occurs where the yl oxygen atom of one actinyl anion directly bonds to an additional actinyl cation, serving as an equatorial ligand of the latter. In a CCI, the actinyl ion associated with the yl bond is considered to be the 'donor', whereas the actinyl ion that is coordinated by the oxygen atom in the equatorial plane is the 'receiver'. Although U^{6+} uranyl cation-cation interactions are rare, there is a growing body of literature that identifies these as important in U^{5+} compounds (Jones *et al*. 2013, Jones & Gaunt 2013, Chatelain *et al*. 2014), as has long been recognized for Np^{5+} compounds (Grigoriev *et al*. 1988, Grigoriev *et al*. 1989). The interested reader is directed to a review article provided by Krot & Grigoriev (2004) as well as the structural hierarchy of Np^{5+} compounds presented by Forbes *et al*. (2008).

Burns (2005) lists only six U^{6+} compounds that contain CCIs, and there are currently 20 reported in the literature (Table 18). Figure 19 illustrates schematically, *via* the direction of the arrow, the three types of donor configurations (D$_c$-I through D$_c$-III) and three types of receiver configurations (R$_c$-I through R$_c$-III) that are observed in the compounds listed in Table 18. Consistent with the approach used elsewhere in this article for other structural classifications, the CCI compounds have been separated into structures based on chains, sheets, and complex frameworks.
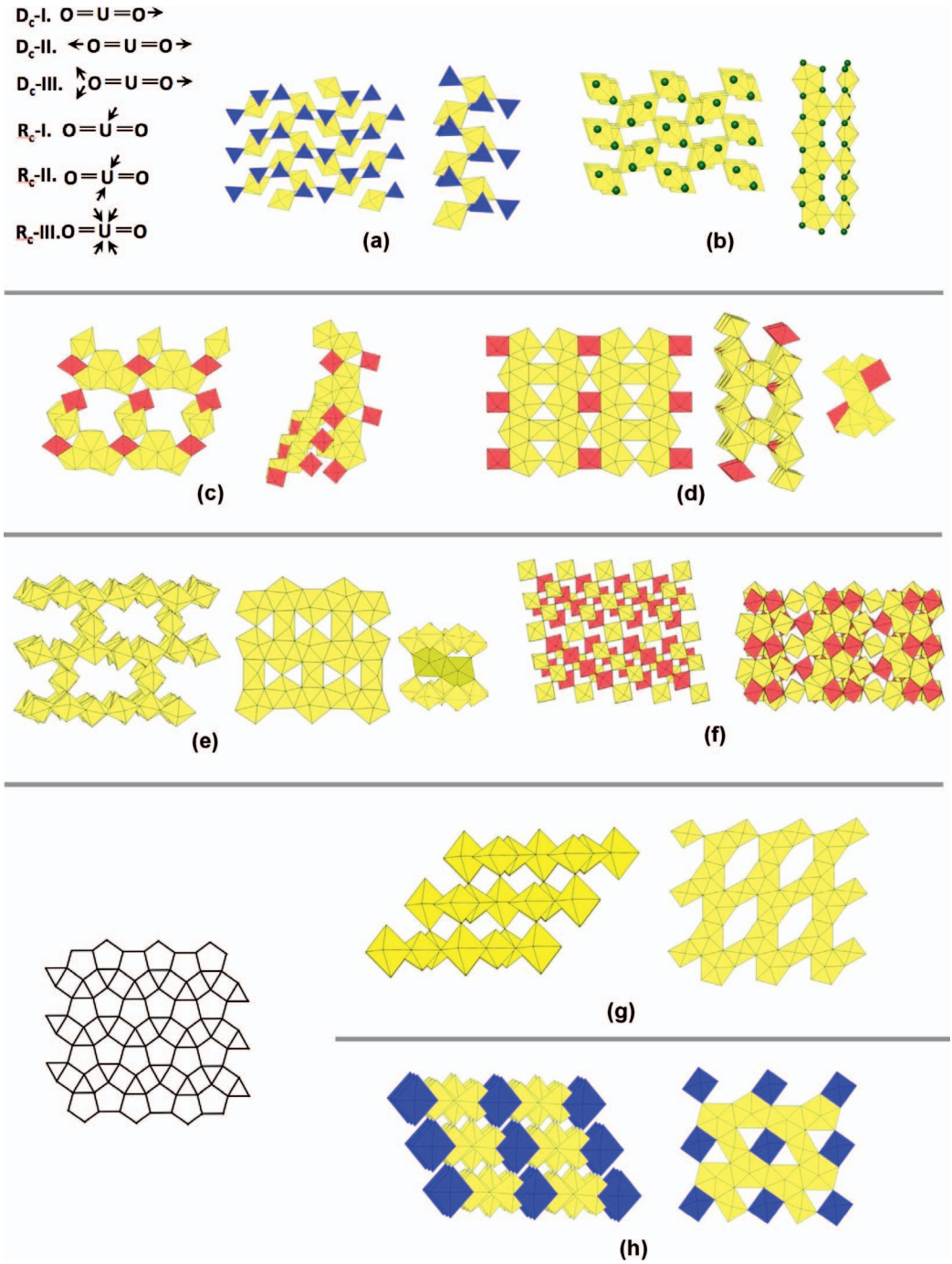
FIG. 19. Framework structures that contain cation-cation interactions. The corresponding compounds are listed in Table 18.
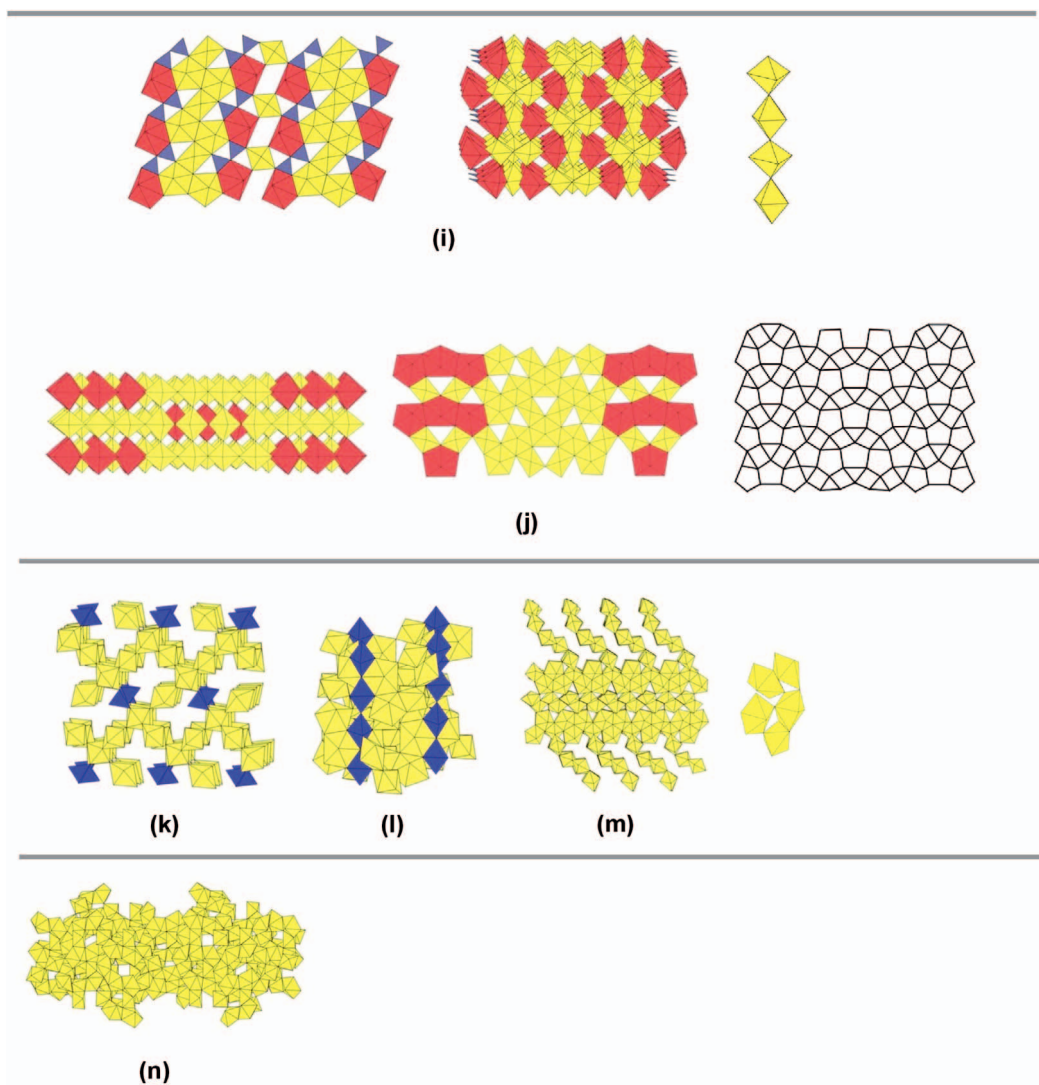
FIG. 19. Continued.

Five compounds have CCIs that are incorporated into infinite chains of uranyl polyhedra. The three isostructural compounds α-[(UO$_2$)(SeO$_4$)], α-[(UO$_2$)(SO$_4$)], and α-[(UO$_2$)(MoO$_4$)] (Fig. 19a) are based on infinite chains of vertex-sharing CCI-linked uranyl polyhedra. The compound [(UO$_2$)Cl$_2$] is also based on infinite chains of edge-sharing uranyl pentagonal bipyramids (Fig. 19b), but in this case the CCIs are not directly part of the infinite chains, but instead the edge-sharing chains are linked *via* the CCI bond. In this compound, all the equatorial anions are halogens (Cl), with the important exception of the equatorial oxygen atom that participates in the CCI interaction.

Topologically complex chains occur in the isostructural compounds [X(UO$_2$)$_3$(HIO$_6$)(H$_2$O)(OH)O]1.5-H$_2$O (X = Li, Na, K, Rb, Cs; Fig. 19c). These chains are formed by edge-sharing trimers of uranyl pentagonal bipyramids and are directly linked to each other by CCIs. Additional linkages in each chain are provided by (IO$_6$) octahedra with both vertex- and edge-sharing configurations. Consequently, this structure may also be considered as a framework of interpenetrating chains.

There are eight compounds that are based on infinite sheets of uranyl polyhedra that are linked into a framework by CCIs. The compound Na$_2$Li$_6$

$[(UO_2)_{11}O_{12}(WO_5)_2]$ contains sheets with the β-U_3O_8 anion topology in which the squares are occupied by (WO_6) octahedra (Fig. 19d). These sheets are linked by uranyl hexagonal bipyramids *via* edge-sharing (two edges shared above, two edges shared below). Similarly, the structure of $Sr_5[(UO_2)_{20}(UO_6)_2$ $O_{16}(OH)_6](H_2O)_6$ (Fig. 19e) contains sheets with the β-U_3O_8 anion topology that are linked by edge-sharing dimers of uranyl pentagonal bipyramids. The compound $Li_2[(UO_2)_4(WO_4)_4O]$ (Fig. 19f) contains sheets of vertex-sharing polyhedra that are linked into a framework by uranyl square bipyramids, where the equatorial bonds link to the yl oxygen atoms of uranyl polyhedra of the sheets.

The compounds $[H_2U_3O_{10}]$ and $[CuU_3O_{10}]$ contain sheets based on the uranophane anion topology, with the squares vacant in the former compound (Fig. 19g). The anion positions of these squares are occupied by (OH) groups, and the H bonds contribute to sheet stability by both inter- and intra-sheet bonding. In the latter compound (Fig. 19h), the squares of the anion topology are occupied by the equatorial planes of Jahn-Teller distorted CuO_6 octahedra. In both structures, the sheets are directly linked to each other by a CCI that exists between the two uranyl ions of the adjacent sheets across the bridging anion.

The structure of $[Ca(UO_2)(BO_3)_2]$ (Fig. 19i) contains sheets with a novel sheet topology. Triangles and squares of the topology are occupied by (BO_3) groups and uranyl ions, respectively. Half of the uranyl ions occupying the squares are oriented perpendicular to the sheet, whereas the other half are oriented within the plane of the sheet. Although all of the pentagons are occupied, half correspond to the pentagonal plane of irregular CaO_7 bipyramids. These sheets are stacked on top of each other, such that the uranyl square bipyramids are linked by vertex-sharing to form infinite chains oriented perpendicular to the plane of the sheets. The orientation of the uranyl ion thus alternates in each second polyhedron, such that a CCI occurs.

The isostructural compounds $[Sr_3(U_{11}O_{36})]$ and $[Pb_3(U_{11}O_{36})]$ contain the complex interrupted sheets topologies shown in Fig. 19j. The divalent cations are both [7]-coordinated in pentagonal bipyramids. Fragments of the β-U_3O_8 structure in the sequence form continuous, ribbon-like chains within each sheet. The adjacent sheets are linked by both CCIs and vertex-sharing with Sr^{2+} (or Pb^{2+}).

There are seven CCI-containing compounds that have structures best described as complex [3]-dimensional frameworks. The compound $Li_4[(UO_2)_{10}O_{10}$ $(Mo_2O_6)]$ (Fig. 19k) consists of sheets of edge-sharing uranyl pentagonal bipyramids that intersect at 90°, forming a complex framework structure in which the

CCI occurs at the point where the sheets intersect. The structures of $X[(UO_6)_2(U_2O_2)_9(GeO_4)(GeO_3(OH)]$ [X = $(NH_4)^+$, Ba^{2+}, K^+] (Fig. 19l) are complex frameworks of edge-sharing uranyl pentagonal bipyramids and U^{6+} in a distorted octahedral coordination. These structures show considerable topological complexity. Sheets of uranyl pentagonal bipyramids and UO_6 octahedra exist that contain CCIs. These sheets are linked by additional uranyl pentagonal bipyramids and by chains of (GeO_5) polyhedra. However, the exact configurations of the GeO_x polyhedra are ambiguous. The two Ge sites are positionally disordered with half occupancy, and thus correspond to either isolated GeO_4 tetrahedra or infinite chains of vertex-sharing GeO_5 trigonal bipyramids along [001].

The structure of $(Pb_2(H_2O))[(UO_2)_{10}UO_{12}(OH)_6$ $(H_2O)_2]$ (Fig. 19m) contains topologically complex chains of uranyl polyhedra oriented in both the [110] and [1$\bar{1}$0] directions and that consist of edge- and vertex-sharing uranyl pentagonal and square bipyramids, as well as distorted $U^{6+}O_6$ octahedra. These two chains are linked into a framework of interpenetrating chains with elongated channels between the chains that are occupied by Pb^{2+}. The structure contains a single CCI that links the chains together. Lastly, the structure of $Cs[(UO_2)_9U_3O_{16}(OH_5)]$ (Fig. 19n) consists of an extremely complex topology of vertex- and edge-sharing uranyl square bipyramids and irregular $(U^{6+}O_6)$ octahedra.

Frameworks based on miscellaneous topologies

There are 12 compounds with framework structures gathered here as miscellaneous types, and these are listed in Table 19. The isostructural compounds $[X_3UO_9Cl_3]$ (X = La, Pr, Nd) have the complex, densely packed framework topology illustrated in Figure 20a. The complete structure is generated by the direct stacking of the illustrated slice perpendicular to the plane of projection. Here U^{6+} is coordinated in unusual trigonal prismatic polyhedra that are edge-sharing with $(X\Phi_{10})$ polyhedra.

The structure of $[U_2Ta_6O_{19}]$ (Fig. 20b) consists in part of sheets of bi-capped trigonal prisms that are occupied by U^{6+} and that are linked by edge sharing. Viewed perpendicular to this sheet, the prisms have hexagonal outlines, and one-third of the hexagons are vacant. The structure also contains sheets of irregular (TaO_6) octahedra that are linked by vertex-sharing. These sheets are linked *via* polyhedral edge sharing such that each uranium sheet is sandwiched between two (TaO_6) sheets. These larger sheets are, in turn, linked to each other *via* vertex-sharing to form the framework structure. In the structure of $[Na_3Ca_{1.5}$ $(UO_6)]$ (Fig. 20c), all cations occur in octahedral

TABLE 19. U(VI) COMPOUNDS CONTAINING FRAMEWORK STRUCTURES WITH MISCELLANEOUS TOPOLOGIES

MINERAL	FORMULA	SG	a (Å)	b (Å)	c (Å)	α (°)	β (°)	γ (°)	SYN[a]	FIG	REF
	[La$_3$(UO$_6$Cl$_3$)]	$P6_3/m$	9.516	9.516	5.613	—	—	120		20a	1
	[Pr$_3$(UO$_6$Cl$_3$)]	$P6_3/m$	9.396	9.396	5.547	—	—	120		20a	1
	[Nd$_3$(UO$_6$Cl$_3$)]	$P6_3/m$	9.367	9.367	5.530	—	—	120		20a	1
	[U$_2$Ta$_6$O$_{19}$]	$P6_3/mcm$	6.266	6.266	19.860	—	—	120		20b	2
	[Na$_3$Ca$_{1.5}$UO$_6$]	$Fddd$	6.657	9.611	20.116	—	—	—	Flx[800]	20c	3
Miscellaneous compounds with isolated uranium polyhedra											
	K$_{3.48}$[(UO$_2$)H$_{1.52}$(VO)$_4$(PO$_4$)$_5$]	$Immm$	7.380	9.158	17.089	—	—	—	HT[190]	20d	4
	K$_2$[(UO$_2$)$_2$(VO)$_2$(IO$_6$)$_2$O](H$_2$O)	$Pba2$	9.984	16.763	4.977	—	—	—	HT[120]	20e	5
	Ca[UMo$_4$O$_{16}$]	$P\bar{1}$	13.239	6.651	8.236	—	90.38	120.16		20f	6
	Cr[UO$_6$]	$P\bar{3}1m$	4.988	4.988	4.620	—	—	120	HT[325]	20g	7
	Cs$_4$[Ge$_8$UO$_{20}$]	$P2_1/n$	7.432	12.378	12.235	—	90.13	—	HT[585]	20h	8
Cliffordite	[(UO$_2$)(Te$_3$O$_7$)]	$Pa\bar{3}$	11.370	11.370	11.370	—	—	—		20i	9
	(UO$_2$)(B$_8$O$_{11}$(OH)$_4$)	Cc	6.448	16.741	10.964	—	90.68	—		14aj	10

Note: Double lines (⸗) indicate major differences in the stoichiometry of the structural unit, as indicated by the corresponding header in the table; single lines (–) indicates different topologic configurations; and dotted lines (- -) separate graphical isomers.
[a] Synthesis column data. HT[T] and SS[T] correspond to hydrothermal and solid state synthesis, respectively, at maximum reported temperature T (℃); V-Cl: vapor phase chlorination; A, aqueous (Ae denotes evaporation to dryness); Ac, concentrated acid; Flx, molten flux; SDg, slow diffusion in gel.
References: (1) Henche *et al.* (1993); (2) Schleifer *et al.* (2000); (3) Roof *et al.* (2010b); (4) Shvareva *et al.* (2007); (5) Sykora & Albrecht-Schmitt (2003); (6) Lee & Jaulmes (1987); (7) Hoekstra & Siegel (1971); (8) Nguyen & Lii (2011); (9) Galy & Meunier (1971); (10) Wang *et al.* (2011b).

coordination, and there is no uranyl ion. The octahedra are close-packed in a halite-like (NaCl) structure and show an extremely complex, yet fully ordered, occupancy pattern.

Although the final seven compounds listed in Table 19 are placed in the category of miscellaneous frameworks, they all contain uranium polyhedra that are isolated in a complex framework of additional edge- and vertex-sharing polyhedra containing high-valence cations. The structure of K$_{3.48}$[(UO$_2$)H$_{1.52}$(VO)$_4$(PO$_4$)$_5$] (Fig. 20d) contains uranyl square bipyramids in which the four equatorial anions bridge to tetrahedral ligand polyhedra. These finite clusters are directly linked to edge-sharing dimers of (VO$_5$) pyramids to form the complete framework. This arrangement results in the presence of channels throughout the structure that are occupied by K$^+$.

In two compounds, the isolated uranium polyhedra are linked to the structural unit *via* edge-sharing chains of non-uranium polyhedra. The structure of K$_2$[(UO$_2$)$_2$(VO)$_2$(IO$_6$)$_2$O](H$_2$O) (Fig, 20e) consists of uranyl square bipyramids that link (by vertex-sharing) to infinite parallel chains of edge-sharing (IO$_6$) octahedra. This configuration results in wide, somewhat rectangular-shaped channels that are occupied by K$^+$ cations. In the structure of Ca[UMo$_6$O$_{16}$] (Fig. 20f), dimers of edge-sharing (MoO$_6$) octahedra are stacked directly on top of each other to form infinite chains. Both the uranyl ions and Ca^{2+} cations occur in pentagonal bipyramidal coordination. Each yl oxygen

links to a (CaO$_7$) polyhedra, and *vice versa*, forming an infinite chain of stacked pentagonal bipyramids. These two types of chains are linked together by sharing equatorial edges with uranyl pentagonal bipyramids.

The structure of [Cr$_2$UO$_6$] (Fig. 20g) consists of uranium octahedra (without uranyl) that occupy space between gibbsite-types sheets of (CrO$_6$) octahedra. In the gibbsite-type sheets, one-third of the octahedra are vacant, and the (UO$_6$) octahedra are located directly above these vacancies, with the sheets linked by vertex-sharing.

In the structure of Cs[Ge$_8$UO$_{20}$] (Fig. 20h), U^{6+} is present in irregular octahedral coordination without uranyl ions present. Each octahedron vertex-shares with six (GeO$_4$) tetrahedra. To form the complete framework, tetrahedra are linked together into three-membered rings. Dimers of edge-sharing (GeO$_5$) polyhedra link the [3]-membered rings together to form [8]-membered polyhedral rings. Cesium occupies the center of these larger rings.

Cliffordite, (UO$_2$)(TeO$_7$) (Fig. 20i) is among the few anhydrous uranyl minerals. Here, each uranyl hexagonal bipyramid shares six edges with irregular TeO$_4$ polyhedra. Adjacent clusters, in turn, link *via* both edge- and vertex-sharing to form a topologically complex, dense framework. In the structure of [(UO$_2$)(B$_8$O$_{11}$(OH)$_4$)] (Fig. 20j) uranyl hexagonal bipyramids each share three edges with boron polyhedra (two BO$_4$ tetrahedron and one BO$_3$
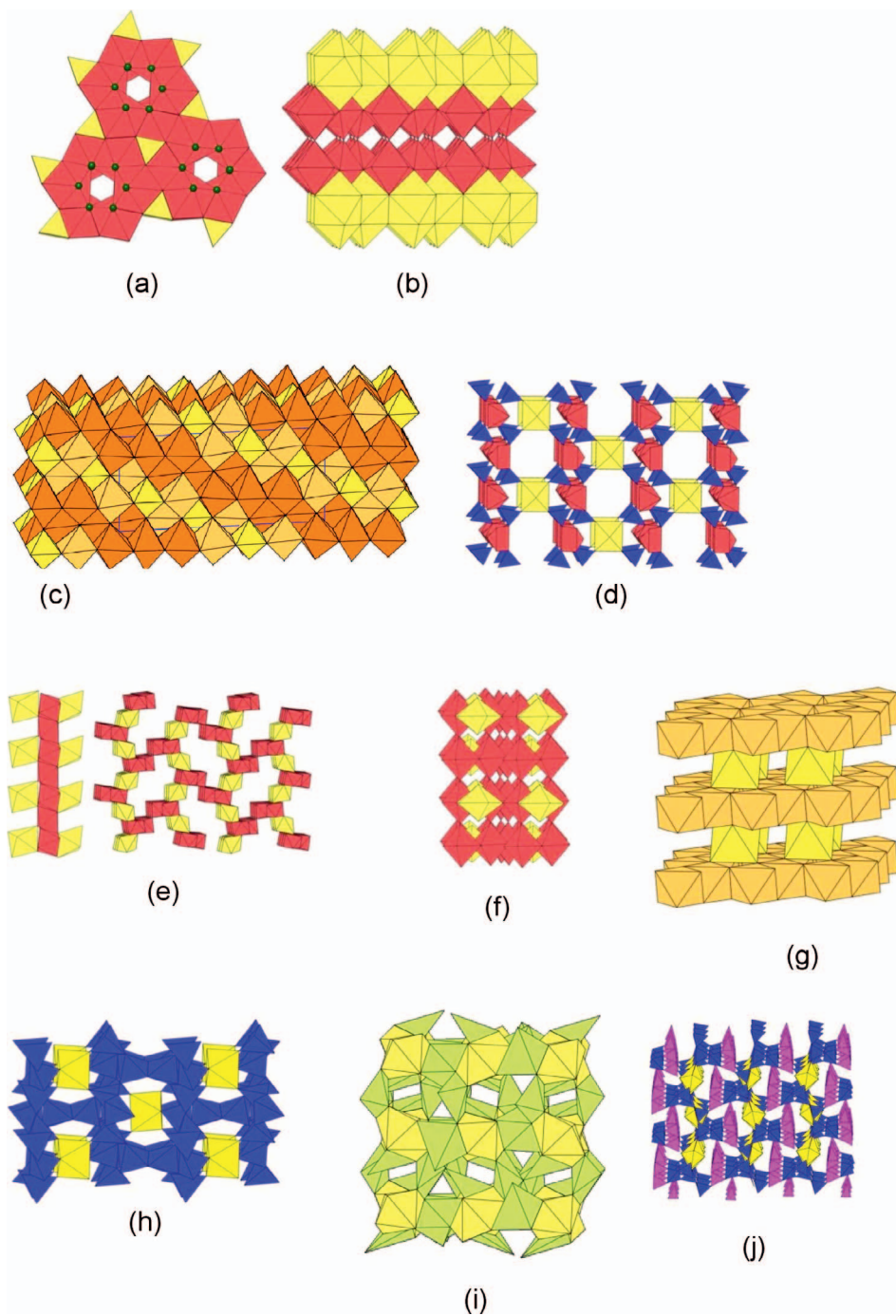
Fɪɢ. 20. Framework structures based on miscellaneous topologies (*i.e.*, failing to fit in the preceding categories). The corresponding compounds are listed in Table 19.
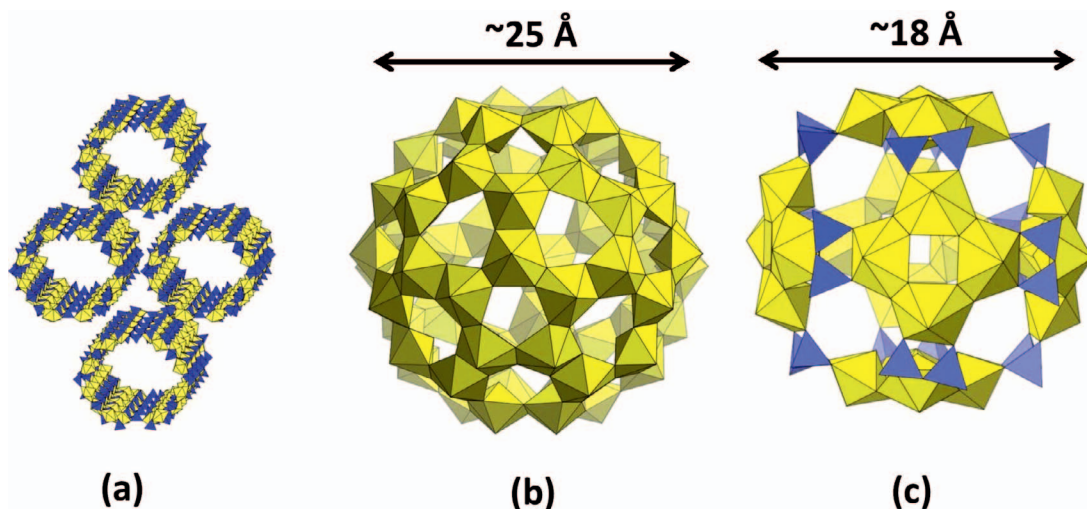
Fig. 21. Selected examples of nanostructured uranyl materials; (a) uranyl selenate tubules; (b) {U_{60}}; and (c) {$U_{24}Py_{12}$}.

triangle). These clusters are linked through a complex network of additional BO_x polyhedra to form the resulting framework. It is noteworthy that in both pervious structures, there is sufficient linkage between the ligand polyhedra to form a coherent framework, *i.e.*, with the uranyl bipyramids essentially located in the interstices.

NANOSTRUCTURED MATERIALS

Recent research has shown a growing number of inorganic compounds that contain uranyl polyhedra arranged to form discrete macromolecular structures (typically on the scale of nanometers). For example, infinite sheets of vertex-sharing uranyl pentagonal bipyramids and selenate tetrahedra (with topology derived from the {3.6.3.6} parent graph shown in 5o) can wrap onto themselves, forming infinite $[(UO_2)_{10}(SeO_4)_{17}(H_2O)]^{14-}$ nanotubules (Krivovichev *et al*. 2005g, h). These tubules have very large effective diameters ($\sim$12.6 Å) and arrange themselves in a parallel, close-packed manner to form crystals, as shown in Figure 21a.

The first uranyl peroxo-nanoclusters were reported by Burns *et al*. (2005). Since this publication, approximately 60 additional clusters have been synthesized and are summarized in Qiu & Burns (2013) and Burns (2011). Each of these contains uranyl-peroxide bipyramids (of the type illustrated in Fig. 1). The polymerization of such bipyramids, bridged by the peroxide ligand, induces the necessary curvature to promote the formation of discrete, caged clusters. The known clusters vary considerably in size and composition. The two examples shown in Figure

21 illustrate this point. Figure 21b shows the {U_{60}} cluster ($Li_{40}K_{20}[UO_2(O_2)(OH)]_{60}(H_2O)_{214}$). The outer cage of this cluster consists solely of edge-sharing uranyl di-peroxo hexagonal bipyramids (diamter $\sim$25 Å). This icosahedral cluster is topologically identical to the well-known C_{60} buckminsterfullerene (Kroto *et al*. 1985), with each carbon atom replaced by the uranyl ion. The cluster consists of 12 pentagonal and 20 hexagonal rings or uranyl ions. In contrast, the {$U_{24}Py_{12}$} cluster ($Na_8[(UO_2)_{24}(O_2)_{24}(P_2O_7)_{12}]$) is shown in Figure 21c. Here, the outer cage consists of six [4]-membered rings of uranyl di-peroxo hexagonal bipyramids, linked by the peroxo bridges. These are linked by 12 vertex-sharing pyrophosphate (P_2O_7) groups. The diameter is $\sim$18 Å. The development of nanostructured materials greatly adds to the diversity of uranyl chemistry and offers new promises for novel useful technologies.

SUMMARY

Uranium is a geologically, economically, and technologically important element. Demand for uranium to fuel the global nuclear energy industry will almost certainly continue to increase in the future. An advanced understanding of the crystal chemical behavior of uranium is critical to developing efficient and effective methods of exploration, exploitation, and eventually disposal that are essential to meeting this demand.

Owing to the efforts of many groups of dedicated scientists worldwide, our knowledge of the crystal chemical possibilities and complexities of U^{6+} has vastly improved over the past decade, with a near

doubling of the number of known structures. Many of these contributions have come from laboratories focused on synthetic chemistry, but the efforts of a few dedicated mineralogists are also fueling discovery of new and fascinating uranyl minerals. Some of these have structures that were initially discovered by synthetic chemists, and others further demonstrate the uniqueness and complexity of geochemical conditions that result in their formation. Some of the newly discovered compounds and minerals will be important in fuel cycle applications, environmental remediation, nuclear reactor accidents, and our understanding and optimization of geological repository performance for nuclear waste. Studies of the crystal chemistry, solid-state chemistry, synthetic chemistry, and nanoscience of U^{6+} are vibrant and important today, and will be for the foreseeable future. Indeed, the high rate of discovery of new compounds continues to accelerate as researchers move into different synthetic realms and geochemical environments.

The continued development of a structure hierarchy of inorganic U^{6+} compounds is a necessary step towards ordering and refining our understanding of U^{6+} solid-state chemistry. It facilitates comparison between the behaviors of seemingly disparate chemical systems and allows a better understanding of the governing mechanisms that promote phase stability, moving us closer to being able to predict how U^{6+} will behave in complex, potentially ecologically sensitive environments.

Behavior prediction is a key issue in overcoming one of the greatest challenges involving uranium geochemistry – the long-term disposal of spent nuclear fuel and other highly radioactive wastes in geologic repositories. Successful disposal requires the immobilization of the waste package upon failure of engineered barriers and the eventual introduction of groundwater. Current models used to predict uranium transport over time are often restricted to the more common uranyl phases (*e.g.*, uranophane, autunite), although new uranyl minerals continue to be discovered even from classic localities. The enormous number of phases presented here, however, indicates that focusing on a few uranyl compounds is likely an oversimplification, and refined models will require incorporation of additional potential phases (as either kinetic or thermodynamic products) as well as nanostructured materials (*e.g.*, soluble cage clusters).

The following key statements and observations can be made:

During the past decade there has been a near two-fold increase in the number of fully-characterized inorganic U^{6+} structures (up from the 368 structures described in Burns 2005), with the majority of the increase corresponding to structures containing sheets and frameworks.

Sheet structures continue to be the most common structural unit observed, with these occurring either as discrete sheets (separated by an interstitial complex of weak bonds), sheets linked by polyhedra containing high valence cations, or sheets that are directly linked. The latter two categories may also be considered as framework structures.

The number of compounds with framework structures has shown the greatest proportional increase over the past decade, prompting the development of the more comprehensive framework classification scheme presented here. The current hierarchy now separates frameworks into the following categories: (1) of element-sharing polyhedra; (2) of clusters linked by vertex-sharing; (3) of linked chains (parallel and cross-linked); (4) of linked sheets; and (5) containing cation-cation interactions. The rapid increase in framework structures appears to arise from exploration of new synthetic realms that are often at higher temperatures or pressures.

For most elements in the periodic table, crystalline compounds containing U^{6+} have been characterized (minerals and synthetics). Despite this, a relatively small number of ligands (and cations) dominate our understanding of uranium crystal chemistry (*e.g.*, Na^+, K^+, Rb^+, Cs^+, Ca^{2+}, Sr^{2+}, Pb^{2+}, Cu^{2+}, Mo^{6+}, V^{5+}, PO_4, SO_4, $SeO_{3/4}$, AsO_4, SiO_4, CrO_4). This is no doubt due to an intentional bias towards those elements that are important in environmental and nuclear waste realms.

References

Aberg, M. (1969) Crystal structure of $(UO_2)_2(OH)_2Cl_2$ $(H_2O)_4$. *Acta Chemica Scandinavica* **23**, 791–810.

ABERG, M. (1976) Crystal-structure of $(UO_2)_4Cl_2O_2(OH)_2$ $(H_2O)_6 \bullet 4H_2O$, a compound containing a tetranuclear aquachlorohydroxooxo complex of uranyl(VI). *Acta Chemica Scandinavica, Series A: Physical and Inorganic Chemistry* **30**, 507–514.

ABERG, M. (1978) Crystal-structure of hexaaqua-tri-mu-hydroxo-mu-3-oxo-triuranyl(vi) nitrate tetrahydrate, $(UO_2)_3O(OH)_3(H_2O)_6NO_3 \bullet 4H_2O$. *Acta Chemica Scandinavica, Series A: Physical and Inorganic Chemistry* **32**, 101–107.

ALCOCK, N.W. (1968) Crystal and molecular structure of sodium uranyl triperoxide. *Journal of the Chemical Society A: Inorganic Physical Theoretical*, 1588–1594.

ALCOCK, N.W., ROBERTS, M.M., & CHAKRAVORTI, M.C. (1980) Structure of potassium catena-di-mu-fluoro-difluorotetraoxo-di-mu-sulphato-diuranate(VI) hydrate. *Acta Crystallographica Section B: Structural Science* **36**, 687–690.

ALCOCK, N.W., ROBERTS, M.M., & BROWN, D. (1982) Actinide structural studies, Part 3: The crystal and molecular-structures of $UO_2SO_4 \bullet H_2SO_4.5H_2O$ and $2NpO_2SO_4 \bullet H_2SO_4 \bullet 4H_2O$. *Journal of the Chemical Society, Dalton Transactions*, 869–873.

ALEKSEEV, E.V., SULEIMANOV, E.V., CHUPRUNOV, E.V., & FUKIN, G.K. (2004) The crystal structure of $Ba(VUO_6)_2$. *Journal of Structural Chemistry* **45**, 518–522.

ALEKSEEV, E.V., SULEIMANOV, E.V., CHUPRUNOV, E.V., & FUKIN, G.K. (2005a) Crystal structure of $CoUO_2$ $(SO_4)_2.5H_2O$ at 293 K. *Crystallography Reports* **50**, 914–917.

ALEKSEEV, E.V., SULEIMANOV, E.V., CHUPRUNOV, E.V., & FUKIN, G.K. (2005b) Crystal structure of monohydrate of gamma-modification of rubidium uranoniobate. *Radiokhimiya* **47**, 492–494.

ALEKSEEV, E.V., SULEIMANOV, E.V., CHUPRUNOV, E.V., & FUKIN, G.K., & ALEKSEEVA, L.G. (2005c) Crystal structure of $KAsUO_6 \bullet 3H_2O$ at 100 and 293 K. *Journal of Structural Chemistry* **46**, 936–940.

ALEKSEEV, E.V., KRIVOVICHEV, S.V., DEPMEIER, W., ARMBRUSTER, T., KATZKE, H., SULEIMANOV, E.V., & CHUPRUNOV, E.V. (2006a) One-dimensional chains in uranyl tungstates: Syntheses and structures of $A_8(UO_2)_4$ $(WO_4)_4(WO_5)_2)$ (A = Rb, Cs) and $Rb_6(UO_2)_2O(WO_4)_4)$. *Journal of Solid State Chemistry* **179**, 2977–2987.

ALEKSEEV, E.V., KRIVOVICHEV, S.V., DEPMEIER, W., SIIDRA, O.I., KNORR, K., SULEIMANOV, E.V., & CHUPRUNOV, E.V. (2006b) $Na_2Li_8(UO_2)_{11}O_{12}(WO_5)_2$: Three different uranyl-ion coordination geometries and cation–cation interactions. *Angewandte Chemie International Edition* **45**, 7233–7235.

ALEKSEEV, E.V., SULEIMANOV, E.V., CHUPRUNOV, E.V., MARYCHEV, M.O., IVANOV, V.A., & FUKIN, G.K. (2006c) Crystal structure and nonlinear optical properties of the $K_2(UO_2)(SO_4)_2 \cdot 2H_2O$ compound at 293 K. *Crystallography Reports* **51**, 29–33.

ALEKSEEV, E.V., SULEIMANOV, E.V., MARYCHEV, M.O., CHUPRUNOV, E.V., & FUKIN, G.K. (2006d) Crystal structure of uranyl tungstate $Cs_2U_2WO_{10}$. *Journal of Structural Chemistry* **47**, 881–886.

ALEKSEEV, E.V., KRIVOVICHEV, S.V., ARMBRUSTER, T., DEPMEIER, W., SULEIMANOV, E.V., CHUPRUNOV, E.V., & GOLUBEV, A.V. (2007a) Dimensional reduction in alkali metal uranyl molybdates: Synthesis and structure of Cs_2 $(UO_2)O(MoO_4)$. *Zeitschrift Für Anorganische und Allgemeine Chemie* **633**, 1979–1984.

ALEKSEEV, E.V., KRIVOVICHEV, S.V., & DEPMEIER, W. (2007b) $K_2(UO_2)As_2O_7$ - the first uranium polyarsenate. *Zeitschrift Für Anorganische und Allgemeine Chemie* **633**, 1125–1126.

ALEKSEEV, E.V., KRIVOVICHEV, S.V., DEPMEIER, W., MALCHEREK, T., SULEIMANOVL, E.V., & CHUPRUNOV, E.V. (2007c) The crystal structure of $Li_4(UO_2)_2(W_2O_{10})$ and crystal chemistry of Li uranyl tungstates. *Zeitschrift Für Kristallographie* **222**, 391–395.

ALEKSEEV, E.V., KRIVOVICHEV, S.V., MALCHEREK, T., & DEPMEIER, W. (2007d) One-dimensional array of two- and three-center cation–cation bonds in the structure of $Li_4(UO_2)_{10}O_{10}(Mo_2O_8)$. *Inorganic Chemistry* **46**, 8442–8444.

ALEKSEEV, E.V., SULEIMANOV, E.V., CHUPRUNOV, E.V., GOLUBEV, A.V., FUKIN, G.K., & MARYCHEV, M.O. (2007e) Synthesis and crystal structure of a new representative of the $Rb_2U_2MoO_{10}$ uranomolybdate series. *Russian Journal of Inorganic Chemistry* **52**, 1446–1449.

ALEKSEEV, E.V., KRIVOVICHEV, S.V., DEPMEIER, W., & KNORR, K. (2008a) Complex topology of uranyl polyphosphate frameworks: Crystal structures of α-, β-$K(UO_2)(P_3O_9)$ and $K(UO_2)_2(P_3O_{10})$. *Zeitschrift Für Anorganische Und Allgemeine Chemie* **634**, 1527–1532.

ALEKSEEV, E.V., KRIVOVICHEV, S.V., MALCHEREK, T., & DEPMEIER, W. (2008b) Crystal chemistry of anhydrous Li uranyl phosphates and arsenates. I. Polymorphism and structure topology: Synthesis and crystal structures of α-$Li(UO_2)(PO_4)$, α-$Li(UO_2)(AsO_4)$, β-$Li(UO_2)(AsO_4)$ and $Li_2(UO_2)_3(P_2O_7)_2$. *Journal of Solid State Chemistry* **181**, 3010–3015.

ALEKSEEV, E.V., KRIVOVICHEV, S.V., & DEPMEIER, W. (2009a) Crystal chemistry of anhydrous Li uranyl phosphates and arsenates. II. Tubular fragments and cation-cation interactions in the 3D framework structures of $Li_6(UO_2)_{12}$ $(PO_4)_8(P_4O_{13})$, $Li_5(UO_2)_{13}(AsO_4)_9(As_2O_7)$, $Li(UO_2)_4$ $(AsO_4)_3$ and $Li_3(UO_2)_7(AsO_4)_5O$. *Journal of Solid State Chemistry* **182**, 2977–2984.

ALEKSEEV, E.V., KRIVOVICHEV, S.V., & DEPMEIER, W. (2009b) Novel layered uranyl arsenates, Ag_6 $(UO_2)_2(As_2O_7)$ (As_4O_{13}) and A^I_6 $(UO_2)_2(AsO_4)_2(As_2O_7)$ (A^I = Ag and Na): first observation of a linear $As_4O_{13}{}^{6-}$ anion and structure type evolution. *Journal of Materials Chemistry* **19**, 2583–2587.

ALEKSEEV, E.V., KRIVOVICHEV, S.V., & DEPMEIER, W. (2009c) Rubidium uranyl phosphates and arsenates with polymeric tetrahedral anions: Syntheses and structures of Rb_4 $(UO_2)_6(P_2O_7)_4(H_2O)$, $Rb_2(UO_2)_3(P_2O_7)(P_4O_{12})$ and $Rb(UO_2)_2(As_3O_{10})$. *Journal of Solid State Chemistry* **182**, 2074–2080.

ALEKSEEV, E.V., KRIVOVICHEV, S.V., & DEPMEIER, W. (2011) Structural Complexity of Barium Uranyl Arsenates: Synthesis, Structure, and Topology of $Ba_4(UO_2)_2$ $(As_2O_7)_3$, $Ba_3(UO_2)_2(AsO_4)_2(As_2O_7)$, and $Ba_5Ca(UO_2)_8$ $(AsO_4)_4O_8$. *Crystal Growth & Design* **11**, 3295–3300.

ALLEN, P.G., BUCHER, J.J., CLARK, D.L., EDELSTEIN, N.M., EKBERG, S.A., GOHDES, J.W., HUDSON, E.A., KALTSOYANNIS, N., LUKENS, W.W., NEU, M.P., PALMER, P.D., REICH, T., SHUH, D.K., TAIT, C.D., & ZWICK, B.D. (1995) Multinuclear NMR, Raman, EXAFS, and X-Ray diffraction studies of uranyl carbonate complexes in near-neutral aqueous solution. X-Ray structure of $[C(NH_2)_3(UO_2)_3(CO_3)_6] \cdot 6.5H_2O$. *Inorganic Chemistry* **34**, 4797–4807.

ALLPRESS, J.G. & WADSLEY, A.D. (1964) Crystal structure of caesium uranyl oxychloride $Cs_x(UO_2)OCl_x$ (x approximately 0.9). *Acta Crystallographica* **17**, 41–46.

ALMOND, P.M. & ALBRECHT-SCHMITT, T.E. (2002a) Expanding the remarkable structural diversity of uranyl tellurites: Hydrothermal preparation and structures of KUO_2 $Te_2O_5(OH)$, $Tl_3\{(UO_2)_2Te_2O_5(OH)(Te_2O_6)\}\cdot 2H_2O$, β-$Tl_2(UO_2(TeO_3))_2$, and $Sr_3((UO_2)(TeO_3))_2(TeO_3)_2$. *Inorganic Chemistry* **41**, 5495–5501.

ALMOND, P.M. & ALBRECHT-SCHMITT, T.E. (2002b) Hydrothermal syntheses, structures, and properties of the new uranyl selenites $Ag_2(UO_2)_2(SeO_3)_2$, $M(UO_2)(HSeO_3)$ (SeO_3) (M = K, Rb, Cs, Tl), and $Pb(UO_2)(SeO_3)_2$. *Inorganic Chemistry* **41**, 1177–1183.

ALMOND, P.M. & ALBRECHT-SCHMITT, T.E. (2004) Hydrothermal synthesis and crystal chemistry of the new strontium uranyl selenites, $Sr((UO_2)_3(SeO_3)_2)O_2 \cdot 4H_2O$ and $Sr(UO_2)(SeO_3)_2$. *American Mineralogist* **89**, 976–980.

ALMOND, P.M., MCKEE, M.L., & ALBRECHT-SCHMITT, T.E. (2002a) Unusual uranyl tellurites containing Te_2O_6 (4^-) ions and three-dimensional networks. *Angewandte Chemie International Edition* **41**, 3426–3429.

ALMOND, P.M., PEPER, S.M., BAKKER, E., & ALBRECHT-SCHMITT, T.E. (2002b) Variable dimensionality and new uranium oxide topologies in the alkaline-earth metal uranyl selenites $AE(UO_2)(SeO3)_2$ (AE=Ca, Ba) and $Sr(UO_2)(SeO_3)_2 \cdot 2H_2O$. *Journal of Solid State Chemistry* **168**, 358–366.

ANDERSON, A., CHIEH, C., IRISH, D.E., & TONG, J.P.K. (1980) An X-ray crystallographic, Raman, and infrared spectral study of crystalline potassium uranyl carbonate, K_4UO_2 $(CO_3)_3$. *Canadian Journal of Chemistry - Revue Canadienne De Chimie* **58**, 1651–1658.

ANSON, C.E., ALJOWDER, O., JAYASOORIYA, U.A., & POWELL, A.K. (1996) Dirubidium tetrachlorodioxouranium(VI) - Water (1:2). *Acta Crystallographica Section C: Crystal Structure Communications* **52**, 279–281.

APPLEMAN, D.E. & EVANS, H.T. (1965) Crystal structures of synthetic anhydrous carnotite $K_2(UO_2)_2V_2O_8$ and its cesium analogue $CS_2(UO_2)_2V_2O_8$. *American Mineralogist* **50**, 825–842.

ATENCIO, D., NEUMANN, R., SILVA, A., & MASCARENHAS, Y.P. (1991) Phurcalite from Peru, Sau-Paulo Brazil, and redetermination of its crystal-structure. *Canadian Mineralogist* **29**, 95–105.

ATENCIO, D., CARVALHO, F.M.S., & MATIOLI, P.A. (2004) Coutinhoite, a new thorium uranyl silicate hydrate, from Urucum mine, Galileia, Minas Gerais, Brazil. *American Mineralogist* **89**, 721–724.

BACHET, B., BRASSY, C., & COUSSON, A. (1991) Structure of $Mg(UO_2)(AsO_4)_2 \cdot 4H_2O$. *Acta Crystallographica Section C: Crystal Structure Communications* **47**, 2013–2015.

BACKER, T. & MUDRING, A.V. (2010) Sodium trinitratouranylate(VI) $Na(UO_2)(NO_3)_3$. *Zeitschrift Für Anorganische Und Allgemeine Chemie* **636**, 1002–1005.

BACMANN, M. & BERTAUT, E.F. (1966) Parametres atomiques et structure magnetique de $MnUO_4$. *Journal De Physique* **27**, 726–734.

BAEVA, E.E., VIROVETS, A.V., PERESYPKINA, E.V., & SEREZHKINA, L.B. (2006) Crystal structure of $Na_2[(UO_2)_2(SeO_4)_3(H_2O)_2)] \cdot 6.5(H_2O)$. *Zhurnal Neorganicheskoi Khimii* **51(2)**, 253–262.

BASNAKOVA, G., FINLAY, J.A., & MACASKIE, L.E. (1998) Nickel accumulation by immobilized biofilm of *Citrobacter* sp. containing cell-bound polycrystalline hydrogen uranyl phosphate. *Biotechnology Letters* **20**, 949–952.

BEAN, A.C. & ALBRECHT-SCHMITT, T.E. (2001) Cation effects on the formation of the one-dimensional uranyl iodates $A_2(UO_2)_3(IO_3)_4O_2$ (A = K, Rb, Tl) and AE $(UO_2)_2(IO_3)_2$ $O_2(H_2O)$ (AE = Sr, Ba, Pb). *Journal of Solid State Chemistry* **161**, 416–423.

BEAN, A.C., CAMPANA, C.F., KWON, O., & ALBRECHT-SCHMITT, T.E. (2001a) A new oxoanion: $[IO_4]^{3-}$ containing I(V) with a stereochemically active lone-pair in the silver uranyl iodate tetraoxoiodate(V), $Ag_4(UO_2)_4(IO_3)_2)$ $(IO_4)_2O_2$. *Journal of the American Chemical Society* **123**, 8806–8810.

BEAN, A.C., PEPER, S.M., & ALBRECHT-SCHMITT, T.E. (2001b) Structural relationships, interconversion, and optical properties of the uranyl iodates, $UO_2(IO_3)_2$ and $UO_2(IO_3)_2(H_2O)$: A comparison of reactions under mild and supercritical conditions. *Chemistry of Materials* **13**, 1266–1272.

BEAN, A.C., RUF, M., & ALBRECHT-SCHMITT, T.E. (2001c) Excision of uranium oxide chains and ribbons in the novel one-dimensional uranyl iodates $K_2[(UO_2)_3(IO_3)_4)O_2]$ and $Ba[(UO_2)_2(IO_3)_2O_2(H_2O)]$. *Inorganic Chemistry* **40**, 3959–3963.

BEAN, A.C., XU, Y.W., DANIS, J.A., ALBRECHT-SCHMITT, T.E., SCOTT, B.L., & RUNDE, W. (2002) Aqueous reactions of U(VI) at high chloride concentrations: Syntheses and

structures of new uranyl chloride polymers. *Inorganic Chemistry* **41**, 6775–6779.

BEHM, H. (1985) Hexapotassium (cyclo-octahydroxotetracosaoxohexadecaborato)dioxouranate(VI) dodecahydrate, $K_6(UO_2)(B_{16}O_{24}(OH)_8)\cdot12H_2O$. *Acta Crystallographica Section C: Crystal Structure Communications* **41**, 642–645.

BELAI, N., FRISCH, M., ILTON, E.S., RAVEL, B., & CAHILL, C.L. (2008) Pentavalent Uranium Oxide via Reduction of UO_2^{2+} Under Hydrothermal Reaction Conditions. *Inorganic Chemistry* **47**, 10135–10140.

BELOMESTNYKH, V.I., SVESHNIKOVA, L.B., MIKHAILOV, Y.N., & KANISHCHEVA, A.S. (2011) Crystal and molecular structure of ammonium trinitratouranylate $(NH_4)(UO_2)(NO_3)_3$. *Russian Journal of Inorganic Chemistry* **56**, 1894–1898.

BENARD, P., LOUER, D., DACHEUX, N., BRANDEL, V., & GENET, M. (1994) $U(UO_2)(PO_4)_2$, a new mixed-valence uranium orthophosphate - *ab-initio* structure determination from powder diffraction data and optical and X-ray photoelectro spectra. *Chemistry of Materials* **6**, 1049–1058.

BERTAUT, E.F., DELAPALME, A., FORRAT, F., & PAUTHENET, R. (1962) Etude des uranates de cobalt et de manganese. *Journal de Physique et du Radium* **23**, 477–483.

BETKE, U. & WICKLEDER, M.S. (2012) Oleum and Sulfuric Acid as Reaction Media: The Actinide Examples $UO_2(S_2O_7)$-lt (low temperature), $UO_2(S_2O_7)$-ht (high temperature), $UO_2(HSO_4)(_2)$, $An(SO_4)(_2)$ (An = Th, U), $Th_4(HSO_4)_2(SO_4)_7$ and $Th(HSO_4)_2(SO_4)$. *European Journal of Inorganic Chemistry*, 306–317.

BLATON, N., VOCHTEN, R., PEETERS, O.M., & VAN SPRINGEL, K. (1999) The crystal structure of $Na_2(UO_2)_2(SiO_4)F_2$, a compound structurally related to soddyite, and formed during uranyl silicate synthesis in Teflon-lined bombs. *Neues Jahrbuch Für Mineralogie-Monatshefte*, 253–264.

BLATOV, V.A., SEREZHKINA, L.B., SEREZHKIN, V.N., & TRUNOV, V.K. (1989) Crystal-structure of $nH_4UO_2SeO_4F\cdot H_2O$. *Zhurnal Neorganicheskoi Khimii* **34**, 162–164.

BORENE, J. & CESBRON, F. (1970) Crystal structure of nickel uranyl vanadate tetrahydrate $Ni(UO_2)_2(VO_4)_2\cdot4H_2O$. *Bulletin De La Societe Francaise Mineralogie Et De Cristallographie* **93**, 426–432.

BORENE, J. & CESBRON, F. (1971) Crystal structure of curienite, $Pb(UO_2)_2(VO_4)_2\cdot5H_2O$. *Bulletin De La Societe Francaise Mineralogie Et De Cristallographie* **94**, 8–14.

BOUGON, R., FAWCETT, J., HOLLOWAY, J.H., & RUSSELL, D.R. (1979) Interaction between uranium tetrafluoride oxide and antimony pentafluoride; Fluorine-19 Nuclear Magnetic Resonance Investigations in Solution; Preparation and characterization of the adducts $UF_4O\cdot nSBF_5$ ($n = 1$–3) and crystal-structure of $UF_4O\cdot2SbF_5$. *Journal of the Chemical Society: Dalton Transactions*, 1881–1885.

BRANDENBURG, N.P. & LOOPSTRA, B.O. (1978) Beta-uranyl sulfate and uranyl selenate. *Acta Crystallographica Section B: Structural Science, Crystal Engineering, and Materials* **34**, 3734–3736.

BRANDSTATTER, F. (1981) Synthesis and crystal-structure determination, of $Pb_2[UO_2][TeO_3]_3$. *Zeitschrift Für Kristallographie* **155**, 193–200.

BRAY, T.H., BEITZ, J.V., BEAN, A.C., YU, Y.Q., & ALBRECHT-SCHMITT, T.E. (2006) Structural polarity induced by cooperative hydrogen bonding and lone-pair alignment in the molecular uranyl iodate $Na_2[UO_2(IO_3)_4(H_2O)]$. *Inorganic Chemistry* **45**, 8251–8257.

BRUGGER, J., BURNS, P.C., & MEISSER, N. (2003) Contribution to the mineralogy of acid drainage of uranium minerals: Marecottite and the zippeite-group. *American Mineralogist* **88**, 676–685.

BRUGGER, J., KRIVOVICHEV, S.V., BERLEPSCH, P., MEISSER, N., ANSERMET, S., & ARMBRUSTER, T. (2004) Spriggite, $Pb_3(UO_2)_6O_8(OH)_2(H_2O)_3$, a new mineral with β-U_3O_8-type sheets: Description and crystal structure. *American Mineralogist* **89**, 339–347.

BURCIAGA-VALENCIA, D.C., REYES-CORTES, M., REYES-ROJAS, A., RENTERIA-VILLALOBOS, M., ESPARZA-PONCE, H., FUENTES-COBAS, L., FUENTES-MONTERO, L., SILVA-SAENZ, M., HERRERA-PERAZA, E., MUNOZ, A., & MONTERO-CABRERA, M.E. (2010) Characterization of uranium minerals from Chihuahua using synchrotron radiation. *Revista Mexicana De Fisica* **56**, 75–81.

BURNS, P.C. (1997) A new uranyl oxide hydrate sheet in vandendriesscheite: Implications for mineral paragenesis and the corrosion of spent nuclear fuel. *American Mineralogist* **82**, 1176–1186.

BURNS, P.C. (1998a) The structure of boltwoodite and implications of solid solution toward sodium boltwoodite. *Canadian Mineralogist* **36**, 1069–1075.

BURNS, P.C. (1998b) The structure of compreignacite, $K_2[(UO_2)_3O_2(OH)_3]_2(H_2O)_7$. *Canadian Mineralogist* **36**, 1061–1067.

BURNS, P.C. (1998c) The structure of richetite, a rare lead uranyl oxide hydrate. *Canadian Mineralogist* **36**, 187–199.

BURNS, P.C. (1999a) The Crystal Chemistry of Uranium. *Reviews in Mineralogy* **38**, 23–90.

BURNS, P.C. (1999b) Cs boltwoodite obtained by ion exchange from single crystals: Implications for radionuclide release in a nuclear repository. *Journal of Nuclear Materials* **265**, 218–223.

BURNS, P.C. (1999c) A new complex sheet of uranyl polyhedra in the structure of wolsendorfite. *American Mineralogist* **84**, 1661–1673.

BURNS, P.C. (2000) A new uranyl phosphate chain in the structure of parsonsite. *American Mineralogist* **85**, 801–805.

BURNS, P.C. (2001a) A new uranyl silicate sheet in the structure of haiweeite and comparison to other uranyl silicates. *Canadian Mineralogist* **39**, 1153–1160.

BURNS, P.C. (2001b) A new uranyl sulfate chain in the structure of uranopilite. *Canadian Mineralogist* **39**, 1139–1146.

BURNS, P.C. (2005) U^{6+} minerals and inorganic compounds: Insights into an expanded structural hierarchy of crystal structures. *Canadian Mineralogist* **43**, 1839–1894.

BURNS, P.C. (2011) Nanoscale uranium-based cage clusters inspired by uranium mineralogy. *Mineralogical Magazine* **75**, 1–25.

BURNS, P.C. & DEELY, K.M. (2002) A topologically novel sheet of uranyl pentagonal bipyramids in the structure of Na[(UO$_2$)$_4$O$_2$(OH)$_5$](H$_2$O)$_2$. *Canadian Mineralogist* **40**, 1579–1586.

BURNS, P.C. & FINCH, R.J. (1999) Wyartite: Crystallographic evidence for the first pentavalent-uranium mineral. *American Mineralogist* **84**, 1456–1460.

BURNS, P.C. & HANCHAR, J.M. (1999) The structure of masuyite, Pb[(UO$_2$)$_3$O$_3$(OH)$_2$](H$_2$O)$_3$, and its relationship to protasite. *Canadian Mineralogist* **37**, 1483–1491.

BURNS, P.C. & HAYDEN, L.A. (2002) A uranyl sulfate cluster in Na$_{10}$[(UO$_2$)$_4$(SO$_4$)$_4$(SO$_4$)$_2$]·3H$_2$O. *Acta Crystallographica Section C: Crystal Structure Communications* **58**, I121–I123.

BURNS, P.C. & HILL, F.C. (2000a) Implications of the synthesis and structure of the Sr analogue of curite. *Canadian Mineralogist* **38**, 175–181.

BURNS, P.C. & HILL, F.C. (2000b) A new uranyl sheet in K$_5$[(UO$_2$)$_{10}$O$_8$(OH)$_9$](H$_2$O): New insight into sheet anion-topologies. *Canadian Mineralogist* **38**, 163–173.

BURNS, P.C. & HUGHES, K.A. (2003) Studtite, [UO$_2$)(O$_2$)(H$_2$O)$_2$](H$_2$O)$_2$: the first structure of a peroxide mineral. *American Mineralogist* **88**, 1165–1168.

BURNS, W.L. & IBERS, J.A. (2009) Syntheses and structures of three *f*-element selenite/hydroselenite compounds. *Journal of Solid State Chemistry* **182**, 1457–1461.

BURNS, P.C. & LI, Y.P. (2002) The structures of becquerelite and Sr-exchanged becquerelite. *American Mineralogist* **87**, 550–557.

BURNS, P.C., MILLER, M.L., & EWING, R.C. (1996) U^{6+} minerals and inorganic phases: A comparison and hierarchy of crystal structures. *Canadian Mineralogist* **34**, 845–880.

BURNS, P.C., EWING, R.C., & HAWTHORNE, F.C. (1997a) The crystal chemistry of hexavalent uranium: Polyhedron geometries, bond-valence parameters, and polymerization of polyhedra. *Canadian Mineralogist* **35**, 1551–1570.

BURNS, P.C., FINCH, R.J., HAWTHORNE, F.C., MILLER, M.L., & EWING, R.C. (1997b) The crystal structure of ianthinite, [U$_2^{4+}$(UO$_2$)$_4$O$_6$(OH)$_4$(H$_2$O)$_4$](H$_2$O)$_5$: a possible phase for Pu^{4+} incorporation during the oxidation of spent nuclear fuel. *Journal of Nuclear Materials* **249**, 199–206.

BURNS, P.C., OLSON, R.A., FINCH, R.J., HANCHAR, J.M., & THIBAULT, Y. (2000) KNa$_3$[(UO$_2$)$_2$(Si$_4$O$_{10}$)$_2$](H$_2$O)$_4$, a new compound formed during vapor hydration of an actinide-bearing borosilicate waste glass. *Journal of Nuclear Materials* **278**, 290–300.

BURNS, P.C., DEELY, K.M., & HAYDEN, L.A. (2003) The crystal chemistry of the zippeite group. *Canadian Mineralogist* **41**, 687–706.

BURNS, P.C., ALEXOPOULOS, C.M., HOTCHKISS, P.J., & LOCOCK, A.J. (2004) An unprecedented uranyl phosphate framework in the structure of [(UO$_2$)$_3$(PO$_4$)O(OH)(H$_2$O)$_2$](H$_2$O). *Inorganic Chemistry* **43**, 1816–1818.

BURNS, P.C., KUBATKO, K.A., SIGMON, G., FRYER, B.J., GAGNON, J.E., ANTONIO, M.R., & SODERHOLM, L. (2005) Actinyl peroxide nanospheres. *Angewandte Chemie International Edition* **44**, 2135–2139.

CAHILL, C.L. & BURNS, P.C. (2000) The structure of agrinierite: a Sr-containing uranyl oxide hydrate mineral. *American Mineralogist* **85**, 1294–1297.

CHAPELET-ARAB, B., NOWOGROCKI, G., ABRAHAM, F., & GRANDJEAN, S. (2005) U(IV)/Ln(III) unexpected mixed site in polymetallic oxalato complexes. Part I. Substitution of Ln(III) for U(IV) from the new oxalate (NH$_4$)$_2$U$_2$(C$_2$O$_4$)$_5$•0.7H$_2$O. *Journal of Solid State Chemistry* **178**, 3046–3054.

CHAPELET-ARAB, B., DUVIEUBOURG, L., NOWOGROCKI, G., ABRAHAM, F., & GRANDJEAN, S. (2006) U(IV)/Ln(III) mixed site in polymetallic oxalato complexes. Part III: Structure of NaYb(C$_2$O$_4$)$_2$(H$_2$O)•3H$_2$O and the derived quadratic series (NH$_4^+$)$_{(1−x)}$Ln$_{(1−x)}$U$_x$(C$_2$O$_4$)$_2$(H$_2$O)•(3+x)H$_2$O, Ln = Y, Pr-Sm, Gd, Tb. *Journal of Solid State Chemistry* **179**, 4029–4036.

CHATELAIN, L., WALSH, J.P.S., PECAUT, J., TUNA, F., & MAZZANTI, M. (2014) Self-Assembly of a 3*d*-5*f* Trinuclear Single-Molecule Magnet from a Pentavalent Uranyl Complex. *Angewandte Chemie International Edition* **53**, 13434–13438.

CHEN, C.S., CHIANG, R.K., KAO, H.M., & LII, K.H. (2005a) High-temperature, high-pressure hydrothermal synthesis, crystal structure, and solid-state NMR spectroscopy of Cs$_2$(UO$_2$)(Si$_2$O$_6$) and variable-temperature powder X-ray diffraction study of the hydrate phase Cs$_2$(UO$_2$)(Si$_2$O$_6$)•0.5H$_2$O. *Inorganic Chemistry* **44**, 3914–3918.

CHEN, C.S., KAO, H.M., & LII, K.H. (2005b) K$_5$(UO$_2$)$_2$[Si$_4$O$_{12}$(OH)]: A uranyl silicate containing chains of four silicate tetrahedra linked by SiO...HOSi hydrogen bonds. *Inorganic Chemistry* **44**, 935–940.

CHEN, C.L., NGUYEN, Q.B., CHEN, C.S., & LII, K.H. (2012) Mixed-Valence Uranium Germanate and Silicate: Cs$_x$(U^{V}O)(U$^{IV/V}$O)$_2$(Ge$_2$O$_7$)$_2$ (*x* = 3.18) and Cs$_4$(U^{V}O)(U$^{IV/V}$O)$_2$(Si$_2$O$_7$)$_2$. *Inorganic Chemistry* **51**, 7463–7465.

CHERNORUKOV, N.G., KNYAZEV, A.V., & DASHKINA, Z.S. (2010) Synthesis, Structures, and Physicochemical Properties of Sr$_2$A^{II}(UO$_6$) (A^{II} = Mg, Ca, Sr, Ba, Mn, Fe, Co,

Ni, Zn, and Cd) Compounds. *Russian Journal of Inorganic Chemistry* **55**, 904–912.

CHEVALIER, R. & GASPERIN, M. (1968) Crystalline structure of a double oxide UNb$_3$O$_{10}$. *Comptes rendus hebdomadaires des seances de l'academie des sciences Serie C* **267**, 481–483.

CHEVALIER, R. & GASPERIN, M. (1969) Monocrystal synthesis and crystal structure of UTiNb$_2$O$_{10}$ oxide. *Comptes rendus hebdomadaires des seances de l'academie des sciences Serie C* **268**, 1426–1429.

CHUKANOV, N.V., PUSHCHAROVSKY, D.Y., PASERO, M., MERLINO, S., BARINOVA, A.V., MOCKEL, S., PEKOV, I.V., ZADOV, A.E., & DUBINCHUK, V.T. (2004) Larisaite, Na(H$_3$O)[(UO$_2$)$_3$(SeO$_3$)$_2$]O$_2$•4H$_2$O, a new uranyl selenite mineral from Repete mine, San Juan County, Utah, USA. *European Journal of Mineralogy* **16**, 367–374.

CLARK, D.L., HOBART, D.E., & NEU, M.P. (1995) Actinide carbonate complexes and their importance in actinide environmental chemistry. *Chemical Reviews* **95**, 25–48.

COOPER, M.A. & HAWTHORNE, F.C. (1995) The crystal-structure of guilleminite, a hydrated Ba-U-Se sheet structure. *Canadian Mineralogist* **33**, 1103–1109.

COOPER, M.A. & HAWTHORNE, F.C. (2001) Structure topology and hydrogen bonding in marthozite, Cu^{2+}(UO$_2$)$_3$ (SeO$_3$)$_2$)O$_2$(H$_2$O)$_8$, a comparison with guilleminite, Ba(UO$_2$)$_3$(SeO$_3$)$_2$)O$_2$(H$_2$O)$_3$. *Canadian Mineralogist* **39**, 797–807.

CORDFUNKE, E.H.P., VANVLAANDEREN, P., ONINK, M., & IJDO, D.J.W. (1991) Sr$_3$U$_{11}$O$_{36}$ - crystal-structure and thermal-stability. *Journal of Solid State Chemistry* **94**, 12–18.

CRAWFORD, M.J., ELLERN, A., KARAGHIOSOFF, K., MAYER, P., NOTH, H., & SUTER, M. (2004) Synthesis and characterization of heavier dioxouranium(VI) dihalides. *Inorganic Chemistry* **43**, 7120–7126.

CREMERS, T.L., ELLER, P.G., LARSON, E.M., & ROSENZWEIG, A. (1986) Single-crystal structure of lead uranate(VI). *Acta Crystallographica Section C: Crystal Structure Communications* **42**, 1684–1685.

DALLEY, N.K., MUELLER, M.H., & SIMONSEN, S.H. (1971) Neutron diffraction study of uranyl nitrate dihydrate. *Inorganic Chemistry* **10**, 323–328.

DAO, N.Q., CHOUROU, S., RODIER, N., & BASTEIN, P. (1979) Chimie minerale. - Structure cristalline de monoaquo-octafluoro-triuranylate de potassium trihydrate K$_2$((UO$_2$)$_3$F$_8$(H$_2$O))(H$_2$O)$_3$. *Comptes Rendus Hebdomadaires des Seances de l'Academie des Sciences, Serie C: Sciences Chimiques* **289**, 405–408.

DE JONG, W.A., APRA, E., WINDUS, T.L., NICHOLS, J.A., HARRISON, R.J., GUTOWSKI, K.E., & DIXON, D.A. (2005) Complexation of the carbonate, nitrate, and acetate anions with the uranyl dication: Density functional studies with relativistic effective core potentials. *Journal of Physical Chemistry A* **109**, 11568–11577.

DEBETS, P.C. (1966) The Structure of β-UO3. *Acta Crystallographica* **21**, 589–593.

DEBETS, P.C. (1968) Structures of uranyl chloride and its hydrates. *Acta Crystallographica Section B: Structural Science, Crystal Engineering, and Materials* **B24**, 400–402.

DELIENS, M. & PIRET, P. (1983) Metastudtite, UO$_4$·2H$_2$O, a new mineral from Shinkolobwe, Shaba, Zaire. *American Mineralogist* **68**, 456–458.

DEMARTIN, F., DIELLA, V., DONZELLI, S., GRAMACCIOLI, C.M., & PILATI, T. (1991) The importance of accurate crystal-structure determination of uranium minerals. I. Phosphuranylite KCa(H$_3$O)$_3$(UO$_2$)$_7$(PO$_4$)$_4$O$_4$·8H$_2$O. *Acta Crystallographica Section B: Structural Science, Crystal Engineering, and Materials* **47**, 439–446.

DEMARTIN, F., GRAMACCIOLI, C.M., & PILATI, T. (1992) The importance of accurate crystal-structure determination of uranium minerals. II. Soddyite (UO$_2$)$_2$(SiO$_4$).2H$_2$O. *Acta Crystallographica Section C: Crystal Structure Communications* **48**, 1–4.

DICKENS, P.G., STUTTARD, G.P., BALL, R.G.J., POWELL, A.V., HULL, S., & PATAT, S. (1992) Powder neutron-diffraction study of the mixed uranium vanadium-oxides Cs$_2$(UO$_2$)$_2$ (V$_2$O$_8$) and UVO$_5$. *Journal of Materials Chemistry* **2**, 161–166.

DICKENS, P.G., STUTTARD, G.P., & PATAT, S. (1993) Structure of CuU$_3$O$_{10}$. *Journal of Materials Chemistry* **3**, 339–341.

DION, C., OBBADE, S., RAEKELBOOM, E., ABRAHAM, F., & SAADI, M. (2000) Synthesis, crystal structure, and comparison of two new uranyl vanadate layered compounds: M_6(UO$_2$)$_5$ (VO$_4$)$_2$)O$_5$ with M = Na, K. *Journal of Solid State Chemistry* **155**, 342–353.

DURIBREUX, I., DION, C., ABRAHAM, F., & SAADI, M. (1999) CsUV$_3$O$_{11}$, a new uranyl vanadate with a layered structure. *Journal of Solid State Chemistry* **146**, 258–265.

DURIBREUX, I., SAADI, M., OBBADE, S., DION, C., & ABRAHAM, F. (2003) Synthesis and crystal structure of two new uranyl oxychloro-vanadate layered compounds: M_7(UO$_2$)$_8$(VO$_4$)$_{(2)}$O$_8$Cl with M = Rb, Cs. *Journal of Solid State Chemistry* **172**, 351–363.

EBY, R.K. & HAWTHORNE, F.C. (1993) Structural relations in copper oxysalt minerals .1. structural hierarchy. *Acta Crystallographica Section B: Structural Science, Crystal Engineering, and Materials* **49**, 28–56.

EFFENBERGER, H. & MEREITER, K. (1988) Structure of a cubic sodium strontium magnesium tricarbonatodioxouranate(VI) hydrate. *Acta Crystallographica Section C: Crystal Structure Communications* **44**, 1172–1175.

FAWCETT, J., HOLLOWAY, J.H., LAYCOCK, D., & RUSSELL, D.R. (1982) Fluoride-ion donor properties of UF$_2$O$_2$ - preparation and characterization of the adducts UF$_2$O$_2$·nSbF$_5$(n = 2 OR 3) and crystal-structure of UF$_2$O$_2$ 3SbF$_5$. *Journal*

of the Chemical Society: Dalton Transactions, 1355–1360.

FEJFAROVÁ, K., PLÁŠIL, J., YANG, H., ČEJKA, J., DUŠEK, M., DOWNS, R.T., BARKLEY, M.C., & ŠKODA, R. (2012) Revision of the crystal structure and chemical formula of weeksite, $K_2(UO_2)_2(Si_5O_{13})•4H_2O$. *American Mineralogist* **97**, 750–754.

FINCH, R.J. & MURAKAMI, T. (1999) Systematics and paragenesis of uranium minerals. *In* Uranium: Mineralogy, Geochemistry and the Environment **38** (P.C. Burns & R.J. Finch, eds.). Mineral Society of America, Washington, D.C., United States (91–179).

FINCH, R.J., COOPER, M.A., HAWTHORNE, F.C., & EWING, R.C. (1996) The crystal structure of schoepite, $(UO_2)_8O_2(OH)_{12})(H_2O)_{12}$. *Canadian Mineralogist* **34**, 1071–1088.

FINCH, R.J., COOPER, M.A., HAWTHORNE, F.C., & EWING, R.C. (1999) Refinement of the crystal structure of rutherfordine. *Canadian Mineralogist* **37**, 929–938.

FINCH, R.J., BURNS, P.C., HAWTHORNE, F.C., & EWING, R.C. (2006) Refinement of the crystal structure of billietite, $Ba[(UO_2)_6O_4(OH)_6](H_2O)_8$. *Canadian Mineralogist* **44**, 1197–1205.

FISCHER, A. (2003) Competitive coordination of the uranyl ion by perchlorate and water - The crystal structures of $UO_2(ClO_4)_2·3H_2O$ and $UO_2(ClO_4)_2·5H_2O$ and a redetermination of $UO_2(ClO_4)_2·H_2O$. *Zeitschrift Für Anorganische Und Allgemeine Chemie* **629**, 1012–1016.

FITCH, A.N. & COLE, M. (1991) The structure of $KUO_2PO_4·3D_2O$ refined from neutron and synchrotron-radiation powder diffraction data. *Materials Research Bulletin* **26**, 407–414.

FITCH, A.N. & FENDER, B.E.F. (1983) The structure of deuterated ammonium uranyl phosphate trihydrate, $ND_4UO_2PO_4.3D_2O$ by powder neutron-diffraction. *Acta Crystallographica Section C: Crystal Structure Communications* **39**, 162–166.

FITCH, A.N., FENDER, B.E.F., & WRIGHT, A.F. (1982) The structure of deuterated lithium uranyl arsenate tetrahydrate $LiUO_2AsO_4•4D_2O$ by powder neutron-diffraction. *Acta Crystallographica Section B: Structural Science, Crystal Engineering, and Materials* **38**, 1108–1112.

FITCH, A.N., BERNARD, L., HOWE, A.T., WRIGHT, A.F., & FENDER, B.E.F. (1983) The room-temperature structure of $DUO_2ASO_5·4D_2O$ by powder neutron diffraction. *Acta Crystallographica, Section C: Crystal Structure Communications* **39**, 159–162.

FORBES, T.Z., GOSS, V., JAIN, M., & BURNS, P.C. (2007) Structure determination and infrared spectroscopy of $K(UO_2)(SO_4)(OH)(H_2O)$ and $K(UO_2)(SO_4)(OH)$. *Inorganic Chemistry* **46**, 7163–7168.

FORBES, T.Z., WALLACE, C., & BURNS, P.C. (2008) Neptunyl compounds: polyhedron geometries, bond-valence parameters, and structural hierarchy. *Canadian Mineralogist* **46**, 1623–1645.

FU, W.T., AU, Y.S., AKERBOOM, S., & IJDO, D.J. (2008) Crystal structures and chemistry of double perovskites $Ba_2M(II)M'(VI)O_6$ ($M =$ Ca, Sr, $M' =$ Te, W, U). *Journal of Solid State Chemistry* **181**, 2523–2529.

GALUSKIN, E.V., ARMBRUSTER, T., GALUSKINA, I.O., LAZIC, B., WINIARSKI, A., GAZEEV, V.M., DZIERZANOWSKI, P., ZADOV, A.E., PERTSEV, N.N., WRZALIK, R., GURBANOV, A.G., & JANECZEK, J. (2011) Vorlanite ($CaU^{6+})O_4$ - A new mineral from the Upper Chegem caldera, Kabardino-Balkaria, Northern Caucasus, Russia. *American Mineralogist* **96**, 188–196.

GALY, J. & MEUNIER, G. (1971) Cliffordite UTe_3O_8 - system UO_3–TeO_2 at 700 degrees C - crystal structure of UTe_3O_9. *Acta Crystallographica Section B: Structural Science, Crystal Engineering, and Materials* **B27**, 608–616.

GASPERIN, M. (1986) $(Cs_{0.75}K_{0.25})(Nb,Ti)U_2O_{11}$ - An alkaline niobotitanouranate with a new structure. *Acta Crystallographica Section C: Crystal Structure Communications* **42**, 136–138.

GASPERIN, M. (1987a) Structure of uranium borate UB_2O_6. *Acta Crystallographica Section C: Crystal Structure Communications* **43**, 2031–2033.

GASPERIN, M. (1987b) Synthesis and structure of 3 niobouranates of mono-valent ions - $TiNb_2U_2O_{11.5}$, $KNbUO_6$ and $RbNbUO_6$. *Journal of Solid State Chemistry* **67**, 219–224.

GASPERIN, M. (1987c) Synthesis and structure of calcium borouranate, $CaB_2U_2O_{10}$. *Acta Crystallographica Section C: Crystal Structure Communications* **43**, 1247–1250.

GASPERIN, M. (1987d) Synthesis and structure of $CsNbUO_6$. *Acta Crystallographica Section C: Crystal Structure Communications* **43**, 404–406.

GASPERIN, M. (1987e) Synthesis and structure of magnesium diborouranate, MgB_2UO_7. *Acta Crystallographica Section C: Crystal Structure Communications* **43**, 2264–2266.

GASPERIN, M. (1988) Synthesis and structure of sodium borowranate, $NaBUO_5$. *Acta Crystallographica Section C: Crystal Structure Communications* **44**, 415–416.

GASPERIN, M. (1989) Synthesis and structure of nickel tetraborouranate, $Ni_7B_4UO_{16}$. *Acta Crystallographica Section C: Crystal Structure Communications* **45**, 981–983.

GASPERIN, M. (1990) Synthesis and structure of $LiBUO_5$. *Acta Crystallographica Section C: Crystal Structure Communications* **46**, 372–374.

GASPERIN, P.M., REBIZANT, J., DANCAUSSE, J.P., MEYER, D., & COUSSON, A. (1991) Structure of $K_9BIU_6O_{24}$. *Acta Crystallographica Section C: Crystal Structure Communications* **47**, 2278–2279.

GEBERT, E., HOEKSTRA, H.R., REIS, A.H., & PETERSON, S.W. (1978) Crystal-structure of lithium uranate. *Journal of Inorganic & Nuclear Chemistry* **40**, 65–68.

GESING, T.M. & RUSCHER, C.H. (2000) Structure and properties of $UO_2(H_2AsO_4)_2 \bullet H_2O$. *Zeitschrift Für Anorganische Und Allgemeine Chemie* **626**, 1414–1420.

GINDEROW, D. (1988) Structure of uranophane alpha, $Ca(UO_2)_2(SIO_3OH)_2 \bullet 5H_2O$. *Acta Crystallographica Section C: Crystal Structure Communications* **44**, 421–424.

GINDEROW, D. & CESBRON, F. (1983a) Structure of demesmaekerite, $Pb_2Cu_5(SeO_3)_6(UO_2)_2(OH)_6 \bullet H_2O$. *Acta Crystallographica Section C: Crystal Structure Communications* **39**, 824–827.

GINDEROW, D. & CESBRON, F. (1983b) The structure of derriksite, $CU_4(UO_2)(SeO_3)_2(OH)_6$. *Acta Crystallographica Section C: Crystal Structure Communications* **39**, 1605–1607.

GINDEROW, D. & CESBRON, F. (1985) The structure of roubaultite, $Cu_2(UO_2)_3(CO_3)_2O_2(OH)_2 \bullet 4H_2O$. *Acta Crystallographica Section C: Crystal Structure Communications* **41**, 654–657.

GLATZ, R.E., LI, Y.P., HUGHES, K.A., CAHILL, C.L., & BURNS, P.C. (2002) Synthesis and structure of a new Ca uranyl oxide hydrate, $Ca(UO_2)_4O_3(OH)_4(H_2O)_2$, and its relationship to becquerelite. *Canadian Mineralogist* **40**, 217–224.

GOFF, G.S., BRODNAX, L.F., CISNEROS, M.R., PEPER, S.M., FIELD, S.E., SCOTT, B.L., & RUNDE, W.H. (2008) First identification and thermodynamic characterization of the ternary U(VI) species, $(UO_2)_2(O_2)(CO_3)_2)_4$, in UO_2–H_2O_2–K_2CO_3 solutions. *Inorganic Chemistry* **47**, 1984–1990.

GORBUNOVA, I.E., LINDE, S.A., LAVROV, A.V., & POBEDINA, A.B. (1980) Synthesis and structure of crystals of Na_{6-X} $(UO_2)_3(H_xPO_4)(PO_4)_3$(x = ~0.5). *Doklady Akademii Nauk SSSR* **251**, 385–389.

GRIGORIEV, M.S., IANOVSKII, A.I., FEDOSEEV, A.M., BUDANTSEVA, N.A., STRUCHKOV, I.T., KROT, N.N., & SPITSYN, V.I. (1988) Cation–cation interaction in neptunoyl sulfate dihydrate, $(NpO_2)_2SO_4 \bullet 2H_2O$. *Doklady Akademii Nauk SSSR* **300**, 618–622.

GRIGORIEV, M.S., YANOVSKII, A.I., STRUCHKOV, I.T., BESSONOV, A.A., AFONAS'EVA, T.V., & KROT, N.N. (1989) Cation–cation interactions in neptunium(V) formates. *Radiokhimiya* **31**, 37–44.

GUESDON, A., CHARDON, J., PROVOST, J., & RAVEAU, B. (2002) A copper uranyl monophosphate built up from CuO_2 infinity chains: $Cu_2UO_2(PO_4)_2$. *Journal of Solid State Chemistry* **165**, 89–93.

GURZHIY, V.V., BESSONOV, A.A., KRIVOVICHEV, S.V., TANANAEV, I.G., ARMBRUSTER, T., & MYASOEDOV, B.F. (2009) Crystal chemistry of selenates with mineral-like structures: VIII. Butlerite chains in the structures of $K(UO_2)(SeO_4)(OH)(H_2O)$. *Geology of Ore Deposits* **51**, 833–837.

GURZHIY, V.V., TYUMENTSEVA, O.S., KRIVOVICHEV, S.V., TANANAEV, I.G., & MYASOEDOV, B.F. (2011) Synthesis and structural studies of new potassium uranyl selenates

$K_2(H_5O_2)(H_3O)[UO_2)_2(SeO_4)_4(H_2O)_2](H_2O)_4$ and $K_3(H_3O)[(UO_2)_2(SeO_4)_4(H_2O)_2](H_2O)_5$. *Radiochemistry* **53**, 569–575.

GURZHIY, V.V., TYUMENTSEVA, O.S., KRIVOVICHEV, S.V., TANANAEV, I.G., & MYASOEDOV, B.F. (2012) Synthesis and structural studies of a new potassium uranyl selenate $K(H_5O_2)[(UO_2)_2(SeO_4)_3(H_2O)]$. *Radiochemistry* **54**, 43–47.

GURZHIY, V.V., TYUMENTSEVA, O.S., KORNYAKOV, I.V., KRIVOVICHEV, S.V., & TANANAEV, I.G. (2014) The role of potassium atoms in the formation of uranyl selenates: the crystal structure and synthesis of two novel compounds. *Journal of Geosciences* **59**, 123–133.

HAWTHORNE, F.C. (1983) Graphical enumeration of polyhedral clusters. *Acta Crystallographica Section A* **39**, 724–736.

HAWTHORNE, F.C. (2014) The structure hierarchy hypothesis. *Mineralogical Magazine* **78**, 957–1027.

HAWTHORNE, F.C. & HUMINICKI, D.M.C. (2002) The crystal chemistry of beryllium. *Beryllium: Mineralogy, Petrology, and Geochemistry* **50**, 333–403.

HAWTHORNE, F.C., BURNS, P.C., & GRICE, J.D. (1996) The crystal chemistry of boron. *Boron* **33**, 41–115.

HAWTHORNE, F.C., KRIVOVICHEV, S.V., & BURNS, P.C. (2000) The crystal chemistry of sulfate minerals. *Sulfate Minerals - Crystallography, Geochemistry, and Environmental Significance* **40**, 1–112.

HAWTHORNE, F.C., FINCH, R.J., & EWING, R.C. (2006) The crystal structure of dehydrated wyartite, $Ca(CO_3)U^{5+}$ $(U^{6+}O_2)_2O_4(OH)(H_2O)_3$. *Canadian Mineralogist* **44**, 1379–1385.

HAYDEN, L.A. & BURNS, P.C. (2002a) A novel uranyl sulfate cluster in the structure of $Na_6(UO_2)(SO_4)_4(H_2O)_2$. *Journal of Solid State Chemistry* **163**, 313–318.

HAYDEN, L.A. & BURNS, P.C. (2002b) The sharing of an edge between a uranyl pentagonal bipyramid and sulfate tetrahedron in the structure of $KNa_5(UO_2)(SO_4)_4(H_2O)$. *Canadian Mineralogist* **40**, 211–216.

HENCHE, G., FIEDLER, K., & GRUEHN, R. (1993) $Ln_3UO_6Cl_3$ (Ln = La, Pr, Nd) - the 1st oxochlorouranates of the rare-earths. *Zeitschrift Für Anorganische Und Allgemeine Chemie* **619**, 77–87.

HENNIG, C., SCHMEIDE, K., BRENDLER, V., MOLL, H., TSUSHIMA, S., & SCHEINOST, A.C. (2007) EXAFS investigation of U(VI), U(IV), and Th(IV) sulfato complexes in aqueous solution. *Inorganic Chemistry* **46**, 5882–5892.

HILL, F.C. & BURNS, P.C. (1999) The structure of a synthetic Cs uranyl oxide hydrate and its relationship to compreignacite. *Canadian Mineralogist* **37**, 1283–1288.

HOEKSTRA, H.R. & SIEGEL, S. (1971) Preparation and properties of Cr_2UO_6. *Journal of Inorganic & Nuclear Chemistry* **33**, 2867–2873.

Huang, J., Wang, X., & Jacobson, A.J. (2003) Hydrothermal synthesis and structures of the new open-framework uranyl silicates $Rb_4(UO_2)_2(Si_8O_{20})$ (USH-2Rb), $Rb_2(UO_2)(Si_2O_6)\cdot H_2O$ (USH-4Rb) and $A_2(UO_2)(Si_2O_6)\cdot 0.5H_2O$ (USH-5A; A = Rb, Cs). *Journal of Materials Chemistry* **13**, 191–196.

Hughes, K.A. & Burns, P.C. (2003a) A new uranyl carbonate sheet in the crystal structure of fontanite, $Ca[(UO_2)_3(CO_3)_2O_2](H_2O)_6$. *American Mineralogist* **88**, 962–966.

Hughes, K.A. & Burns, P.C. (2003b) Uranyl dinitrate trihydrate, $UO_2(NO_3)_2(H_2O)_3$. *Acta Crystallographica Section C: Crystal Structure Communications* **59**, I7–I8.

Hughes, K.A., Burns, P.C., & Kolitsch, U. (2003) The crystal structure and crystal chemistry of uranosphaerite, $Bi(UO_2)O_2OH$. *Canadian Mineralogist* **41**, 677–685.

Huminicki, D.M.C. & Hawthorne, F.C. (2002) The crystal chemistry of the phosphate minerals. *In* Chapter 5 - Phosphates: Geochemical, Geobiological, and Materials Importance (M.J. Kohn, J. Rakovan, & J.M. Hughes, eds.). *Reviews in Mineralogy & Geochemistry* **48**, 123–253.

Huys, D., Van Deun, R., Pattison, P., Van Meervelt, L., & Van Hecke, K. (2010) Redetermination of di-mu-hydroxido-bis diaquachloridodioxidouranium(VI) from single-crystal synchrotron data. *Acta Crystallographica Section E: Structure Reports Online* **66**, I11.

Ijdo, D.J.W. (1993a) $Pb_3U_{11}O_{36}$, A Rietveld refinement of neutron powder diffraction data. *Acta Crystallographica Section C: Crystal Structure Communications* **49**, 654–656.

Ijdo, D.J.W. (1993b) Redetermination of tristrontium uranate(VI) - a Rietveld refinement of neutron powder diffraction data. *Acta Crystallographica Section C: Crystal Structure Communications* **49**, 650–652.

Ivanov, V.A., Mikhailov, Y.N., Kuznetsov, N.T., & Davidovich, R.L. (1981) The crystal structure of $Ni_3[(UO_2)_2F_7]_2(H_2O)_{18}$. *Zhurnal Strukturnoi Khimii* **22**, 188–1491.

Ivanov, S.B., Mikhailov, Y.N., & Davidovich, R.L. (1982) The crystal structure of nickel tetrafluorodooxouranate heptahydrate. *Koordinatsionnaya Khimiya* **8**.

Jackson, J.M. & Burns, P.C. (2001) A re-evaluation of the structure of weeksite, a uranyl silicate framework mineral. *Canadian Mineralogist* **39**, 187–195.

Jones, M.B. & Gaunt, A.J. (2013) Recent Developments in Synthesis and Structural Chemistry of Nonaqueous Actinide Complexes. *Chemical Reviews* **113**, 1137–1198.

Jones, G.M., Arnold, P.L., & Love, J.B. (2013) Oxo-Group-14-Element Bond Formation in Binuclear Uranium(V) Pacman Complexes. *Chemistry - A European Journal* **19**, 10287–10294.

Jouffret, L.J., Krivovichev, S.V., & Burns, P.C. (2011) Polymorphism in Alkali Metal Uranyl Nitrates: Synthesis and Crystal Structure of γ-$K(UO_2)(NO_3)_3$. *Zeitschrift Für Anorganische Und Allgemeine Chemie* **637**, 1475–1480.

Jove, J., Cousson, A., & Gasperin, M. (1988) Synthesis and crystal-structure of K_2U_2O7 and Mössbauer (NP-237) studies of $K_2NP_2O_7$ and $CaNPO_4$. *Journal of the Less-Common Metals* **139**, 345–350.

Juan, W., Xin, L., Ziying, L., Yuyan, Z., & Shiyuan, C. (2010) Synthesis and crystal structure of a uranyl containing complex $(U(CO_3)_3(H_2O)_2)\bullet 2(H_2O)$. *Wuji Huaxue Xuebao* **26**, 351–354.

Kampf, A.R., Mills, S.J., Housley, R.M., Marty, J., & Thorne, B. (2010) Lead-tellurium oxysalts from Otto Mountain near Baker, California: IV. Markcooperite, $Pb(UO_2)Te^{6+}O_6$, the first natural uranyl tellurate. *American Mineralogist* **95**, 1554–1559.

Kampf, A.R., Plášil, J., Kasatkin, A.V., & Marty, J. (2014) Belakovskiite, $Na_7(UO_2)(SO_4)_4(SO_3OH)(H_2O)_3$, a new uranyl sulfate mineral from the Blue Lizard mine, San Juan County, Utah, USA. *Mineralogical Magazine* **78**, 639–649.

Kapshukov, I.I., Volkov, Y.F., Moskvitse, E.P., Lebedev, I.A., & Yakovlev, G.N. (1971) Crystal Structure of Uranyl Tetranitrate. *Zhurnal Strukturnoi Khimii* **12**, 94–98.

Karimova, O.V. & Burns, P.C. (2007) Structural units in three uranyl perrhenates. *Inorganic Chemistry* **46**, 10108–10113.

Khosrawan-Sazedj, F. (1982a) The crystal-structure of meta-uranocircite-II, $Ba(UO_2)_2(PO_4)_2\bullet 6H_2O$. *Tschermaks Mineralogische Und Petrographische Mitteilungen* **29**, 193–204.

Khosrawan-Sazedj, F. (1982b) On the space group of threadgoldite. *Tschermaks Mineralogische Und Petrographische Mitteilungen* **30**, 111–115.

Khrustalev, V.N., Andreev, G.B., Antipin, M.Y., Fedoseev, A.M., Budantseva, N.A., & Shirokova, I.B. (2000) Synthesis and crystal strucutre of rubidium dimolybdouranylate monohydrate $Rb_2UO_2(MoO_4)\cdot H_2O$. *Zhurnal Neorganicheskoi Khimii* **45**, 1845–1847.

Knyazev, A.V. & Kuznetsova, N.Y. (2009) Crystal structure of compounds $CsA^{5+}A'^{6+}O_6(A^{5+}= Sb, Ta; A'^{6+} = W, U)$. *Radiochemistry* **51**, 1–4.

Knyazev, A.V., Chernorukov, N.G., Dashkina, Z.S., Bulanov, E.N., & Ladenkov, I.V. (2011) Synthesis, structures, physicochemical properties, and crystal-chemical systematics of $M_2^{II}A^{II}UO_6$ (M^{II} = Pb, Ba, Sr; A^{II} = Mg, Ca, Sr, Ba, Mn, Fe, Co, Ni, Cu, Zn, Cd, Pb) compounds. *Russian Journal of Inorganic Chemistry* **56**, 888–898.

Kolitsch, U. & Giester, G. (2001) Revision of the crystal structure of ulrichite, $CaCu^{2+}(UO_2)(PO_4)_2\bullet 4H_2O$. *Mineralogical Magazine* **65**, 717–724.

Koskenlinna, M. & Valkonen, J. (1996) Ammonium uranyl hydrogenselenite selenite. *Acta Crystallographica Section C: Crystal Structure Communications* **52**, 1857–1859.

KOSKENLINNA, M., MUTIKAINEN, I., LESKELA, T., & LESKELA, M. (1997) Low-temperature crystal structures and thermal decomposition of uranyl hydrogen selenite monohydrate, $(UO_2)(HSeO_3)_2 \cdot H_2O$ and diammonium uranyl selenite hemihydrate, $(NH_4)_2(UO_2)(SeO_3)_2 \cdot 0.5H_2O$. *Acta Chemica Scandinavica* **51**, 264–269.

KOSTER, A.S., RENAUD, J.P.P., & RIECK, G.D. (1975) Crystal-structures at 20 and 1000 degrees C of bismuth uranate, Bi_2UO_6. *Acta Crystallographica Section B: Structural Science, Crystal Engineering, and Materials* **31**, 127–131.

KOVBA, L.M. (1971) Crystal structures of potassium and sodium monouranates. *Soviet Radiochemistry* (English Translation) **13**.

KOVBA, L.M. (1972) Crystal structure of $K_2U_7O_{22}$. *Zhurnal Strukturnoi Khimii* **13**, 256–258.

KOVBA, L.M., IPPOLITOVA, E.A., SIMANOV, Y.P., & SPITSYN, V.I. (1958) An X-ray study of alkali metal uranates. *Doklady Akademii Nauk SSSR* **120**, 1042–1044.

KRAUSE, W., EFFENBERGER, H., & BRANDSTATTER, F. (1995) Orthowalpurgite, $(UO_2)Bi_4O_4(AsO_4)_2 \cdot 2H_2O$, a new mineral from the Black Forest, Germany. *European Journal of Mineralogy* **7**, 1313–1324.

KRIVOVICHEV, S.V. (2004) Combinatorial topology of salts of inorganic oxoacids: zero-, one- and two-dimensional units with corner-sharing between coordination polyhedra. *Crystallography Reviews* **10**, 185–232.

KRIVOVICHEV, S.V. (2008a) Crystal chemistry of selenates with mineral-like structures: V. Crystal structures of $(H_3O)_2[(UO_2)(SeO_4)_2(H_2O)](H_2O)_2$ and $(H_3O)_2[(UO_2)(SeO_4)_2(H_2O)](H_2O)$, new compounds with rhomboclase and goldichite topology. *Geology of Ore Deposits* **50**, 789–794.

KRIVOVICHEV, S.V. (2008b) Crystal chemistry of selenates with mineral-like structures. VI. Hydrogen bonds in the crystal structure of $(H_5O_2)(H_3O)(H_2O)(UO_2)(SeO_4)_2$. *Geology of Ore Deposits* **50**, 795–800.

KRIVOVICHEV, S.V. (2008c) Crystal Struture of $KNa_3[(UO_2)_5O_6(SO_4)]$. *Radiochemistry* **50**, 450–454.

KRIVOVICHEV, S.V. (2009) Crystal Chemistry of Selenates with Mineral-Like Structures: VII. The Structure of $(H_3O)(UO_2)(SeO_4)(SeO_2OH)$ and Some Structural Features of Selenite-Selenates. *Geology of Ore Deposits* **51**, 663–667.

KRIVOVICHEV, S.V. (2014) $K_2N_8(UO_2)_8MO_4O_{24}[(S,Mo)O_4]$, the first uranium molybdosulfate: synthesis, crystal structure, and comparison to related compounds. *Journal of Geosciences* **59**, 115–121.

KRIVOVICHEV, S.V. & BURNS, P.C. (2000) Crystal chemistry of uranyl molybdates. I. The structure and formula of umohoite. *Canadian Mineralogist* **38**, 717–726.

KRIVOVICHEV, S.V. & BURNS, P.C. (2000) The crystal chemistry of uranyl molybdates. II. The crystal structure of iriginite. *Canadian Mineralogist* **38**, 847–851.

KRIVOVICHEV, S.V. & BURNS, P.C. (2001a) Crystal chemistry of uranyl molybdates. III. New structural themes in $Na_6(UO_2)_2O(MoO_4)_4$, $Na_6(UO_2)_2(MoO_4)_4$ and $K_6(UO_2)_2O(MoO_4)_4$. *Canadian Mineralogist* **39**, 197–206.

KRIVOVICHEV, S.V. & BURNS, P.C. (2001b) Crystal chemistry of uranyl molybdates. IV. The structures of $M_2[(UO_2)_6(MoO_4)_7(H_2O)_2]$ (M = Cs, NH_4). *Canadian Mineralogist* **39**, 207–214.

KRIVOVICHEV, S.V. & BURNS, P.C. (2002a) Crystal chemistry of rubidium uranyl molybdates: Crystal structures of $Rb_6[(UO_2)(MoO_4)_4$, $Rb_6[(UO_2)_2O(MoO_4)_4]$, $Rb_2[(UO_2)(MoO_4)_2]$, $Rb_2[(UO_2)_2(MoO_4)_3]$ and $Rb_2[(UO_2)_6(MoO_4)_7(H_2O)_2]$. *Journal of Solid State Chemistry* **168**, 245–258.

KRIVOVICHEV, S.V. & BURNS, P.C. (2002b) Crystal chemistry of uranyl molybdates. VI. New uranyl molybdate units in the structures of $Cs_4[(UO_2)_3O(MoO_4)_2(MoO_5)]$ and $Cs_6[(UO_2)(MoO_4)_4]$. *Canadian Mineralogist* **40**, 201–209.

KRIVOVICHEV, S.V. & BURNS, P.C. (2002c) Crystal chemistry of uranyl molybdates. VII. An iriginite-type sheet of polyhedra in the structure of $(UO_2)Mo_2O_7(H_2O)_2$. *Canadian Mineralogist* **40**, 1571–1577.

KRIVOVICHEV, S.V. & BURNS, P.C. (2002d) Synthesis and structure of $Ag_6[(UO_2)_3O(MoO_4)_5]$: A novel sheet of triuranyl clusters and MoO_4 tetrahedra. *Inorganic Chemistry* **41**, 4108–4110.

KRIVOVICHEV, S.V. & BURNS, P.C. (2003) Combinatorial topology of uranyl molybdate sheets: syntheses and crystal structures of $(C_6H_{14}N_2)_3[(UO_2)_5(MoO_4)_8](H_2O)_4$ and $(C_2H_{10}N_2)[(UO_2)(MoO_4)_2]$. *Journal of Solid State Chemistry* **170(1)**, 106–117.

KRIVOVICHEV, S.V. & BURNS, P.C. (2003b) Crystal chemistry of uranyl molybdates. IX. A novel uranyl molybdate sheet in the structure of $Tl_2(UO_2)_2O(MoO_5)$. *Canadian Mineralogist* **41**, 1225–1231.

KRIVOVICHEV, S.V. & BURNS, P.C. (2003c) Crystal chemistry of uranyl molybdates. VIII. Crystal structures of $Na_3Tl_3[(UO_2)(MoO_4)_4]$, $Na_{13-x}Tl_{3+x}[(UO_2)(MoO_4)_3]_4(H_2O)_{6+x}$ (x = 0.1), $Na_3Tl_5[(UO_2)(MoO_4)_3]_2(H_2O)_3$ and $Na_2[(UO_2)(MoO_4)_2](H_2O)_4$. *Canadian Mineralogist* **41**, 707–719.

KRIVOVICHEV, S.V. & BURNS, P.C. (2003d) Crystal chemistry of uranyl molybdates. X. The crystal structure of $Ag_{10}[(UO_2)_8O_8(Mo_5O_{20})]$. *Canadian Mineralogist* **41**, 1455–1462.

KRIVOVICHEV, S.V. & BURNS, P.C. (2003e) The first sodium uranyl chromate, $Na_4(UO_2)(CrO_4)_3$: Synthesis and crystal structure determination. *Zeitschrift Für Anorganische Und Allgemeine Chemie* **629**, 1965–1968.

KRIVOVICHEV, S.V. & BURNS, P.C. (2003f) Geometrical isomerism in uranyl chromates I. Crystal structures of $(UO_2)(CrO_4)(H_2O)_2$, $[(UO_2)(CrO_4)(H_2O)_2](H_2O)$ and $[(UO_2)(CrO_4)(H_2O)_2]_4(H_2O)_9$. *Zeitschrift Für Kristallographie* **218**, 568–574.

KRIVOVICHEV, S.V. & BURNS, P.C. (2003g) Structural topology of potassium uranyl chromates: crystal structures of $K_8[(UO_2)(CrO_4)_4](NO_3)_2$, $K_5[(UO_2)(CrO_4)_3](NO_3)(H_2O)_3$, $K_4[(UO_2)_3(CrO_4)_5](H_2O)_8$ and $K_2(UO_2)_2(CrO_4)_3(H_2O)_2](H_2O)_4$. *Zeitschrift Für Kristallographie* **218**, 725–732.

KRIVOVICHEV, S.V. & BURNS, P.C. (2003h) Synthesis and crystal structure of $Li_2[(UO_2)(MoO_4)_2]$, a uranyl molybdate with chains of corner-sharing uranyl square bipyramids and MoO_4 tetrahedra. *Solid State Sciences* **5**, 481–485.

KRIVOVICHEV, S.V. & BURNS, P.C. (2003i) A novel rigid uranyl tungstate sheet in the structures of $Na_2[(UO)_2W_2O_8]$ and α- and β-$Ag_2[(UO_2)W_2O_8]$. *Solid State Sciences* **5**, 373–381.

KRIVOVICHEV, S.V. & BURNS, P.C. (2004a) Crystal structure of $K[UO_2(NO_3)_3]$ and some features of compounds $M[UO_2(NO_3)_3]$ (M = K, Rb and Cs). *Radiochemistry* **46**, 16–19.

KRIVOVICHEV, S.V. & BURNS, P.C. (2004b) Synthesis and crystal structure of $Cs_4[UO_2(CO_3)_3]$. *Radiochemistry* **46**, 12–15.

KRIVOVICHEV, S.V. & BURNS, P.C. (2004c) Synthesis and Crystal Structure of $Cu_2\{(UO_2)_3[(S,Cr)O_4]_5\}(H_2O)_{17}$. *Radiochemistry* **46**, 441–445.

KRIVOVICHEV, S.V. & BURNS, P.C. (2005) Crystal chemistry of uranyl molybdates. XI. Crystal structures of $Cs_2[(UO_2)(MoO_4)_2]$ and $Cs_2[(UO_2)(MoO_4)_2](H_2O)$. *Canadian Mineralogist* **43**, 713–720.

KRIVOVICHEV, S.V. & BURNS, P.C. (2014) The modular structure of the novel uranyl sulfate sheet in [Co$(H_2O)_6]_3[(UO_2)_5(SO_4)_8(H_2O)](H_2O)_5$. *Journal of Geosciences* **59**, 135–143.

KRIVOVICHEV, S.V. & KAHLENBERG, V. (2004) Synthesis and crystal structures of α- and β-Mg_2 $(UO_2)_3(SeO_4)_5](H_2O)_{16}$. *Zeitschrift Für Anorganische Und Allgemeine Chemie* **630**, 2736–2742.

KRIVOVICHEV, S.V. & KAHLENBERG, V. (2005a) Crystal structure of $(H_3O)_6[(UO_2)_5(SeO_4)_8(H_2O)](H_2O)_5$. *Radiochemistry* **47**, 456–459.

KRIVOVICHEV, S.V. & KAHLENBERG, V. (2005b) Crystal Structure of $(H_3O)_2[(UO_2)_2(SeO_4)_3(H_2O)_2](H_2O)_{3.5}$. *Radiochemistry* **47**, 452–455.

KRIVOVICHEV, S.V. & KAHLENBERG, V. (2005c) Preparation and crystal structures of $M(UO_2)_2(SeO_4)_2(H_2O)](H_2O)_4$ (M = Mg, Zn). *Zeitschrift Für Naturforschung Section B - A Journal of Chemical Sciences* **60**, 538–542.

KRIVOVICHEV, S.V. & KAHLENBERG, V. (2005d) Structural diversity of sheets in rubidium uranyl oxoselenates: Synthesis and crystal structures of $Rb_2[(UO_2)(SeO_4)_2(H_2O)](H_2O)$, $Rb_2(UO_2)_2(SeO_4)_3(H_2O)_2](H_2O)_4$, and $Rb_4[(UO_2)_3(SeO_4)_5(H_2O)]$. *Zeitschrift Für Anorganische Und Allgemeine Chemie* **631**, 739–744.

KRIVOVICHEV, S.V. & KAHLENBERG, V. (2005e) Synthesis and crystal structure of $Zn_2[(UO_2)_3(SeO_4)_5](H_2O)_{17}$. *Journal of Alloys and Compounds* **389**, 55–60.

KRIVOVICHEV, S.V. & KAHLENBERG, V. (2005f) Synthesis and crystal structures of $M_2[(UO_2)_3(SeO_4)_5](H_2O)_{16}$ (M = Co, Zn). *Journal of Alloys and Compounds* **395**, 41–47.

KRIVOVICHEV, S.V., CAHILL, C.L., & BURNS, P.C. (2002a) Syntheses and crystal structures of two topologically related modifications of $Cs_2[(UO_2)_2(MoO_4)_3]$. *Inorganic Chemistry* **41**, 34–39.

KRIVOVICHEV, S.V., FINCH, R.J., & BURNS, P.C. (2002b) Crystal chemistry of uranyl molybdates. V. Topologically distinct uranyl dimolybdate sheets in the structures of $Na_2[(UO_2)(MoO_4)_2]$ and $K_2(UO_2)_3O(Mo_4)_2](H_2O)$. *Canadian Mineralogist* **40**, 193–200.

KRIVOVICHEV, S.V., CAHILL, C.L., & BURNS, P.C. (2003) A novel open framework uranyl molybdate: Synthesis and structure of $(NH_4)_4[(UO_2)_5(MoO_4)_7](H_2O)_5$. *Inorganic Chemistry* **42**, 2459–2464.

KRIVOVICHEV, S.V., KAHLENBERG, V., KAINDL, R., MERSDORF, E., TANANAEV, I.G., & MYASOEDOV, B.F. (2005g) Nanoscale tubules in uranyl selenates. *Angewandte Chemie International Edition* **44**, 1134–1136.

KRIVOVICHEV, S.V., KAHLENBERG, V., TANANAEV, I.G., KAINDL, K., MERSDORF, E., & MYASOEDOV, B.F. (2005h) Highly porous uranyl selenite nanotubules. *Journal of the American Chemical Society* **127**, 1072–1073.

KRIVOVICHEV, S.V., LOCOCK, A.J., & BURNS, P.C. (2005i) Lone electron pair stereoactivity, cation arrangements and distortion of heteropolyhedral sheets in the structures of $Tl_2[(UO_2)(AO_4)_2]$ (A = Cr, Mo). *Zeitschrift für Kristallographie* **220**, 10–18.

KROT, N.N. & GRIGORIEV, M.S. (2004) Cation–cation interaction in crystalline actinide compounds. *Uspekhi Khimii* **73**, 94–106.

KROTO, H.W., HEATH, J.R., OBRIEN, S.C., CURL, R.F., & SMALLEY, R.E. (1985) C_{60} - buckminsterfullerene. *Nature* **318**, 162–163.

KUBATKO, K.-A. & BURNS, P.C. (2004a) The crystal structure of a novel uranyl tricarbonate, $K_2Ca_3[(UO_2)(CO_3)_3]_2(H_2O)_6$. *Canadian Mineralogist* **42**, 997–1003.

KUBATKO, K.-A.H. & BURNS, P.C. (2004b) The Rb analogue of grimselite, Rb_6Na_2 $[(UO_2)(CO_3)_3]_2(H_2O)$. *Acta Crystallographica Section C: Crystal Structure Communications* **60**, I25–I26.

KUBATKO, K.-A. & BURNS, P.C. (2006a) Expanding the crystal chemistry of actinyl peroxides: Open sheets of uranyl polyhedra in $Na_5[(UO_2)_3(O_2)_4(OH)_3](H_2O)_{13}$. *Inorganic Chemistry* **45**, 6096–6098.

KUBATKO, K.-A. & BURNS, P.C. (2006b) Cation–cation interactions in $Sr_5(UO_2)_{20}(UO_6)_2O_{16}(OH)_6(H_2O)_6$ and $Cs(UO_2)_9U_3O_{16}(OH)_5$. *Inorganic Chemistry* **45**, 10277–10281.

KUBATKO, K.-A. & BURNS, P.C. (2006c) A novel arrangement of silicate tetrahedra in the uranyl silicate sheet of

oursinite, $(Co_{0.8}Mg_{0.2})(UO_2)(SiO_3OH)_2(H_2O)_6$. *American Mineralogist* **91**, 333–336.

KUBATKO, K.-A.H., HELEAN, K.B., NAVROTSKY, A., & BURNS, P.C. (2003) Stability of peroxide-containing uranyl minerals. *Science* **302**, 1191–1193.

KUBATKO, K.-A., FORBES, T.Z., KLINGENSMITH, A.L., & BURNS, P.C. (2007) Expanding the crystal chemistry of uranyl peroxides: Synthesis and structures of di- and triperoxodioxouranium(VI) complexes. *Inorganic Chemistry* **46**, 3657–3662.

LEE, M.R. & JAULMES, S. (1987) A new series of isotypical oxides with a structure reminiscent of α-U_3O_8: $M^{II}UMo_4O_{16}$. *Journal of Solid State Chemistry* **67**, 364–368.

LEE, C.S., WANG, S.L., CHEN, Y.H., & LII, K.H. (2009) Flux Synthesis of Salt-Inclusion Uranyl Silicates: $K_3Cs_4F(UO_2)_3(Si_2O_7)_2$ and $NaRb_6F(UO_2)_3(Si_2O_7)_2$. *Inorganic Chemistry* **48**, 8357–8361.

LEE, C.S., LIN, C.H., WANG, S.L., & LII, K.H. (2010) $[Na_7U^{IV}O_2(U^VO)_2(U^{V/VI}O_2)_2Si_4O_{16}]$: A Mixed-Valence Uranium Silicate. *Angewandte Chemie International Edition* **49**, 4254–4256.

LEGROS, J.P. & JEANNIN, Y. (1975) Coordination of uranium by germanate ion. 2. structure of uranium germanate dihydrate of formula $(UO_2)_2GeO_4(H_2O)_2$. *Acta Crystallographica Section B: Structural Science, Crystal Engineering, and Materials* **31**, 1140–1143.

LI, Y.P. & BURNS, P.C. (2000a) Investigations of crystalchemical variability in lead uranyl oxide hydrates. I. Curite. *Canadian Mineralogist* **38**, 727–735.

LI, Y.P. & BURNS, P.C. (2000b) Investigations of crystalchemical variability in lead uranyl oxide hydrates. II. Fourmarierite. *Canadian Mineralogist* **38**, 737–749.

LI, Y.P. & BURNS, P.C. (2000c) Synthesis and crystal structure of a new Pb uranyl oxide hydrate with a framework structure that contains channels. *Canadian Mineralogist* **38**, 1433–1441.

LI, Y.P. & BURNS, P.C. (2001a) The crystal structure of synthetic grimselite, $K_3Na[(UO_2)(CO_3)_3](H_2O)$. *Canadian Mineralogist* **39**, 1147–1151.

LI, Y.P. & BURNS, P.C. (2001b) The structures of two sodium uranyl compounds relevant to nuclear waste disposal. *Journal of Nuclear Materials* **299**, 219–226.

LI, Y.P. & BURNS, P.C. (2002) New structural arrangements in three Ca uranyl carbonate compounds with multiple anionic species. *Journal of Solid State Chemistry* **166**, 219–228.

LI, Y.P., BURNS, P.C., & GAULT, R.A. (2000) A new rareearth-element uranyl carbonate sheet in the structure of bijvoetite-(Y). *Canadian Mineralogist* **38**, 153–162.

LI, Y.P., CAHILL, C.L., & BURNS, P.C. (2001a) Synthesis, structural characterization, and topological rearrangement of a novel open framework U-O material: $(NH_4)_3$ $(H_2O)_2\{(UO_2)_{10}O_{10}(OH)(UO_4)(H_2O)_2\}$. *Chemistry of Materials* **13**, 4026–4031.

LI, Y.P., KRIVOVICHEV, S.V., & BURNS, P.C. (2001b) The crystal structure of $Na_4[(UO_2)(CO_3)_3]$ and its relationship to schrockingerite. *Mineralogical Magazine* **65**, 297–304.

LIN, C.-H. & LII, K.-H. (2008) $A_3[(U_2O_4)(Ge_2O_7)]$ (A = Rb, Cs): Mixed-Valence Uranium(V,VI) Germanates. *Angewandte Chemie International Edition* **47**, 8711–8713.

LIN, C.-H., CHIANG, R.-K., & LII, K.-H. (2009) Synthesis of thermally stable extra-large pore crystalline materials: a uranyl germanate with 12-ring channels. *Journal of the American Chemical Society* **131**, 2068–2069.

LINDE, S.A., GORBUNOVA, I.E., LAVROV, A.V., & KUZNETSOV, V.G. (1978) Synthesis and structure of crystals of $CsUO_2(PO_3)_3$. *Doklady Akademii Nauk SSSR* **241**, 1083–1085.

LINDE, S.A., GORBUNOVA, I.E., & LAVROV, A.V. (1980) Formation of $K_4UO_2(PO_4)_2$ crystals. *Zhurnal Neorganicheskoi Khimii* **25**, 1992–1994.

LINDE, S.A., GORBUNOVA, I.E., LAVROV, A.V., & POBEDINA, A.B. (1981) Synthesis and structure of crystals of uranyl pyrophosphates $M_2UO_2P_2O_7$ (M = Rb, Cs). *Izvestiya Akademii Nauk SSSR* **17**.

LINDE, S.A., GORBUNOVA, I.E., LAVROV, A.V., & POBEDINA, A.B. (1984) Synthesis and formation of $Na_2UO_2P_2O_7$ sodium uranylpyrophosphate crystals. *Zhurnal Neorganicheskoi Khimii* **29**, 1533–1537.

LING, J. & ALBRECHT-SCHMITT, T.E. (2007) Intercalation of iodic acid into the layered uranyl iodate, $UO_2(IO_3)_2(H_2O)$. *Inorganic Chemistry* **46**, 346–347.

LING, J., WU, S., CHEN, F., SIMONETTI, A., SHAFER, J.T., & ALBRECHT-SCHMITT, T.E. (2009) Does Iodate Incorporate into Layered Uranyl Phosphates Under Hydrothermal Conditions? *Inorganic Chemistry* **48**, 10995–11001.

LING, J., MORRISON, J.M., WARD, M., POINSATTE-JONES, K., & BURNS, P.C. (2010a) Syntheses, structures, and characterization of open-framework uranyl germanates. *Inorganic Chemistry* **49**, 7123–7128.

LING, J., SIGMON, G.E., WARD, M., ROBACK, N., & BURNS, P.C. (2010b) Syntheses, structures, and IR spectroscopic characterization of new uranyl sulfate/selenate 1D-chain, 2D-sheet and 3D-framework. *Zeitschrift Für Kristallographie* **225**, 230–239.

LING, J., WARD, M., & BURNS, P.C. (2011) Hydrothermal syntheses and structures of the uranyl tellurates $AgUO_2(HTeO_5)$ and $Pb_2UO_2(TeO_6)$. *Journal of Solid State Chemistry* **184**, 401–404.

LIU, H.K., CHANG, W.J., & LII, K.H. (2011) High-Temperature, High-Pressure Hydrothermal Synthesis and Characterization of an Open-Framework Uranyl Silicate with Nine-Ring Channels: $Cs_2UO_2Si_{10}O_{22}$. *Inorganic Chemistry* **50**, 11773–11776.

LOCOCK, A.J. (2007) Trends in actinide compounds with the autunite sheet-anion topology. *Proceedings of the Russian Mineralogical Society* **136**, 115–137.

LOCOCK, A.J. & BURNS, P.C. (2002a) The crystal structure of triuranyl diphosphate tetrahydrate. *Journal of Solid State Chemistry* **163**, 275–280.

LOCOCK, A.J. & BURNS, P.C. (2002b) Crystal structures of three framework alkali metal uranyl phosphate hydrates. *Journal of Solid State Chemistry* **167**, 226–236.

LOCOCK, A.J. & BURNS, P.C. (2003a) The crystal structure of bergenite, a new geometrical isomer of the phosphuranylite group. *Canadian Mineralogist* **41**, 91–101.

LOCOCK, A.J. & BURNS, P.C. (2003b) The crystal structure of synthetic autunite, $Ca[(UO_2)_2(PO_4)_2](H_2O)_{11}$. *American Mineralogist* **88**, 240–244.

LOCOCK, A.J. & BURNS, P.C. (2003c) Crystal structures and synthesis of the copper-dominant members of the autunite and meta-autunite groups: torbernite, zeunerite, metatorbernite and metazeunerite. *Canadian Mineralogist* **41**, 489–502.

LOCOCK, A.J. & BURNS, P.C. (2003d) Structures and syntheses of framework triuranyl diarsenate hydrates. *Journal of Solid State Chemistry* **176**, 18–26.

LOCOCK, A.J. & BURNS, P.C. (2003e) Structures and synthesis of framework Rb and Cs uranyl arsenates and their relationships with their phosphate analogues. *Journal of Solid State Chemistry* **175**, 372–379.

LOCOCK, A.J. & BURNS, P.C. (2003f) The structure of huegelite, an arsenate of the phosphuranylite group, and its relationship to dumontite. *Mineralogical Magazine* **67**, 1109–1120.

LOCOCK, A.J. & BURNS, P.C. (2004) Revised Tl(I)–O bond valence parameters and the structures of thallous dichromate and thallous uranyl phosphate hydrate. *Zeitschrift Für Kristallographie* **219**, 259–266.

LOCOCK, A.J., BURNS, P.C., DUKE, M.J.M., & FLYNN, T.M. (2004a) Monovalent cations in structures of the meta-autunite group. *Canadian Mineralogist* **42**, 973–996.

LOCOCK, A.J., BURNS, P.C., & FLYNN, T.M. (2004b) Divalent transition metals and magnesium in structures that contain the autunite-type sheet. *Canadian Mineralogist* **42**, 1699–1718.

LOCOCK, A.J., SKANTHAKUMAR, S., BURNS, P.C., & SODERHOLM, L. (2004c) Syntheses, structures, magnetic properties, and X-ray absorption spectra of carnotite-type uranyl chromium(V) oxides: $A(UO_2)_2Cr_2O_8](H_2O)_n$ ($A = K_2$, Rb_2, Cs_2, Mg; $n = 0$, 4). *Chemistry of Materials* **16**, 1384–1390.

LOCOCK, A.J., BURNS, P.C., & FLYNN, T.M. (2005a) The role of water in the structures of synthetic hallimondite, $Pb_2[(UO_2)(AsO_4)]_2(H_2O)_n$ and synthetic parsonsite, $Pb_2[(UO_2)(PO_4)](H_2O)_n$, $0 \leq n \leq 0.5$. *American Mineralogist* **90**, 240–246.

LOCOCK, A.J., BURNS, P.C., & FLYNN, T.M. (2005b) Structures of strontium- and barium-dominant compounds that contain the autunite-type sheet. *Canadian Mineralogist* **43**, 721–733.

LOCOCK, A.J., KINMAN, W.S., & BURNS, P.C. (2005c) The structure and composition of uranospathite $Al1-x$ square(x) $(UO_2)(PO_4)_2(H_2O)_{20+3x}F_{1-3x}$, $0 < x < 0.33$, a non-centrosymmetric flourine-bearing mineral of the autunite group, and of a related synthetic lower hydrate, $Al_{0.67}\square_{0.33}[(UO_2)(PO_4)_2](H_2O)_{15.5}$. *Canadian Mineralogist* **43**, 989–1003.

LOOPSTRA, B.O. (1970) Structure of β-U_3O_8. *Acta Crystallographica Section B: Structural Science, Crystal Engineering, and Materials* **B26**, 656–657.

LOOPSTRA, B.O. (1977) Crystal-structure of α-U_3O_8. *Journal of Inorganic & Nuclear Chemistry* **39**, 1713–1714.

LOOPSTRA, B.O. & BRANDENBURG, N.P. (1978) Uranyl selenite and uranyl tellurite. *Acta Crystallographica Section B: Structural Science, Crystal Engineering, and Materials* **34**, 1335–1337.

LOOPSTRA, B.O. & CORDFUNKE, E.H. (1966) On structure of α-UO_3. *Recueil Des Travaux Chimiques Des Pays-Bas* **85**, 135–142.

LOOPSTRA, B.O. & RIETVELD, H.M. (1969) Structure of some alkaline-earth metal uranates. *Acta Crystallographica Section B: Structural Science, Crystal Engineering, and Matierals* **B25**, 787–791.

LOOPSTRA, B.O., TAYLOR, J.C., & WAUGH, A.B. (1977) Neutron powder profile studies of gamma-uranium trioxide phases. *Journal of Solid State Chemistry* **20**, 9–19.

LYCHEV, A.A., MASHIROV, L.G., SMOLIN, Y.I., & SHEPELEV, Y.F. (1986) Refinement of the crystal-structure of $K_3UO_2F_5$. *Soviet Radiochemistry* **28**, 622–625.

MACASKIE, L.E., BONTHRONE, K.M., YONG, P., & GODDARD, D.T. (2000) Enzymically mediated bioprecipitation of uranium by a Citrobacter sp.: a concerted role for exocellular lipopolysaccharide and associated phosphatase in biomineral formation. *Microbiology – United Kingdom* **146**, 1855–1867.

MAKAROV, E.S. & IVANOV, V.I. (1960) The crystal structure of meta-autunite, $Ca(UO_2)_2(PO_4)_2(H_2O)_6$. *Doklady Akademii Nauk SSSR* **132**, 673–676.

MARTINEZ, R.J., BEAZLEY, M.J., TAILLEFERT, M., ARAKAKI, A.K., SKOLNICK, J., & SOBECKY, P.A. (2007) Aerobic uranium (VI) bioprecipitation by metal-resistant bacteria isolated from radionuclide- and metal-contaminated subsurface soils. *Environmental Microbiology* **9**, 3122–3133.

MARUKHNOV, A.V., PUSHKIN, D.V., PERESYPKINA, E.V., VIROVETS, A.V., & SEREZHKINA, L.B. (2008a) Synthesis and structure of $NaUO_2(SeO_3)(HSeO_3) \cdot 4H_2O$. *Russian Journal of Inorganic Chemistry* **53**, 831–836.

MARUKHNOV, A.V., SEREZHKIN, V.N., PUSHKIN, D.V., SMIRNOV, O.P., & PLAKHTII, V.P. (2008b) Neutron diffraction study

of $UO_2SeO_4 \cdot 2D_2O$. *Russian Journal of Inorganic Chemistry* **53**, 1283–1287.

MAYER, H. & MEREITER, K. (1986) Synthetic bayleyite, $Mg_2UO_2(CO_3)_3 \cdot 18H_2O$ - thermochemistry, crystallography and crystal-structure. *Tschermaks Mineralogische Und Petrographische Mitteilungen* **35**, 133–146.

MER, A., OBBADE, S., RIVENET, M., RENARD, C., & ABRAHAM, F. (2012) $La(UO_2)(V_2O_7)(UO_2)(VO_4)$ the first lanthanum uranyl-vanadate with structure built from two types of sheets based upon the uranophane anion-topology. *Journal of Solid State Chemistry* **185**, 180–186.

MERCIER, R., PHAM THI, M., & COLOMBAN, P. (1985) Structure, Vibrational Study and Conductivity of the Trihydrated Uranyl Bis(Dihydrogenphosphate): $UO_2(H_2PO_4)_2 \cdot 3(H_2O)$. *Solid State Ionics* **15**, 113–126.

MEREITER, K. (1982a) The crystal-structure of johannite, $Cu(UO_2)_2(OH)_2(SO_4) \cdot 2.8H_2O$. *Tschermaks Mineralogische Und Petrographische Mitteilungen* **30**, 47–57.

MEREITER, K. (1982b) The crystal-structure of liebigite, $Ca_2UO_2(CO_3)_3 \cdot \sim 11H_2O$. *Tschermaks Mineralogische Und Petrographische Mitteilungen* **30**, 277–288.

MEREITER, K. (1982c) The crystal-structure of walpurgite, $(UO_2)Bi_4O_4(AsO_4) \cdot 2.2H_2O$. *Tschermaks Mineralogische Und Petrographische Mitteilungen* **30**, 129–139.

MEREITER, K. (1986a) Crystal-structure and crystallographic properties of a schrockingerite from Joachimsthal. *Tschermaks Mineralogische Und Petrographische Mitteilungen* **35**, 1–18.

MEREITER, K. (1986b) Crystal-structure refinements of two francevillites, $(Ba,Pb)(UO_2)_2V_2O_8 \cdot 5H_2O$. *Neues Jahrbuch Für Mineralogie-Monatshefte*, 552–560.

MEREITER, K. (1986c) Structure of strontium tricarbonatodioxouranate(VI) octahydrate. *Acta Crystallographica Section C: Crystal Structure Communications* **42**, 1678–1681.

MEREITER, K. (1986d) Structure Of Thallium Tricarbonatodioxouranate(VI). *Acta Crystallographica Section C: Crystal Structure Communications* **42**, 1682–1684.

MEREITER, K. (1986e) Synthetic swartzite, $CaMgUO_2(CO_3)_3 \cdot 12H_2O$, and its strontium analogue, $SrMgUO_2(CO_3)_3 \cdot 12H_2O$ - crystallography and crystal-structures. *Neues Jahrbuch Für Mineralogie-Monatshefte*, 481–492.

MEREITER, K. (1986f) Neue kristallographische daten ueber das uranmineral andersonit. *Anzeiger der Oesterreichischen Akademie der Wissenschaften, Mathematisch-Naturwissenschaftliche Klasse* **3**, 39–41.

MEREITER, K. (1988) Structure of cesium tricarbonatodioxouranate(VI) hexahydrate. *Acta Crystallographica Section C: Crystal Structure Communications* **44**, 1175–1178.

MEREITER, K. (2013) Description and crystal structure of albrechtschraufite, $MgCa_4F_2[UO_2(CO_3)_3] \cdot 17–18H_2O$. *Mineralogy and Petrology* **107**, 179–188.

MEUNIER, G. & GALY, J. (1973) Crystal-structure of synthetic schmitterite $UTeO_5$. *Acta Crystallographica Section B: Structural Science, Crystal Engineering, and Materials* **B29**, 1251–1255.

MIJLHOFF, F.C., IJDO, D.J.W., & CORDFUNKE, E.H.P. (1993) The crystal-structure of α-$Cs_2U_2O_7$ and β-$Cs_2U_2O_7$. *Journal of Solid State Chemistry* **102**, 299–305.

MIKHAILOV, Y.N., KOKH, L.A., KUZNETSOV, V.G., GREVTSEVA, T.G., SOKOL, S.K., & ELLERT, G.V. (1977) Synthesis and crystal structure of potassium trisulfatouranylate $K_4(UO_2(SO_4)_3$. *Koordinatsionnaya Khimiya* **3**, 500–513.

MIKHAILOV, Y.N., GORBUNOVA, Y.E., BAEVA, E.E., SEREZHKINA, L.B., & SEREZHKIN, V.N. (2001a) Crystal structure of $Na_2UO_2(SeO_4)_2 \cdot 4H_2O$. *Russian Journal of Inorganic Chemistry* **46**, 1841–1845.

MIKHAILOV, Y.N., GORBUNOVA, Y.E., SHISHKINA, O.V., SEREZHKINA, L.B., & SEREZHKIN, V.N. (2001b) Crystal Structure of $Cs_2[(UO_2(SeO_4)_2(H_2O)](H_2O)$. *Zhurnal Neorganicheskoi Khimii* **46**, 1828–1832.

MIKHAILOV, Y.N., GORBUNOVA, Y.E., MIT'KOVSKAYA, E.V., SEREZHKINA, L.B., & SEREZHKINA, V.N. (2002a) Crystal Structure of $Rb(UO_2(SO_4)F)$. *Radiochemistry* **44**, 315–318.

MIKHAILOV, Y.N., GORBUNOVA, Y.E., STOLYAROV, I.P., & MOISEEV, I.I. (2002b) The synthesis and structure of a new modification of monoaquadifluorouranyl hydrate. *Zhurnal Neorganicheskoi Khimii* **47**, 1980–1986.

MILLER, S.A. & TAYLOR, J.C. (1986) The crystal-structure of saleeite, $Mg[UO_2PO_4]_2 \cdot 10H_2O$. *Zeitschrift Für Kristallographie* **177**, 247–253.

MILLS, S.J., BIRCH, W.D., KOLITSCH, U., MUMME, W.G., & GREY, I.E. (2008) Lakebogaite, $CaNaFe^{3+}_2H(UO_2)_2(PO_4)_4(OH)_2(H_2O)_8$, a new uranyl phosphate with a unique crystal structure from Victoria, Australia. *American Mineralogist* **93**, 691–697.

MISTRYUKOV, V.E. & MIKHAILOV, Y.N. (1983) The characteristic properties of the structural function of the selenitogroup in the uranyl complex with neutral ligands. *Koordinatsionnaya Khimiya* **9**, 97–102.

MISTRYUKOV, V.E. & MIKHAILOV, Y.N. (1985) Crystal structure of $Rb(UO_2(HPO_3)(H_2PO_3))_3H_2O$ and $K_2(UO_2(HPO_3)_2)_2(H_2O)$. *Koordinatsionnaya Khimiya* **11**, 1393–1398.

MIT'KOVSKAYA, E.V., MIKHAILOV, Y.N., GORBUNOVA, Y.E., SEREZHKINA, L.B., & SEREZHKIN, V.N. (2003) Crystal structure of $(H_3O)_3(UO_2)_3O(OH)_3(SeO_4)_2$. *Russian Journal of Inorganic Chemistry* **48**, 666–670.

MOLL, H., REICH, T., HENNIG, C., ROSSBERG, A., SZABO, Z., & GRENTHE, I. (2000) Solution coordination chemistry of uranium in the binary UO_2^{2+}–SO_4^{2-} and the ternary UO_2^{2+}–SO_4^{2-}–OH system. *Radiochimica Acta* **88**, 559–566.

MOROSIN, B. (1978) Hydrogen uranyl phosphate tetrahydrate, a hydrogen-ion solid electrolyte. *Acta Crystallographica Section B: Structural Science, Crystal Engineering, and Materials* **34**, 3732–3734.

MORRISON, J.M., MOORE-SHAY, L.J., & BURNS, P.C. (2011) U(VI) Uranyl cation-cation interactions in framework germanates. *Inorganic Chemistry* **50**, 2272–2277.

NAZARCHUK, E.V., KRIVOVICHEV, S.V., & BURNS, P.C. (2005a) Crystal structure and phase transformations of Ca[(UO$_2$)$_6$(MoO$_4$)$_7$(H$_2$O)$_2$](H$_2$O)$_n$ (n = 7.6). *Zapiski Vserossijskogo Mineralogicheskogo Obshchestva* **134**, 110–117.

NAZARCHUK, E.V., KRIVOVICHEV, S.V., & BURNS, P.C. (2005b) Crystal structure of Tl$_2$[(UO$_2$)$_2$(MoO$_4$)$_3$] and crystal chemiistry of the compounds M_2[(UO$_2$)$_2$(MoO$_4$)$_3$] (M = Tl, Rb, Cs). *Radiochemistry* **47**, 447–451.

NAZARCHUK, E.V., KRIVOVICHEV, S.V., & BURNS, P.C. (2005c) Crystal Structure of Tl$_2$[(UO$_2$)$_2$(MoO$_4$)$_3$] and crystal chemistry of the compounds M_2[(UO$_2$)$_2$(MoO$_4$)$_3$] (M = Tl, Rb, Cs). *Radiochemistry* **47**, 447–451.

NAZARCHUK, E.V., SIIDRA, O.I., KRIVOVICHEV, S.V., MALCHEREK, T., & DEPMEIER, W. (2009) First Mixed Alkaline Uranyl Molybdates: Synthesis and Crystal Structures of CsNa$_3$(UO$_2$)$_4$O$_4$(Mo$_2$O$_8$) and Cs$_2$Na$_8$(UO$_2$)$_8$O$_8$(Mo$_5$O$_{20}$). *Zeitschrift Für Anorganische Und Allgemeine Chemie* **635**, 1231–1235.

NAZARCHUK, E.V., SIIDRA, O.I., & KRIVOVICHEV, S.V. (2011) Crystal chemistry of uranyl halides containing mixed (UO$_2$)(X_mO$_n$)$_5$ bipyramids (X = Cl, Br): synthesis and crystal structure of Cs$_2$(UO$_2$)(NO$_3$)Cl$_3$. *Zeitschrift Für Naturforschung Section B: A Journal of Chemical Sciences* **66**, 142–146.

NEUEFEIND, J., SKANTHAKUMAR, S., & SODERHOLM, L. (2004) Structure of the UO$_2^{2+}$–SO$_4^{2-}$ ion pair in aqueous solution. *Inorganic Chemistry* **43**, 2422–2426.

NGUYEN, Q.B. & LII, K.H. (2011) Cs$_4$UGe$_8$O$_{20}$: A tetravalent uranium germanate containing four- and five-coordinate germanium. *Inorganic Chemistry* **50**, 9936–9938.

NGUYEN, Q.D., CHOUROU, S., & HECKLY, J. (1981) The crystal structure and some physico-chemical properties of the compound (Na$_3$(UO$_2$)$_2$F$_7$)(H$_2$O)$_6$. *Journal of Inorganic & Nuclear Chemistry* **43**, 1835–1839.

NGUYEN, Q.B., LIU, H.K., CHANG, W.J., & LII, K.H. (2011) Cs$_8$U^{IV}((U^{VI}O$_2$)O)$_3$(Ge$_3$O$_9$)$_3$•3H$_2$O: A Mixed-Valence Uranium Germanate with 9-Ring Channels. *Inorganic Chemistry* **50**, 4241–4243.

NGUYEN-TRUNG, C., BEGUN, G.M., & PALMER, D.A. (1992) Aqueous Uranium Complexes. 2. Raman Spectroscopic Study of the Complex Formation of the Dioxouranium(V1) Ion with a Variety of Inorganic and Organic Ligands. *Inorganic Chemistry* **31**, 5280–5287.

NIINISTO, L. (1979) Uranyl (VI) Compounds. II. The Crystal Structure Of Potassium Uranyl Sulfate Dihydrate, K$_2$UO$_2$(SO$_4$)$_2$•2H$_2$O. *Acta Chemica Scandinavica* **33**, 621–624.

NIINISTO, L., TOIVONEN, J., & VALKONEN, J. (1978) Uranyl (VI) compounds. I. The crystal structure of ammonium uranyl sulfate dihydrate, (NH$_4$)$_2$UO$_2$(SO$_4$)$_2$(H$_2$O)$_2$. *Acta Chemica Scandinavica, Series A* **32**, 647–651.

NYMAN, M., RODRIGUEZ, M.A., & CAMPANA, C.F. (2010) Self-Assembly of Alkali-Uranyl-Peroxide Clusters. *Inorganic Chemistry* **49**, 7748–7755.

OBBADE, S., DION, C., BEKAERT, E., YAGOUBI, S., SAADI, M., & ABRAHAM, F. (2003a) Synthesis and crystal structure of new uranyl tungstates M_2(UO$_2$)(W$_2$O$_8$) (M = Na, K), M_2(UO$_2$)$_2$(WO$_5$)O (M = K, Rb), and Na$_{10}$(UO$_2$)$_8$(W$_5$O$_{20}$)O$_8$. *Journal of Solid State Chemistry* **172**, 305–318.

OBBADE, S., DION, C., DUVIEUBOURG, L., SAADI, M., & ABRAHAM, F. (2003b) Synthesis and crystal structure of α- and β-Rb$_6$U$_5$V$_2$O$_{23}$, a new layered compound. *Journal of Solid State Chemistry* **173**, 1–12.

OBBADE, S., YAGOUBI, S., DION, C., SAADI, M., & ABRAHAM, F. (2003c) Synthesis, crystal structure and electrical characterization of two new potassium uranyl molybdates K$_2$(UO$_2$)$_2$(MoO$_4$)O$_2$ and K$_8$(UO$_2$)$_8$(MoO$_5$)$_3$O$_6$. *Journal of Solid State Chemistry* **174**, 19–31.

OBBADE, S., DION, C., RIVENET, M., SAADI, M., & ABRAHAM, F. (2004a) A novel open-framework with non-crossing channels in the uranyl vanadates A(UO$_2$)$_4$(VO$_4$)$_3$ (A = Li, Na). *Journal of Solid State Chemistry* **177**, 2058–2067.

OBBADE, S., DION, C., SAADI, M., & ABRAHAM, F. (2004b) Synthesis, crystal structure and electrical characterization of Cs$_4$(UO$_2$)$_2$(V$_2$O$_7$)O$_2$, a uranyl divanadate with chains of corner-sharing uranyl square bipyramids. *Journal of Solid State Chemistry* **177**, 1567–1574.

OBBADE, S., DION, C., SAADI, M., YAGOUBI, S., & ABRAHAM, F. (2004c) Pb(UO$_2$)(V$_2$O$_7$), a novel lead uranyl divanadate. *Journal of Solid State Chemistry* **177**, 3909–3917.

OBBADE, S., YAGOUBI, S., DION, C., SAADI, M., & ABRAHAM, F. (2004d) Two new lithium uranyl tungstates Li$_2$(UO$_2$)(WO$_4$)$_2$ and Li$_2$(UO$_2$)$_4$(WO$_4$)$_4$O with framework based on the uranophane sheet anion topology. *Journal of Solid State Chemistry* **177**, 1681–1694.

OBBADE, S., DUVIEUBOURG, L., DION, C., & ABRAHAM, F. (2007) Three-dimensional framework of uranium-centered polyhedra with non-intersecting channels in the uranyl oxy-vanadates A_2(UO$_2$)$_3$(VO$_4$)$_2$O (A = Li, Na). *Journal of Solid State Chemistry* **180**, 866–872.

OBBADE, S., RENARD, C., & ABRAHAM, F. (2009) New open-framework in the uranyl vanadates A_3(UO$_2$)$_7$(VO$_4$)$_5$O (A = Li, Ag) with intergrowth structure between A(UO$_2$)$_4$(VO$_4$)$_3$ and A_2(UO$_2$)$_3$(VO$_4$)$_2$O. *Journal of Solid State Chemistry* **182**, 413–420.

OK, K.M., BAEK, J., HALASYAMANI, P.S., & O'HARE, D. (2006) New layered uranium phosphate fluorides: Syntheses, structures, characterizations, and ion-exchange properties of A(UO$_2$)F(HPO$_4$)•xH$_2$O (A = Cs$^+$, Rb$^+$, K$^+$; x = 0–1). *Inorganic Chemistry* **45**, 10207–10214.

OMALY, J., & BADAUD, J.P. (1972) Preparation and properties of URh$_2$O$_6$ phase. *Comptes rendus hebdomadaires des seances de l'academie des sciences serie C* **275**, 371.

PADEL, L., POIX, P., & MICHEL, A. (1972) Preparation and crystallographic study of system Ba$_2$(UMg)O$_6$–Ba$_2$(U$_{2/3}$Fe$_{4/3}$)O$_6$. *Revue De Chimie Minerale* **9**, 337.

PAGOAGA, M.K., APPLEMAN, D.E., & STEWART, J.M. (1987) Crystal-structures and crystal-chemistry of the uranyl oxide hydrates becquerelite, billietite, and protasite. *American Mineralogist* **72**, 1230–1238.

PEETERS, O.M., VOCHTEN, R., & BLATON, N. (2008) The crystal structures of synthetic potassium transition-metal zippeite-group phases. *Canadian Mineralogist* **46**, 173–182.

PERRIN, A. (1976) Crystal-structure of dihydroxodiuranyl nitrate tetrahydrate. *Acta Crystallographica Section B: Structural Science, Crystal Engineering, and Materials* **32**, 1658–1661.

PERRIN, A. (1977) Preparation, structural and vibrational study of M$_2$U$_2$O$_5$Cl$_4$•2H$_2$O (M = Rb, Cs) - preparation of tetranuclear anion. *Journal of Inorganic & Nuclear Chemistry* **39**, 1169–1172.

PERRIN, A. & LE MAROUILLE, J.Y. (1977) Crystal and molecular-structure of tetranuclear complex K$_2$(UO$_2$)$_4$O$_2$(OH)$_2$Cl$_4$(H$_2$O)$_6$. *Acta Crystallographica Section B: Structural Science, Crystal Engineering, and Materials* **33**, 2477–2481.

PINACCA, R., VIOLA, M.C., PEDREGOSA, J.C., MUNOZ, A., ALONSO, J.A., MARTINEZ, J.L., & CARBONIO, R.E. (2005) Crystal and magnetic structure of the double perovskite Sr$_2$CoUO$_6$: a neutron diffraction study. *Dalton Transactions*, 447–451.

PINACCA, R.M., VIOLA, M.C., PEDREGOSA, J.C., MARTINEZ-LOPE, M.J., CARBONIO, R.E., & ALONSO, J.A. (2007) Preparation, crystal structure and magnetic behavior of new double perovskites Sr$_2$B'UO$_6$ with B' = Mn, Fe, Ni, Zn. *Journal of Solid State Chemistry* **180**, 1582–1589.

PIRET, P. (1985) The crystal-structure of fourmarierite Pb(UO$_2$)$_4$O$_3$(OH)$_4$•4H$_2$O. *Bulletin de Mineralogie* **108**, 659–665.

PIRET, P. & DECLERCQ, J.P. (1983) Crystal-structure of upalite Al(UO$_2$)$_3$O(OH)(PO$_4$)$_2$•7H$_2$O - an example of mimetic twin. *Bulletin de Mineralogie* **106**, 383–389.

PIRET, P. & DELIENS, M. (1982) Vanmeersscheite U(UO$_2$)$_3$(PO$_4$)$_2$(OH)$_6$·4H$_2$O and meta-vanmeersscheite U(UO$_2$)$_3$(PO$_4$)$_2$(OH)$_6$·2H$_2$O, new minerals. *Bulletin de Mineralogie* **105**, 125–128.

PIRET, P. & DELIENS, M. (1987) Uranyl and aluminum phosphates from Kobokobo. IX. althupite, AlTh(UO$_2$)(UO$_2$)$_3$O(OH)(PO$_4$)$_2$(OH)$_3$•15H$_2$O, a new mineral - properties and crystal-structure. *Bulletin de Mineralogie* **110**, 65–72.

PIRET, P. & PIRETMEUNIER, J. (1988) New crystal-structure determination of dumontite Pb$_2$(UO$_2$)$_3$O$_2$(PO$_4$)$_2$•5H$_2$O. *Bulletin de Mineralogie* **111**, 439–442.

PIRET, P. & PIRETMEUNIER, J. (1994) Crystal-structure of seelite from Rabejac (France). *European Journal of Mineralogy* **6**, 673–677.

PIRET, P. & PIRETMEUNIER, J., & DECLERCQ, J.P. (1979) Structure of phuralumite. *Acta Crystallographica Section B: Structural Science, Crystal Engineering, and Matierals* **35**, 1880–1882.

PIRET, P., DECLERCQ, J.P., & WAUTERSSTOOP, D. (1980) Crystal-structure of sengierite. *Bulletin de Mineralogie* **103**, 176–178.

PIRET, P., DELIENS, M., PIRETMEUNIER, J., & GERMAIN, G. (1983) Sayrite, Pb$_2$(UO$_2$)$_5$O$_6$(OH)$_2$•4H$_2$O a new mineral - properties and crystal-structure. *Bulletin de Mineralogie* **106**, 299–304.

PIRET, P., DELIENS, M., & PIRETMEUNIER, J. (1988) Francoisite-(Nd), a new uranyl and rare-earth phosphate - properties and crystal-structure. *Bulletin de Mineralogie* **111**, 443–449.

PIRET, P., PIRETMEUNIER, J., & DELIENS, M. (1990) Chemical-composition and crystal-structure of dewindtite Pb$_3$[H(UO$_2$)$_3$O$_2$(PO$_4$)$_2$]$_2$•12H$_2$O. *European Journal of Mineralogy* **2**, 399–405.

PLÁŠIL, J., ČEJKA, J., SEJKORA, J., HLOUŠEK, J., & GOLIÁŠ, V. (2009) New data for metakirchheimerite from Jáchymov (St. Joachimsthal), Czech Republic. *Journal of Geosciences* **54**, 373–384.

PLÁŠIL, J., SEJKORA, J., ČEJKA, J., NOVÁK, M., VIÑALS, J., ONDRUŠ, P., VESELOVSKÝ, F., ŠKÁCHA, P., JEHLIČKA, J., GOLIÁŠ, V., & HLOUŠEK, J. (2010a) Metarauchite, Ni[(UO$_2$)$_2$(AsO$_4$)$_2$]•8H$_2$O, from Jáchymov, Czech Republic, and Schneeberg, Germany: a new member of the autunite group. *Canadian Mineralogist* **48**, 335–350.

PLÁŠIL, J., SEJKORA, J., ČEJKA, J., ŠKÁCHA, P., GOLIÁŠ, V., & EDEROVÁ, J. (2010b) Characterization of phosphate-rich metalodevite from Příbram, Czech Republic. *Canadian Mineralogist* **48**, 113–122.

PLÁŠIL, J., DUŠEK, M., NOVÁK, M., ČEJKA, J., CÍSAŘOVÁ, I., & ŠKODA, R. (2011a) Sejkoraite-(Y), a new member of the zippeite group containing trivalent cations from Jáchymov (St. Joachimsthal), Czech Republic: Description and crystal structure refinement. *American Mineralogist* **96**, 983–991.

PLÁŠIL, J., MILLS, S.J., FEJFAROVÁ, K., DUŠEK, M., NOVÁK, M., ŠKODA, R., ČEJKA, J., & SEJKORA, J. (2011b) The crystal structure of natural zippeite, K$_{1.85}$H$^+_{0.15}$[(UO$_2$)$_4$O$_2$(SO$_4$)$_2$(OH)$_2$](H$_2$O)$_4$, from Jáchymov, Czech Republic. *Canadian Mineralogist* **49**, 1089–1103.

PLÁŠIL, J., HAUSER, J., PETŘÍČEK, V., MEISSER, N., MILLS, S.J., ŠKODA, R., FEJFAROVÁ, K., ČEJKA, J., SEJKORA, J., HLOUŠEK, J., JOHANNET, J.M., MACHOVIČ, V., & LAPČÁK, L. (2012a) Crystal structure and formula revision of deliensite,

Fe$(UO_2)_2(SO_4)_2(OH)_2(H_2O)_7$. *Mineralogical Magazine* **76**, 2837–2860.

PLÁŠIL, J., HLOUŠEK, J., VESELOVSKÝ, F., FEJFAROVÁ, K., DUŠEK, M., ŠKODA, R., NOVÁK, M., ČEJKA, J., SEJKORA, J., & ONDRUŠ, P. (2012b) Adolfpateraite, K(UO_2) $(SO_4)(OH)(H_2O)$, a new uranyl sulphate mineral from Jáchymov, Czech Republic. *American Mineralogist* **97**, 447–454.

PLÁŠIL, J., FEJFAROVÁ, K., ČEJKA, J., DUŠEK, M., ŠKODA, R., & SEJKORA, J. (2013a) Revision of the crystal structure and chemical formula of haiweeite, Ca$(UO_2)_2(Si_5O_{12})$ $(OH)_2 \bullet 6H_2O$. *American Mineralogist* **98**, 718–723.

PLÁŠIL, J., FEJFAROVÁ, K., DUŠEK, M., ŠKODA, R., & ROHLÍČEK, J. (2013b) Revision of the symmetry and the crystal structure of čejkaite, Na$_4(UO_2)(CO_3)_3$. *American Mineralogist* **98**, 549–553.

PLÁŠIL, J., FEJFAROVÁ, K., ŠKODA, R., DUŠEK, M., MARTY, J., & ČEJKA, J. (2013c) The crystal structure of magnesiozippeite, Mg$(UO_2)_2O_2(SO_4)(H_2O)_{3.5}$, from East Saddle Mine, San Juan County, Utah (USA). *Mineralogy and Petrology* **107**, 211–219.

PLÁŠIL, J., KAMPF, A.R., KASATKIN, A.V., MARTY, J., ŠKODA, R., SILVA, S., & ČEJKA, J. (2013d) Meisserite, Na$_5(UO_2)$ $(SO_4)_3(SO_3OH)(H_2O)$, a new uranyl sulfate mineral from the Blue Lizard mine, San Juan County, Utah, USA. *Mineralogical Magazine* **77**, 2975–2988.

PLÁŠIL, J., KASATKIN, A.V., ŠKODA, R., NOVÁK, M., KALLISTOVÁ, A., DUŠEK, M., SKÁLA, R., FEJFAROVÁ, K., ČEJKA, J., MEISSER, N., GOETHALS, H., MACHOVIČ, V., & LAPČÁK, L. (2013e) Leydetite, Fe$(UO_2)(SO_4)_2(H_2O)_{11}$, a new uranyl sulfate mineral from Mas d'Alary, Lodeve, France. *Mineralogical Magazine* **77**, 429–441.

PLÁŠIL, J., DUŠEK, M., ČEJKA, J., & SEJKORA, J. (2014a) The crystal structure of rabejacite, the Ca^{2+}-dominant member of the zippeite group. *Mineralogical Magazine* **78**, 1249–1264.

PLÁŠIL, J., KAMPF, A.R., KASATKIN, A.V., & MARTY, J. (2014b) Bluelizardite, Na$_7(UO_2)(SO_4)_4Cl(H_2O)_2$, a new uranyl sulfate mineral from the Blue Lizard mine, San Juan County, Utah, USA. *Journal of Geosciences* **59**, 145–158.

PLÁŠIL, J., PALATINUS, L., ROHLÍČEK, J., HOUDKOVÁ, L., KLEMENTOVÁ, M., GOLIÁŠ, V., & ŠKÁCHA, P. (2014c) Crystal structure of lead uranyl carbonate mineral widenmannite: Precession electron-diffraction and synchrotron powder-diffraction study. *American Mineralogist* **99**, 276–282.

PLÁŠIL, J., VESELOVSKÝ, F., HLOUŠEK, J., ŠKODA, R., NOVÁK, M., SEJKORA, J., ČEJKA, J., ŠKÁCHA, P., & KASATKIN, A.V. (2014d) Mathesiusite, K$_5(UO_2)_4(SO_4)_4(VO_5)(H_2O)_4$, a new uranyl vanadate-sulfate from Jáchymov, Czech Republic. *American Mineralogist* **99**, 625–632.

PLÁŠIL, J., HLOUŠEK, J., KASATKIN, A.V., NOVÁK, M., ČEJKA, J., & LAPČÁK, L. (2015) Svornostite, K$_2$Mg $[(UO_2)(SO_4)_2]_2 \cdot$ 8H$_2$O, a new uranyl sulfate mineral from Jáchymov, Czech Republic. *Journal of Geosciences* **60**, 113–121.

POBEDINA, A.B. & ILYUKHIN, A.B. (1997) Synthesis, properties, and structure of Cs$_{11}$Eu$_4(UO_2)_2(P_2O_7)_6(PO_4)$. *Zhurnal Neorganicheskoi Khimii* **42**, 1120–1124.

PUSHCHAROVSKY, D.Y., RASTSVETAEVA, R.K., & SARP, H. (1996) Crystal structure of deloryite, Cu$_4(UO_2)Mo_2O_8$ $(OH)_6$. *Journal of Alloys and Compounds* **239**, 23–26.

PUSHCHAROVSKII, D.Y., SULEIMANOV, E.V., PASERO, M., MERLINO, S., BARINOVA, A.V., & ALEKSEEV, E.V. (2003) Crystal structure of Sr$(AsUO_6)_2 \bullet 8H_2O$. *Crystallography Reports* **48**, 212–215.

QIU, J. & BURNS, P.C. (2013) Clusters of Actinides with Oxide, Peroxide, or Hydroxide Bridges. *Chemical Reviews* **113**, 1097–1120.

RASTSVETAEVA, R.K., ARAKCHEEVA, A.V., PUSHCHAROVSKY, D.YU., ATENCIO, D., & MENEZES FILHO, L.A.D. (1997) A new silicon band in the haiweeite [sic] structure. *Crystallographic Reports* **42**, 927–933.

RASTSVETAEVA, R.K., SIDORENKO, G.A., IVANOVA, A.G., & CHUKANOV, N.V. (2008) Structural model of uramarsite. *Crystallography Reports* **53**, 771–774.

REIS, A.H., HOEKSTRA, H.R., GEBERT, E., & PETERSON, S.W. (1976) Redetermination of crystal-structure of barium uranate. *Journal of Inorganic & Nuclear Chemistry* **38**, 1481–1485.

RENARD, C., OBBADE, S., & ABRAHAM, F. (2009) Channels occupancy and distortion in new lithium uranyl phosphates with three-dimensional open-frameworks. *Journal of Solid State Chemistry* **182**, 1377–1386.

REYNOLDS, E., KENNEDY, B.J., THOROGOOD, G.J., GREGG, D.J., & KIMPTON, J.A. (2013) Crystal structure and phase transitions in the uranium perovskite. *Journal of Nuclear Materials* **433**, 37–40.

RIVENET, M., VIGIER, N., ROUSSEL, P., & ABRAHAM, F. (2007) Hydrothermal synthesis, structure and thermal stability of diamine templated layered uranyl-vanadates. *Journal of Solid State Chemistry* **180**, 713–724.

RIVENET, M., VIGIER, N., ROUSSEL, P., & ABRAHAM, F. (2009) [Ni$(H_2O)_4]_3$[U$(OH,H_2O)(UO_2)_8O_{12}(OH)_3$], crystal structure and comparison with uranium minerals with U_3O_8-type sheets. *Journal of Solid State Chemistry* **182**, 905–912.

ROOF, I.P., SMITH, M.D., & ZUR LOYE, H.C. (2010a) Crystal growth of K$_2UO_4$ and Na$_4UO_5$ using hydroxide fluxes. *Journal of Crystal Growth* **312**, 1240–1243.

ROOF, I.P., SMITH, M.D., & ZUR LOYE, H.C. (2010b) Crystal growth of uranium-containing complex oxides Ba$_2$Na$_{0.83}$ U$_{1.17}O_6$, BaK$_4U_3O_{12}$ and Na$_3$Ca$_{1.5}UO_6$. *Solid State Sciences* **12**, 1941–1947.

ROOF, I.P., SMITH, M.D., & ZUR LOYE, H.C. (2010c) High Temperature Flux Crystal Growth of Uranium-Containing Perovskites: Sr$_2UO_6$ and Ba$_2$MUO$_6$ (M = Cu, Ni, Zn). *Journal of Chemical Crystallography* **40**, 491–495.

Rosenzweig, A. & Ryan, R.R. (1975) Refinement of crystal-structure of cuprosklodowskite, $Cu(UO_2)_2(SIO_3OH)_2 \bullet 6H_2O$. *American Mineralogist* **60**, 448–453.

Rosenzweig, A. & Ryan, R.R. (1977a) Kasolite, $Pb(UO_2)(SiO_4) \bullet H_2O$. *Crystal Structure Communications* **6**, 617–621.

Rosenzweig, A. & Ryan, R.R. (1977b) Vandenbrandeite $Cu(UO_2)(OH)_4$. *Crystal Structure Communications* **6**, 53–56.

Ross, M. & Evans, H.T. (1960) The crystal structure of cesium biuranyl trisulphate, $Cs_2(UO_2)_2(SO_4)_3$. *Journal of Inorganic & Nuclear Chemistry* **15**, 338–351.

Ross, M. & Evans, H.T. (1964) Studies of torbernite minerals. I. crystal structure of abernathyite and structurally related compounds $NH_4(UO_2AsO_4) \bullet 3H_2O$ and $K(H_3O)(UO_2 AsO_4)_2 \bullet 6H_2O$. *American Mineralogist* **49**, 1578–1602.

Rutsch, M., Geipel, G., Brendler, V., Bernhard, G., & Nitsche, H. (1999) Interaction of uranium(VI) with arsenate(V) in aqueous solution studied by time-resolved laser-induced fluorescence spectroscopy (TRLFS). *Radiochimica Acta* **86**, 135–141.

Ryan, R.R. & Rosenzweig, A. (1977) Sklodowskite, $MgO[(UO_3)_2(SiO_2)_2](H_2O)_7$. *Crystal Structure Communications* **6**, 611–615.

Saad, S., Obbade, S., Yagoubi, S., Renard, C., & Abraham, F. (2008) A new uranyl niobate sheet in the cesium uranyl niobate $Cs_9(UO_2)_8O_4(NbO_5)(Nb_2O_8)_2$. *Journal of Solid State Chemistry* **181**, 741–750.

Saad, S., Obbade, S., Renard, C., & Abraham, F. (2009) Synthesis, crystal structure, infrared and electrical conductivity of the layered rubidium uranate $Rb_4U_5O_{17}$. *Journal of Alloys and Compounds* **474**, 68–72.

Saadi, M., Dion, C., & Abraham, F. (2000) Synthesis and crystal structure of the pentahydrated uranyl orthovanadate $(UO_2)_3(VO_4)_2 \bullet 5H_2O$, precursor for the new $(UO_2)_3 (VO_4)_2$ uranyl-vanadate. *Journal of Solid State Chemistry* **150**, 72–80.

Sadikov, G.G., Krasovskaya, T.I., Polyakov, Y.A., & Nikolaev, V.P. (1988) Structural and spectral studies on potassium dimolybdatouranylate. *Inorganic Materials* **24**, 91–96.

Saine, M.C. (1987) Demonstration of a new family of compounds analogous to the perovskites. *Journal of the Less-Common Metals* **134**, 245–248.

Saine, M.C. (1989) Synthesis and structure of monoclinic $K_2U_2O_7$. *Journal of the Less-Common Metals* **154**, 361–365.

Sandino, A. & Bruno, J. (1992) The solubility of $(UO_2)_3 (PO_4)_2 \bullet 4H_2O(S)$ and the formation of U(VI) phosphate complexes - their influence in uranium speciation in natural-waters. *Geochimica et Cosmochimica Acta* **56**, 4135–4145.

Sarin, V.A., Linde, S.A., Fykin, L.E., Dudarev, V.Y., & Gorbunova, Y.E. (1983) Neutron graphic study of $UO_2H(PO_3)_3$ monocrystals. *Zhurnal Neorganicheskoi Khimii* **28**, 1538–1541.

Sawyer, J.O. (1972) The crystal structure of alpha $WSrUO_4$. *Journal of Inorganic & Nuclear Chemistry* **34**, 3268–3271.

Schleifer, M., Busch, J., Albert, B., & Gruehn, R. (2000) Synthesis and crystal structure of U_2TaO_{19}, a new compound with ''Jahnberg-structure'' and a note to the first oxide chlorides in the systems Th/Nb/O/Cl and Th/Zr(Hf)/Nb/O/Cl. *Zeitschrift Für Anorganische Und Allgemeine Chemie* **626**, 2299–2306.

Serezhkin, V.N. & Trunov, V.K. (1981) The crystal-structure of $UO_2CrO_4 \bullet 5.5H_2O$. *Kristallografiya* **26**, 301–304.

Serezhkin, V.N., Efremov, V.A., & Trunov, V.K. (1980a) Crystal-structure of $\alpha-UO_2MoO_4 \bullet 2H_2O$. *Kristallografiya* **25**, 861–865.

Serezhkin, V.N., Trunov, V.K., & Makarevich, L.G. (1980b) The refined crystal structure of uranyl molybdate. *Kristallografiy* **25**, 858–860.

Serezhkin, V.N., Soldatkina, M.A., & Efremov, V.A. (1981a) Crystal-structure of $MgUO_2(SO_4)_2 \bullet 11H_2O$. *Journal of Structural Chemistry* **22**, 454–457.

Serezhkin, V.N., Soldatkina, M.A., & Efremov, V.A. (1981b) Crystal-structure of uranyl selenate tetrahydrate. *Journal of Structural Chemistry* **22**, 451–454.

Serezhkin, V.N., Boiko, N.V., & Trunov, V.K. (1982) Crystal-structure of $SrUO_2(OH)CrO_4 \bullet 2.8H_2O$. *Journal of Structural Chemistry* **23**, 270–273.

Serezhkin, V.N., Soldatkina, M.A., & Boiko, N.V. (1983) Refinement of the crystal-structure of $(NH_4)_4UO_2(CO_3)_3$. *Journal of Structural Chemistry* **24**, 770–774.

Serezhkin, V.N., Verevkin, A.G., Smirnov, O.P., & Plakhtii, V.P. (2010) Neutron diffraction study of $Rb_2UO_2 (SeO_4)_2 \bullet 2D_2O$. *Russian Journal of Inorganic Chemistry* **55**, 1600–1606.

Serezhkina, L.B., Trunov, V.K., Kholodkovskaya, L.N., & Kuchumova, N.V. (1990) Crystalline-structure of $KUO_2CrO_4(OH) \bullet 1.5H_2O$. *Koordinatsionnaya Khimiya* **16**, 1288–1291.

Serezhkina, L.B., Mikhailov, Y.N., Gorbunova, Y.E., Medrish, I.V., & Serezhkin, V.I. (2004) Crystal structure of $Rb_2(UO_2(SO_4)_2H_2O) \cdot (H_2O)$. *Zhurnal Neorganicheskoi Khimii* **49**, 414–418.

Serezhkina, L.B., Vologzhanina, A.V., Marukhnov, A.V., Pushkin, D.V., & Serezhkin, N. (2009) Synthesis and Crystal Structure of $Na_3(H_3O)[UO_2(SeO_3)_2]_2 \bullet H_2O$. *Crystallography Reports* **54**, 852–857.

Serezhkina, L.B., Peresypkina, E.V., Virovets, A.V., Pushkin, D.V., & Verevkin, A.G. (2010) Synthesis and

structure of Cs[UO₂(SeO₄)(OH)]•nH₂O (n = 1.5 or 1). *Kristallografiya* **55**, 416–420.

SEREZHKINA, L.B., VOLOGZHANINA, A.V., VEREVKIN, A.G., & SEREZHKIN, V.N. (2011) An X-ray diffraction study of Rb[UO₂(SeO₄)F]•H₂O. *Radiochemistry* **53**, 301–303.

SHANNON, R.D. (1976) Revised effective ionic-radii and systematic studies of interatomic distances in halides and chalcogenides. *Acta Crystallographica Section A* **32**, 751–767.

SHASHKIN, D.P., LURE, E.A., & BELOV, N.V. (1974) Crystal-structure Na₂(UO₂)SiO₄. *Kristallografiya* **19**, 958–963.

SHISHKINA, O.V., MIKHAILOV, Y.N., GORBUNOVA, Y.E., SEREZHKINA, L.B., & SEREZHKIN, V.N. (2001) Rubidium Aquadioxoselenato(VI)hydroxouranate. *Doklady Akademii Nauk* **376**, 356–360.

SHUVALOV, R.R. & BURNS, P.C. (2003) A monodinic polymorph of uranyl dinitrate trihydrate, UO₂(NO₃)₂(H₂O)₂•H₂O. *Acta Crystallographica Section C: Crystal Structure Communications* **59**, I71–I73.

SHVAREVA, T.Y. & ALBRECHT-SCHMITT, T.E. (2006) General route to three-dimensional framework uranyl transition metal phosphates with atypical structural motifs: The case examples of Cs₂{(UO₂)₄[Co(H₂O)₂]2(HPO₄)(PO₄)₄} and Cs₃₊ₓ[(UO₂)₃CuH₄₋ₓ(PO₄)₅]•H₂O. *Inorganic Chemistry* **45**, 1900–1902.

SHVAREVA, T.Y., ALMOND, P.M., & ALBRECHT-SCHMITT, T.E. (2005a) Crystal chemistry and ion-exchange properties of the layered uranyl iodate KUO₂(IO₃)₃. *Journal of Solid State Chemistry* **178**, 499–504.

SHVAREVA, T.Y., BEITZ, J.V., DUIN, E.C., & ALBRECHT-SCHMITT, T.E. (2005b) Polar open-framework structure, optical properties, and electron paramagnetic resonance of the mixed-metal uranyl phosphate Cs₂[UO₂(VO₂)₂(PO₄)₂]•0.59H₂O. *Chemistry of Materials* **17**, 6219–6222.

SHVAREVA, T.Y., SULLENS, T.A., SHEHEE, T.C., & ALBRECHT-SCHMITT, T.E. (2005c) Syntheses, structures, and ion-exchange properties of the three-dimensional framework uranyl gallium phosphates, Cs₄[(UO₂)₂(GaOH)₂(PO₄)₄)]•H₂O and Cs[UO₂Ga(PO₄)₂]. *Inorganic Chemistry* **44**, 300–305.

SHVAREVA, T.Y., SKANTHAKUMAR, S., SODERHOLM, L., CLEARFIELD, A., & ALBRECHT-SCHMITT, T.E. (2007) Cs+-selective ion exchange and magnetic ordering in a three-dimensional framework uranyl vanadium(IV) phosphate. *Chemistry of Materials* **19**, 132–134.

SIEGEL, S. & HOEKSTRA, H.R. (1968) Crystal structure of copper uranium tetroxide. *Acta Crystallographica Section B: Structural Science, Crystal Engineering, and Mateirals* **B24**, 967–970.

SIEGEL, S., HOEKSTRA, H.R., & GEBERT, E. (1972a) Structure of gamma-uranyl dihydroxide, UO₂(OH)₂. *Acta Crystallographica Section B: Structural Science, Crystal Engineering, and Materials* **28**, 3469–3473.

SIEGEL, S., TANI, B., VISTE, A., & HOEKSTRA, H.R. (1972b) Structure of hydrogen triuranate. *Acta Crystallographica Section B: Structural Science, Crystal Engineering, and Materials* **B28**, 117–121.

SIIDRA, O.I., NAZARCHUK, E.V., & KRIVOVICHEV, S.V. (2012a) Highly Kinked Uranyl Chromate Nitrate Layers in the Crystal Structures of A(UO₂)(CrO₄)(NO₃) (A = K, Rb). *Zeitschrift Für Anorganische und Allgemeine Chemie* **638**, 982–986.

SIIDRA, O.I., NAZARCHUK, E.V., & KRIVOVICHEV, S.V. (2012b) Syntheses and crystal structures of two novel alkaline uranyl chromates A_2(UO₂)(CrO₄)₂ (A = Rb, Cs) with bidentate coordination mode of uranyl ions by chromate anions. *Journal of Solid State Chemistry* **187**, 286–290.

SIIDRA, O.I., NAZARCHUK, E.V., KAYUKOV, R.A., BUBNOVA, R.S., & KRIVOVICHEV, S.V. (2013) Transition in uranyl chromium compounds: Synthesis and high-temperature x-ray diffraction study of Cs₂[(UO₂)₂(CrO₄)₃]. *Zeitschrift für Anorganische und Allgemeine Chemmie* **639**, 2302–2306.

SLADKOV, V. (2010) Interaction of uranyl with Se(IV) and Se(VI) in aqueous acid solutions by means of capillary electrophoresis. *Electrophoresis* **31**, 3482–3491.

SODERHOLM, L., SKANTHAKUMAR, S., & ANTONIO, M.R. (2007) Synchrotron studies of actinide speciation in solution. *Abstracts of Papers of the American Chemical Society* **234**.

SOKOLOVA, E., HAWTHORNE, F.C., BELAKOVSKIY, D.I., & PAUTOV, L.A. (2005) The OD (order-disorder) structure of holfertite, hydrated uranyl titanate mineral from Searle Canyon, Thomas Range, Utah, USA. *Canadian Mineralogist* **43**, 1545–1552.

SPITSYN, V.I., KOVBA, L.M., TABACHENKO, V.V., TABACHENKO, N.V., & MIKHAILOV, Y.N. (1982) Study of the structure of basic uranyl salts and polyuranates. *Izvestiya Akademii Nauk SSSR* **1982**, 807–812.

STERNS, M., PARISE, J.B., & HOWARD, C.J. (1986) Refinement of the structure of trilead(II) uranate(VI) from neutron powder diffraction data. *Acta Crystallographica Section C: Crystal Structure Communications* **42**, 1275–1277.

STROBEL, S. & SCHLEID, T. (2004) CuGdSe₂, ein noch unbekanntes Kupfer-Lanthanoid-Selenid im CuLaS₂-Typ. *Zeitschrift Für Anorganische und Allgemeine Chemie* **630**, 1761.

SULLENS, T.A., JENSEN, R.A., SHVAREVA, T.Y., & ALBRECHT-SCHMITT, T.E. (2004) Cation-cation interactions between uranyl cations in a polar open-framework uranyl periodate. *Journal of the American Chemical Society* **126**, 2676–2677.

SULLIVAN, J.C., ZIELEN, A.J., & HINDMAN, J.C. (1961) Specific interaction between Np(V) and U(VI) in aqueous perchloric acid media. *Journal of the American Chemical Society* **83**, 3373–3378.

SURBLE, S., OBBADE, S., SAAD, S., YAGOUBI, S., DION, C., & ABRAHAM, F. (2006) The $A_{(1−x)}$UNbO$_{(6−x/2)}$ compounds (x

= 0, A = Li, Na, K, Cs and x = 0.5 A = Rb, Cs): from layered to tunneled structure. *Journal of Solid State Chemistry* **179**, 3238–3251.

SWIHART, G.H., SENGUPTA, P.K., SCHLEMPER, E.O., BACK, M.E., & GAINES, R.V. (1993) The Crystal-structure of moctezumite PbUO$_2$(TeO$_3$)$_2$. *American Mineralogist* **78**, 835–839.

SYKORA, R.E. & ALBRECHT-SCHMITT, T.E. (2003) Self-assembly of a polar open-framework uranyl vanadyl hexaoxoiodate(VII) constructed entirely from distorted octahedral building units in the first uranium hexaoxoio-date: K$_2$[(UO$_2$)$_2$(VO)$_2$(IO$_6$)$_2$O]•(H$_2$O). *Inorganic Chemistry* **42**, 2179–2181.

SYKORA, R.E. & ALBRECHT-SCHMITT, T.E. (2004) Hydrothermal synthesis and crystal structure of Cs$_6$[(UO$_2$)$_4$(W$_5$O$_{21}$)(OH)$_2$(H$_2$O)$_2$]: a new polar uranyl tungstate. *Journal of Solid State Chemistry* **177**, 3729–3734.

SYKORA, R.E., MCDANIEL, S.M., WELLS, D.M., & ALBRECHT-SCHMITT, T.E. (2002a) Mixed-metal uranium(VI) iodates: Hydrothermal syntheses, structures, and reactivity of Rb[UO$_2$(CrO$_4$)(IO$_3$)(H$_2$O)], A_2[UO$_2$(CrO$_4$)(IO$_3$)$_2$] (A = K, Rb, Cs), and K$_2$[UO$_2$(MoO$_4$)(IO$_3$)$_2$]. *Inorganic Chemistry* **41**, 5126–5132.

SYKORA, R.E., WELLS, D.M., & ALBRECHT-SCHMITT, T.E. (2002b) Hydrothermal synthesis and structure of a new one-dimensional, mixed-metal U(VI) iodate, Cs$_2$[(UO$_2$)(CrO$_4$)(IO$_3$)$_2$]. *Inorganic Chemistry* **41**, 2304–2306.

SYKORA, R.E., BEAN, A.C., SCOTT, B.L., RUNDE, W., & ALBRECHT-SCHMITT, T.E. (2004a) New one-dimensional uranyl and neptunyl iodates: crystal structures of K$_3$(UO$_2$)$_2$(IO$_3$)$_6$(IO$_3$)•H$_2$O and KNpO$_2$(IO$_3$)$_3$·1.5H$_2$O. *Journal of Solid State Chemistry* **177**, 725–730.

SYKORA, R.E., KING, J.E., ILLIES, A.J., & ALBRECHT-SCHMITT, T.E. (2004b) Hydrothermal synthesis, structure, and catalytic properties of UO$_2$Sb$_2$O$_4$. *Journal of Solid State Chemistry* **177**, 1717–1722.

SYKORA, R.E., MCDANIEL, S.M., & ALBRECHT-SCHMIDTT, T.E. (2004c) Hydrothermal synthesis and structure of K$_6$(UO$_2$)$_4$(CrO$_4$)$_7$•6H$_2$O: A layered uranyl chromate with a new uranyl sheet topology. *Journal of Solid State Chemistry* **177**, 1431–1436.

TABACHENKO, N.V., SEREZHKIN, N., SEREZHKINA, L.B., & KOVBA, L.M. (1979) Crystal structure of manganese sulfatouranylate Mn(UO$_2$)(SO$_4$)$_2$(H$_2$O)$_5$. *Koordinatsionnaya Khimiya* **5**, 1563–1568.

TABACHENKO, N.V., KOVBA, L.M., & SEREZHKIN, N. (1983) The crystal structure of molybdatouranylates of magnesium and zinc of composition M(UO$_2$)$_3$(MoO$_4$)$_4$(H$_2$O)$_8$ (M = Mg, Zn). *Koordinatsionnaya Khimiya* **9**, 1568–1571.

TABACHENKO, N.V., KOVBA, L.M., & SEREZHKIN, N. (1984a) Crystal structures of Mg(UO$_2$)$_6$(MoO$_4$)$_7$(H$_2$O)$_{18}$ and Sr(UO$_2$)$_6$(MoO$_4$)$_7$(H O)$_{15}$. *Koordinatsionnaya Khimiya* **10**, 558–562.

TABACHENKO, V.V., BALASHOV, V.L., KOVBA, L.M., & SEREZHKIN, V.N. (1984b) Crystal-structure of barium molybdateuranylate Ba(UO$_2$)$_3$(MoO$_4$)$_4$.4H$_2$O. *Koordinatsionnaya Khimiya* **10**, 854–857.

TABACHENKO, V.V., KOVBA, L.M., & SEREZHKIN, V.N. (1984c) Crystalline-structure of Mg(UO$_2$)$_6$(MoO$_4$)$_7$·18H$_2$O and Sr(UO$_2$)$_6$(MoO$_4$)$_7$·15H$_2$O. *Koordinatsionnaya Khimiya* **10**, 558–562.

TALI, R., TABACHENKO, N.V., & KOVBA, L.M. (1993) Crystal structure of Cu$_4$UO$_2$(MoO$_4$)$_2$(OH)$_6$. *Zhurnal Neorganicheskoi Khimii* **38**, 1450–1452.

TANCRET, N., OBBADE, S., & ABRAHAM, F. (1995) Ab initio structure determination of urany divanadate (UO$_2$)$_2$V$_2$O$_7$ from powder X-ray diffraction data. *European Journal of Solid State Inorganic Chemistry* **32**, 195–207.

TANNER, P.A. & MAK, T.C.W. (1999) Synthesis, structure, and spectroscopy of rare earth hypophosphites. II. Uranyl hypophosphite monohydrate and uranyl hypophosphite-hypophosphorous acid (1/1). *Inorganic Chemistry* **38**, 6024–6031.

TAYLOR, J.C. (1971) Structure of α-form of uranyl hydroxide. *Acta Crystallographica Section B: Structural Science, Crystal Engineering, and Materials* **B27**, 1088–1091.

TAYLOR, J.C. & BANNISTER, M.J. (1972) Neutron-diffraction study of anisotropic thermal-expansion of beta-uranyl dihydroxide. *Acta Crystallographica Section B: Structural Science, Crystal Engineering, and Materials* **B28**, 2995–2999.

TAYLOR, J.C. & MUELLER, M.H. (1965) A neutron diffraction study of uranyl nitrate hexahydrate. *Acta Crystallographica* **19**, 536–543.

TAYLOR, J.C. & WILSON, P.W. (1973) Structure of anhydrous uranyl chloride by powder neutron diffraction. *Acta Crystallographica Section B: Structural Science, Crystal Engineering, and Materials* **B29**, 1073–1076.

TAYLOR, J.C. & WILSON, P.W. (1974) Structure of uranyl chloride monohydrate by neutron-diffraction and disorder of water molecule. *Acta Crystallographica Section B: Structural Science, Crystal Engineering, and Materials* **B30**, 169–175.

TROMBE, J.C., GLEIZES, A., & GALY, J. (1985) Structure of a uranyl diselenite, UO$_2$Se$_2$O$_5$. *Acta Crystallographica Section C: Crystal Structure Communications* **41**, 1571–1573.

TUTOV, A.G., PLAKHTII, V.P., USOV, O.A., BUBLYAEV, R.A., & CHERNENKOV, Y.P. (1991) Neutron-diffraction refinement of the structure of a nonlinear optical-crystal of dicesiumuraniltetrachloride Cs$_2$UO$_2$Cl$_4$. *Kristallografiya* **36**, 1135–1138.

UNRUH, D.K., BURTNER, A., & BURNS, P.C. (2009) Expanding the Crystal Chemistry of Actinyl Peroxides: mu-eta(2): eta(1) Peroxide Coordination in Trimers of U^{6+} Polyhedra. *Inorganic Chemistry* **48**, 2346–2348.

UNRUH, D.K., BARANAY, M., BARANAY, M., & BURNS, P.C. (2010) Uranium(VI) Tetraoxido Core Coordinated by Bidentate Nitrate. *Inorganic Chemistry* **49**, 6793–6795.

VAN DEN BOSSCHE, G., SPIRLET, M.R., REBIZANT, J., & GOFFART, J. (1987) Structure of diammonium tetrabromodioxouranate(VI) dihydrate. *Acta Crystallographica Section C: Crystal Structure Communications* **43**, 383–384.

VAN DER PUTTEN, N. & LOOPSTRA, B.O. (1974) Uranyl sulphate 2.5H_2O, $UO_2SO_4(H_2O)_{2.5}$. *Crystal Structure Communications* **3**, 377–380.

VAN DUIVENBODEN, H.C. & IJDO, D.J.W. (1986) Redetermination of tricalcium uranate(VI) - a rietveld refinement of neutron powder diffraction data. *Acta Crystallographica Section C: Crystal Structure Communications* **42**, 523–525.

VAN EGMOND, A.B. (1976) Investigations on cesium uranates. V. crystal-structures of Cs_2UO_4, $Cs_4U_5O_{17}$, $Cs_2U_7O_{22}$ and $Cs_2U_{15}O_{46}$. *Journal of Inorganic & Nuclear Chemistry* **38**, 1649–1651.

VEREVKIN, A.G., VOLOGZHANINA, A.V., SEREZHKINA, L.B., & SEREZHKIN, V.N. (2010) X-Ray Diffraction Study of $Rb_2[(UO_2)_2(CrO_4)_3(H_2O)_2] \bullet 4H_2O$. *Crystallography Reports* **55**, 602–608.

VILLA, E.M., MARR, C.J., JOUFFRET, L.J., ALEKSEEV, E.V., DEPMEIER, W., & ALBRECHT-SCHMITT, T.E. (2012) Systematic evolution from uranyl(VI) phosphites to uranium(IV) phosphates. *Inorganic Chemistry* **51**, 6548–6558.

VILLA, E.M., DIWU, J.A., ALEKSEEV, E.V., DEPMEIER, W., & ALBRECHT-SCHMIDT, T.E. (2013a) Structural changes within the alkaline earth uranyl phosphites. *Dalton Transactions* **42**, 9637–9644.

VILLA, E.M., JUAN, D., ALEKSEEV, E.V., DEPMEIER, W., & ALBRECHT-SCHMITT, T.E. (2013b) Structural changes within the alkaline earth uranyl phosphites. *Dalton Transactions* **42**, 9637–9644.

VISWANATHAN, K. & HARNEIT, O. (1986) Refined crystal-structure of β-uranophane, $Ca(UO_2)_2(SIO_3OH) \bullet 2.5H_2O$. *American Mineralogist* **71**, 1489–1493.

VLČEK, V., ČEJKA, J., CÍSAŘOVÁ, I., GOLIÁŠ, V., & PLÁŠIL, J. (2009) Crystal structure of $UO_2SO_4 \bullet 2.5H_2O$: Full anisotropic refinement and vibration characteristics. *Journal of Molecular Structure* **936**, 75–79.

VOCHTEN, R., VAN HAVERBEKE, L., VAN SPRINGEL, K., BLANTON, N., & PEETERS, O.M. (1994) The structure and physiochemical characteristics of a synthetic phase compositionally intermediate between liebigite and andersonite. *Canadian Mineralogist* **32**, 553–561.

WALENTA, K., HATERT, F., THEYE, T., LISSNER, F., & ROELLER, K. (2009) Nielsbohrite, a new potassium uranyl arsenate from the uranium deposit of Menzenschwand, southern Black Forest, Germany. *European Journal of Mineralogy* **21**, 515–520.

WALLWORK, K.S., JAMES, M., & CARTER, M.L. (2006) The crystal chemistry, structure and properties of a synthetic carnotite-type compound, $Ba_2[(UO_2)_2Ti_2O_8]$. *Canadian Mineralogist* **44**, 433–442.

WANG, X.Q., HUANG, J., LIU, L.M., & JACOBSON, A.J. (2002) The novel open-framework uranium silicates $Na_2(UO_2)(Si_4O_{10}) \cdot 2.1H_2O$ (USH-1) and $RbNa(UO_2)(Si_2O_6) \cdot H_2O$ (USH-3). *Journal of Materials Chemistry* **12**, 406–410.

WANG, S., ALEKSEEV, E.V., LING, J., SKANTHAKUMAR, S., SODERHOLM, L., DEPMEIER, W., & ALBRECHT-SCHMITT, T.E. (2010a) Neptunium diverges sharply from uranium and plutonium in crystalline borate matrixes: insights into the complex behavior of the early actinides relevant to nuclear waste storage. *Angewandte Chemie International Edition* **49**, 1263–1266.

WANG, S., ALEKSEEV, E.V., STRITZINGER, J.T., DEPMEIER, W., & ALBRECHT-SCHMITT, T.E. (2010b) Crystal chemistry of the potassium and rubidium uranyl borate families derived from boric acid fluxes. *Inorganic Chemistry* **49**, 6690–6696.

WANG, S., ALEKSEEV, E.V., STRITZINGER, J.T., DEPMEIER, W., & ALBRECHT-SCHMITT, T.E. (2010c) How are centrosymmetric and noncentrosymmetric structures achieved in uranyl borates? *Inorganic Chemistry* **49**, 2948–2953.

WANG, S., ALEKSEEV, E.V., JUAN, D., MILLER, H.M., OLIVER, A.G., LIU, G., DEPMEIER, W., & ALBRECHT-SCHMITT, T.E. (2011a) Functionalization of borate networks by the incorporation of fluoride: syntheses, crystal structures, and nonlinear optical properties of novel actinide fluoroborates. *Chemistry of Materials* **23**, 2931–2939.

WANG, S.A., VILLA, E.M., DIWU, J.A., ALEKSEEV, E.V., DEPMEIER, W., & ALBRECHT-SCHMITT, T.E. (2011b) Role of Anions and Reaction Conditions in the Preparation of Uranium(VI), Neptunium(VI), and Plutonium(VI) Borates. *Inorganic Chemistry* **50**, 2527–2533.

WELLER, M.T., DICKENS, P.G., & PENNY, D.J. (1988) The structure of δ-UO_3. *Polyhedron* **7**, 243–244.

WELLER, M.T., LIGHT, M.E., & GELBRICH, T. (2000) Structure of uranium(VI) oxide dihydrate, $UO_3 \cdot 2H_2O$; synthetic meta-schoepite $(UO_2)_4O(OH)_6 \cdot 5H_2O$. *Acta Crystallographica Section B: Structural Science, Crystal Engineering, and Materials* **56**, 577–583.

WENG, Z.H., WANG, S.A., LING, J., MORRISON, J.M., & BURNS, P.C. (2012) $(UO_2)_2[UO_4(trz)_2](OH)_2$: A U(VI) coordination intermediate between a tetraoxido core and a uranyl ion with cation–cation interactions. *Inorganic Chemistry* **51**, 7185–7191.

WILSON, R.E., SKANTHAKUMAR, S., CAHILL, C.L., & SODERHOLM, L. (2011) Structural studies coupling X-ray diffraction and high-energy X-ray scattering in the UO_2^{2+}–HBr_{aq} system. *Inorganic Chemistry* **50**, 10748–10754.

WOLF, R. & HOPPE, R. (1985) New investigations about oxo uranates - on α-Li_6UO_6. with a remark about β-Li_6UO_6. *Zeitschrift Für Anorganische und Allgemeine Chemie* **528**, 129–137.

WOLF, R. & HOPPE, R. (1986) New information on oxouranates. VI. Na$_4$UO$_5$ and K$_4$UO$_5$. *Revue De Chimie Minerale* 23, 828–848.

WOLF, R. & HOPPE, R. (1987) A new oxouranate(VI) - K$_2$Li$_4$UO$_6$ - with a remark about Rb$_2$Li$_4$UO$_6$ and Cs$_2$Li$_4$UO$_6$. *Zeitschrift Für Anorganische und Allgemeine Chemie* 554, 34–42.

WOODWARD, J.D. & ALBRECHT-SCHMITT, T.E. (2005) Molten salt flux synthesis and structure of the new layered uranyl tellurite, K$_4$[(UO$_2$)$_5$(TeO$_3$)$_2$O$_5$]. *Journal of Solid State Chemistry* 178, 2922–2926.

WOODWARD, J.D., ALMOND, P.M., & ALBRECHT-SCHMITT, T.E. (2004) Synthesis and crystal structures of the layered uranyl tellurites A_2[(UO$_2$)$_3$(TeO$_3$)$_2$O$_2$] (A = K, Rb, Cs). *Journal of Solid State Chemistry* 177, 3971–3976.

WU, S.J., LING, J., WANG, S.A., SKANTHAKUMAR, S., SODERHOLM, L., ALBRECHT-SCHMITT, T.E., ALEKSEEV, E.V., KRIVOVICHEV, S.V., & DEPMEIER, W. (2009) Uranium(VI) adopts a tetraoxido core. *European Journal of Inorganic Chemistry*, 4039–4042.

WU, S., BEERMANN, O., WANG, S., HOLZHEID, A., DEPMEIER, W., MALCHEREK, T., MODOLO, G., ALEKSEEV, E.V., & ALBRECHT-SCHMITT, T.E. (2012) Synthesis of uranium materials under extreme conditions: UO$_2$[B$_3$Al$_4$O$_{11}$(OH)], a complex 3D aluminoborate. *Chemistry - A European Journal* 18, 4166–4169.

YAGOUBI, S., OBBADE, S., DION, C., & ABRAHAM, F. (2005) Crystal structures of Rb$_2$U$_2$O$_7$ and Rb$_8$U$_9$O$_{31}$, a new layered rubidium uranate. *Journal of Solid State Chemistry* 178, 3218–3232.

YAGOUBI, S., OBBADE, S., SAAD, S., & ABRAHAM, F. (2011) From $_\infty^1$[(UO$_2$)$_2$O(MoO$_4$)$_4$]$^{6-}$ to $_\infty^1$[(UO$_2$)$_2$(MoO$_4$)$_3$ (MoO$_5$)]$^{6-}$ infinite chains in A$_6$U$_2$Mo$_4$O$_{21}$ (A = Na, K, Rb, Cs) compounds: Synthesis and crystal structure of Cs$_6$[(UO$_2$)$_2$(MoO$_4$)$_3$(MoO$_5$)]. *Journal of Solid State Chemistry* 184, 971–981.

YAGOUBI, S., RENARD, C., ABRAHAM, F., & OBBADE, S. (2013) Molten salt flux synthesis and crystal structure of a new open framework uranyl phosphate Cs$_3$(UO$_2$)$_2$(PO$_4$)O$_2$: Spectroscopic characterization and cationic mobility studies. *Journal of Solid State Chemistry* 200, 13–21.

YAKUBOVICH, O.V., STEELE, I.M., ATENCIO, D., MENEZES, L.A., & CHUKANOV, N.V. (2008) Crystal structure of the (Mg,Fe)[UO$_2$(P,As)O$_4$]$_2$•10H$_2$O solid solution - A novel mineral variety of saleeite. *Crystallography Reports* 53, 764–770.

YAMASHITA, T., FUJINO, T., MASAKI, N., & TAGAWA, H. (1981) The crystal-structures of α-CdUO$_4$ and β-CdUO$_4$. *Journal of Solid State Chemistry* 37, 133–139.

YU, Y.Q., JIANG, K., & ALBRECHT-SCHMITT, T.E. (2009) [Hg$_5$O$_2$(OH)$_4$][(UO$_2$)$_2$(AsO$_4$)$_2$]: A complex mercury(II) uranyl arsenate. *Journal of Solid State Chemistry* 182, 1867–1871.

ZALKIN, A., RUBEN, H., & TEMPLETON, D.H. (1978) Structure of a new uranyl sulfate hydrate, α-2UO$_2$SO$_4$•7H$_2$O. *Inorganic Chemistry* 17, 3701–3702.

ZALKIN, A., TEMPLETON, L.K., & TEMPLETON, D.H. (1989) Structure of rubidium uranyl(VI) trinitrate. *Acta Crystallographica Section C: Crystal Structure Communications* 45, 810–811.

ZEHNDER, R.A., PEPER, S.M., SCOTT, B.L., & RUNDE, W.H. (2005) Tetrapotassium dicarbonatodioxoperoxouranium(VI) 2.5-hydrate, K$_4$[U(CO$_3$)$_2$O$_2$(O$_2$)]•2.5H$_2$O. *Acta Crystallographica Section C: Crystal Structure Communications* 61, I3–I5.

ZEHNDER, R.A., BATISTA, E.R., SCOTT, B.L., PEPER, S.M., GOFF, G.S., & RUNDE, W.H. (2008) Synthesis, crystallographic characterization, and conformational prediction of a structurally unique molecular mixed-ligand U(VI) solid, Na$_6$[(UO$_2$)(O$_2$)$_2$(OH)$_2$](OH)$_2$•14H$_2$O. *Radiochimica Acta* 96, 575–578.